20 June 2008 | $10

Science

AAAS

Custom-fit RNAi tools for your research

Rarely, one size fits all. Small, medium or large — your research needs are your own. So, our technology comes custom-fit with your basic and applied research in mind.

Sigma's RNAi tools are tailored to your needs for gene silencing — from single gene analysis and high throughput screens to cutting-edge applications for drug discovery and target validation.

- Guaranteed siRNA, shRNA, miRNA for high performance
- Lentiviral manufacturing to fit your specifications (volume, titer, scale)
- Large scale production for *in vivo* RNAi and more
- Custom cloned shRNAs for experimental flexibility
- Coming Soon: Zinc Finger Nuclease technology for Targeted Genome Editing

What's your custom fit?

Design your own lab coat at sigma.com/lookcloser. After all, you know what fits you best.

Enter your design to win.

Grand prize is an all expense paid* three-day, hands-on RNAi Workshop and 20 customized lab coats of your design. Additional prizes for runner-ups.

For a chance to win custom-designed lab coats and to learn from the experts, enter our MISSION® RNAi Lab Coat Design Contest.

For more information and to enter your custom lab coat design, visit ***sigma.com/lookcloser.***

SIGMA Life Science

Our Innovation, Your Research — Shaping the Future of Life Science

MISSION is a registered trademark of Sigma-Aldrich Co. and its affiliate Sigma-Aldrich Biotechnology, LP.

*Visit sigma.com/lookcloser for official contest details and rules.

SIGMA-ALDRICH®

Custom-fit RNAi tools for your research

Rarely, one size fits all. Small, medium or large — your research needs are your own. So, our technology comes custom-fit with your basic and applied research in mind.

Sigma's RNAi tools are tailored to your needs for gene silencing — from single gene analysis and high throughput screens to cutting-edge applications for drug discovery and target validation.

- Guaranteed siRNA, shRNA, miRNA for high performance
- Lentiviral manufacturing to fit your specifications (volume, titer, scale)
- Large scale production for *in vivo* RNAi and more
- Custom cloned shRNAs for experimental flexibility
- Coming Soon: Zinc Finger Nuclease technology for Targeted Genome Editing

What's your custom fit?

Design your own lab coat at sigma.com/lookcloser. After all, you know what fits you best.

Enter your design to win.

Grand prize is an all expense paid* three-day, hands-on RNAi Workshop and 20 customized lab coats of your design. Additional prizes for runner-ups.

For a chance to win custom-designed lab coats and to learn from the experts, enter our MISSION® RNAi Lab Coat Design Contest.

For more information and to enter your custom lab coat design, visit ***sigma.com/lookcloser.***

SIGMA Life Science

Our Innovation, Your Research — Shaping the Future of Life Science

MISSION is a registered trademark of Sigma-Aldrich Co. and its affiliate Sigma-Aldrich Biotechnology, LP.

*Visit sigma.com/lookcloser for official contest details and rules.

SIGMA-ALDRICH®

Statistical Analysis is NOT a daunting task anymore -

NEW! *SigmaPlot 11 can show you how !*

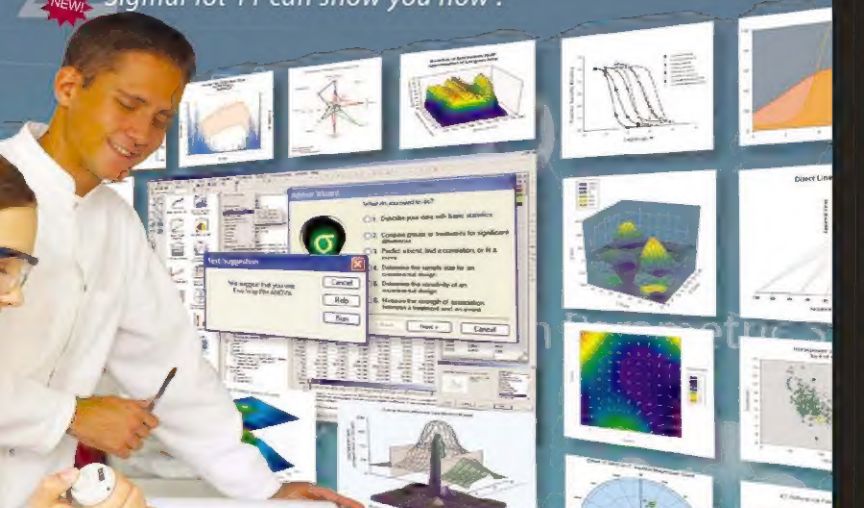

The Simplest and Most Effective Way to Analyze and Graph Data !

Join the more than 250,000 researchers worldwide who use SigmaPlot to easily customize every graphic detail and create compelling publication-quality graphs that clearly present their results for technical publications, presentations or the web. Gain deeper insight into your data with easy-to-use data analysis tools — from sophisticated curve fitting to advanced mathematical calculations. SigmaPlot 11 has 50 of the most frequently used statistical tests to analyze scientific data right within SigmaPlot's statistics menu or take advantage of the Advisor Wizard that walks the non-statistician through the analysis of their data.

With SigmaPlot 11 you can:

- Perform over 50 of the most frequently used statistical tests in scientific research with step-by-step guidance that includes suggestion of the most appropriate statistical test, checking for violations of data assumptions and generation of an easy-to-interpret report that has minimal statistical jargon.
- Fit your data easily and accurately to solve simple and advanced curve fitting problems including Global Curve Fitting.
- Choose from over 100 easily customizable 2D and 3D graph types to create publication-quality graphs that communicate exactly what you want. Use pre-formatted worksheets to easily arrange your data according to the required graph type.
- Take advantage of an updated look-and-feel across the entire application and customize your workspace according to your usage.
- Automate repetitive tasks to save your time and effort.

"I find SigmaPlot to be the most user-friendly and advanced... It really is quite exceptional, especially for someone who doesn't have a huge statistical background."

- Carmen Cuffari, MD
Associate Professor
Department of Pediatrics

SIGMAPLOT
Exact Graphs and Data Analysis

Systat Software USA
phone: 866-797-7401
Email: info-usa@systat.com

Systat Software UK
phone: +44-(0)208-538 0128
Email: info@systat.co.uk

Systat Software Germany
phone: +49-2104-9540
Email: kontakt@systat.de

Systat Software Asia-Pac
phone: +91 - 80 - 4112 0000
Email: info-in@systat.com

FREE INTERACTIVE DEMOS & 30-DAY TRIAL SOFTWARE AVAILABLE AT WWW.SYSTAT.COM OR CALL 1-800-797-7401

GE Healthcare

Whatman®

Whatman is now part of GE Healthcare.

Creating a centre of excellence in separation technology.

The considerable expertise of Whatman in the fields of sample preparation and filtration technologies has earned them an outstanding reputation world wide. Whatman has key enabling technologies used in the understanding of gene and protein functions. Combining the skills of the two companies will enable GE Healthcare to create strong added value for customers giving unparalleled support to a wide range of research and lab applications.

For more information visit www.gelifesciences.com/whatman

imagination at work

Volume 320, Issue 5883

COVER

False-color image of a section of the Semarkona meteorite. The round objects are chondrules; the large one near the bottom center is about 2 millimeters across. Magnesium-rich minerals (olivine and pyroxene) appear red, sodium-rich glass appears yellow, and the iron-rich material surrounding the chondrules includes matrix (greenish) and sulfides, metal, and oxides (blue). The sodium in the glass suggests that the chondrules formed in extremely dusty environments in the early solar system. See page 1617.

Image: Jeffrey Grossman/USGS

DEPARTMENTS

EDITORIAL

NEWS OF THE WEEK

NEWS FOCUS


1578

LETTERS

BOOKS *ET AL.*


1597 & 1638

POLICY FORUM

PERSPECTIVES

CONTENTS continued >>

Sample technologies by QIAGEN

Prepare for results

Rely on QIAGEN sample technologies for:

- **DNA, RNA, and protein purification**
- **Automated sample preparation**
- **Whole genome and transcriptome amplification**
- **Epigenetics sample preparation**
- **Sample collection and stabilization**

Contact QIAGEN today or visit www.qiagen.com/goto/SampleTech .

QIAGEN®

Sample & Assay Technologies

Science

SCIENCE EXPRESS

www.sciencexpress.org

CLIMATE CHANGE

High-Resolution Greenland Ice Core Data Show Abrupt Climate Change Happens in Few Years
J. P. Steffensen et al.
Greenland's climate flipped to a different state within 1 to 3 years more than once during the last deglaciation.
10.1126/science.1157707

IMMUNOLOGY

Censoring of Autoreactive B Cell Development by the Pre-B Cell Receptor
R. A. Keenan et al.
A protein that helps newly rearranged antibody chains arrive at the cell surface of immature immune cells is found to help delete cells with potential autoreactivity.
10.1126/science.1157533

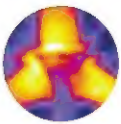

APPLIED PHYSICS

Control of Exciton Fluxes in an Excitonic Integrated Circuit
A. A. High, E. E. Novitskaya, L. V. Butov, M. Hanson, and A. C. Gossard
Coupled quantum-wells structures, patterned to create electron-hole circuits, can perform simple logic operations on optical input signals.
10.1126/science.1157845

IMMUNOLOGY

Modulation of Gene Expression via Disruption of NF-κB Signaling by a Bacterial Small Molecule
V. V. Kravchenko et al.
A small molecule produced by a common pathogenic bacterium inhibits the activity of a key immune transcription factor.
10.1126/science.1156499

TECHNICAL COMMENT ABSTRACTS

PLANETARY SCIENCE

REVIEW

ECONOMICS

1595 & 1622

BREVIA

PLANT SCIENCE

REPORTS

ASTRONOMY

PHYSICS

METEORITICS

GEOCHEMISTRY

CONTENTS continued >>

Pioneering What does the Curie family have in common with the settlers of the New World? Leica Microsystems has mapped its corporate values. For more information visit our website.

"Cells work quickly and precisely – just like our Leica AM TIRF MC system."

Our work is concentrated on depicting polarized protein transport in epithelial cells. The incorporation of newly synthetisized proteins into the plasma membrane can be tracked in the Leica AM TIRF MC microscope – living up to new insights in life.

Prof. Dr. Ralf Jacob, University Marburg, Department of Clinical Cytobiology and Cytopathology, Marburg, Germany

www.leica-microsystems.com

Living up to Life

Leica

MICROSYSTEMS

REPORTS CONTINUED

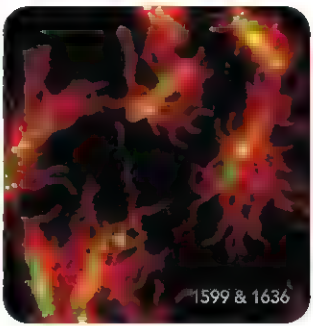

ADVANCING SCIENCE, SERVING SOCIETY

SCIENCE (ISSN 0036-8075) is published weekly on Friday, except the last week in December, by the American Association for the Advancement of Science, 1200 New York Avenue, NW, Washington, DC 20005. Periodicals Mail postage (publication No. 484420) paid at Washington, D.C. and additional mailing offices. Copyright © 2008 by the American Association for the Advancement of Science. The title SCIENCE is a registered trademark of the AAAS. Domestic Institutional subscription (51 issues): $1349; GST (Canada) $94; GST (Australia) $103; Canadian Institutional subscription $1,349; Foreign postage extra. Member subscriber rate and $65 other countries rate and additional $25 first class, airmail, student and emeritus rate are reduced. Canadian rate with GST available upon request. GST #125439372. Publications Mail Agreement Number 1074626. **Printed in the U.S.A.**

Changes of address: Allow 4 weeks, giving old and new addresses and 8-digit account number. **Postmaster:** send change of address to AAAS, P.O. Box 96178, Washington, DC 20090-6178. **Single-copy sales:** $10.00 current issue; $15.00 back issue prepaid includes surface postage; bulk discounts requested. **Authorization to photocopy materials** for internal or personal use under circumstances not falling within the fair use provisions of the Copyright Act is granted by AAAS to libraries and other users registered with the Copyright Clearance Center (CCC) Transactional Reporting Service, provided that $25.00 per article is paid directly to CCC, 222 Rosewood Drive, Danvers, MA 01923. The identification code for Science is 0036-8075. Science is indexed in the *Reader's Guide to Periodical Literature* and in several specialized indexes.

CONTENTS continued >>

Challenge presented, scientists accept

Promega

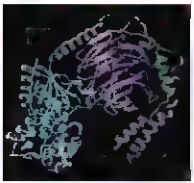

A heterotrimeric G protein.

SCIENCE SIGNALING
www.sciencesignaling.org

REVIEW: Dissociation of Heterotrimeric G Proteins in Cells
N. A. Lambert
G proteins may function as activated heterotrimers, as well as dissociated subunits.

PERSPECTIVE: Does Contractile Ca^{2+} Control Calcineurin-NFAT Signaling and Pathological Hypertrophy in Cardiac Myocytes?
S. R. Houser and J. D. Makarewich
Are calcium signaling pathways in the heart regulated by bulk cytoplasmic calcium or by calcium in specialized microdomains?

PERSPECTIVE: A Cunning Stunt—An Alternative Mechanism of Eukaryotic Translation Initiation
S. J. Morley and M. J. Coldwell
Translation of cellular inhibitor of apoptosis 2 transcripts appears to involve a ribosome shunting mechanism, permitting translation in periods of stress.

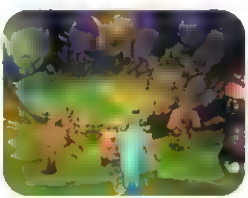

SCIENCE ONLINE FEATURE

THE GONZO SCIENTIST: Slaying Monsters for Science
An article and video highlight the first scientific conference held in Azeroth, the online universe of the role-playing game World of Warcraft
www.sciencemag.org/scientistgonzo.dtl

SCIENCENOW
www.sciencenow.org

How Is a Lizard Like a Motorcycle?
Study answers century-old mystery of why lizards "pop a wheelie" while running.

Life Cooked Up in Outer Space?
Meteorite fragments contain makings of DNA.

The Importance of Being Frightened
Wide eyes and flared nostrils may have saved our ancestors on more than one occasion.

Finding opportunities in toxins.

SCIENCE CAREERS
www.sciencecareers.org/career_development

In Toxicology, Opportunities Abound
B. Vastag
Toxicology encompasses a wide range of disciplines and offers a wide range of jobs.

Tooling Up: What Really Matters in a Job Talk
D. Jensen
The key to giving a good job talk is giving what your audience is looking for

Training in Academia—and Industry
E. Pain
Physicist Sylvain Schwartz has won acclaim from both the private sector and the ivory tower

Held-Over Feature: Sustaining Forests in a Changing World
E. Pain
Science Careers reviews career opportunities in forest ecology.

SCIENCE PODCAST
www.sciencemag.org/about/podcast.dtl

Download the 20 June *Science* Podcast to hear about a molecular clutch on flagella, judging fuel efficiency, analyzing the recent China earthquake, and more

FREE PROTEIN LADDER SAMPLE
available with any purchase

NEW ENGLAND BIOLABS

The New Protein Ladder from New England Biolabs

ACHIEVE ACCURACY IN YOUR PROTEIN EXPRESSION ANALYSIS

Choose the new Protein Ladder from New England Biolabs and experience a more consistent banding pattern that is ideal for accurate size determination. A mixture of our recombinant, highly purified proteins, this ladder will resolve into 12 sharp, evenly spaced bands when analyzed by SDS-PAGE. Bring precision to your protein sample analysis with the new Protein Ladder from NEB.

Advantages:

- Suitable for analysis of a wide range of proteins
- Sharp, uniform bands in the range of 10 - 250 kDa
- Convenient band spacing for accurate molecular weight determination
- Easy-to-identify reference bands
- Value pricing

Ordering information:

Protein Ladder (10 - 250 kDa)	**P7703S**
Other Protein Markers Available from New England Biolabs	
Protein Marker, Broad Range (2 - 212 kDa)	**P7702S/L**
Prestained Protein Marker, Broad Range (7 - 175 kDa)	**P7708V/S/L**
ColorPlus Prestained Protein Marker, Broad Range (7 - 175 kDa)	**P7709V/S/L**

Receive a FREE PROTEIN LADDER SAMPLE with the purchase of any product by including P7703S with your order. Limit one sample per order. Valid in the U.S. Only. Offer expires July 31, 2008.

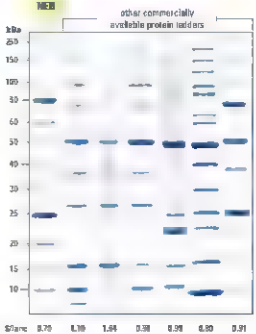

Compare the quality, consistency and value of the NEB Protein Ladder to other commercially available protein ladders. *Cost/Gene is based on current catalog price and manufacturer's recommendations for loading a mini-gel.*

For more information and our international distribution network, please visit: www.neb.com

New England Biolabs Inc. 240 County Road, Ipswich, MA 01938-2723, USA • Tel: (978) 927-5054 • Fax: (978) 921-1350 • info@neb.com
Canada • Tel: (800) 387-1095 • info@ca.neb.com • **China** • Tel: 0-800-8324318 • beijing@neb-china.com • **Germany** • Tel: 0800/746 5427 • info@de.neb.com
Japan • Tel: +81 (0)3 5669 6191 • info@nub-japan.com • **UK** • Tel: (0800) 318486 • info@uk.neb.com

NEW ENGLAND BioLabs Inc.
the leader in enzyme technology

CREDITS: TOP TO BOTTOM: MAX PLANCK INSTITUTE OF QUANTUM OPTICS/LABORATORY FOR ATTOSECOND AND HIGH-FIELD PHYSICS; NELSEN ET AL.

<< Toward Attosecond Technology

The interaction between intense light pulses and rare (noble) gas atoms results in the ionization of the atoms and the subsequent emission of shorter light pulses of much shorter wavelength, extending into the ultraviolet. Control over this process is necessary for the development of attosecond technology. Optimizing the interaction, Goulielmakis *et al.* (p. 1614) demonstrate the single-cycle ionization of neon atoms by an intense single-cycle infrared driving pulse and the concomitant generation of isolated, sub-100-attosecond pulses of extreme ultraviolet light. Such short pulses enter the atomic unit of time scales where electrons in atoms and electron-electron effects can start to be probed.

Enigmatic Chondrules

The conditions that formed the most abundant solids in the early solar system, known as chondrules, have been enigmatic. Chondrules record high-energy processes in the solar nebula and represent an important starting condition for understanding the subsequent evolution of the solar system, including the distribution of material and the formation of larger planetesimals. **Alexander *et al.*** (p. 1627, cover) show that the sodium concentration of chondrules is too high to be explained by current models, which invoke evaporation at modest to low particle densities. Instead, chondrules seem to have formed in locally dense regions of the nebula. While this suggestion accounts for the general chemistry of the chondrules, explaining the existence of such locally dense regions remains a challenge.

Motivation, Morals, and Behavior

The design of social programs often relies upon Adam Smith's "invisible hand" whereby individuals are assumed to choose their actions primarily on the basis of self-interest. Society may often therefore structure economic incentives that are likely to induce individuals to act in a fashion that benefits the social group as a whole. On the other hand, empirical observations and experimental investigations have demonstrated in individuals the existence of prosocial behaviors, such as altruism. **Bowles** (p. 1605) reviews these recent studies and describes how the failure to take these behaviors into account when designing incentives can lead to entirely unexpected and counterproductive outcomes.

Constant Constants?

Fundamental constants such as the speed of light, the gravitational constant, and the electron mass are thought to be both basic to a physical picture of the universe and unchanging over time and space. As measurements get more and more precise, the constancy of the constants can be checked. One approach involves ever more precise atomic clocks, but these are restricted to terrestrial laboratory measurements. What about the possibility of changes in physical constants at great distance or just after the Big Bang? **Murphy *et al.*** (p. 1611) use absorption of light by molecular clouds between our solar system and a distant quasar to establish a bound on the possible variation of the ratio of the proton mass to the electron mass.

A Greener Greenland

Melting of the Greenland ice sheet is expected to cause much of the rise in sea level that will occur as global climate continues to warm, although it still is not clear how much of the ice sheet will disappear as air temperatures rise. One way to infer how vulnerable the ice sheet is to temperature variations is to determine how it was affected by climate change in the past. **De Vernal and Hillaire-Marcel** (p. 1622, see the Perspective by **Steig and Wolfe**) constructed a pollen record for southern Greenland for the past million years, from a marine sediment core just off the coast. Large changes in ice extent and vegetation accompanied changes in temperature, illustrating the susceptibility of the ice sheet to climate change, and providing a guide as to what to expect with future warming.

Changes in Altitude

The rate at which the ice sheets in Greenland and the Antarctic change mass is determined by the difference between the rate of ice loss at the margins and ice gain in the center, both of which are largely uncertain. Mass gain in the interior of the Antarctic ice sheet has been particularly difficult to determine, because snow accumulation varies over multiple time scales, and the thickness of the firn (the porous, upper layer of the ice sheet formed by fallen snow and not yet fully transformed into ice) is difficult to document for large regions. **Nelsen *et al.*** (p. 1626, published online 29 May; see the Perspective by **Cuffey**) show that accumulation variability dictates changes in firn layer thickness, and thus mainly determines ice sheet elevation changes as observed by satellite radar altimetry.

Guts Galore

Spectacular numbers of microbes live in mammalian guts and lend their hosts important nutritional functions. **Ley *et al.*** (p. 1647, published

Continued on page 1561

Genome Sequencer FLX System

Longer sequencing reads mean more applications.

Sequencing-by-Synthesis: Using an enzymatically coupled reaction, light is generated when individual nucleotides are incorporated. Hundreds of thousands of individual DNA fragments are sequenced in parallel.

In 2005, the Genome Sequencer 20 System was launched
- Read length: 100 bases
- 20 million bases in less than 5 hours

In 2007, the Genome Sequencer FLX System was launched
- Read length: 250 to 300 bases
- 100 million bases in less than 8 hours

Available in 2008, the Genome Sequencer FLX with improved chemistries
- Read length: >400 bases
- 1 billion bases in less than 24 hours

More applications lead to more publications.

Proven performance with an expanding list of applications and more than 130 peer-reviewed publications.
Visit ***www.genome-sequencing.com*** to learn more.

454
SEQUENCING

For life science research only. Not for use in diagnostic procedures.

Roche Diagnostics GmbH
Roche Applied Science
68298 Mannheim, Germany

Roche

Continued from page 1559

online 22 May) have made a comparative metagenomic study of the fecal flora of human beings and 60 other mammal species, living in zoos and in the wild, to see how taxonomic position and diet affect the composition of the internal flora and to learn how these relationships have co-evolved. Although there is a general trend to herbivores harboring the most diverse communities and carnivores the least, overall the relationship between a flora and its host is specific: Baboons in the St. Louis Zoo have much the same gut flora as wild baboons in Namibia.

Phylogenetic Error Correction

Molecular sequence alignment methodology is a key tool for analyzing evolutionary relationships. However **Löytynoja and Goldman** (p. 1632) show that current methods are making systematic errors that bias results of evolutionary inferences, e.g., in comparative genomics. These errors are not corrected by sampling more sequence data—indeed, the error grows in response to denser sampling. These systematic errors can be avoided by performing multiple alignments for studies in phylogenetics and sequence evolution.

Clutching the Flagellum

The bacterial flagellum is one of a very few rotating motors in biology and has been extensively studied with respect to its assembly and function. A variety of transcription factors control flagellar gene expression and chemotaxis systems control the direction of flagellar rotation and cell behavior. **Blair *et al.*** (p. 1636, see the Perspective by **Berry and Armitage**) identify a novel functional component of the motor, a clutch that allows the cell to arrest flagellar rotation. This clutch protein appears to play a role in motility control and is co-regulated with biofilm formation, when bacteria will stop moving.

Glial Cell Tuning

Astrocytes are the major class of nonneuronal cells in the brain and account for close to half of the cells in the mammalian cerebral cortex, yet their function is virtually unknown. Evidence is now accumulating for an active role of astrocytes in brain function. **Schummers *et al.*** (p. 1638; see the Perspective **Wolf and Kirchhoff**) investigated astroglial calcium responses in the visual cortex of the ferret by two-photon laser-scanning microscopy. Visual cue–induced calcium signals were monitored in neurons and astrocytes simultaneously at high temporal and cellular resolution. The receptive field properties (response kinetics, orientation, and localization) of the astroglial network consistently followed neuronal activity. Simultaneous recordings of hemodynamic signals and calcium responses in neurons and astroglia revealed that astrocytes have a key role in coupling neuronal activity to vascular signals critical for noninvasive brain imaging.

Shorter Messages in Proliferating Cells

Sequences in the 3′ untranslated regions (UTRs) of messenger RNAs (mRNAs) control mRNA stability, translation, and subcellular localization. **Sandberg *et al.*** (p. 1643) analyzed changes in the expression of mRNA isoforms differing in their 3′UTRs in response to activation of T lymphocytes. Activated cells tend to express higher proportions of shorter 3′UTR isoforms, which lack regulatory sequences such as microRNA target sites that commonly inhibit protein expression. This shift toward expression of shorter 3′UTR isoforms occurs in activated immune cells in both human and mouse and correlates with cellular proliferation across many cell types and tissues.

Intracellular Subversion Strategy

A large number of putative bacterial proteins contain eukaryotic ankyrin repeat homology domains (ank). These same bacteria also possess potential type IV secretion systems, which can inject bacterial effector proteins into their eukaryotic host cell cytosol. It is thus possible that these ank-containing genes could encode such effector proteins. Now **Pan *et al.*** (p. 1651) show that ank-containing genes in both the facultative intracellular pathogen *Legionella pneumophila* and the obligate intracellular pathogen *Coxiella burnetii* encode proteins that are indeed translocated into host cells during infection by a process that requires the bacterial Dot/Icm type IV secretion system. One of the *L. pneumophila* ank-containing proteins, AnkX, prevented microtubule–dependent vesicle transport and helped internalize *L. pneumophila* to evade phagosome-lysosome fusion.

CREDITS: SCHUMMERS ET AL.

Call for Papers

Science Signaling

Now accepting original research submissions

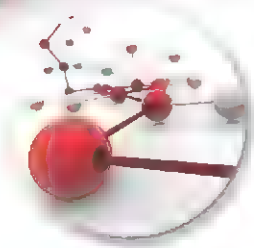

ISSN: 1937 9145

From the publishers of ***Science***, ***Science Signaling***, formerly known as ***Science***'s STKE, will add original research starting September 2008. Each week the journal will publish leading-edge findings in addition to the current features, including Perspectives, Reviews, Protocols, Meeting Reports, Book Reviews, Teaching Resources, and the Database of Cell Signaling.

Science Signaling showcases high-impact research in cellular regulation in such fields as molecular biology, development, immunology, neuroscience, microbiology, physiology and medicine, pharmacology, biochemistry, cell biology, bioinformatics, and systems biology. Submit your research that provides new concepts and new understanding of biological signal transduction for consideration.

Subscribing to ***Science Signaling*** ensures that you and your lab have the latest cell signaling resources. From basic science to design of therapeutics, from molecules to networks and systems design, read the best source – ***Science Signaling***.

Announcing Chief Scientific Editor for *Science Signaling* –

Michael B. Yaffe, M.D., Ph.D.
Associate Professor, Department of Biology
Massachusetts Institute of Technology

Submit your paper to:
stke.sciencemag.org/about/help/research.dtl

Science Signaling
AAAS

Garret A. FitzGerald is director of the Institute for Translational Medicine and Therapeutics at the University of Pennsylvania and serves on the Institute of Medicine Forum on Drug Discovery, Development, and Translation and on the Science Board of the FDA. E-mail: garret@spirit.gene.upenn.edu

Drugs, Industry, and Academia

This week, international academic and industry leaders, investors, and policy-makers participated in the Biotechnology Industry Organization's International Convention in San Diego, a reminder that prospects for new drugs seem bleak. Only 17 new molecular entities were approved by the U.S. Food and Drug Administration (FDA) in 2007, a fall from 53 in 1996. Coincident trends worsen the situation: a decline in prescription drug sales, the flight of investors, corporate layoffs, and pricing inequities in advanced economies that fuse with demands from poorer countries to gain cheap and immediate access to new drugs.

The paradox is that this comes as high-throughput screening, combinatorial chemistry, and rationalized drug design have revolutionized the discovery of new drugs and their targets. Ironically, just as the conventional business model appears fallible, academia has been lured by funding to re-engage in translational science (moving basic research findings into clinical application). However, academia lacks features intrinsic to drug discovery and development: incentives for "team science," relevant infrastructure, and the capacity for large-scale production. So, like star-crossed lovers, industry and academia face both challenge and opportunity. How might they reposition themselves to interact effectively and bring new drugs to the table?

Initiatives such as the Medicines for Malaria Venture and the TB Alliance exemplify shifting global alliances of academia and industry to collaborate on treating neglected diseases of the developing world, from drug discovery through development. Governments, the private sector, and philanthropies have responded altruistically to such enterprises. The keys have been focus, flexibility [such as with intellectual property (IP) rights], tight timelines, and sufficient resources. This model of cooperation might provide a blueprint for optimizing the interface between both sectors to speed drug development more generally.

The capacity of the academic sector for drug development is illustrated by its experience with vaccines and biologicals (such as inhibitors of inflammation). Moreover, discoveries of niche applications for compounds that have failed in their primary application by industry (such as compounds with a new use in reducing cholesterol) suggest that the revision of outmoded approaches to IP might enable such academia/industry interactions to expand further.

Academia and industry might explore models to interact that are unconstrained by IP. One example would be secure Internet chat rooms for industry chemists and academic biologists to become acquainted and hatch projects, whose specifics would only then determine the division of IP. Presently, IP agreements occur before an academic even identifies chemists in a company, let alone discusses science with them. Similarly, both sectors are investing independently in defining biological networks of genes and proteins for target selection and drug development. This effort might be more efficient as a precompetitive public/private partnership, leaving the subsequent selection of targets and the attendant chemistry to IP.

A major bottleneck in drug development is in human capital. Investigators who project their science across disciplines are fundamental to producing safe and efficacious drugs. Such integrated expertise is scarce. But recent initiatives, such as the Wellcome Trust's Training Program in Translational Medicine and Therapeutics, are providing trainee experience across sectors.

Regulatory agencies need to be empowered with funds for inspections that meet global standards and for harnessing academia to explore claims of drug efficacy and safety, independent of the sponsor but respectful of proprietary interest. Labeling might also be revised to indicate drugs that are truly innovative, because approval might be accelerated for drugs that are the first to safely address unmet clinical needs.

What if political pressures that threaten to drive down prescription drug costs also depress reimbursements for health care delivery, the lifeblood of science in many U.S. medical schools? Both industry and academia are poorly positioned to respond in the financial landscape. Such a scenario might occur rapidly, just like the rise in the price of oil, and alter both the livelihood of academic research and the industrial approach to drug development. But a crisis can present opportunities if both sectors strengthen their relationship. The time to revise the building code is not when the earthquake strikes.

– Garret A. FitzGerald

10.1126/science.1161006

PHYSICS

Rolling Out Single Photons

Carbon nanotubes (CNTs) have been studied exhaustively in terms of electronic and mechanical properties. A large repertoire of potential applications has been demonstrated for these one-dimensional systems of rolled-up sheets of carbon. To date, most of the optical studies on CNTs have focused more on characterization. Hogele *et al.* now show that CNTs exhibit quantum optical behavior. Photons, being bosons, like to bunch together. However, in quantum systems such as atoms and artificial atoms, the confinement of carriers can split the pack behavior, resulting in the photons being emitted one at a time. For applications such as quantum communication, such antibunching behavior is desirable. These authors excite a single CNT with a laser pulse and observe that light is emitted as single photons upon relaxation. The results suggest that CNTs may extend their repertoire beyond logic circuits and other electronic devices, finding application in quantum optoelectronics. — ISO

Phys. Rev. Lett. **100**, 217401 (2008)

BIOCHEMISTRY

Autoactivation Is the Key

Protein tyrosine kinases (PTKs) regulate cellular activities by transferring phosphate groups from ATP to other proteins. PTKs must first be activated by autophosphorylation of their own specific tyrosine residues. The structural basis for eukaryotic PTK activation involves displacement of an amino acid loop, which initially blocks access to the active site but shifts out of the way upon autophosphorylation. Much less is known about prokaryotic PTKs, which do not have significant sequence homology to eukaryotic PTKs.

Lee *et al.* have determined the crystal structure of a prokaryotic PTK domain from the *Escherichia coli* tyrosine kinase Etk, alone and with ADP bound. The side chain of tyrosine 574 (Y574), which must be autophosphorylated in order to activate Etk, is positioned facing ADP in the active site and blocks access by peptide substrates. Although Y574 is not part of a flexible loop, a phosphorylated Y574 side chain could rotate away from the active site into an alternate conformation that would be stabilized by a salt bridge to a nearby arginine and multiple hydrogen bonds to surrounding amino acids. The Etk structure therefore suggests a new mechanism of activation of PTKs, in which phosphorylation-triggered displacement of only a single amino acid side chain suffices to unlock the door to the active site. — NM*

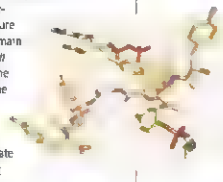

Arginine pulls the phosphotyrosine (lower right) away from the substrate binding site.

EMBO J. **27**, 10.1038/emboj.2008.97 (2008)

*Nilah Monnier is a summer intern in *Science*'s editorial department.

CELIA JESSEN

Spotting Hazards

Anal. Chem. **80**, 10.1021/ac8004428 (2008).

GENETICS

Genomes of a Feather

The zebra finch (*Taeniopygia guttata*) belongs to the most populous bird order (the perching birds or Passeriformes) and is having its genome sequenced. Stapley *et al.* have created a linkage map of the zebra finch and compared it to that of the distantly related chicken (Galliformes). There was extensive synteny, or conservation of genes on the same chromosomes, indicative of a low amount of interchromosomal rearrangement between bird orders. However, a number of intrachromosomal differences were found between the

CREDITS (TOP TO BOTTOM): KARSTEN SCHNEIDER/PHOTORESEARCHERS; *EE ET AL. EMBO J.* 27, 10.1038/EMBOJ.2008.97 (2008)

zebra finch, reed warbler (another Passerine), and chicken, especially on the five macrochromosomes, suggesting that gene order is not conserved even among close relatives. A comparison of recombination rates reveals that chickens have high rates relative to other birds whereas reed warblers experience less recombination. —MZ

Genetics **179**, 651 (2008).

NEUROSCIENCE

Multiple Choice Testing

When we make economic decisions, for example the purchase of a good or a service, our brain has to perform at least three computations. First, it has to assess the goal value of the good in economic terms, our maximal willingness to pay. Second, it has to assess the decision value of the good, the goal value minus the unavoidable costs. Third, there is a prediction error, which indicates the deviation from one's expectations of reward; the prediction error is positive when something better than expected happens and negative when the opposite occurs. Unfortunately, these three related quantities are intermingled and are often highly correlated, making it challenging to isolate the neural regions performing these computations.

Hare *et al.* have attempted to measure goal value, decision value, and prediction error in a single neuroimaging task so that they could dissociate these parameters. They found that ventral striatum activation reflected prediction error and not goal or decision value. However, activity in the medial orbitofrontal cortex and the central orbitofrontal cortex correlated with goal value and decision value, respectively. — PRS

J. Neurosci. **28**, 5623 (2008).

CHEMISTRY

A Question of Geometry

The varied metal clusters that proteins use to handle diatomic gases are remarkable not only for the unsurpassed chemistry they support but also for the fine tuning of the geometric properties of the metal atoms by their ligands. By synthesizing a series of dinuclear FeNi complexes, Ohki *et al.* demonstrate how the Ni can be switched between octahedral, square pyramidal, and square planar geometries. In the precursor compound, the Fe atom carries three CO ligands, there are three bridging thiolates, and the Ni adopts a slightly distorted square pyramidal structure. Adding a bidentate thioether–thiolate ligand onto the Ni atom resulted in the release of one of the bridging thiolates and a square planar configuration. In contrast, adding a phenolate–thioether ligand yielded an octahedral Ni that retained the three Ni–μ-S bonds, with Ni–O and Ni–S links to the bidentate ligand and a Ni–O bond to a molecule of solvent (methanol). The reversible loss of methanol was accompanied by ejection of one of the bridging thiolates and conversion into the square planar configuration. Integrating these findings with earlier work on the [NiFe] hydrogenase and other dinuclear complexes (NiRu and GeRu), these authors propose that the hydrogenase NiFe cluster binds H_2 by shifting the square pyramidal Ni into an octahedral configuration and that heterolysis of H_2 leads to loss of the bridging OH ligand as H_2O. — GJC

Proc. Natl. Acad. Sci. U.S.A. **105**, 7652 (2008).

CREDIT: JUPITERIMAGES

www.sciencemag.org

Science

1200 New York Avenue, NW
Washington, DC 20005
Editorial: 202-326-6550; FAX 202-289-7562
News: 202-326-6501; FAX 202-371-9227
Rittenham House, 82-88 Hills Road
Cambridge, UK CB2 1LQ
+44 (0) 1223 326500; FAX +44 (0) 1223 326501

SUBSCRIPTION SERVICES: For change of address, missing issues, new orders and renewals, and payment questions: 866-434-AAAS (2227) or 202-326-6417. FAX 202-842-1065. Mailing addresses: AAAS, PO Box 96178, Washington, DC 20090-6178 or AAAS Member Services, 1200 New York Avenue, NW, Washington, DC 20005

INSTITUTIONAL SITE LICENSES: please call 202-326-6755 for any questions or information

REPRINTS: Author inquiries 800-635-7181
Commercial inquiries 803-359-4578

PERMISSIONS: 202 326-7074, FAX 202-682-0816

MEMBER BENEFITS: AAAS/Barnes & Noble.com bookstore www.aaas.org/offer AAAS Online Store: http://membership.sciencemag.com/store/code/40CNL AAAS Travel: Betchart Expeditions 800-252-4910; Apple Store www.apple.com/education/aaas; Bank of America MasterCard: 1-800-833-6262 priority code FA8396; Cold Spring Harbor Laboratory Press Publications www.cshlpress.com/affiliates/aaas.htm. GEICO Auto Insurance www.geico.com/landingpage/si31.htm?logo=17624 Hertz 800-654-2200 CDP#343467. Offer Expires: http://hertz.com/clubpass. Quikbook 877-218-0686. Subaru: Symbol of the Future 800-424-9883. Subaru VIP Program 202-326-6417. VIP Moving Services http://www.vipmoyalflower.com/domestic/indexhtml. Other Benefits: AAAS Member Services 202-326-6417 or www.aaas.org/member.org.

Science: letters@aaas.org (for general letters of interest)
science_letters@aaas.org (for queries about letters)
science_reviews@aaas.org (for returning manuscript reviews)
science_bookrev@aaas.org (for book review queries)

Published by the American Association for the Advancement of Science (AAAS) which serves its readers as a forum for the consideration and discussion of important issues related to the advancement of science, including the presentation of minority or conflicting points of view, rather than by publishing only material on which a consensus has been reached. Accordingly, all articles published in Science—including editorials, news and comment, and book reviews—are signed and reflect the individual views of the authors and not official points of view adopted by AAAS or the institutions with which the authors are affiliated.

AAAS was founded in 1848 and incorporated in 1874. Its mission is to advance science, engineering, and innovation throughout the world for the benefit of all people. The goals of the association are to enhance communication among scientists, engineers, and the public; promote and defend the integrity of science and its use; strengthen support for the science and technology enterprise; provide a voice for science on national issues; promote the responsible use of science in public policy; strengthen and diversify the science and technology workforce; foster education in science and technology for everyone; increase public engagement with science and technology; and advance international cooperation in science.

INFORMATION FOR AUTHORS
See pages 634 and 635 of the 1 February 2008 issue or access www.sciencemag.org/about/authors

Unlock the Power of Gene Expression Analysis

coming soon

The 7900HT Fast Real-Time PCR with TaqMan Arrays are the right combination for high-throughput gene expression analysis

- Fast 384-well Real-Time PCR System
- Gold standard performance from [illegible]
- Customizable plate formats: 96-well, 384-well
- Process [illegible] samples in as little as 24 hours
- [illegible]

- [illegible]
- Proven quality, speed, [illegible]
- [illegible] TaqMan [illegible]
- [illegible]
- [illegible] and pathways
- Increased sensitivity and precision

Unlock the right combination. Learn more at www.7900HT.com

Applied Biosystems

A Fiery, Dark Day

To poet John Greenleaf Whittier, it was "A horror of great darkness" when "Men prayed, and women wept." By noon of 19 May 1780, the pall cast over coastal New England was so deep that citizens of Portland, Boston, and Providence had to eat their midday meals by candlelight. Many thought the Day of Judgment was at hand.

After the darkness lifted the next day, all manner of explanations came forth, including volcanic outpourings and celestial machinations. Now, researchers say they have traced the source of the darkness to forest fires 600 kilometers to the northwest.

Erin McMurry of the University of Missouri, Columbia, and colleagues base their conclusion on tree ring records from fire-damaged trees around North America. In the *International Journal of Wildland Fire*, the researchers report that 1780 was a big year for forest fires in eastern North America, due in part to drought around the Great Lakes. New England's noontime darkness, they found, most likely resulted from the smoke of fires that spanned at least 2000 square kilometers in southern Ontario. At one Ontario burn site, fire swept in just after distinctive wood tissue began forming early in the growing season, consistent with the timing of the darkness.

The forest-fire hypothesis "is plausible," says Stephen Pyne of Arizona State University in Tempe, author of *Fire in America*. Proving it, however, would require better records of weather and winds on that day, he says—points on which the tree rings are silent.

Rating Big Pharma

This week, the Access to Medicine Foundation, a charity based in the Netherlands, issued its first ranking of 20 pharmaceutical companies' efforts to make key medicines available to the world's poor. The Access to Medicine Index, designed to help investors put their money into companies that are good global citizens, is based on eight criteria, including investment in R&D "that reflects both the global disease burden and neglected diseases," patenting practices, and commitment to equitable pricing. Top laurels went to GlaxoSmithKline, in part for its recent licensing agreement with a Canadian generics company to manufacture two of its patented antiretroviral drugs for distribution in Rwanda.

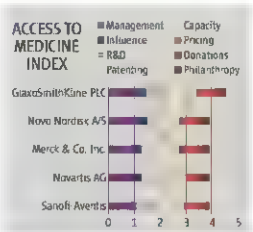

Face Genes

Genetic anthropologist Talal Mohammad based his Ph.D. thesis on tracing the ancestry of Bedouin tribes in the Gulf states, including his native Kuwait. Now he's embarked on a more unusual project: identifying genes that determine facial features in hopes of illuminating how individual differences evolved.

With start-up funds of $70,000 from International Financial Advisors in Kuwait, Mohammad and colleagues at the University of Cambridge in the U.K. plan to begin next fall by getting cheek swabs from about 500 Kuwaitis. Collaborators at the University of Toronto will fly to Kuwait to do computed tomography scans of their heads. Mohammad says that the team will categorize faces by a list of "landmarks," which will be compared with up to a million DNA markers. Height, pigmentation, and facial expressions will also be measured. One goal is to test the theory that all humans originated in Africa by comparing modern skulls with ancient ones from the Middle East and Africa.

Mohammad says Kuwait's homogeneous population should help researchers pinpoint genetic links. He plans to expand the project to other Gulf states, starting with Iran, and ultimately would like to cover the whole world.

Evolutionary geneticist Chris Tyler-Smith of Cambridge's Sanger Institute (who is not involved in the project) says Mohammad's study marks a departure from past ones that focused solely on the genetics of abnormal features such as those in Down syndrome. "It's a very interesting biological question," he says. "Why do we all look different, and how are these differences genetically determined?"

CREDITS: PEP TO BOYTSOVA, COURTESY OF ACCESS TO MEDICINE INDEX; MARK DAFFEY/LONELY PLANET IMAGES

The Perfect Crime Gets Harder

Criminals beware: A scientist at the University of Leicester, U.K., has come up with a way of revealing latent fingerprints on metallic objects such as bullet cartridges and guns.

Physicist John Bond built on a 2001 discovery that salts from skin can corrode hot metal surfaces, producing an imprint that persists even after the metal is cleaned. Various research groups are exploring ways to reveal these hidden prints, such as heating the metals to spur chemical reactions with the salts.

In July's *Journal of Forensic Sciences*, Bond describes a way to detect fingerprints on brass and copper at room temperature. After dusting an object such as a bullet with a black conducting powder, he applies an electric potential that increases the resistivity of the metal at the site of a finger's contact, thus bringing out the image. "Potentially, this will make it possible to reopen old cold cases," says Bond, who is collaborating with the local police.

Chemist Neil McMurray of Swansea University in Wales likes the idea but notes that Bond's method won't work if previous examinations of a bullet or gun have disturbed the fingerprints. And, he says, looking for DNA can involve liquid treatments that "will move the salt around."

DID YOU FIND IT?

A poster was included in the May 23 issue of *Science* mailed to subscribers who work in a selection of fields relevant to viral gene delivery. This special educational poster was created to enhance the understanding of those technologies available to scientists using, or considering using, virally based gene delivery techniques.

If you didn't receive the insert—or you read a communal copy of the journal and someone got to it first –you can sign up at www.stratagene.com/viralposter to obtain your own personal copy of the poster by mail.

The poster is also available as a downloadable PDF on the *Science* magazine website. Just go to: www.sciencemag.org/products

Science

AAAS

This poster is brought to you by the *Science*/AAAS Business Office and is sponsored by Stratagene, an Agilent Technologies company

'Tis the Season to Be Honored

Just as spring heralds a slew of entertainment awards, summer seems to be the season for scientists. A number of prestigious prizes for career achievements have been announced in the past few weeks. Here is a sampling, recognizing researchers in fields from astronomy to pediatric surgery.

DUTCH NOBELS

Research in brain abnormalities, magnetism, cheese, and Irish culture have garnered four scientists the Spinoza Prize, the Netherlands' biggest scientific honor. Each awardee will receive €1.5 million from the Netherlands Organisation for Scientific Research for their research.

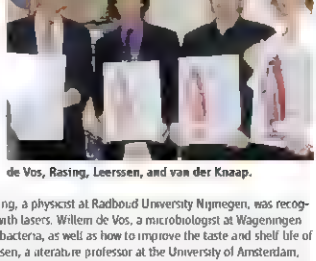

de Vos, Rasing, Leerssen, and van der Knaap.

Marjo van der Knaap, a child neurologist at VU University Amsterdam, was selected for identifying new diseases affecting the nerve fibers of brain cells and improving their diagnosis. Theo Rasing, a physicist at Radboud University Nijmegen, was recognized for manipulating magnetism with lasers. Willem de Vos, a microbiologist at Wageningen University, has worked on intestinal bacteria, as well as how to improve the taste and shelf life of cheese. Also honored was Joep Leerssen, a literature professor at the University of Amsterdam, for studies of Irish cultural history and how stereotypes are formed. The awards will be presented by Dutch Education Minister Ronald Plasterk in November.

CREDITS (TOP TO BOTTOM): CHRIBER PRIZE FOUNDATION; RIVOLIER/HOPE FILM; THE ASAHI GLASS FOUNDATION; BEN CARSON SR.

BLUE PLANET PRIZE

Two scientists have been honored for lifetime contributions to addressing global environmental problems. Claude Lorius (left), director emeritus of research at CNRS, the French national research agency, headquartered in Paris, and José Goldemberg of the University of São Paulo in Brazil are this year's recipients of the Blue Planet Prize.

Lorius is being recognized for work dating from the 1950s on ancient levels of atmospheric carbon dioxide. The results, obtained from Antarctic ice cores, helped to bolster the case for human-induced global warming in modern times. Goldemberg helped launch Brazil's bioethanol program in the 1970s and pioneered the concept of "technological leapfrogging," in which developing countries adopt renewable energy technologies. He was environment minister when Brazil hosted the 1992 Earth Summit. The Blue Planet Prize is funded by the Asahi Glass Foundation in Tokyo. Each scientist will receive $463,000.

MEDAL OF FREEDOM

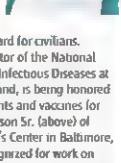

An AIDS expert, a pediatric neurosurgeon, and a former top U.S. health official are among six Americans selected last week to receive the Presidential Medal of Freedom, the nation's highest award for civilians.

Anthony Fauci, director of the National Institute of Allergy and Infectious Diseases at NIH in Bethesda, Maryland, is being honored for research on treatments and vaccines for HIV/AIDS. Benjamin Carson Sr. (above) of Johns Hopkins Children's Center in Baltimore, Maryland, is being recognized for work on neurological disorders and creating scholarships for deserving high school graduates. Donna Shalala, president of the University of Miami, Florida, and secretary of Health and Human Services under President Bill Clinton, is being lauded for efforts to improve health care and education.

GRUBER PRIZE

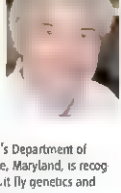

Allan Spradling has won this year's Gruber Genetics Prize from the Peter and Patricia Gruber Foundation based in St. Thomas, U.S. Virgin Islands. Spradling, who directs the Carnegie Institution's Department of Embryology in Baltimore, Maryland, is recognized for his work on fruit fly genetics and developmental biology.

Spradling pioneered methods to insert DNA into the *Drosophila melanogaster* genome, helping to make it a premier model organism for studying how genes control development. In their work on the fruit fly ovary, he and his colleagues were the first to describe a stem cell niche, the group of cells that surround stem cells and help guide their behavior. Spradling will receive $500,000 and a gold medal at the International Congress of Genetics next month in Berlin, Germany.

ASIAN NOBELS

The 2008 Shaw Prizes have been awarded to six researchers in astronomy, life science and medicine, and mathematical sciences. The prize, which carries a $1 million award, was begun in 2004 by Hong Kong movie and TV entrepreneur Run Run Shaw.

Reinhard Genzel, managing director of the Max Planck Institute for Extraterrestrial Physics in Garching, Germany, won the astronomy award for work demonstrating that the Milky Way has a supermassive black hole at its center. Ian Wilmut of the University of Edinburgh, U.K., and Keith Campbell of the University of Nottingham, U.K., will split half of the life science and medicine prize, with the other half going to Shinya Yamanaka of Kyoto University in Japan. The award recognizes their work on reversing the process of cell differentiation in mammals. Ludwig Faddeev of the Petersburg Department of Steklov Institute of Mathematics in St. Petersburg, Russia, and Vladimir Arnold of the Steklov Mathematical Institute in Moscow will share the mathematical sciences award for their contributions to mathematical physics.

Got a tip for this page? E-mail, people@aaas.org

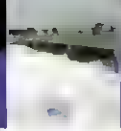

Energy from tides 1574

Promoting Australian science 1576

SCIENCE EDUCATION

Louisiana Opens School Door For Opponents of Evolution

Louisiana school teachers have been given license to supplement the existing science curricula with material that they feel "promotes critical thinking skills." The seemingly innocuous language, in a bill passed overwhelmingly by the state legislature and expected to become law as early as next week, marks the latest attack in the United States on the teaching of evolution and mainstream scientific thought on global warming and other topics.

"The only thing this bill does is give a green light for the school board to protect teachers who want to use creationist supplementary materials," says Barbara Forrest, a philosopher at Southeastern Louisiana University in Hammond who has been fighting the legislation.

Under the banner of "academic freedom," opponents of evolution have made some headway in Florida and have attracted support in Michigan and South Carolina (*Science*, 9 May, p. 731). But their greatest success has come in Louisiana, where state legislators have invited educators to hold "an open and objective discussion of scientific theories being studied, including but not limited to evolution, the origins of life, global warming, and human cloning."

The approach appeals to Louisiana's Republican Governor Bobby Jindal, who is expected to sign the bill. "Some want only to teach intelligent design. Some only want to teach evolution. I think both views are wrong," he told a television interviewer last weekend. "As a parent, I want [children] to be presented with the best thinking. I don't want any facts or theories or explanations to be withheld from them because of political correctness. The way we are going to have smart and intelligent kids is exposing them to the very best science."

Science educators say the new wording is intended simply to circumvent rulings by U.S. courts that creationism and intelligent design are unconstitutional religious intrusions into a public school science curriculum. It's also unnecessary, adds Brenda Nixon of Louisiana State University in Baton Rouge, who co-directs a statewide effort to improve science and math education and also works with the Louisiana Science Teachers Association, because teachers already explore these topics in class. Teachers are required to follow the Louisiana Comprehensive Curriculum, which encourages teachers to keep up to date and allows them to incorporate outside materials as long as the content is consistent with the state framework. "We have had overwhelming support from our science teacher members, who don't want to see this approved," Nixon says about the association's 1600 members.

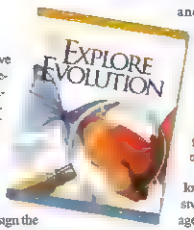

Politics, science? This 2007 book takes a view in sync with supporters of the Louisiana legislation.

The bill requires the Louisiana board of education to implement the language in time for the 2008–09 academic year. But Forrest and others worry that it will be very difficult for any government body to make sure that the supplementary materials meet agreed upon standards. **–FAYANA RICHARDS**

BIOBANKS

Canada Launches Massive Study of Adult Cancer Precursors

TORONTO, CANADA—Canada has joined the global stampede of countries gathering biological data over decades on a large population cohort in hopes of better understanding the genetic, social, and environmental factors that affect human health.

The Canadian Partnership for Tomorrow Project, launched last week, will follow 300,000 adults over the age of 35 for 30 years, gathering saliva, blood, urine, fecal, and toenail samples as well as answers to questions about the health effects of influences including diet, physical fitness, and environmental conditions. The goal is "a comprehensive data set for research into the causes of cancer," says Heather Bryant, vice president of cancer control for the Canadian Partnership Against Cancer in Toronto, a federally funded organization helping to lead the study. But she says the project will also "provide a platform for numerous other research topics."

The project builds on a cancer-risk study in Alberta that examined the interaction of lifestyle, behavioral, environmental, and genetic factors. Five provincial public health agencies have kicked in an initial $82 million to recruit participants in what is expected to be a $3.5-million-a-year effort. Researchers have already obtained funding to probe the effects of vitamin D in northern climes, measure compliance with public health recommendations for physical activity, and chart the effects of dietary supplements as varied as alcohol, vitamins, and traditional native diets, notes Phillip Branton, head of the Canadian Institutes of Health Research's Institute of Cancer Research, who will oversee research.

The Canadian study is intended to dovetail with the efforts of more than a dozen biobank studies around the world, says Branton. "One of the biggest questions to be tackled is, 'Who are the people first at risk for cancer as diets and lifestyles rapidly change in different societies?'" Epidemiologist Michael Thun, who is recruiting 500,000 participants for a biobank to be managed by the American Cancer Society in Atlanta, Georgia, says the Canadian study will add "useful further capacity. The

CREDIT: DISCOVERY INSTITUTE

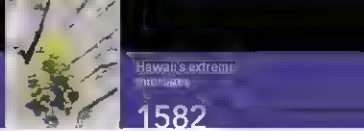

BIODEFENSE

Senate Bill Would Alter Biosafety, Select Agent Rules

As U.S. biodefense research has expanded since 2001, so has scientists' frustration with the red tape involved in studying potential bioweapons. Last week, a bipartisan pair of U.S. senators introduced a bill that would address some of these problems as well as safety concerns at the nation's biodefense labs. Some researchers hope the legislation will trigger a broader debate on finding better ways for science and security to coexist.

The Select Agent Program and Biosafety Improvement Act of 2008 would reauthorize an arrangement under which 325 research organizations and nearly 10,000 individuals have been approved by the Centers for Disease Control and Prevention since 2002 to work with anthrax and botulinum toxin and other so-called select agents. The bill (S. 3127), introduced by senators Richard Burr (R-NC) and Edward Kennedy (D-MA), calls for "minimum standards" for biosafety and biosecurity training, a voluntary, anonymous accident reporting system, and inclusion of newly created organisms. It would also have the National Academies study whether the select agent program has hindered research, including international collaborations.

Microbiologists say strict rules for shipping samples have stymied investigations of outbreaks abroad, and a requirement that collaborators abroad follow U.S. rules has made some joint research projects impossible. "The Select Agent Program is an important part of ensuring the nation's safety and security," Burr said in a press release, "and I look forward to working with my colleagues to reauthorize and improve the program."

Stanford University microbiologist David Relman, a member of the National Science Advisory Board for Biosecurity (NSABB), says he hopes the provision to update the existing list of select agents will "open up a larger discussion about how we prioritize concerns." He worries that a definition based on nomenclature is not specific enough and may be hindering research. The bill also asks the U.S. Attorney General to clarify language adopted in 2004 that would ban work on poxviruses genetically similar to smallpox but fairly benign (*Science*, 11 March 2005, p. 1540). NSABB, which offers advice on the oversight of research that could be potentially useful to terrorists, advised that the language should be repealed.

The senators also want to address biosafety concerns—including the fear that many accidents aren't reported (*Science*, 12 October 2007, p. 182). The bill calls for a system, similar to what's used by the aviation industry, that would allow researchers to learn from one another's mistakes.

"It's very exciting. It has a lot of things that I completely agree with," says Gigi Kwik Gronvall of the University of Pittsburgh Center for Biosecurity in Baltimore, Maryland, who's also encouraged that the bill asks for an assessment of whether the many new labs are needed. But Janet Shoemaker, public affairs director of the American Society for Microbiology, says the bill, although worthy, "needs further refinement." She suggests deferring action on any reporting system until after an interagency task force examining biosafety submits its report later this year.

With little time left on the legislative calendar and Kennedy recovering from brain surgery, prospects for the bill appear dim this year. But Senate staffers hope that its introduction will stimulate interest in the House and lay the groundwork for passage in the next Congress.

–JOCELYN KAISER

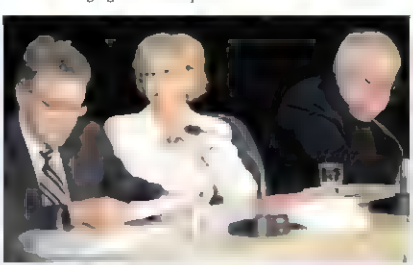

The .org view. Canadian cancer scientists Jeffrey Lozon (*left*) and Phil Branton flank study participant Mary O'Nei

CREDIT: COURTESY OF THE CANADIAN PARTNERSHIP AGAINST CANCER

more communication there is among early stage cohorts, the more that can be gained."

Co-principal investigator Louise Fortier, who directs an international biobank consortium centered at Montreal's CARTaGENE biobank with information on 20,000 Quebec participants, predicts that "environmental measures are likely to become an important and novel focus" as the new study progresses. "We will have samples as well as really good information on the subjects' homes and environments," she explains.

That says the decentralization of private and public health records in the United States makes it difficult to collect and manage such data from larger populations. He hopes that the Canadian study can take advantage of centralized public health systems in each province that are capable of collecting and managing a wide array of data from large populations.

The Canadian study is enrolling adults from five provinces from eastern, central, and western Canada. Instead of canvassing for volunteers, researchers will seek a cross section of "ordinary Canadians," says Bryan, perhaps by calling a randomized list of telephone numbers. She believes that such a pool will be of greater value to other researchers. "If you don't build the platform," she says, "you can't ask the questions."

–PAUL WEBSTER

Paul Webster is a freelance writer in Toronto, Canada.

RENEWABLE ENERGY

U.K. Ponders World's Biggest Tidal Power Scheme

Harnessing nature's energy to produce up to 5% of the United Kingdom's electricity without any carbon emissions sounds too good to be true. It is, according to a report last week from 10 environmental groups opposing plans to build the world's largest tidal power scheme.

Britain is under pressure to combat climate change with more renewable energy. According to the European Union's (E.U.'s) common energy policy, 15% of the U.K.'s total energy consumption should come from renewables by 2020. Wind turbines and other renewables now provide less than 5% of U.K. electricity. As a result, the government is reviving mothballed plans for a dam, or barrage, across the Severn estuary, which separates southwest England from south Wales.

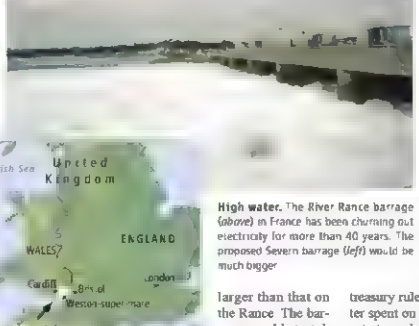

High water. The River Rance barrage (*above*) in France has been churning out electricity for more than 40 years. The proposed Severn barrage (*left*) would be much bigger.

But wildlife and environmental groups, including the Royal Society for the Protection of Birds (RSPB), the Worldwide Fund for Nature, and The National Trust, who argue that it will damage a unique ecosystem, now also assert that it will cost too much. "The report shows that this exorbitantly expensive and massively damaging proposal cannot be justified on economic grounds—there are simply too many cheaper options for clean energy generation," says RSPB Chief Graham Wynne.

Positioned across an estuary or inlet, a tidal barrage is essentially the same as a hydroelectric dam, but the rise and fall of the tides drives water through its turbines. The first such barrage began operating on France's River Rance in 1966. Because of high construction costs and fears of ecological damage, there have been only two, smaller imitators, in Canada and Russia.

The River Severn has the second highest tidal range in the world—15 meters between high and low tide. The first of many plans for a tidal power scheme there dates from 1925, but none has left the drawing board. The $29 billion scheme now being considered by the U.K. government is an order of magnitude larger than that on the Rance. The barrage would stretch 16 kilometers from Weston-super-Mare in Somerset to Cardiff in south Wales and would generate 17 terawatt-hours of energy per year, equivalent to the output of two 1 gigawatt power stations. A tidal barrage has lower operating costs than a nuclear station and would last up to three times longer, as long as 120 years.

The Severn barrage would have locks to accommodate ships and perhaps a road or rail link along its top. Proponents say that the water behind it would be safe for shipping and watersports and would reduce the threat of floods.

Then there are the drawbacks. Apart from cost, the barrage will irrevocably change the ecosystem of the enclosed estuary. The groups that sponsored last week's report say that it would threaten 35,000 hectares of protected wetlands, home to 68,000 birds in winter and more in summer. The barrage will also disrupt the migration of salmon, shads, lampreys, and sea trout to their spawning grounds. "The estuary is truly exceptional for its ecological value," says Wynne.

In 2007, the government funded Sustainable Development Commission (SDC) issued a report supporting a Severn barrage, as long as it does not contravene E.U. environmental directives. The directives allow for schemes that alter habitats if there is overwhelming public benefit—such as combating climate change—and if compensatory habitats are provided, either by restoring damaged habitats or creating new habitats somewhere else. SDC also recommended that the project should be government funded and owned to avoid higher commercial interest rates. In January, the U.K. government launched a 2-year feasibility study into the barrage.

Last week's report, drawn up by the consultancy group Frontier Economics, argues that there is no compelling reason for the government to bankroll a project that the private sector could do equally well. Doing so, it adds, may actually contravene U.K. treasury rules. Public money would be better spent on other types of renewable project, it concludes.

Researchers are divided over both the economic and the environmental arguments. "I'd rather see more distributed, smaller [schemes] built sooner," says ecologist Peter Randerson of Cardiff University in the U.K., who believes a barrage would take 20 years to build. Hydraulic engineer Richard Burrows of the University of Liverpool in the U.K. notes that E.U. targets have Britain getting 60% of its energy from renewables by 2050 and that small-scale schemes will never reach such a target. "You have to capture a larger part of the tidal power out there," he says.

The barrage's environmental impact is also debatable. "There will be environmental modification but not necessarily degradation," says Burrows. "You could argue that there will be a richer ecological state inside the impounded reservoir." Oceanographer Robert Kirby, who has studied the estuary for 40 years, predicts that the barrage will be good for the estuary, slowing the fast tides that stir up sediments and blocking sunlight from the water.

Randerson says that this is a "tantalizing argument" but that as yet there have been "no serious studies" of the idea. In any case, he expects the decision to be made on political rather than scientific grounds. "It's very attractive for politicians to have a big, megabucks, grandiose scheme to hang their credentials on," he says. "It's inevitable for all the wrong reasons."

–DANIEL CLERY

CREDIT: ATTAR MAHER/CORBIS SYGMA

Heinz Center Wants Feds to Build Ecosystem Indicator Partnership

WASHINGTON, D.C.—The nonpartisan Heinz Center this week issued a comprehensive update on the health of U.S. ecosystems—along with a plea for the U.S. government to coordinate and fund future assessments.

The 368-page report, titled *The State of the Nation's Ecosystems 2008*, summarizes 108 environmental indicators, some new and many improved, on the state of farmland, forests, and four other major ecosystems. "We've proved that it is possible to have credible improvements and refinements" of the indicators, says Robin O'Malley, who heads the center's Environmental Reporting Program. And now the center is ready to turn over the reins to the U.S. government. A companion policy document, released along with the updated report here on 17 June, lays out the center's vision for a congressionally chartered future.

Following the suggestion of the Clinton Administration's Office of Science and Technology Policy, the Heinz Center took on the challenge of designing a U.S. system of environmental indicators in 1997. It convened more than 150 representatives from environmental groups, industry, academia, and government agencies, who eventually agreed on 103 indicators. But 44% of the indicators contained in the 2002 report were essentially left blank because of insufficient data (*Science*, 27 September 2002, p. 2191).

The updated report contains new data for 68 indicators, 41 of those now have multi-year trends, a 32% increase from the first iteration. But significant holes remain. For 40 indicators, as opposed to 45 in the earlier report, no adequate data exist.

The group also redesigned or refined 56 indicators and added six more in areas that had been underemphasized. One new national indicator is change to stream flows, which O'Malley says is already revealing the impact of climate change. Carbon storage is another new indicator. Although nationwide estimates aren't yet possible for most ecosystems, the report finds that carbon storage in agricultural soils increased by 11 million tons a year from 1995 to 2005, perhaps due to no-till management that lessens soil erosion. Tracking such changes could help policymakers decide which practices are worth encouraging to reduce atmospheric carbon dioxide levels, O'Malley notes.

The Heinz Center, which has spent $9.2 million on the project, hopes the U.S. Congress will create a new public-private partnership to take over the process and create a system of national indicators. Meanwhile, the White House this week announced a federal pilot project to create national indicators of water quantity and quality. William Clark of Harvard University, who chaired the design committee of the Heinz report, says the key steps are to sell the next Administration on the concept and persuade Congress to fund it.

–ERIK STOKSTAD

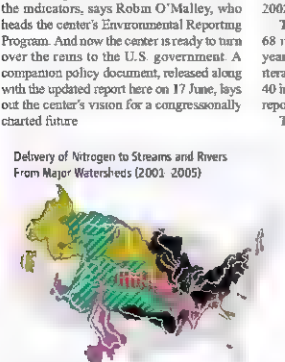

DATA SOURCE: U.S. GEOLOGICAL SURVEY'S MASSACHUSETTS AND FEDERAL-STATE COOPERATIVE PROGRAM

New trend? Nitrate runoff is most severe in the Mississippi River watershed (map, *above*), but the amount flowing from the Mississippi River into the Gulf of Mexico may have begun a downward trend since the 2002 report.

SCIENCESCOPE

A Bio Billion for Massachusetts

Massachusetts Governor Deval Patrick this week signed into law a plan to dole out $1 billion over 10 years to help the state's biotech industry. Proposed a year ago, the legislation includes $250 million in grants, $250 million in tax incentives for biotech companies, and another $500 million for new facilities with n the state university system. The presidents of Harvard University, the Massachusetts Institute of Technology, and the University of Massachusetts have criticized earmarks inserted by lawmakers that would funnel some of that money to nonscience projects that include a highway interchange and a sewage-treatment plant. California, Texas, and North Carolina have approved similar legislation to bolster life sciences and health research. –ANDREW LAWLER

Quake Shakes Panda Breeders

CHENGDU—Chinese scientists are surveying the Sichuan highlands to see how badly the 12 May Wenchuan earthquake disturbed the country's charismatic giant pandas. But it's clear that the panda breeding facilities face a long recovery. Five staff members at the panda research center in Wolong Nature Reserve near the epicenter died in the quake, and landslides destroyed much of the compound. Last week, the reserve announced plans to rebuild its center from scratch.

Meanwhile, the Chengdu Research Base of Giant Panda Breeding has suffered collateral damage. The center, which cares for 48 of the world's 239 captive pandas, has delayed an expansion to be funded largely by gate receipts after tourism in the usually busy spring season dropped 90%. The expansion is aimed at relieving overcrowding and boosting the captive population to allow more reintroductions into the wild. –RICHARD STONE

Chinese Postal Ban Pinches Labs

BEIJING—Chinese researchers may be forced to curtail some experiments because of a 5-month ban on transporting hazardous substances that took effect last month in anticipation of the Olympic Games in August and the Paralympic Games in September. The Chinese postal service has stopped accepting parcels containing any liquids, gels, powders, or "chemical products." Labs countrywide scrambled to stock up on reagents and solvents such as ethanol, says He Shigang, a neuroscientist at the Institute of Biophysics in Beijing. But those stockpiles are likely to run out long before the ban is lifted in October. "We might as well take the summer off," says He. –HAO XIN

AUSTRALIA

Science Minister Drives Push to Strengthen Innovation

Kim Carr readily admits that he's not a scientist and that he has never run a company. But as Australia's minister of innovation, industry, science, and research for the Labor government that took office in November, Carr is convinced that he's the right man to foster collaboration between university researchers and industry. This is one of the key planks in Prime Minister Kevin Rudd's attempt to put the country's science and technology base to better use in growing the economy. "I don't have to be an expert in scientific research, I have to be an expert in public policy," explains Carr, a 52-year-old senator from Victoria with strong ties to the Socialist wing of his party.

Carr was a history teacher at a technical school. "The only science I took was political science," he cracks—and a union strategist before entering politics in 1993. His portfolio includes Australia's research councils and the Commonwealth Scientific and Industrial Research Organisation (CSIRO), the country's largest scientific and industrial research agency, giving him a foot in both industry and higher education camps. He's been busy on both fronts.

On 6 June, he and Education Minister Julie Gillard jointly laid out the rules for grants from the $11 billion Education Investment Fund to help rebuild the country's academic-research infrastructure. The program was created in the waning days of the previous government, and Rudd has expanded it beyond universities to include technical and vocational schools. But his government's first budget (*Science*, 23 May, p. 998), which featured a near doubling of that fund, also contained a $60 million cut to the $1 billion CSIRO as part of a 2% belt-tightening across all agencies. Already unhappy over what they see as the government's disregard for the basic research they conduct for industry, CSIRO scientists staged a 1-day protest last week over delays in contract negotiations. Next month, a blue-ribbon commission reviewing the nation's innovation system—all government policies affecting science and technology—is due to submit its report, a document that is expected to have a major impact on future budgets.

Carr is a cheerleader for the country's manufacturing sector, and last week he went to Japan with his boss to trumpet a $35 million grant to Toyota, from a new $500 million green car fund, to help the company build a hybrid Camry in Melbourne. "It drives innovation across the economy," Carr says of the auto industry. "That's why I'm interested in it."

However, the government's wooing of automakers runs counter to the recommendations of the independent, influential Productivity Commission, which takes a dim view of industrial subsidies. And some scientists see other motives. "He comes from a labor background that would make him a bit dogmatic on the issue of protecting jobs, and the subsidy to Toyota is possibly symptomatic," says Kurt Lambeck, a geophysicist at Australian National University in Canberra and president of the Australian Academy of Science.

At the same time, Lambeck says that Carr, who held the same portfolio in Labor's shadow Cabinet, is passionate about innovation. "He recognizes that science and technology are important, and he's certainly seeking input from the community. But it's too soon to tell if he's listening."

Carr is currently visiting the United States to drum up support for all manner of industrial collaborations. He's also promoting Australia's bid to host the Square Kilometre Array (SKA), a proposed $2 billion radio telescope with a 50-fold increase in sensitivity that will allow scientists to "see" back to the very young universe (*Science*, 18 August 2006, p. 910). *Science* caught up with him during a daylong visit to Washington, D.C., that was sandwiched between stops in Detroit, Michigan. –JEFFREY MERVIS

Capital visitor. Australia's Kim Carr told a Washington, D.C., audience that improving innovation "is an endurance event, not a sprint."

CREDIT: COURTESY OF THE EMBASSY OF AUSTRALIA, WASHINGTON, D.C.

On the innovation review:

K.C.: There are a whole range of approaches, which boil down to one simple proposition. And that's talking to people. We have received more than 700 submissions. [The commission] has also undertaken considerable research on the nation's innovation system and the gaps in it.

On university-industry ties:

K.C.: There is the expectation among universities that business is there to be plundered, that is, that industry will fund whatever we say. And there is the view in some sectors of business that universities are there simply to do the research that companies won't do themselves and that scientists should be at the direction of the private firm. Well, none of those things are right. But there is a need to find projects that people see the value of working together on.

In Australia, the historical pattern is such that business will simply not be spending a lot of money on basic research. We [also] don't have the same strength of philanthropy that you do in the States.

On the infrastructure fund:

K.C.: There's an infinite level of demand and a finite level of resources. But the current arrangement shouldn't be seen as the end of the story. There will be additional funding made available in future budgets. . . . We are also looking at [ways] to get universities to take more responsibility for what they do with the money they receive from the government.

On the value of SKA:

K.C.: We are using technologies developed in conjunction with the SKA for monitoring baggage in airports, testing engines, diagnosis and treatment of cancer, tracking of icebergs, identification of crime suspects, and monitoring climate change . . . Basic research in radio astronomy, or astronomy more generally, has produced these practical outcomes. That's not the reason you do it. But it's a good place to start.

VIROLOGY

Alzheimer's Risk Factor Also Aids HIV

The defective lipid carrier apolipoprotein E4 (apoE4) has accumulated a nasty record. Not only are people who have the gene for apoE4 famously predisposed to Alzheimer's disease, but the same risk factor can also worsen several nervous system disorders and promote cardiovascular disease. A study out this week suggests that apoE4 also hastens the death of people infected with HIV, possibly by allowing the virus easy entry into cells.

This discovery already has scientists wondering if the new genetic risk factor could help guide AIDS treatment and if prospective Alzheimer's drugs could one day fight HIV as well. But some remain skeptical, noting that it's not clear how many of the apoE4-linked deaths were due to AIDS.

Apolipoprotein E is supposed to ferry cholesterol and lipoproteins through the plasma and cerebrospinal fluid to cells. One version of the protein, apoE3, does the job just fine—but two other versions, E2 and E4, are associated with different diseases. People possess two copies of the gene for apoE, and having even one copy for apoE4 is a major risk factor for Alzheimer's disease.

Some research has also hinted at a role for E4 in infectious diseases. One 1998 study, for example, found that among 44 HIV patients, individuals with at least one copy of the E4 gene were twice as likely as other patients to develop HIV-associated dementia.

Intrigued by that dementia link, a team led by physician-scientist Sunil Ahuja of the University of Texas Health Science Center in San Antonio recently studied the apoE gene status of 1267 people with HIV—mostly servicemen—who received free military health care for up to 20 years. The E4-dementia connection did not hold up in this larger study—perhaps because new antiviral drugs have nearly eliminated the condition, suggests Colin Hall, a neurologist at the University of North Carolina, Chapel Hill, who led the 1998 study.

What Ahuja and his team do report this week in the *Proceedings of the National Academy of Sciences* is a dramatic effect of E4 status on survival. 10 years after diagnosis, almost all of the 27 patients who had two copies of the E4 gene had died, but among those with other gene combinations, even one E4 gene, half were still alive. Double E4 patients also developed AIDS-related diseases such as toxoplasmosis twice as fast as the other patients.

"The clinical differences are really not subtle," says Michael Lederman, a molecular biologist at Case Western Reserve University in Cleveland, Ohio. "People should hustle after [this]."

It's not clear whether E4 is detrimental or E3 is protective. But by adding purified E4 or E3 to an HIV cell infection assay, Ahuja's team showed that the virus most frequently infected cells incubated with E4.

Ahuja predicts that a role for apoE in infectious disease is "a broader theme that's going to emerge down the road." Linking E4 to AIDS progression could lead to new HIV drugs. Robert Mahley, a pathologist at the J. David Gladstone Institutes in San Francisco, Califor-

Risky. HIV (*inset*) may more easily infect cells of people who produce only apolipoprotein E4 (*right*) instead of the more common E3 (*left*).

COURTESY OF R. W. HARVEY AND R. W. MAHLEY, THE J. DAVID GLADSTONE INSTITUTES; JOSEPH A. SULPIZIO/SCIENCE

nia, and an author of the study, is working with Merck to develop Alzheimer's drugs that would force apoE4 to assume an E3-like structure. Those compounds, however, aren't even ready for animal tests.

Robert Shamburek, who specializes in lipoprotein metabolism at the National Heart, Lung, and Blood Institute in Bethesda, Maryland, agrees that the new study is provocative. But he worries that Ahuja's team doesn't define the cause of death among those with the E4 gene. Instead of AIDS, they may be dying of other causes, such as cardiovascular problems that would respond better to cholesterol-lowering drugs than to aggressive antiviral treatment.

—ELSA YOUNGSTEADT

Bad Grades for U.S. Science Office

The White House Office of Science and Technology Policy (OSTP) needs a "critical upgrade" to more effectively tackle important science issues, says a report released this week by the Woodrow Wilson International Center for Scholars. In a 17 June briefing, the report's authors and other experts said that the current office, headed by John Marburger with a staff of 50 and a $5.2 million budget, is often ignored by the president and does a mediocre job of coordinating science policy among federal agencies. In that way, said consultant and co-author Mark Schaefer, it resembles science offices in previous Administrations. The report itself was more circumspect, calling for four assistants (up from two) who are confirmed by the Senate, offices in the Old Executive Office Building adjacent to the West Wing (OSTP currently sits in another building slightly farther away), and more face time with the next president.

"If you're not able to forge the relationships in the inner sanctuary, . . . you can't get stuff done," said Deborah Wince-Smith, president of the Council on Competitiveness and a former OSTP staffer. But Marburger calls the additional top staff "management overkill" and says the report's recommendation to give his office more clout by making it a Cabinet-level agency "in my experience would not be necessary."

—ELI KINTISCH

Genetic Test Kits Under Fire

California has told 13 companies to stop offering genetic tests directly to its residents. The action followed an investigation by state public health officials, who received complaints from consumers about the accuracy and cost of these tests, which are sold over the Internet.

Direct-to-consumer genetic testing is a new and rapidly expanding area, and genetic researchers and physicians have expressed concern over whether the tests, which are often based on gene mutations that only slightly raise risk of disease, can provide meaningful information. The companies, including California-based Navigenics and 23andMe, as well as some outside the United States, were ordered to "cease and desist performing genetic testing" on Californians until they prove that they are following state laws for laboratory licenses and that they require orders from a physician before selling tests. New York state has made similar requests of 26 companies.

—JENNIFER COUZIN

An Unpredictably Violent Fault

Chinese researchers placed a dense array of seismometers around a dangerous-looking seam in the rocks of Sichuan—only to be blindsided by the true killer

BEIJING—Geophysicists knew that the rugged mountains of Sichuan Province were primed for a "big one." But they didn't know when or which fault would give way first. Two years ago, Liu Qiyuan, a geophysicist at the China Earthquake Administration's (CEA's) Institute of Geology, bet on the Anninghe fault, which has been shifting to the east about 10 millimeters a year as the Indian subcontinent shoves the Tibetan Plateau against the Sichuan Basin. Liu deployed 300 broadband seismometers—the $6 million array is one of the densest in the world—around Anninghe and two faults to the north. Thanks to a prodigious 1.8 terabytes of seismic data per year, he began compiling a high-resolution three-dimensional map of the underlying crust.

Liu and his colleagues guessed wrong.

Northeast of Anninghe, on 12 May, a complex fault system ruptured under the Longmenshan, or Dragon's Gate Mountains, releasing energy equivalent to about 2000 Hiroshima-size atomic bombs. Nearly 70,000 people are known to have died, thousands are missing, and more than 1.5 million people lost their homes in the magnitude-7.9 Wenchuan earthquake. Land west of the Longmenshan fault system had been edging eastward toward the Sichuan Basin at a rate of only a couple of millimeters per year, according to Global Positioning System (GPS) measurements. Liu says the GPS readings blinded researchers to the real threat. "We did not imagine such a big event happening in Longmenshan."

Scientists will need to redraw seismic-intensity maps that guide planners on safe areas for construction and how much shaking buildings must be designed to withstand. The U.S. Geological Survey (USGS) estimates that the Wenchuan earthquake subjected 1.3 million people to violent or extreme shaking. The revisions must be made posthaste in Sichuan, which is keen to begin reconstruction.

But with many of China's 1.3 billion people living in seismic zones, every province will have to check its intensity maps. Municipalities will have to upgrade building codes and strengthen enforcement. "They can begin to prepare for the inevitable," says geophysicist Walter Mooney, USGS's top expert on China. But in the long run, a deeper understanding of the titanic forces at play in Earth's crust is necessary to refine predictions of where future big quakes might strike.

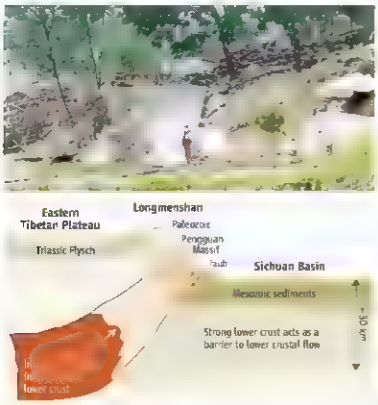

Mountain building. During the Wenchuan earthquake, land west of Longmenshan lurched eastward. At Shiyan village in Beichuan County, the rupture lifted a road more than 4 meters, destroying houses along the scarp.

CREDITS: (TOP TO BOTTOM) CHEN XUEZHANG-LA PRESSE/CORBIS; AP; CHEN ZU-AGE/USGS

Other revelations are sure to follow. For the past month, a few dozen Chinese scientists have been braving strong aftershocks to survey the rupture on the central Longmenshan fault and a shorter gash on a parallel fault. Their observations, coupled with readings from the northeastern corner of Liu's Sichuan array, which covers much of the Longmenshan system, should give an unprecedented look at how a powerful temblor warps geological structure. "The Sichuan earthquake is very important because it's rare to see this happen on a thrust fault inside a continent," says seismologist David Simpson, president of Incorporated Research Institutions for Seismology in Washington, D.C., a university consortium that has wired up the world with digital seismometers. Not surprisingly, Liu has been barraged with requests for data from the CEA array; he expects to release preliminary analyses in the next several weeks.

In the shadow of Dragon's Gate

For someone who has spent nearly three solid weeks surveying Longmenshan and ducking aftershock-induced landslides, geologist Wen Xue-ze looks surprisingly refreshed. Chengdu is sweltering on 5 June, but Wen, after a couple of arduous days in the field around Wenchuan, has just showered and changed and can now review his team's copious findings at the Sichuan Seismological Bureau (SSB) in Chengdu, CEA's biggest provincial bureau.

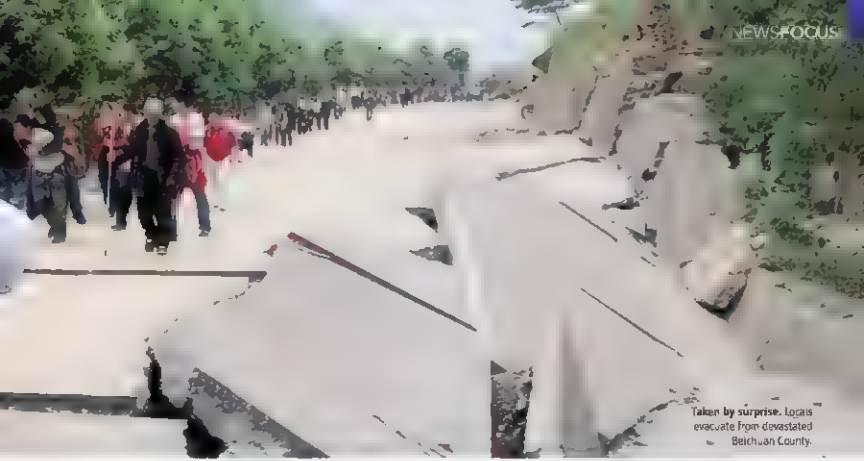

Taken by surprise. Locals evacuate from devastated Beichuan County.

At 2.28 p.m. on 12 May, when the earthquake shook the bureau violently, "we realized it was a big one, but we didn't know where it struck," Wen says. In a few minutes, they learned that the epicenter was Wenchuan, just 70 kilometers northwest of Chengdu. That brought a fresh worry: the possibility that the 156 meter-high Zipingpu Dam, several kilometers east of the epicenter, would collapse. Engineers determined that Zipingpu suffered cracking but was structurally sound. Some Chinese and Western geophysicists privately say it's necessary to investigate whether the dam, completed less than 2 years ago, triggered the earthquake.

A couple of hours after the quake struck, Wen and other SSB staff reached the historic town of Dujiangyan, situated on the edge of the Sichuan Basin in the shadow of the Longmenshan. Much of the town lay in ruins, the road winding through the mountains to Wenchuan blocked by landslides. To aid relief efforts, Sichuan officials in Dujiangyan asked SSB to produce a map of the hardest hit areas. Based on aftershocks in the first several hours after main shock, Wen and SSB Director Wu Yao-qiang circled an area encompassing a mind-numbing 20,000 square kilometers. That night, SSB delivered the sobering map to authorities. "They realized the destroyed area was enormous," Wen says.

Wen led a team into the field on 17 May to look for surface ruptures. Their first stop was Beichuan, which straddled the main fault and had been reduced to rubble. Wen's group found that land on the northwestern side of the fault had been thrust up as much as 5 meters. "This is mountain building," says Liu. (The third-largest temblor ever recorded—the magnitude-9.3 earthquake off Sumatra that spawned the tsunami in 2004—ruptured 1600 kilometers, shifting the seabed fault a staggering 20 meters in places.)

Based on the dramatic scar at Beichuan, CEA chiefs in Dujiangyan asked Wen to rev up his survey work and assigned him a team of 30 scientists. They fanned out in eight groups and over 2 weeks mapped a rupture running more than 200 kilometers along the main fault. In addition to lifting 3 to 5 meters, the fault had shifted areas to the west 1 to 4 meters relative to those in the east. "The earthquake lifted up the mountains and pushed them to the side," says Mooney. The section near Beichuan showed a strike-slip movement, a grinding twist as two slabs of crust moved in opposite directions. Aftershocks have rattled 300 kilometers of the main fault, including a roughly 100-kilometer section to the northeast that Wen says did not rupture. His team also discovered a rupture more than 50 kilometers long on a secondary fault 10 to 20 kilometers to the southeast. A third fault in the Longmenshan system northwest of the main one appears not to have ruptured.

Before the Wenchuan earthquake, Wen and his colleagues, like Liu, perceived two immediate threats. One was the Anninghe fault, which has a 90-kilometer seismic gap, or eerily quiet stretch with few tremors. The other was the Xianshuihe fault, which runs southwest to northeast, forming a "V" with the Longmenshan fault, and which, like Anninghe, has been moving about 10 millimeters per year. Longmengshan's giving way before the others, says Wen, "is a challenge to the traditional idea of active fault segmentation."

Out of the blue?

The Wenchuan earthquake certainly wrong-footed CEA headquarters. After the quake struck, it took less than 6 minutes for the initial seismic waves to leave Chinese soil. By the time the waves had reached the far corners of the globe 20 minutes later, USGS's National Earthquake Information Center in Colorado had pinpointed the epicenter and assigned a preliminary magnitude of 7.5. Meanwhile, CEA's automated software determined, erroneously, that a magnitude-3.9 earthquake had struck the Beijing suburb of Tongzhou and posted the information to CEA's Web site. Minutes later, CEA identified the correct epicenter and updated the Web site. By evening, a 230-person-strong CEA team had arrived in Dujiangyan (*Science*, 23 May, p. 996). But an incorrect calculation of the moment tensor—a mathematical description of a fault's movement during a quake—lingered on the Web site for 4 days.

The errors left CEA's cadre of scientists red-faced. The massive agency employs some 10,000 people, but only about 100 are Ph.D. scientists. "The problem is at the top,"

says Chen Yuntai, honorary director of CEA's Institute of Geophysics. "The root cause of the mistakes is not placing importance on the science." Perhaps as a result, says Peking (Beijing) University geophysicist Huang Qinghua, "CEA is isolated from the scientific community."

One long-standing gripe is a lack of data sharing. The main entities involved in earthquake research—CEA, China's Geological Survey, the Chinese Academy of Sciences, and universities under the Ministry of Education—each collect similar data using their own instruments. "We need a policy to force scientists to upload data to a common server," says Zhou Shiyong, a geophysicist at Peking University. Collaboration across disciplines must also improve. "Before, seismologists and geohazards researchers were working completely separately. Now we realize we have to cooperate," says Cui Peng, a geomorphologist at the Institute of Mountain Hazards and Environment in Chengdu.

Peking University and CEA last year established a joint seismology research center. "Theoretically, we can get data from CEA," says Huang. But it hasn't worked very well. U.S. experts, meanwhile, complain that China's policy of delaying the release of seismic data by 30 minutes impedes emergency response. Chinese researchers say their hands are tied by the military, but some say the Wenchuan quake may give momentum to arguments for real-time data release.

A more fundamental issue is CEA's mission, not only to monitor and respond to earthquakes but also to predict them. "CEA issues many earthquake warnings, but they are just guessing. It's not science," says Zhou. One recognized precursor of some major quakes is foreshocks that increase in frequency and intensity, but "very few earthquakes have identifiable foreshocks," says Simpson—and Wenchuan had none.

Reading portents

Nonseismic warning signs are even more problematic. In the hours before the Wenchuan earthquake, a Taiwanese meteorology satellite reportedly detected a decrease in density of charged particles in the ionosphere above Wenchuan. Although some researchers speculate that it may have been due to radon seeping into the air, Huang notes that a link between earthquakes and ionosphere anomalies is controversial. A few days before that, the streets of a Sichuan village near the fault were filled with toads migrating from the mountains. "Everyone hopes that animals can tell us something us humans don't know," says Mooney. "But animal behavior is way too unreliable." Even in hindsight, he and others say, they've seen no geophysical connection between these anomalies and the earthquake.

Chinese scientists devoted considerable energy to research on potential precursors after the late Premier Zhou Enlai in 1966 tasked CEA with earthquake prediction. But a decade later, a disaster laid bare the limitations of this effort. On 28 July 1976, a magnitude-7.8 earthquake leveled Tangshan, 160 kilometers east of Beijing. Officially, 240,000 people died, the highest earthquake death toll in the 20th century. Before the quake, the geology beneath Tangshan was restless. In early July, for example, locals reported fluctuations in the water table, and on the eve of the disaster, there were reports of odd lights emanating from the ground. Some experts were convinced an earthquake was imminent, but others "were waiting for the foreshocks," says Chen Xiaofei, a geophysicist at Peking University. None came. "Tangshan is why I believe that precursors exist, but we don't understand them yet," says Huang. The primitive state of the field, says a senior CEA geophysicist, is similar to that of weather forecasting a century ago, when people relied on sky observations and animal behavior. "Meteorologists have made the transition from empirical to physical prediction," he says. "We haven't."

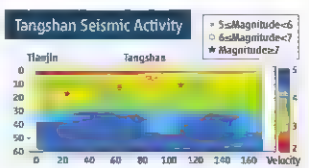

The danger below. CEA's seismometer array near Beijing has revealed a tumultuous—and still dangerous—geology beneath the city of Tangshan, which was leveled by an earthquake in 1976.

In the past decade, Chinese research has largely followed the lead of Japanese and U.S. efforts that focus on deep geophysical processes. For instance, Liu notes, CEA's other broadband array—107 seismometers in the "Capital Circle" region around Beijing—has revealed a convoluted geology under Tangshan caused by a localized upwelling of magma into the crust (see diagram, above). Such mapping can flag hot spots for future megaquakes where GPS reveals little deformation. "The findings suggest that Tangshan remains perilous," warns Liu.

Other Chinese scientists argue that their country should chart its own course, with an emphasis on characterizing nonseismic anomalies preceding major temblors. "We pay too much attention to deep structure," argues Zhou, who would like to see China's seismically restive Xinjiang Province turned into an earthquake prediction laboratory. Huang says that "rigorous and reliable" research could allow scientists to design a precursor monitoring network. "We should study geophysical and geochemical signals," says Liu. But he cautions that precursors are likely to be more complicated than the earthquakes they presumably foretell. "Some of my colleagues are in too big a hurry to succeed in earthquake prediction," he says.

In the short term, all eyes will be on Sichuan. Liu's team is processing data from the Longmenshan broadband stations, only three of the pricey seismometers were damaged. Wen's group will mount field surveys and comb records of past earthquakes in Longmenshan to better estimate the intervals between major quakes. "We want to understand the relationship between this large earthquake and historical seismicity," he says. The SSB researchers will also investigate whether the Wenchuan earthquake transferred stress to surrounding faults such as southwestern Longmenshan and Anninghe.

Geophysicists will help guide reconstruction, which the Sichuan government aims to complete in 3 years. "We want people to have a better life than they had before the earthquake," says Cui, whose mountain hazards institute is one of dozens of organizations participating in reconstruction planning. The most urgent task, Wen says, is to remap the faults. Within the next few weeks, he says, a CEA team will produce an active fault map of the region, which will be revised as new information comes in.

Although geophysicists do not expect another huge earthquake in the 12 May rupture zone for another century or two, Sichuan authorities have already chosen another location for a new Beichuan; there are no plans to rebuild other villages on the Longmenshan fault. "People feel the area is no good," says Cui. Adding to the agony is the observation that many buildings that collapsed were poorly constructed. That was the biggest lesson of the Wenchuan earthquake, says the senior CEA geophysicist. "We got this knowledge at the expense of many lives. We should never let it happen again."

—RICHARD STONE

With reporting by Hao Xin.

CREDIT: COURTESY OF LIU QIFANG

BEHAVIORAL GENETICS

Abuzz About Behavior

Researchers are tracking down the genes underlying variations in alcohol dependence, sleepiness, and other behaviors by studying specially bred fruit flies

RALEIGH, NORTH CAROLINA—Humans can be short-tempered or mild mannered, shy or boisterous, neat or slovenly—and every combination in between. Understanding the complex genetic networks that underlie behavior—and, ultimately, what makes each of us unique—is a mind-boggling task. Now Robert Anholt, Trudy Mackay, and their colleagues have developed a resource that may help researchers begin to figure out how genes make us who we are.

Together with a dozen colleagues at North Carolina State University (NCSU) in Raleigh, as well as collaborators in Europe and Canada, this husband-and-wife team has established a collection of inbred fruit flies (*Drosophila melanogaster*) from a wild population in North Carolina and are correlating patterns of gene expression with specific behaviors in the insects. The work could steer biomedical researchers to genes that influence aspects of human behavior, says Anholt. "What Trudy and Robert are doing will be very important for the discovery of genetic changes that contribute to behavior," says Catherine "Katie" Peichel, an evolutionary geneticist at the Fred Hutchinson Cancer Research Center in Seattle, Washington.

The project began a decade ago. Twice, in 1999 and 2002, Mackay's NCSU collaborator Richard Lyman showed up at Raleigh's farmers' market and picked off the fruit flies that emerged as crates of freshly harvested peaches were opened. Individual females were placed in vials, and each fly that reproduced became the progenitor of a single line of flies. Their offspring were allowed to mate only with each other, resulting, after several generations, in a line of genetically identical individuals that display consistent behavior. Each line is genetically—and behaviorally—different from all the others. The overall goal is to capture the genetic variation in the North Carolina wild fruit fly population in these wild-derived inbred lines.

To date, the NCSU group has established 345 lines, and the researchers have used microarrays to determine the level of activity of 18,000 genes in 40 of them. Surprisingly, the expression of about 10,000 genes varies from one line to the next, Mackay and Anholt reported at the annual meeting here earlier this month of the American Genetic Association.

The team has also tracked variation in behavior from line to line under different conditions. Then, by looking for differences in gene expression in lines that differ most in a particular behavior, they can zoom in on genes likely to underlie that particular behavior. And, drilling down further, the researchers use existing lines of *D. melanogaster* with mutations in every gene, as well as techniques for manipulating genes in this species, to pin down what each gene does and how it might influence a particular behavior.

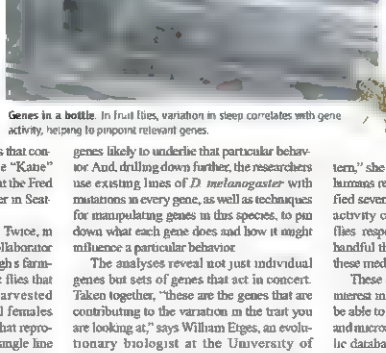

Genes in a bottle. In fruit flies, variation in sleep correlates with gene activity, helping to pinpoint relevant genes.

The analyses reveal not just individual genes but sets of genes that act in concert. Taken together, "these are the genes that are contributing to the variation in the trait you are looking at," says William Etges, an evolutionary biologist at the University of Arkansas, Fayetteville. Synchronized genes are likely to be part of a common biochemical pathway; thus known genes in a set provide clues about the function of uncharacterized genes in that cluster.

To get at the genetic underpinnings of sleep, for example, NCSU's Susan Harbison has compared gene-expression patterns of flies that keep quite different schedules, some spending 20 hours a day resting, others barely pausing for four. She reported that different sets of genes were turned up for nappers and for nighttime snoozers—out of the hundreds correlated with sleep, only 78 were common to night and day resting, she reported.

Another project, spearheaded by NCSU postdoc Tatiana Morozova, is probing the genetic underpinnings of the fruit flies' responses to alcohol. Morozova monitors which lines are sensitive to ethanol vapor—measured by how long it takes individuals to lose their ability to cling to a tilted screen—and which ones become more tolerant when the exposure is repeated. In people, tolerance is a risk factor for alcoholism. She found a wide range in both sensitivity and tolerance, but the two traits were not linked. "You can't tell who will develop tolerance" based on who is sensitive, Morozova reported.

The gene-expression analysis revealed 195 genes that appear to play a role in sensitivity to alcohol and about 600 linked to tolerance. Many of the genes that underlie sensitivity and tolerance play a role in metabolism, but few were common to both responses. And many have human counterparts. Anholt, Mackay, and Morozova are now investigating whether some of these genes correlate with alcohol tolerance in humans.

NCSU postdoctoral fellow Katherine Jordan is using the inbred lines to look for genes that regulate the insects' responses to a variety of psychoactive drugs. "There's no uniform pattern," she reported. "It's very similar to how humans react to these drugs." She has identified several dozen genes whose variations in activity correlated with differences in the flies' responses, and she is now focusing on a handful that might influence the efficacy of these medications.

These early results are fueling widespread interest in the inbred lines. Soon, anyone will be able to order the lines from a stock center, and microarray data will be available on a public database. And the U.S. National Human Genome Research Institute in Bethesda, Maryland, has just awarded Baylor College of Medicine $5.75 million to sequence the genomes of individuals from 192 of the lines, the sequences will be publicly available once they are completed, Mackay notes. "It's the next generation [of genetic studies]," predicts Michael Ritchie, an evolutionary biologist at the University of St. Andrews in Fife, U.K. "You can see people asking not just about two or three genes but about [whole] networks."

–ELIZABETH PENNISI

CREDITS: TOP TO BOTTOM: KEAN LEAHEY & MARKSON AND C. COUCHMAN/L. JAPPOT CONSORTIUM

MICROBIAL ECOLOGY

Out of Thin Air

On a volcano, [illegible] takes a trip back [illegible] how microbes [illegible] life on lava fields and [illegible]

New beginning. Lava flows from Mauna Kea in Hawaii create new land and reset the volcano's biological clock.

VOLCANOES NATIONAL PARK, HAWAII—On a warm, humid day in early May, Gary King is watching an ecosystem come alive. Here, the glowing lava of Kilauea regularly destroys the slopes' forests, then cools into dark gray, gold-flaked phantasmagorical forms. For decades, these lava fields bake under the hot sun, seemingly lifeless. But eventually, a fern or a koa sapling springs up timidly from a crevice, precursors of the forest that will ultimately rise again. A walk across the park takes King back through time, allowing him to get a close look at the specialized bacteria that are midwives to this rebirth.

"Here, you can study how the microbes colonize the lava, how they provide nutrients for the first plants, and how the microbial community evolves as the amount of plants grows," says King, a slight, soft-spoken 54-year-old microbiologist from Louisiana State University in Baton Rouge.

Through field and lab work, he and his colleagues have discovered that these microbial pioneers first survive by processing dust, rainwater, atmospheric hydrogen, and, to a surprising degree, carbon monoxide. Only a few dozen species were known to use this typically toxic gas. Now, King's genetic analyses have uncovered more than 100. His studies of the interactions between the bacteria, flora, and atmosphere are showing how these microbes help control Earth's balance of greenhouse gases—both directly, through their metabolism, and indirectly, by creating hospitable landscapes for plants that can sequester carbon.

"King is studying this very important step of how life takes hold and discovering keystone organisms that play a critical role in the Earth's biogeochemical cycles," says Matthew Kane, a program director at the U.S. National Science Foundation in Washington, D.C. As King pins down the carbon monoxide–oxidizing species, "he will eventually figure out what they like and don't like," adds Ortwin Meyer, a microbiologist at the University of Bayreuth in Germany. "Then we should be able to tell decision-makers what to do and not to do" about putting these organisms to good use in the fight against global warming.

Today, with Kane looking on, King bends over a crevice at the rim of a 30-meter-deep smoking caldera. He scrapes off tiny bits of 34-year-old lava and puts them into a tube filled with a solution that preserves any DNA that they contain. There's probably a billion bacteria per gram, he says. Examining the 50,000 expected to have carbon monoxide–processing capabilities "will tell us what the diversity is like at this site, and we can compare it to the diversity at other sites, older or younger, and that way we can track the whole process of microbial succession."

He and Kane then move on to the next site, one of eight scheduled for sampling on this 2-day visit. Later, they head to the leafy, everrainy Volcano Village and stop at the rented house that serves as the temporary lab for King's team. There, graduate student Carolyn Weber is running a gas chromatograph that measures how much carbon monoxide is being consumed by bacteria samples brought back from the volcanoes.

The work being done here, says Ralf Conrad, a biochemist at the Max Planck Institute for Terrestrial Microbiology in Marburg, Germany, will make it easier to find these bacteria in more complex soils around the world, and that "will help us understand their global role."

Hungry for carbon monoxide

Although carbon dioxide, the chief greenhouse gas, grabs many of the global warming headlines, its oxygen-deprived cousin, carbon monoxide, plays a role as well. Industrialization has caused carbon monoxide concentrations to rise. Once in the air, it turns into carbon dioxide within 3 months by reacting with hydrogen radicals. These radicals also break down methane, another greenhouse gas. "So when carbon monoxide uses up these radicals, there's less left to break down the methane, and the methane increases," King explains. Thus, removing carbon monoxide from the air "is important."

Meyer estimates that at least 15% of the carbon monoxide being released into the atmosphere is absorbed by bacteria living on the first cen-

Life returns. Bacterial pioneers enrich sunbaked lava soil with ammonia, enabling plants to take hold.

CREDITS: (TOP TO BOTTOM) JIM ELLIS/NOAA; CHRISTOPHER PALA

timeter of the world's soil cover, even though this gas is toxic to most organisms, including microbes. King, long curious about how bacteria affect carbon monoxide concentrations in the atmosphere, had been comparing samples from Georgia and Maine; he first came to Hawaii a decade ago to see how these bacteria worked in a seasonless environment.

Intrigued by what new "soils" such as newly hardened lava deposits—would do, King measured the rates of carbon monoxide and hydrogen removal from the air on lava flows laid down anywhere from 25 to 300 years ago. He was surprised to find that some of the youngest—seemingly barren, fractured surfaces—were able to remove these gases from the air as rapidly as mature continental forest soils that support rich communities of bacteria. He wondered if such high consumption was the key to survival for microbes settling on new lava, given the scarcity of other energy sources.

By comparing rates of carbon monoxide and hydrogen uptake with total rates of respiration in the bacteria, King showed in 2003 that the two gases account for more than 20% of the bacteria's energy needs. He then used genetics to learn more about these microbes. From an assortment of soil samples, his team isolated all the copies of a gene for an enzyme critical to carbon monoxide use. By counting and comparing the different versions of the gene—different ones represent different species—the researchers got a sense of the number and diversity of carbon monoxide consumers at various sites. "King is the first to identify bacteria by their carbon monoxide function using genetic probes," says Meyer.

The resulting data showed that microbes that use this gas are far more diverse than he had previously imagined, King says. Moreover, distinctly different communities of carbon monoxide–oxidizing microbes exist on different types of lava—from the ropy "pahoehoe" to the wisps of lava called Pele's hair—and in different types of soils. The newly recognized oxidizers of the gas include important symbiotic partners for peanuts, soybeans, and other plants, as well as plant, animal, and human pathogens. The ability of symbionts and pathogens to use the gas may help explain their survival outside their host organisms, he says.

While they are consuming carbon monoxide, these bacteria are also taking nitrogen from the atmosphere and converting it into ammonia, a fertilizer that enriches the lava and encourages plant growth. King has shown that the iconic acacia koa tree, a Hawaii endemic that's the preferred wood for the oceangoing canoes of the Polynesians (along with much of the handicrafts sold to tourists), thrives on barren soils because lumpy nodules on its roots host these carbon monoxide– and nitrogen-processing bacteria.

As plant communities take hold, the bacteria "eat" less carbon monoxide, King and Weber reported online 29 November 2007 in *The ISME Journal*. Now the microbes feast on organic matter and on carbon dioxide and really begin to thrive. "We've found that in the forested area, there are five times as many species of these carbon monoxide oxidizers as in the dry area," Weber says. In addition, the expanding plant cover begins to turn the area into a carbon sink.

Pay dirt. King gathers tiny pieces of lava called Pele's hair (inset) to look for carbon monoxide–consuming bacteria.

CREDITS: CHRISTOPHER PALA

Warehousing carbon

During this field visit, King heads beyond the bare lava fields to the cool, humid Pu'u Puai forest. He sticks his trowel into the soft ground, a mix of bits of lightweight dead leaves and humus, holds it up, and says, "*This* is carbon sequestration." The leaves of the endemic flowering tree ohia lehua and the invasive fire tree above King absorb carbon dioxide from the atmosphere, lock up the carbon in carbohydrates, fall on the ground, and die. Bacteria then process that plant matter and release some captured carbon as carbon dioxide. The rest of the carbon stays put, sequestered from the atmosphere. Waving his dirt-filled trowel, he continues, "This stuff is at least 20% carbon, which isn't unusual for an old growth forest. What is unique is that this forest is only 50 years old. In other places, in that time span, you'll find much less soil and carbon." He doesn't understand why these differences develop but thinks that the volcano is the place to find out.

"This is a place that can show us the rules that govern sequestration, because we can follow the process from the beginning," he explains. King stands up and walks out of the forest into a sunlit area of tephra, gravel hurled from exploding volcanoes. The ground is sparsely punctuated by ferns and ohelo bushes laden with bright-red berries, another Hawaiian endemic. "On one side, we have an area that is storing a lot of carbon, and in the other we have an area where there is nothing," he explains. "If we can understand the basic principles of how you go from nothing to a lot in 50 years, then we might be able to better manage carbon storage in other soils to help reduce the rise of carbon dioxide in the atmosphere."

And Christian Giardina of the U.S. Department of Agriculture's Forest Service in Hilo, Hawaii, agrees. "Gary's research is providing fundamental information on how the composition and structure of these microbial communities affect the rate at which they release CO_2."

Later, as we drive to the next site, King cautions that carbon sequestration in plants is no magic bullet against global warming. "We're never going to be able to use plants to remove more greenhouse gases than we're putting in," he says. "But if we understand how these microbes affect carbon in soil, we might be able to manipulate the growth of plants and their decomposition in a way that would influence their effect on these gases in the atmosphere."

–CHRISTOPHER PALA

Christopher Pala is a writer based in Hawaii.

Membrane Makes Plastic Precursor Deliver More Bag for the Buck

TO MAKE THE BIGGEST IMPACT, TACKLE THE biggest problem. That's what Balu Balachandran and his colleagues at Argonne National Laboratory in Illinois did when they set out to reform the making of polyethylene, the world's most abundant commodity plastic. At the meeting, Balachandran reported that his team has developed a novel metal-ceramic membrane that enables them to produce ethylene, the starting material for polyethylene. If adopted widely, the process could cut production costs by 15%, saving millions of dollars a year and dramatically cutting the amount of greenhouse gases released into the atmosphere.

Ronald Pate, an energy and water analyst at Sandia National Laboratories in Albuquerque, New Mexico, says improving the production of ethylene "is a big leverage opportunity." Pate says that the technology still needs to prove itself as a viable industrial-scale process but that "it ought to be looked at to bring the carbon footprint down."

In the world of commodity chemicals, petite ethylene (C_2H_4) is a behemoth. More than 75 million metric tons of the gas are produced each year to make the plastics that go into everything from grocery bags and milk jugs to compact disc cases and wire sheathing. The simple organic molecule can be made from many materials, most commonly by breaking apart, or "cracking," light liquid hydrocarbons with high-temperature steam. Although simple, the process converts only about 64% of the starting materials into ethylene. One reason is that the carbon in the starting hydrocarbons can combine with oxygen from the steam to make CO_2 instead of pairing up with hydrogens to make ethylene.

Big impact. A new approach could slash the cost and carbon footprint of making polyethylene

To make the process more efficient, Balachandran and colleagues looked for a way to crack ethane (C_2H_6) and other hydrocarbons while keeping the oxygen and carbons apart. They settled on using a thick membrane made from a mixture of palladium and a ceramic called yttria-stabilized zirconia. Although Balachandran did not reveal the precise makeup of the new membrane or how it transports hydrogen, he and his Argonne colleagues have developed related membranes to separate hydrogen gas for use in fuel cells. For their current study, Balachandran reported, they put ethane on one side of the membrane and air on the other. Heating the ethane caused most of the molecules to break apart into ethylene and H_2 molecules. The H_2 molecules then traveled through the membrane and combined with oxygen from the air, a reaction that generates heat. In turn, the heat traveled back through the membrane to sustain the ethane-cracking reaction.

The process converted 73.5% of the ethane to ethylene, nearly 10% more than steam reforming does. As a bonus, no additional energy was needed to produce the superheated steam. Balachandran says he suspects that could simplify reactor designs and help drop production costs.

Balachandran acknowledges that the new process is still in its infancy. The next steps are to scale up the process and see if it works with other hydrocarbon feedstocks. If they succeed, your plastic milk jugs of the future may well become a little greener.

Don't Sweat the Small Stuff >>

Nanoparticles are known for packing macro-sized surprises. And that's just what chemist Brian Woodfield and his colleagues at Brigham Young University in Provo, Utah, got when they set out to solve a nanoparticle mystery last year.

Their cerium oxide nanoparticles were displaying odd magnetic behaviors. But they were also spiked with impurities. To see if that's what was causing the odd readings, Woodfield's postdoctoral assistant Shengfeng Liu came up with a new scheme for synthesizing high-purity cerium oxide particles. He found out that the impurities were indeed to blame. But more important, as Woodfield reported at the meeting, Liu hit upon an easy-to-use general technique for making dozens of different types of metal oxide nanoparticles that could have a major impact on everything from catalysts to electronics.

"It opens a very general, cheap, clean, flexible route to nanoparticles for all sorts of applications," says Alexandra Navrotsky, a chemist at the University of California, Davis. Researchers around the globe are already looking to metal oxide nanoparticles to improve everything from fuel cells to optical films. So, Navrotsky says, "the opportunities are pretty widespread."

There are many ways to make nanoparticles. A common method uses heat to vaporize bulk-sized starting materials. As the vapor cools, its atoms coodense into larger nanoparticles. Another approach precipitates nanoparticles from ions in liquids. But such techniques produce highly pure nanoparticles only when the chemistry and kinetics are just right.

Liu chose instead to start with high-purity metal salts, which, like table salt, are a fusion of positively and negatively charged ions that come together to form a neutral compound. He then ground the salt together with ammonium bicarbonate, a white, powdery material used as everything from a leavening agent in breads to fertilizer. The grinding rearranged the chemical partners. Mixing aluminum nitrate and ammonium bicarbonate, for example, produced aluminum hydroxide and ammonium nitrate, with excess carbon and oxygen bubbling off as CO_2 (see diagram, p. 1585). Finally, Liu baked his mixture at 300°C for about an hour. The heating drove off several additional components as gases, leaving behind aluminum oxide nanoparticles. "Voila, you get nanopowder," Woodfield says.

The simple process is a nearly foolproof way to make uniformly sized metal oxide nanoparticles, Woodfield says. He and his colleagues have used

CREDIT: LEW ROBERTSON/STOCKFOOD/GETTY IMAGES

Solar Cells Gear Up to Go Somewhere Under the Rainbow

TODAY'S SOLAR CELLS DO A FAIR JOB OF converting visible light into electricity, but they ignore lower energy infrared (IR) photons, or heat, which don't have enough energy to generate electricity in semiconductors. At the meeting, researchers from the Idaho National Laboratory (INL) in Idaho Falls reported harvesting IR photons with arrays of antennas akin to those on televisions and in cell phones, a first step toward solar cells that convert heat to electricity. If the approach pans out, it could lead to solar cells capable of generating electricity after sunset and using the waste heat from industrial plants.

"It's certainly an intriguing idea," says Michael Naughton, a physicist at Boston College in Chestnut Hill, Massachusetts, whose group has built related antennas. But he notes that converting the energy from the collected IR light to electricity will require a separate set of advances. Says Naughton: "Either it has no chance of working, or it will be fantastic."

The notion of using antennas to capture electromagnetic waves and then convert that energy to electricity is decades old. In 1964, William Brown, an engineer at the U.S. aerospace company Raytheon, demonstrated a flying helicopter that absorbed microwaves and converted their energy to DC power to run a small engine. At the heart of the helicopter's success was a two-part device called a "rectenna": a microwave-absorbing antenna combined with a "rectifier" that converts the microwave energy to electricity. More recent are proposals to transmit microwave energy to Earth from arrays of solar collectors in space.

Several years ago, researchers led by Steven Novack at INL set out to capture and convert IR light, which has a wavelength two to five orders of magnitude shorter than microwaves. That meant the size of each antenna needed to be in the micrometer scale

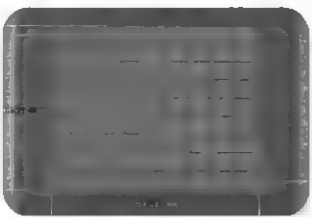

Gotcha. Arrays of gold spiral–shaped antennas absorb infrared photons, or heat, triggering electrons in the antennas to oscillate at 30 trillion times per second. Researchers hope those excited electrons will lead to a new form of solar power

with numerous features in the nanometer range. To capture enough IR photons, Novack and his colleagues needed arrays with millions of the antennas side by side. The good news was that instead of having to use exotic semiconductor alloys to capture the light, they could do so by patterning gold in square spiral structures. Novack's team worked out a way to stamp out millions of gold spiral arrays on either silicon or cheap, flexible plastics. At the meeting, Novack reported that the arrays on silicon capture some 80% of the IR photons that hit them, whereas those on plastic manage a respectable 40% to 50%.

Novack and his colleagues still need to figure out how to get the power out of the antennas. When the IR photons hit the array, they cause electrons in the gold to oscillate back and forth at a frequency of 30 terahertz, or 30 trillion times a second. Conventional electronics operate with a current that oscillates at a plodding 60 times a second. That means Novack's team needs to find devices that can either step down the terahertz electrons or convert them into a DC current.

Unfortunately, Novack and Naughton know of no devices—commercial or otherwise—that can do that, though diodes and rectifiers do the job at lower frequencies. But Novack says theoretical work suggests that sandwichlike devices made from three metal layers separated by ultrathin insulating layers might step down the frequency. And both Novack and Naughton say that a recent surge in terahertz-frequency research is producing rapid advances. Novack says devices that convert to electricity even 30% to 40% of the IR energy absorbed by the antennas could lead to solar cells that beat the efficiency of crystalline silicon cells with a cheap and simple technology that can be printed like newspapers.

ROBERT F. SERVICE

their technique to make some two dozen different metal oxide and mixed-metal oxide particles. And Woodfield says researchers should have little trouble in scaling up the technique. He and his colleagues recently formed a company called Cosmas Inc. to commercialize the process.

Although all the current particles are oxides, Navrotsky says she suspects that the technique could be extended to combine other negatively charged ions with the metals. That should open the door to making a variety of chloride, nitride, and phosphide nanoparticles with a broad palette of exotic optic, electronic, and catalytic properties. If she's right, what is already a powerful technique could become a powerhouse. **R.F.S.**

CREDITS: (TOP TO BOTTOM) IDAHO NATIONAL LABORATORY; I. CHERELIN/SCIENCE

RECIPE FOR NANOPARTICLES

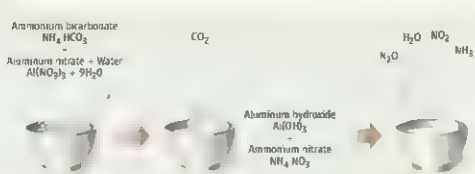

Works every time. Chemists probing a basic mystery of magnetism in cerium oxide nanoparticles discovered this general recipe for making numerous flavors of the tiny grains. Start with a metal salt, add ammonium bicarbonate, stir, heat, and presto! Instant nanoparticles.

LETTERS

edited by Jennifer Sills

Environmental Revolution Starts at Home

THE TITLE OF J. LIU AND J. DIAMOND'S POLICY FORUM, "REVOLUTIONIZING CHINA'S ENVIRONMENTAL protection" (4 January, p. 37), implies a novel solution to China's environmental problems, but suggesting that China must reform its environmental governance is nothing new (*1*). What's more, criticizing a nation because economic performance is still its main criterion for choosing government leaders hardly seems fair. What criterion guides U.S. national leadership? If the U.S. economy appears greener than China's—and less pollution and greenhouse gases are indeed generated per dollar of U.S. GDP—this is only because the United States has exported the "dirty" industries that produce most of what it consumes to China and other nations that need hard currency from abroad to develop their economies.

China's environmental failings reflect the same basic challenge faced by all governments: how to enforce environmental regulations when these conflict with economic development. Even Liu and Diamond admit that China's government has already attempted to couple environmental performance with governance and has a plethora of environmental regulations on the books. The main problem seems to be an inability to enforce most of these in the face of overwhelming economic pressures.

The reason that China has dramatic environmental problems is not a mystery. China's once small economy is booming, moving large numbers of people into a modern consumer life-style. Given that this development is linked to the expansion of China's industry and energy use, as it has been everywhere else, and that a large share of this is dedicated to manufacturing what the rest of the world consumes, those busy consuming the fruits of all of this industrial production should share some of the responsibility for the environmental results.

This would indeed be a revolution: finding a way to make consumers pay for the environmental costs of their consumption, even when they are incurred on the other side of the world. In a globalized economy, the environmental revolution ought to begin at home.

ERLE C. ELLIS

Department of Geography and Environmental Systems, University of Maryland, Baltimore County, Baltimore, MD 21250, USA.

Reference

1. V. Smil, *China's Environmental Crisis: An Inquiry into the Limits of National Development* (M. E. Sharpe, Armonk, NY, 1993).

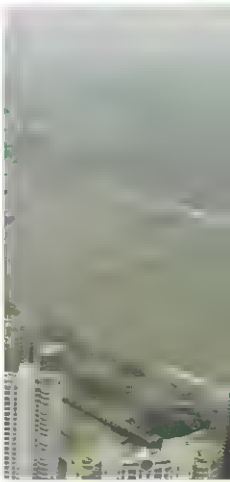

Smog in Shanghai. Pollution in countries such as China is due in part to the outsourcing of "dirty" industries by countries such as the United States.

A Graduate Student Oath

THE HIPPOCRATIC OATH, RECITED BY MEDICAL school graduates worldwide, is arguably the best-known professional honor code. This centuries-old oath instills a commitment to altruism, professionalism, honesty, skill, knowledge, duty, loyalty, and fraternity among medical doctors. The positive impact of the Hippocratic Oath has inspired other professional oaths, notably in schools of pharmacy, dentistry, engineering, physical therapy, veterinary medicine, osteopathy, and law.

The realities of the nuclear age, more frequent acts of bioterrorism, and biotechnological advances such as cloning and stem cells have fueled a call for a similar oath tailored to biomedical scientists that would encourage awareness and discussion of the social and moral responsibilities of students in the life sciences (*1*–*4*). At the Institute of Medical Science (IMS), Faculty of Medicine, University of Toronto, as elsewhere, there is rising recognition of the potential for academic misconduct, in part due to the computer and Internet age, in which there is free access to and exchange of information derived from anonymous sources. Another factor is the increasingly competitive nature and "pressure cooker" milieu of scientific training programs due to the pace of scientific progress. Finally, there is the perception that current students take plagiarism, misrepresentation of facts, and scientific fraud less gravely than did previous generations of scientists. Clearly, the time is ripe to consider improved strategies for instilling basic values about acceptable and expected behavior (*5*, *6*).

We created an oath to be recited voluntarily at the first meeting of each year's new graduate student body in IMS. We specifically chose to hold the oath ceremony at the entry point to graduate studies rather than at graduation day in order to introduce students to these concepts early. In constructing our oath, we took a simple but holistic approach to emphasize three aspects of scientific training at the graduate level: community, professionalism, and ethical conduct, through declarations of pride, integrity, and pursuit. The text of the Institute of Medical Science Graduate Student Oath follows.

CREDIT: KEN ELLIS

"I, [NAME], have entered the serious pursuit of new knowledge as a member of the community of graduate students at the University of Toronto.

"I declare the following.

"Pride: I solemnly declare my pride in belonging to the international community of research scholars.

"Integrity: I promise never to allow financial gain, competitiveness, or ambition cloud my judgment in the conduct of ethical research and scholarship.

"Pursuit: I will pursue knowledge and create knowledge for the greater good, but never to the detriment of colleagues, supervisors, research subjects or the international community of scholars of which I am now a member.

"By pronouncing this Graduate Student Oath, I affirm my commitment to professional conduct and to abide by the principles of ethical conduct and research policies as set out by the University of Toronto."

Our inaugural oath ceremony was held in 2007. We felt it was essential to provide each student with a booklet of information and a personal copy of the oath. The Oath Booklet contained the oath and its purpose; excerpts and Web references to various university codes and policies governing student and ethical conduct, the Canadian Tri-Council policy statement on integrity in research and scholarship; and a reproduction of a speech on science and society by Canadian Nobel Prize recipient John Polanyi (*7*).

To enhance and solidify the ideals embodied in the initiation oath, we also have infused the IMS graduate training program with additional information provided in a variety of formats. For example, currently, our first-year students attend a mandatory seminar course that includes lecture material on issues of scientific misconduct, including plagiarism. In addition, each new student is required to complete the NIH (*8*) or Canadian Tri-Council (*9*) online course on ethics.

We propose that a graduate student oath should constitute a standard requirement of life science graduate programs. This oath should be the cornerstone of a programmatic series of information modules addressing issues of community, professionalism, and ethical conduct provided by the graduate department and reinforced throughout the student's training by their faculty mentor.

KAREN D. DAVIS,[1,2,3]* MARY V. SEEMAN,[2,4] JOSIE CHAPMAN,[1] OR. O. ROTSTE N[1,2,5]

[1]Institute of Medical Science, Faculty of Medicine and School of Graduate Studies, University of Toronto, Toronto, ON M5S 1A8, Canada. [2]Department of Surgery, University of Toronto, Toronto, ON M5G 1L5, Canada. [3]Toronto Western Research Institute, University Health Network, Toronto, ON M5T 2S8, Canada. [4]Department of Psychiatry, University of Toronto, Centre for Addiction and Mental Health, Toronto, ON M5T 1R8, Canada. [5]Keenan Research Centre, 1 Ka Shing Knowledge Institute, St. Michael's Hospital, Toronto, ON M5B 1W8, Canada.

*To whom correspondence should be addressed. E-mail: kdavis@uhnres.utoronto.ca

References and Notes

1. M. L. Jones, *Sci. Eng. Ethics* **13**, 25 (2007).
2. J. Howard, *Nature* **332**, 96 (1984).
3. J. Roskies, *Science* **286**, 1475 (1999).
4. J. Revill, M. R. Dando, *EMBO Rep.* **7** Spec. No., S55 (2006).
5. M. H. Steneck, *Sci. Eng. Ethics* **12**, 53 (2006).
6. B. Glass, *Science* **150**, 1254 (1965).
7. J. Polanyi, "Science, ethics and human destiny" speech given at the 1999 Coudrehing Institute on Public Affairs Conference, 6 August 1999 www.utoronto.ca/jpolanyi/public_affairs/.
8. NIH Office of Extramural Research, Protecting Human Research Participants (PHRP) course, http://phrp.nihtraining.com/users/login.php.
9. Canadian Institutes of Health Research, the Social Science and Humanities Research Council of Canada, and the Natural Sciences and Engineering Research Council of Canada, introductory Tutorial for the Tri-Council Policy Statement: Ethical Conduct for Research Involving Humans (TCPS). www.pre.ethics.gc.ca/english/tutorial/welcome.cfm.
10. We thank S. Pfeiffer, Dean of Graduate Studies, for an inspirational address at the oath ceremony and M. Au for encouragement.

CORRECTIONS AND CLARIFICATIONS

Special issue on Microbial Ecology: News: "Confusing kinships" by J. Bohannon (23 May, p. 1031): David Ward was incorrectly associated with studies of microbial ecotypes in Israel. He studies ecotypes in Yellowstone National Park. Also, the *Bacillus simplex* ecospecies Gram-nifolius should be ecospecies Gramnigrifolius in both the caption and text on p. 1033.

Reports: "The antidepressant fluoxetine restores plasticity in the adult visual cortex" by L. F. Maya Vetencourt *et al.* (18 April, p. 385). The list of supporting online material (SOM) was omitted from the end of the paper. The SOM contains Materials and Methods, figs. S1 to S7, and References. It is available at www.sciencemag.org/cgi/content/full/320/5874/385/DC1.

Perspectives: "Zooming into live cells" by F. Pinaud and M. Dahan (11 April, p. 187). In the credit for the image on the bottom of page 188, the name was misspelled. The credit should have been "Adapted from an image by Graham Johnson." The same credit should have accompanied the image on page 147 of the Table of Contents.

Perspectives: "Titan's hidden ocean" by C. Sotin and G. Tobie (23 March, p. 1629): Titan's obliquity is 0.3°, not 3°.

Perspectives: "The new diamond age?" by P. W. May (16 March, p. 1490). The largest single-crystal diamond substrates supplied by Element Six are 5 mm by 5 mm, not 5 μm by 5 μm.

Reports: "Hybrid neurons in a microRNA mutant are putative evolutionary intermediates in insect CO_2 sensory systems" by P. Cayirlioglu *et al.* (29 February, p. 1256). The introductory paragraph incorrectly stated that CO_2 neurons in the below fly are located in the maxillary palps. They are found in the antennae.

TECHNICAL COMMENT ABSTRACTS

COMMENT ON "Athabasca Valles, Mars: A Lava-Draped Channel System"

David P. Page

Jaeger *et al.* (Reports, 21 September 2007, p. 1709) presented images of the Athabasca Valles channel system on Mars and asserted that the observed deposits are composed of thin, fluid lavas. However, all the features they described are secondary and postdate the surface by many millions of years, as documented by structural relationships with small, young impact craters.

Full text at www.sciencemag.org/cgi/content/full/320/5883/1586b

RESPONSE TO COMMENT ON "Athabasca Valles, Mars: A Lava-Draped Channel System"

W. L. Jaeger, L. P. Keszthelyi, A. S. McEwen, T. N. Titus, C. M. Dundas, P. S. Russell

The recent geologic history of Athabasca Valles, Mars, is controversial. Some studies report ice-rich sediment in its channels, whereas others find only lava. Data from the High-Resolution Imaging Science Experiment camera now confirm that, although certain features exhibit a superficial similarity to ice-related sandforms, solidified lava coats the entire channel system.

Full text at www.sciencemag.org/cgi/content/full/320/5883/1586c

Prized Programs Need Both Eyes and Ears

IN THE ONLINE NEWS STORY "PLAY IT AGAIN, robot" (21 March, Gonzo Scientist series, www.sciencemag.org/scitext/gonzoscientist/), J. Bohannon imprecisely described the Turing test as a chat-only test. In his seminal article "Computing machinery and intelligence" (*1*), Turing used the term "imitation game." He then stated, in reference to computer memory requirements, "I should be surprised if more than 10^9 was required for satisfactory playing of the imitation game, at any rate against a blind man." Presumably, the requirements for playing against a blind man would be different from the requirements for playing against a sighted person in that the game against a sighted person would permit the use of images. At the conclusion of the article, discussing how the computer can be programmed to pass the imitation game, Turing wrote, "It can also be maintained that it is best

to provide the machine with the best sense organs that money can buy, and then teach it to understand and speak English. This process could follow the normal teaching of a child. Things would be pointed out and named, etc."

In keeping with Turing's broad intention, I have required that in order to win The Loebner Prize Gold Medal and $100,000, the program must be able to "intelligently" discuss audio and visual input.

HUGH LOEBNER

Sponsor, The Loebner Prize for Artificial Intelligence, New York, NY 10025, USA.

Reference

1. A. M. Turing, *Mind* **59**, 433 (1950).

Giving Samoan Healers Credit for Prostratin

THE UNIQUE ABILITY OF PROSTRATIN TO ACTIvate latent viral reservoirs while protecting healthy cells from infection makes it of particular interest as a possible adjuvant therapy for HIV/AIDS (*1*). In an effort to provide a short-term supply of prostratin for future Phase II clinical trials, the Government of Samoa is attempting wide-scale cultivation of *Homalanthus nutans*. However, the highest-yielding genotype we have found produces a maximum of 52 grams of prostratin per metric ton of wood (*2*). The partnership between Samoa and University of California, Berkeley, to identify genes responsible for prostratin biosynthesis and to insert them into a prokaryote may eventually provide a low-cost source (*3*).

The elegant synthesis of prostratin and structural analogs in gram quantities by Wender, Kee, and Warrington ("Practical synthesis of prostratin, DPP, and their analogs, adjuvant leads against latent HIV," Reports, 2 May, p. 649) is a major step forward. Synthesis of analogs, however, raises interesting issues concerning indigenous intellectual property rights. Because knowledge of prostratin's antiviral activity originated from ethnobotanical studies with Samoan healers, the AIDS Research Alliance (ARA) and the Government of Samoa agreed that 20 percent of ARA's profit from prostratin will be returned to the Samoan people (*4*). Similarly, Samoa and the University of California, Berkeley, agreed to share equally in commercialization of the prostratin gene sequences (*5*). In the spirit of these previous agreements, we encourage future developers of prostratin analogs for antiviral therapy to negotiate fair and equitable benefits with the Samoan people.

PAUL ALAN COX,[1] HOLLY E. JOHNSON,[1] GAUGAJ TAVANA[2]

[1]Institute for Ethnomedicine, Jackson, WY 83001, USA. [2]National Tropical Botanical Garden, Kalaheo, HI 96741, USA.

References

1. A. Buonaguro *et al.*, *J. Virol.* **78**, 10507 (2004).
2. H. E. Johnson, S. A. Banack, P. A. Cox, abstract presented at the 48th Annual Meeting of the Society for Economic Botany, Lake Forest, IL, 4 to 7 June 2007 (www.econbot.org/_organization_/07_annual_meetings/meetings_by_year/2007/pdf/abstracts/johnson.pdf).
3. M. C. Chang, J. D. Keasling, *Nat. Chem. Biol.* **2**, 674 (2006).
4. P. A. Cox, *Pharm. Biol.* **39**, 33 (2001).
5. A. Coghlan, *New Scientist* **2468**, 8 (2004).

SCIENCE AND RELIGION

For a Redefinition of God

Denis Noble

At a Novartis Foundation meeting 10 years ago on "the limits of reductionism in biology," I presented my work on modeling heart rhythm as an example of downward causation: the idea, which Stuart Kauffman expounds beautifully in *Reinventing the Sacred*, that the whole constrains the parts as much as the parts are necessary to the whole. A colleague objected: "Denis, I would go along with you, but this lets God back into the picture." I disagreed. But Kauffman, now the director of the Institute for Biocomplexity and Informatics at the University of Calgary, would wholeheartedly agree. He is one of the great masters of complexity, an essential component of the systems biology currently in vogue, and readers have found his earlier books (*1*–*3*) thrilling. His new one lives up to that promise. It sparkles from every angle as its author gallops through the relevant science, philosophy, economics, history, ethics, poetry and—well, we had better use the word because Kauffman does: religion.

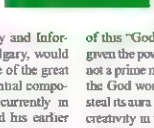

He builds his case step by step, first developing powerful arguments against reductionism. Not only is the world in some sense inexplicable at its lowest level (does anyone really understand quantum mechanics in the sense in which we can say that we understand Newtonian mechanics?), it is also necessarily historically unique in its development at higher levels. There is "ceaseless novelty" in what Kauffman calls the "adjacent present" that cannot be anticipated, just as it would be impossible to anticipate all the future uses to which a new invention might be put. So biology cannot conceivably be reduced to physics. Laplace's calculating demon would not be able to foresee all the future because he would not even be able to specify all the relevant variables.

It is from this phenomenon of "ceaseless creativity" in nature that Kauffman develops his case for reinventing the sacred. His argument is partly based on underlining the awe and humility we must feel at contemplating nature and partly a neat sidestepping of the "ought-is" argument in ethics. For him, ethics have emerged from evolution. They are part of the facts of the world we live in.

Another part of reinventing the sacred comes from the author's conviction that we need to find a new way of expressing human spirituality: "Seeking a new vision of the real world and our place in it has been a central aim of this book: to find common ground between science and religion so that we might collectively reinvent the sacred."

But why should we call any of this "God"? Kauffman's God is not even given the power that the Deists recognize. It is not a prime mover. He feels that "we must use the God word, for my hope is to honorably steal its aura to authorize the sacredness of the creativity in nature." I am sympathetic to this view and, as Kauffman himself notes, there are religions (notably Buddhism) that do not postulate a Creator God and for whom nature is sacred to a high degree.

The weakest part of the book concerns the role of quantum mechanics in the brain. Here Kauffman's principal motivation is to avoid causal closure, a condition in which it would seem that there is no free will. But, my reading of the rest of the book had already convinced me that above certain levels of complexity there is generally no causal closure in nature. I am not sure what quantum mechanics has to contribute to the problem of mind, and the more I read the chapter "The Quantum Brain?" the more I felt convinced that no one really understands quantum mechanics. I don't mean in the sense of understanding the equations—I am sure Kauffman does that. But rather in the sense of understanding what a "quantum mind" would be. As he admits, this is the most "scientifically improbable" of his ideas. Moreover, I don't think the important aspects of his thesis hang on whether his ideas about quantum mind are correct.

The rest of the book is very clearly written. Kauffman is on top of his material. So, could his concept of God as nature's ceaseless creativity be convincing? As he expects, believers in a Creator God will strongly disagree with him, whereas humanists are not likely to adopt a word they have expunged from their language. Yet he is on to something important. Some of the words for "religion" in oriental languages (e.g., *kyō* in Japanese, *jiào* in Chinese, both

CREDIT: BARNEY MAGINNIS/COMIS

Building on creation myths. The Spaniards erected the shrine of Santuario de Chimayó, New Mexico, over a sipapu, a hole sacred to the Pueblo people. (Legend held that sipapus linked the current and lower worlds and that the first people had passed through them.) Seeing such usurpation as "a kind of acknowledgment," Kauffman urges using the word God to gain support for recognizing nature's creativity as sacred.

The reviewer is at the Department of Physiology, Anatomy, and Genetics, Oxford University, Parks Road, Oxford OX1 3PT, UK. E-mail: denis.noble@dpag.ox.ac.uk

usually combined with the word for ancestral) have more of the connotation of teaching—they are also used, for example, in references to teacher and professor. They reveal a semantic frame differing greatly from that familiar to most westerners. I can't help reflecting that Kauffman would have an easier time getting his ideas adopted by religious people outside the three Abrahamic faiths. But these people will likely say that they already have such a religion and do not see why they need anything else. Bringing science and religion together globally in the way that Kauffman wishes is not going to be easy—as other ecumenical movements have repeatedly found—but it is necessary.

References

1. S. A. Kauffman, *The Origins of Order: Self-Organization and Selection in Evolution* (Oxford Univ. Press, New York, 1993).
2. S. A. Kauffman, *At Home in the Universe: The Search for Laws of Self-Organization and Complexity* (Oxford Univ. Press, New York, 1995).
3. S. A. Kauffman, *Investigations* (Oxford Univ. Press, New York, 2000).

10.1126/science.1159912

MICROBIOLOGY

Learning Much from a Bug's Life

Daniel J. Rankin

> Here too are the dreaming landscapes, lunar, derelict. Here too are the masses, the lice of the soil.

So begins "In the Microscope" by the immunologist and poet Miroslav Holub (*1*). Through his microscope's lens, Holub saw "cells, fighters who lay down their lives for a song" and heard "murmuring, the revolt of immense estates." In short, his poem reminds us that all of the ingredients of a good Shakespearean play can be found in the microscopic world.

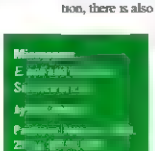

Holub was writing under political oppression in communist Czechoslovakia, and he often took a dark view of the world around him. In *Microcosm: E. coli and the New Science of Life*, Carl Zimmer, a Connecticut-based science writer, paints a rosier picture of his focal organism. The "fighters who lay down their lives" in his book come under the scientific name *Escherichia coli*, an organism that has achieved notoriety thanks to various outbreaks of harmful strains in recent years. However, leafing through the pages of this gripping book, one cannot help but feel pangs of sympathy for this delightful little creature.

Ranging widely across nearly all of contemporary biology, Zimmer presents *E. coli* as a basis from which one can gain a better understanding of almost every facet of biotic life. He moves from the inner workings of the cell, through the social life of *E. coli*, to, in the very last chapter, outer space (where he uses *E. coli* to ask whether life exists on other planets and, if so, what such life may look like).

First impressions never seem to help when looking at microbes. For a long time, scientists did not believe microbes could have sex. The late Joshua Lederberg and colleagues discovered bacterial conjugation, showing that *E. coli* could exchange genes through direct contact with other cells. Not only can *E. coli* have sex but, like higher organisms, it has a rather complex social life. For example, when food is limited, members of a population can signal to one another to enter a stationary phase. The phase improves the chances that at least a few of the members will survive, effectively relying on safety in numbers. However, life is not always so friendly for the star of Zimmer's book. In addition to cooperation, there is also strife in the bacterial world. To compete with other species, or even its own kind, *E. coli* can produce chemical weapons, in the form of antibiotics.

Evolution is never far away from the author's mind. He quotes Charles Darwin's comment that "natural selection will always act with extreme slowness, I fully admit" (*2*). In fact, Darwin would have marveled at *E. coli* and at researchers' ability to use it to confirm many predictions of his theory. Countless laboratory experiments have demonstrated adaptation in the species on time scales short enough for us to observe, and it has played a role in discrediting Lamarckian inheritance.

E. coli has even been presented in defense of evolution itself. The bacterial flagellum, which is rotated to propel the organism, has recently featured in the controversy surrounding intelligent design. Advocates of intelligent design often offer the flagellum as an example of a structure too complex to have evolved through natural selection. Michael Behe testified to that effect for the defense when parents in Dover, Pennsylvania, sued the local school district over the teaching of intelligent design in science classes (*3*). The plaintiff's attorneys countered with scientists who demonstrated how it was possible for the flagellum to have evolved from useful, intermediate structures, even if those structures did not function in bacterial locomotion. Complicated structures such as flagella could therefore have evolved through small evolutionary steps, thus discrediting a central argument used against evolutionary theory.

***E. coli* cluster.** This rod-shaped bacteria was first isolated in 1885, from the diapers of healthy babies, by the German pediatrician Theodor Escherich, who noted the microbe's ability to produce a "massive, luxurious growth."

A large part of the book discusses biotechnology, which owes a lot to *E. coli*. The early days of genetic engineering were fraught with political problems, with many warning of potentially harmful effects for society and the ethical implications of playing God. However, once the benefits for society as a whole became apparent, the science was allowed to proceed. By inserting animal genes into *E. coli*, strains were developed to fill tanks that now pump out gallons of insulin and other drugs every day. As Zimmer notes, *E. coli* genes are now being inserted into animals. For example, researchers have transferred to pigs genes that allow *E. coli* to break down phosphate-bearing compounds, which offers hope that such pigs can one day be used to reduce phosphate pollution from farms.

The reviewer is at the Department of Behavioural Ecology, Institute of Zoology, University of Bern, Wohlenstrasse 50a, CH-3032 Hinterkappelen, Switzerland. E-mail: daniel.rankin@esh.unibe.ch

"The dire warnings," the author writes, "that *E coli* would create tumor plagues and insulin shock epidemics seem quaint today."

A popular science book on *E. coli* may not sound like the most interesting read. However, *Microcosm* is just that. The next time you hear of an outbreak of nasty *E. coli* on the news, spare a thought for this minute creature, which has arguably helped advance humanity far further than any other organism. Not only has it inhabited human guts for as long as we have existed, it has benefited almost all areas of the biosciences, from genetic engineering to evolutionary theory. To really understand life, it seems we must pay close attention to this bug's life.

References

1. M. Hoiab, *Poems Before and After: Collected English Translations* (Bloodaxe Tarset, U.K., 2006).
2. C. Darwin, *On the Origin of Species by Means of Natural Selection* (John Murray, London, 1859).
3. E. Humes, *Monkey Girl: Evolution, Education, Religion, and the Battle for America's Soul* (Ecco, New York, 2007).

10.1126/science.1159301

A TASTE OF THE GONZO SCIENTIST

Scientists Invade Azeroth

A slime-filled sewer deep beneath a city may seem like a strange place to hold a conference, but none of the participants seemed to mind. I was cohosting the first scientific conference (1) held in Azeroth, the virtual world inhabited by millions who play the game World of Warcraft (WoW), and a lively discussion was under way about how to promote data sharing. Virtual worlds such as Azeroth are a treasure trove for psychological, social, and economic research (2). The atmosphere was casual and animated, like the conversations that happen between lectures at a good scientific meeting. But at this conference, the chat was happening on the computer monitors of 200 to 300 people scattered around the globe. The participants were embodied as virtual characters standing in the cavernous chamber, many of them at that moment knee-deep in a green, bubbling pool.

Online
sciencemag.org

For more on this episode, including videos, go to www.gonzoscientist.org

The meeting was organized around three sessions. The first, "Research and World of Warcraft," was chaired by Bonnie Nardi (University of California, Irvine) and Hilde Corneliussen (University of Bergen, Norway). They and three panelists discussed such issues as the potential and pitfalls of using WoW as a laboratory and how to ensure that research subjects give their consent. Following ethical guidelines for research in places like Azeroth may seem trivial now, but the panelists predicted that it will become crucial as the portion of people's lives spent in virtual worlds grows.

Dmitri Williams (University of Southern California) chaired the second session, "Relationships Between WoW and the Real World," which focused mostly on social psychology. It had a reading list as well as working papers put online by the panelists during the meeting. Then participants were introduced to Azeroth's sophisticated gold-based economy, which has a real-world analog fueled by "gold-farmers" who sell their virtual wares for real money.

The closing session, "The Future of Virtual Worlds," was overseen by the conference host, William Sims Bainbridge (U.S. National Science Foundation). The audience joined in a free-for-all forum, with questions ranging from the near-term outlook for the virtual worlds industry to the far-reaching prospects for human immortality in virtual worlds. Azeroth is already dotted with virtual beings who are memorials to real-life people who have died in recent years. "Will our ancestors someday be able to interact with virtual versions of ourselves?" mused Bainbridge.

What happened between the meeting's academic sessions was highly unusual. On the first day, Bainbridge led an anthropological tour across one of Azeroth's vast and dangerous continents. (After conducting over 2000 hours of ethnographic research in this world, Bainbridge knows it better than anyone.) Unfortunately, many of the conference participants were complete newcomers with vulnerable, low-level characters. Although the more powerful characters stayed in the lead, killing monsters along the way, there were a few casualties. Participants on the second day were treated to a concert sung by four banshees in an underground throne room. The third day included a dance that was followed by a massive attack on an enemy fort (which left all the participants dead). This was not your average scientific meeting.

The organizers recorded a transcript of the entire conference—including every comment, question, and answer—and an academic report is planned. Wayne Lutters, a computer scientist (University of Maryland, Baltimore County) who participated, described the conference as "historic." And it has also generated an unexpected byproduct: the first science guild in WoW. Henry Lowood (Stanford University), the guild historian, is helping to create a wiki Web site for the guild that will include scientific forums (both game-related and otherwise), a Facebook-like system for scientists to describe their research (and characters), and a calendar for academic and social events. Visit the guild homepage (3) to learn more or, if you like, to take part.

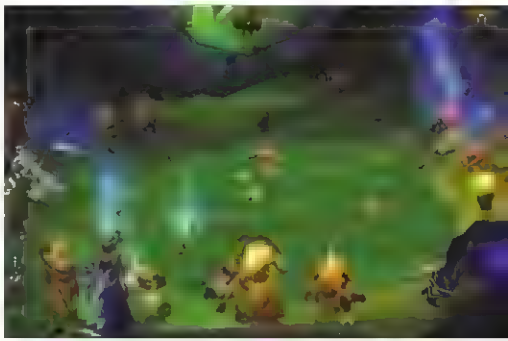

CREDIT: BLIZZARD

References

1. "Convergence of the Real and the Virtual," World of Warcraft, 9 to 11 May 2008.
2. W. S. Bainbridge, *Science* **317**, 472 (2007).
3. www.scienceguild.org.

–JOHN BOHANNON

10.1126/science.1161351

ECONOMICS

The MPG Illusion

Using "miles per gallon" as a measure of fuel efficiency leads people to undervalue the benefits of replacing the most inefficient automobiles.

Richard P. Larrick* and Jack B. Soll

Many people consider fuel efficiency when purchasing a car, hoping to reduce gas consumption and carbon emissions. However, an accurate understanding of fuel efficiency is critical to making an informed decision. We will show that there is a systematic misperception in judging fuel efficiency when it is expressed as miles per gallon (MPG), which is the measure used in the U.S.A. People falsely believe that the amount of gas consumed by an automobile decreases as a linear function of a car's MPG. The actual relationship is curvilinear. Consequently, people underestimate the value of removing the most fuel-inefficient vehicles. We argue that removing the most inefficient vehicles is where policy and popular opinion should be focused and that representing fuel efficiency in terms of amount of gas consumed for a given distance—which is the common representation outside of the United States (e.g., liters per 100 kilometers)—would make the benefits of greater fuel efficiency more transparent (*1*–*3*).

To illustrate these issues, consider the criticism that has been directed at adding hybrid engines to sport utility vehicles (SUVs). In a *New York Times* Op-Ed column, an automotive expert (*4*) has said that hybrid cars are like "fat-free desserts"—they "can make people feel as if they're doing something good, even when they're doing nothing special at all." The writer questions the logic of granting tax incentives to buyers of "a hypothetical hybrid Dodge Durango that gets 14 miles per gallon instead of 12 thanks to its second, electric power source" but not to a "buyer of a conventional, gasoline-powered Honda Civic that gets 40 miles per gallon." The basic argument is correct: The environment would benefit most if all consumers purchased highly efficient cars that get 40 MPG, not 14, and incentives should be tied to achieving such efficiency. An implicit premise in the example, however, is that an improvement from 12 to 14 MPG is negligible. However, the 2 MPG improvement is actually a significant one in terms of reduction in gas consumption. The amount of gas used by a vehicle to drive 10,000 miles at different levels of MPG is shown in the graph above. A car that gets 12 MPG consumes 833 gallons to cover that distance (10,000/12); a car that gets 14 MPG consumes 714 gallons (10,000/14). The roughly 120-gallon reduction in fuel used is larger than the reduction achieved by replacing a car that gets 28 MPG with a car that gets 40 MPG over that distance.

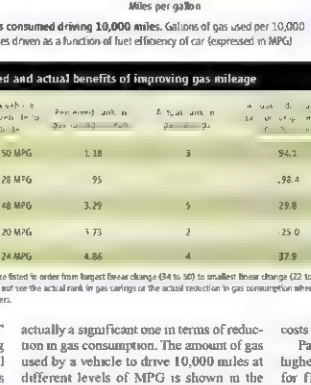

Gas consumed driving 10,000 miles. Gallons of gas used per 10,000 miles driven as a function of fuel efficiency of car (expressed in MPG).

Perceived and actual benefits of improving gas mileage

Change in vehicle pair (old vehicle → new vehicle)*	Perceived rank in gas savings	Actual rank in gas savings	Actual gas savings (gallons per 10,000 miles)
34 MPG to 50 MPG	1.18	3	94.1
18 MPG to 28 MPG	95	1	98.4
42 MPG to 48 MPG	3.29	5	29.8
16 MPG to 20 MPG	3.73	2	25.0
22 MPG to 24 MPG	4.86	4	37.9

*Vehicle pairs are listed in order from largest linear change (34 to 50) to smallest linear change (22 to 24). Participants did not see the actual rank in gas savings or the actual reduction in gas consumption when they gave their answers.

We conducted three experiments to test whether people reason in a linear, but incorrect, fashion about gas mileage. In study 1 (*5*), 77 college students were asked to "assume that a person drives 10,000 miles per year and is contemplating changing from a current vehicle to a new one." They were asked to rank order five pairs of old and new vehicles in order of "their benefit to the environment (i.e., which new car would reduce gas consumption the most compared to the original car)" using 1 for the most beneficial change and 5 for the least beneficial change.

Perceptions of improvement corresponded directly to the linear change in MPG and not to the actual reduction in gas consumption (see table below). Sixty percent of participants ordered the pairs according to linear improvement and 1% according to actual improvement. A third strategy, proportional improvement, was used by 10% of participants (*5*).

Study 2 tested whether the price that people would pay for more efficient vehicles would also show a linear relationship to MPG. College participants (n = 74) were told they had several vehicles from which to choose that were identical except for the efficiency of the engine (*5*). Participants were told to assume "you drive 10,000 miles per year for work, and this total amount cannot be changed. The baseline model gets 15 miles per gallon and costs $20,000."

Participants were then asked to state the highest price they would be willing to pay for five vehicles that varied only in the MPG of their engines. Mean willingness to pay (WTP) showed a clear linear relationship with MPG improvement (see figure, page 1594). The best-fitting strategy for the majority of participants was a linear strategy (62%) followed by a proportional strategy (18%); the actual savings was the best-fitting strategy for only 15% of participants. Participants gave mean WTP values that, compared with expected gas savings,

Fuqua School of Business, Duke University, Durham, NC 27708, USA.

*Author for correspondence. larrick@duke.edu.

significantly undervalued the improvements to 19 and 25 MPG and overvalued the improvement to 55 MPG (6)

Study 3 was designed to test whether the MPG illusion could be decreased if fuel efficiency were framed in terms of gallons per 100 miles (GPM) instead of MPG. The study was presented in an online survey to 171 participants who were drawn from a national subject pool. Participants ranged in age from 18 to 75, with a median age of 35. All participants were given the following scenario (5): "A town maintains a fleet of vehicles for town employee use. It has two types of vehicles. Type A gets 15 miles per gallon. Type B gets 34 miles per gallon. The town has 100 Type A vehicles and 100 Type B vehicles. Each car in the fleet is driven 10,000 miles per year." They were then asked to choose a plan for replacing the original vehicles with corresponding hybrid models if the "overriding goal is to reduce gas consumption of the fleet and thereby reduce harmful environmental consequences."

One group of 78 participants was randomly assigned to a policy choice framed in terms of MPG. They were asked to choose between two options: (option 1) replace the 100 vehicles that get 15 MPG with vehicles that get 19 MPG and (option 2) replace the 100 vehicles that get 34 MPG with vehicles that get 44 MPG. Note that town fuel efficiency is improved more in option 1 (by 14,035 gallons) than in option 2 (by 6,684 gallons). As expected, the majority (75%) of participants in the MPG condition chose option 2, which offers a large gain in MPG but less fuel savings (95% confidence interval (CI) = 65 to 85%).

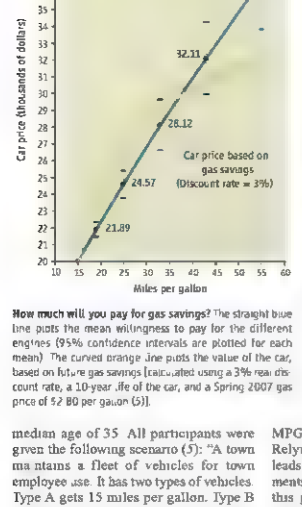

How much will you pay for gas savings? The straight blue line plots the mean willingness to pay for the different engines (95% confidence intervals are plotted for each mean). The curved orange line plots the value of the car, based on future gas savings [calculated using a 3% real discount rate, a 10-year life of the car, and a Spring 2007 gas price of $2.80 per gallon (5)].

Participants in the GPM condition ($n = 93$) were given the same instructions as those in the MPG condition. In addition, they were told that the town "translates miles per gallon into how many gallons are used per 100 miles. Type A vehicles use 6.67 gallons per 100 miles. Type B vehicles use 2.94 gallons per 100 miles." They read the same choice options as used in the MPG condition, including the MPG information, but with an additional stem that translated outcomes into GPM for the hybrid vehicles [(option 1) replace the 100 vehicles that get 6.67 gallons per 100 miles with vehicles that get 5.26 GPM and (option 2) replace the 100 vehicles that get 2.94 gallons per 100 miles with vehicles that get 2.27 GPM]. As expected, the majority of participants (64%) in the GPM frame chose option 1, which offers a small gain in MPG but more fuel savings (CI = 54 to 74%). Overall, the percentage choosing the more fuel-efficient option increased from 25% in the MPG frame to 64% in the GPM frame ($P < 0.01$).

These studies have demonstrated a systematic misunderstanding of MPG as a measure of fuel efficiency. Relying on linear reasoning about MPG leads people to undervalue small improvements on inefficient vehicles. We believe this general misunderstanding of MPG has implications for both public policy and research on environmental decision-making (7–9). From a policy perspective, these results imply that the United States should express fuel efficiency as a ratio of volume of consumption to a unit of distance. Although MPG is useful for estimating the range of a car's gas tank, GPM allows consumers to understand exactly how much gas they are using on a given car trip or in a given year (10–14) and, with additional information, how much carbon they are releasing. GPM also makes cost savings from reduced gas consumption easier to calculate.

Although the current work has focused on misunderstanding the curvilinear relationship between MPG and fuel efficiency, other cognitive processes may also lead people to undervalue small improvements for inefficient cars. For example, if the 50 MPG fuel efficiency of popular small hybrids is used as a standard of comparison, small improvements on inefficient cars (e.g., a 5 MPG improvement from 15 to 20) look like "a drop in the bucket" (15, 16).

The issue of translating car efficiency to gas consumption and carbon emissions is a special case of a general policy problem. People need a common metric to compare the consequences of their activities across a range of daily actions (14, 17). Choosing a more efficient car is just one means to reduce greenhouse gas emissions. Arming consumers with information about the relative greenhouse gas emissions of various activities expressed in a common metric can allow concerned consumers to make beneficial trade-offs in their daily decisions.

References and Notes

1. Decision-makers often focus on the surface attributes of a decision problem and fail to recognize the more fundamental structure (2, 3).
2. C. K. Hsee, F. Yu, J. Zhang, Y. Zhang, *J. Consum. Res.* **30**, 1 (2003).
3. D. Kahneman, S. Frederick, in *Heuristics and Biases: The Psychology of Intuitive Judgment*, T. Gilovich, D. Griffin, D. Kahneman, Eds. (Cambridge Univ. Press, New York, 2002), pp. 49–81.
4. J. L. Kirman, *New York Times*, 16 April 2006, §4, p. 12.
5. Materials, methods, and additional examples and analyses are available as supporting online material (SOM) on *Science* Online.
6. Section IV of the SOM provides additional analyses of WTP versus expected gas savings.
7. J. D. Sterman, L. B. Sweeney, *Clim. Change* **80**, 213 (2007).
8. A. E. Tenbrunsel, K. A. Wade-Benzoni, D. M. Messick, M. H. Bazerman, *Acad. Manag. J.* **43**, 854 (2000).
9. E. U. Weber, *Clim. Change*, **77**, 103 (2006).
10. Section I of the SOM discusses possible GPM measures.
11. Decisions are often improved more by changing the decision context than by trying to improve individual reasoning (12–14).
12. J. Klayman, K. Brown, *Cognition* **49**, 97 (1993).
13. J. W. Payne, J. R. Bettman, D. A. Schkade, *J. Risk Uncertainty*, **19**, 243 (1999).
14. R. H. Thaler, C. R. Sunstein, *Nudge* (Yale Univ. Press, New Haven, CT, 2008).
15. J. Baron, *J. Risk Uncertain.* **14**, 301 (1997).
16. C. Heath, R. P. Larrick, G. Wu, *Cognit. Psychol.* **38**, 79 (1999).
17. J. Baron, *J. Public Policy Market.* **23**, 7 (2004).
18. The authors thank D. T. Robinson for advice on discount rate assumptions in study 3.

10.1126/science.1154983

Supporting Online Material
www.sciencemag.org/cgi/content/full/320/5883/1593/DC1

ATMOSPHERIC SCIENCE

Sprucing Up Greenland

Pollen data suggest that the Greenland ice sheet was much smaller during previous warm periods

Eric J. Steig[1] and Alexander P. Wolfe[2]

How much did the Greenland ice sheet shrink during previous warm episodes of the Pleistocene (from ~1.8 million to ~11,000 years ago)? This question is central to understanding fluctuations in sea level and the future stability of the ice sheet. On page 1622 of this issue, de Vernal and Hillaire-Marcel (*1*) report a record of pollen preserved in marine sediments deposited beyond the ice sheet's margin that sheds considerable new light on the problem.

The Pleistocene was characterized by long periods of extensive Northern Hemisphere glaciation, interrupted by relatively brief interglacials during which continental ice retreated to a few strongholds in the Canadian Arctic and Greenland. During the last interglacial—referred to as marine isotope stage (MIS) 5e—global mean sea level was 4 to 6 m higher than during the current Holocene period (*2*). A substantial fraction of this sea-level rise can be attributed to a smaller Greenland ice sheet (*3*).

The last interglacial is an interesting analog for the future, because the Arctic was several degrees Celsius warmer than during the 20th century (*4*), within the scope of projections for the coming decades. However, the analogy only goes so far, because melting of the Greenland ice sheet during MIS 5e was driven mainly by greater summer insolation, not by increased levels of greenhouse gases. During MIS 11 (three interglacials before MIS 5e), summer insolation was not very different from that during the Holocene (*5*). MIS 11, however, lasted from 425,000 to 375,000 years ago, twice the duration of MIS 5e. This interglacial thus provides a different analog for the future, allowing us to examine what happens to the ice sheet and surrounding land mass when subjected to protracted warmth. MIS 11 cannot easily be studied by looking at ice cores. Any ice this old has long since melted away or has been subject to irreparable thinning and distortion at the base of the ice sheet (*6*). On the other hand, a continuous record exists offshore.

de Vernal and Hillaire-Marcel analyzed a marine sediment core from the Ocean Drilling Program (ODP) site 646, raised from a depth of 3460 m. At this site, sediment has been deposited continuously since at least MIS 17 (*7*). The core contains a rich terrestrial pollen record, because the core is located on the south Greenland continental rise, which captures runoff from the adjacent land mass. Taxa currently extant in southern Greenland are well represented, including spores from mosses and club mosses and pollen from shrub birch and alder. During interglacials, the record is punctuated by marked increases in total pollen concentrations and additional contributions from boreal coniferous trees, namely spruce and pine, neither of which survives in Greenland today. The pollen assemblages differ tremendously between interglacials, with direct implications for the past development of ecosystems in south Greenland. For example, spruce pollen concentrations were three times as high during MIS 13 and 5e, and more than 20 times as high during MIS 11, as during the Holocene. On the other hand, MIS 9 and 7, have unspectacular conifer pollen signatures similar to those in the Holocene.

How can we be sure that spruce grew in southern Greenland during MIS 13, 11, and 5e, and thus that the ice sheet was sufficiently reduced to allow for regional development of boreal forests? The spruce pollen in these interglacial sediments cannot be attributed to enhanced long-distance transport from North America or Europe. Because spruce pollen is far less easily dispersed than pine pollen, long-distance transport would lead to reduced spruce/pine ratios. Instead, increased spruce/pine ratios are found in each warm episode recorded in the core. The exquisite preservation of the spruce grains, and their morphological affinities to Norway spruce, lend further credence to local sources.

There is independent evidence that spruce lived in Greenland in the mid-Pleistocene, in a region now covered by more than 2 km of ice. In 2007, Willerslev *et al.* (*8*) amplified DNA from sediment-rich ice at the base of the Dye 3 ice core, showing not only the presence of spruce but also of pine and yew, consistent with an ancient boreal forest. They could not assign an unambiguous date to the sediments entombing these genetic fossils, but their estimate of between 450,000 and 800,000 years is close enough to MIS 11 to be more than coincidental. Indeed, given current esti-

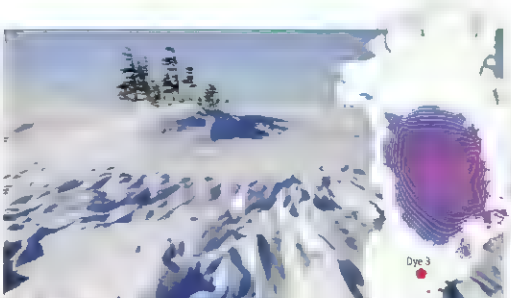

A modern analog. Spruce copses at Churchill, Manitoba, Canada (59°N, 94°W), are an apt modern analog for southern Greenland during interglacial periods MIS 13, 11, and 5e. The inset shows a plausible ice sheet geometry for MIS 11, based on the ice sheet model used in (*3*); contour intervals of ice elevation (blue and purple) are 200 m.

[1]Department of Earth and Space Sciences, University of Washington, Seattle, WA 98195, USA. E-mail: steig@ess.washington.edu [2]Department of Earth and Atmospheric Sciences, University of Alberta, Edmonton, AB T6G 2E3, Canada. E-mail: awolfe@ualberta.ca

mates of DNA degradation kinetics (*9*), the results reported by de Vernal and Hillaire-Marcel point to MIS 11 as the most parsimonious age for the Dye 3 sediments.

Evidently, the Greenland ice sheet was smaller during MIS 5e and 13 than it is today, but ice probably still covered the location of the Dye 3 ice core. During MIS 11, deglaciation must have been much more extensive. The sixfold increase in spruce pollen abundance during MIS 11 relative to MIS 5e and 13 is unlikely to reflect minor differences in ice sheet size. Spruce is absent in Greenland today not because of the high latitude but because there is no land sufficiently removed from the hostile microclimate at the ice sheet margin. Thus, the Dye 3 area must have been completely deglaciated during MIS 11. For that to occur, most of southern Greenland must have been ice free (see the figure).

It seems to have taken some time for the extensive spruce populations of MIS 11 to develop. Global temperatures had risen to Holocene levels by ~425,000 years ago, but spruce abundance increased most dramatically 10,000 to 20,000 years later (*1*). This lag is probably not associated with slow rates of forest propagation; spruce can expand northward at rates of more than 100 km per century as climate warms (*10*). Instead, the data suggest that the ice sheet retreated slowly. This would not be surprising. Once the ice retreats beyond the heads of fjords, removing the possibility of glacier calving, the rate of volume loss is likely to decrease.

It was not exceptional warmth, but time, that diminished the size of the Greenland ice sheet during MIS 11, leaving vast tracts of land available for plant colonization. In the future, the Arctic will likely become warmer than it was during MIS 5e and will stay warmer for thousands of years if greenhouse gas concentrations continue to rise over the next century. The Greenland ice sheet will then have to contend with both time and warmth.

References

1. A. de Vernal, C. Hillaire-Marcel, *Science* **320**, 1622 (2008)
2. C. M. Stirling *et al.*, *Earth Planet. Sci. Lett.* **160**, 745 (1998).
3. B. L. Otto-Bliesner *et al.*, *Science* **311**, 1751 (2006).
4. CAPE Last Interglacial Project members, *Quat. Sci. Rev.* **25**, 1383 (2006).
5. D. Raynaud *et al.*, *Nature* **436**, 39–40 (2005).
6. North Greenland Ice Core Project members, *Nature* **161**, 147 (2004).
7. C. Hillaire-Marcel, A. de Vernal, G. Bilodeau, A. J. Weaver, *Nature* **410**, 1073 (2001).
8. E. Wolff *et al.*, *Science* **317**, 111 (2007).
9. E. Willerslev, A. Cooper, *Proc. R. Soc. London B* **272**, 3 (2005).
10. G. M. MacDonald *et al.*, *Nature* **361**, 243 (1993).

10.1126/science.1160004

CLIMATE CHANGE

A Matter of Firn

Estimating ice sheet mass changes from elevation surveys requires adjustments for snow density variations at the ice sheet surface.

Kurt M. Cuffey

The Antarctic Ice Sheet is vast, about 3000 km wide and up to 4.5 km thick. If it melted completely, sea level would rise by 70 m worldwide. Such a large change is not plausible, except on geologic time scales, but a loss of even 5% of the total mass would radically transform Earth's coastal regions. How has the ice sheet changed in recent years? Measuring the mass change of such a large feature is difficult, but there are methods available for the task (see the figure) (*1*–*3*). On page 1626 of this issue, Helsen *et al.* (*4*) provide key information that will substantially improve some of these important analyses.

Consider one method that is simple in concept. Map the surface elevations everywhere on the ice sheet, then repeat the process some time later. Determine the difference between the two maps, correct for changes in the elevation of the underlying lithosphere, and integrate over the area; the result is the volume change. Multiply this by the density of ice to find the mass change, and celebrate.

Alas, your celebration is premature; the density of the ice sheet is not a constant. The density varies by a factor of 3 from new snow to solid ice, and most of the ice sheet is mantled with a layer of old snow, called firn, that is tens of meters thick (*5*). This layer densifies over time, at a rate that depends on the temperature and the weight of new snow added to its surface. As Helsen *et al.* report, variations of the firn layer's thickness, over years and decades, complicate assessments of Antarctic mass changes based on maps of elevation. When snowfall increases or temperature decreases, the firn layer thickens. The authors show that, in East Antarctica, such effects con-

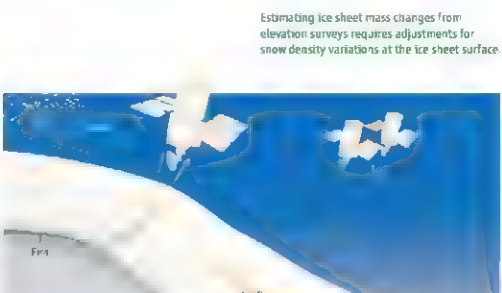

How to track mass changes. Changes in the mass of the Antarctic ice sheets can be measured by subtracting the melt and ice flow from the total snowfall, by sensing changes in the strength of gravity using pairs of satellites, or by repeat mapping of surface elevations from satellites. Helsen *et al.* show that, in the repeated-mapping method, a correction must be made for changes in the density of the firn layer on the ice sheet surface.

CREDIT: ADAPTED BY N. MUELVEY/SCIENCE

Department of Geography, University of California, Berkeley, CA 94720, USA. E-mail: kcuffey@berkeley.edu

tribute as much to recent measured elevation changes as do the mass changes of interest.

Measurements of contemporary changes are essential for understanding what will happen to the Antarctic Ice Sheet as the planet warms. On one hand, warming will increase the water content of the polar atmosphere, and so increase snowfall on the ice sheet's vast interior. On the other hand, warmer ocean waters and increased summer air temperatures will erode the floating ice shelves fringing the continent, and so increase the discharge of ice to the coast, where it is lost as icebergs. This chain of processes now operates on the Antarctic Peninsula (*6*), the one part of Antarctica that has strongly warmed over the last several decades. And warming ocean waters are likely responsible for similar events in West Antarctica, where the giant ice streams flowing into the Amundsen Sea are accelerating, causing the ice sheet to thin (*7*). The region of thinning extends hundreds of kilometers inland.

In the Amundsen Sea region, the ice sheet rests in a basin that is more than 1 km below sea level. The boundary between grounded and floating ice is retreating into the basin, and the water depth at this boundary is thus increasing. Studies of the tidewater glaciers of southern Alaska have shown that a strong positive feedback operates in such a situation (*8*), thinning of the ice brings more of the glacier close to flotation, which increases the flow, thinning, and rate of retreat. This process caused the ice in Glacier Bay, Alaska, to retreat more than 80 km in the last century. A similar fate may await large regions of Antarctica (*9*).

Will increased snowfall come to the rescue? Climate models suggest that snowfall on Antarctica will increase by about 5% for every degree centrigrade of warming (*10*). Most likely, the ice sheet interior will thicken through increased snowfall even while the coastal regions are diminishing. But these processes operate at different time scales, and one cannot assume that their effects on sea level will cancel one another.

These processes cannot yet be predicted with confidence, and observations are essential. The combined effects of snowfall and ice flow on the ice sheet's mass can be determined by using satellite-based sensors for repeated mappings of surface elevations—as long as changes of firn density are taken into account. Helsen *et al.* reinterpret satellite data from the period 1995 to 2003 (*2*) by applying a model of the firn densification process, forced by climate data. Using meteorological models to derive snowfall and temperature patterns, the authors estimate density changes everywhere on the ice sheet. They show convincingly that such changes are a large part of the elevation signal.

Their analysis demonstrates that the declining elevations observed in the Amundsen Sea region do indeed reflect a significant loss of mass from the West Antarctic Ice Sheet. A second result is that the interior of East Antarctica is gaining mass. By how much is not clear, however, and this uncertainty strikes me as a particularly important result of the analysis. The correction for firn thickness changes is substantial. Unfortunately, calculating the correction accurately requires a long history of climate variations. In their analysis of the entire ice sheet, Helsen *et al.* use a 25-year record from meteorological analyses. For a few locations, they can also use longer histories from ice-core data. Results from the longer and shorter histories are different in Wilkes Land, a region of East Antarctica where the ice sheet is growing. The longer history provides the better estimate of firn thickness changes and implies a much smaller rate of ice sheet growth than does the shorter history.

Thus, even with explicit accounting for firn density variations, the elevation data cannot yet tell us by how much the mass of the East Antarctic ice sheet is changing. To do so appears to require a blending of the elevation data and firn models with longer-term climate histories from ice cores. This is an important task ahead. There are other ways to estimate Antarctica's changing mass: by calculating the difference between the total fluxes into and out of the ice sheet (*1*), and by monitoring the regional gravity field (*3*). These methods face difficulties of their own, however, and elevation measurements are essential for providing a complementary perspective on Antarctica's evolution in the coming decades.

References

1. E. Rignot *et al.*, *Ant. Geosci.* **1**, 106 (2008).
2. C. H. Davis *et al.*, *Science* **308**, 1898 (2005).
3. I. Velicogna, J. Wahr, *Science* **311**, 1754 (2006).
4. M. M. Helsen *et al.*, *Science* **320**, 1626 (2008); published online 29 May 2008 (10.1126/science.1153894).
5. W. S. B. Paterson, *The Physics of Glaciers* (Pergamon, Oxford, ed. 3, 1994).
6. E. Rignot *et al.*, *Geophys. Res. Lett.* **31**, L18401 (2004).
7. A. Shepherd, D. Wingham, E. Rignot, *Geophys. Res. Lett.* **31**, L23402 (2004).
8. M. F. Meier, A. Post, *J. Geophys. Res.* **92**, 9051 (1987).
9. J. H. Mercer, *Nature* **271**, 321 (1978).
10. J. M. Gregory, P. Huybrechts, *Philos. Trans. R. Soc. A.* **364**, 1709 (2006).

Published online 29 May 2008.
10.1126/science.1158663
Include this information when citing this paper.

NEUROSCIENCE

Imaging Astrocyte Activity

Fred Wolf[1] and Frank Kirchhoff[2]

Astrocytes, like neurons, respond to visual stimuli, affecting vascular dynamics in the brain that provide the basis for imaging techniques.

Astrocytes are the most abundant type of glial cell in the mammalian central nervous system. They are not only metabolically coupled to neighboring neurons but also communicate with them through signals (neurotransmitters) that were once considered a language exclusive to neurons. The generation of neurons from embryonic glia has also garnered recent attention. Yet, without in vivo experiments, the role of astrocytes in brain function has not been clear. On page 1638 in this issue, Schummers *et al.* (*1*) show that astrocyte activity is functionally coupled to neuronal activity with unanticipated spatial specificity. This suggests that the quality and spatial resolution of noninvasive-imaging techniques that assess brain activity, including functional magnetic resonance imaging, reflect the responses of both cell populations in the brain.

Neurons in the mammalian visual cortex are organized into orientation columns, which consist of neurons that extend vertically through the cortex and respond to visual stimuli of the same orientation (*2*). Columns encoding the complete set of all stimulus orientations are organized around so-called pinwheel centers like the spokes of a wheel (*3*). Remote from these centers, neighboring neurons are activated by stimuli of the same orientation. However, in pinwheel centers, neighboring neurons are selective for very dissimilar orientations, but still form a highly ordered orientation map of neurons.

[1]Max Planck Institute for Dynamics and Self-Organization and Bernstein Center for Computational Neuroscience, Göttingen, Germany. [2]Max Planck Institute of Experimental Medicine and DFG Research Center for Molecular Physiology of the Brain, Göttingen, Germany. E-mail: kirchhoff@em.mpg.de

Schummers *et al* exploit this radial structure, which is highly precise at the level of single cells (*4*), to probe the specificity of neuron-astrocyte interactions.

To investigate whether and how astrocytes respond to visual stimuli, Schummers *et al* examined selected regions in the visual cortex of the ferret by combining intrinsic signal optical imaging (*5*) and high-resolution two-photon laser-scanning microscopy of calcium signals (*6*). The authors first visualized the organization of orientation maps over the cortical surface and then examined selected regions, a few hundred micrometers in diameter, to assess how the responses of individual astrocytes and neurons are organized with single-cell precision. Thousands of cortical cells in these selected regions were labeled with a green fluorescent calcium indicator, whereas astrocytes were labeled with a red fluorescent dye. The authors then simultaneously recorded calcium signals in neurons and astrocytes that were evoked by visual stimuli of different orientations and spatial frequencies.

Presenting a ferret with appropriate visual stimuli elicited similar transient calcium signals in neurons and astrocytes in specific regions of the visual cortex, indicating that both cells types in the same vicinity are organized in the same orientation map. The astrocyte calcium transient was delayed a few seconds compared to that in neurons, corresponding to the time it takes neurotransmitters to be released from neurons and activate cognate receptors in astrocytes (*7*, *8*). But three observations were wholly unexpected. Local injection of *threo*-β-benzyloxyaspartic acid, which blocks neurotransmitter (glutamate) transport in astrocytes, not only reduced the response of astrocytes to a visual stimulus, but increased the neuronal response. The intrinsic optical signals—that is, changes in blood vessel volume (hemodyamic changes) reflecting altered circulation—were nearly abolished. After decades of hemodynamic brain imaging, we are finally able to visualize the cellular mediator of vascular responses in action. Stimulus-evoked neuronal activity is transferred to the hemodynamic changes recorded by noninvasive imaging. Other factors, such as the organization and hydrodynamics of the cortical blood vessel network (*10*), or potential optical anisotropies of the cortical tissue, may also contribute. The results of Schummers *et al* call for a comprehensive reevaluation of the spatial resolution of optical imaging methods.

Schummers *et al* consider three possible explanations for the enhanced tuning of astrocytes compared with that of their connected neurons. The threshold level of

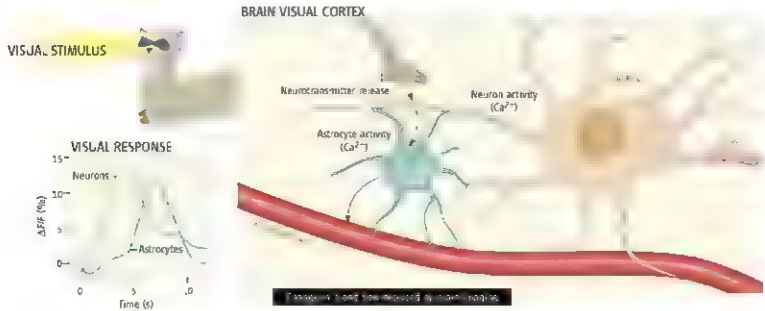

Astrocyte as mediator. In response to a visual stimulus, neuronal activity (measured as change in intracellular calcium concentration) in the cortex is transferred to adjacent astrocytes through the release of neurotransmitters. The calcium transients in astrocytes are similar to those in neurons, but delayed (inset graph is derived from (*1*)). Astrocyte activity affects local blood flow, which can be assessed by noninvasive visual techniques such as functional magnetic resonance imaging.

adjacent astrocytes, which subsequently modulate local blood flow (see the figure).

The other two observations involve the tuning of astrocyte activity in orientation domains and at pinwheel centers. Surprisingly, astrocytes in both regions are more sharply tuned in their response to stimuli than are adjacent neurons. Moreover, astrocytes in pinwheel centers display different orientation preferences compared to many of their immediate neighbors (within tens of micrometers away). The latter finding is particularly intriguing given that innervating synaptic activity adjacent to both astrocytes and neurons showed only weak or no orientation tuning.

In contrast to theoretically predicted limitations and large systematic errors intrinsic to optical signal imaging (*9*), Schummers *et al.* find that assessment of pinwheel centers by two-photon laser-scanning microscopy and optical signal recording generally coincide. The highly tuned activity patterns of astrocytes may improve the spatial resolution of presynaptic activity (in neurons that respond to a visual stimulus and signal to other neurons and astrocytes) that must be overcome to release neurotransmitters (and thus induce a calcium response in associated cells) may differ between astrocytes and neurons. Alternatively, the field of astrocytes that is influenced by neurotransmitter release (so-called receptive field) may be smaller than that of neighboring neurons. Finally, astrocytes may sample presynaptic activity along their anatomical extensions with different preferences.

The idea of astrocytes as individual cells with unique response patterns stands in sharp contrast to the long-standing view that astrocytes form a continuous syncytium in the brain. Indeed, other studies show that some astrocytes may not belong to a labeled syncytium (*11*) and that in the somatosensory cortex, astrocyte networks are restricted to individual barrel fields (*12*). One explanation for the individualistic nature of the astrocytes is that neuronal activity modulates and poten-

CREDIT: ADAPTED BY P. HUEY/*SCIENCE*

tially uncouples the astrocyte syncytium. Identifying the molecular mechanism of astrocyte coupling through direct cellular connections (gap junctions) and its physiological modulators will be a challenge. A less exciting possibility is that the anesthetics used in the imaging experiments by Schummers *et al.* may have blocked gap junctions. Future experiments in awake animals should clarify this.

References and Notes

1. J. Schummers, H. Yu, M. Sur, *Science* **320**, 1638 (2008).
2. D. H. Hubel, T. N. Wiesel, *Proc. R. Soc. London B Biol. Sci.* **198**, 1 (1977).
3. T. Bonhoeffer, A. Grinvald, *Nature* **353**, 429 (1991).
4. K. Obata *et al.*, *Nature* **442**, 920 (2006).
5. A. Grinvald *et al.*, in *Modern Techniques in Neuroscience Research*, U. Windhorst, H. Johansson, Eds. (Springer, New York, 1999), pp. 893–969.
6. J. M. Kerr, W. Denk, *Nat. Rev. Neurosci.* **9**, 195 (2008).
7. L. Pasti, A. Volterra, T. Pozzan, G. Carmignoto, *J. Neurosci.* **17**, 7817 (1997).
8. M. D'Ascenzo *et al.*, *Proc. Natl. Acad. Sci. U.S.A.* **104**, 1995 (2007).
9. J. R. Pobimen, D. Grandpierre, R. J. Wood, E. Schmutz, *Proc. Natl. Acad. Sci. U.S.A.* **102**, 4158 (2005).
10. N. Nishimura, C. B. Schaffer, B. Friedman, P. D. Lyden, D. Kleinfeld, *Proc. Natl. Acad. Sci. U.S.A.* **104**, 365 (2007).
11. V. Houades *et al.*, *Neuron Glia Biol.* **2**, 3 (2006).
12. V. Houades, A. Koulakoff, P. Ezan, C. Seif, C. Giaume, *J. Neurosci.* **28**, 5207 (2008).

13. We acknowledge support by the Max Planck Society.

10.1126/science.1160122

MICROBIOLOGY

How Bacteria Change Gear

Bacterial motility is arrested when a protein that acts as a clutch disables rotation of the flagellar motor

Richard M. Berry[1] and Judith P. Armitage[2]

Many species of bacteria form biofilms, slimy carpets a fraction of a millimeter thick that appear on rocks, leaves, pipes, teeth—pretty much any place that has a supply of nutrients and water. Cells must first attach to a surface, which in many species requires swimming propelled by rotating helical flagella (*1*). Two things typically happen next. Cells stop expressing genes that encode components of the flagellum, and they secrete a sticky matrix of polysaccharides that holds them together on the surface (*2*). Once at a surface, swimming may be a hindrance rather than a help, and an inverse relationship between swimming and attachment has been seen in many diverse species (*3*). However, the molecular details underlying this arrest in motility have not been fleshed out. Are flagella ejected or dismantled? If not, do they keep rotating until they are jammed by the newly formed matrix? On page 1636 of this issue, Blair *et al.* (*4*) show that in the bacterium *Bacillus subtilis* the link between swimming and matrix formation is more subtle than either of these two extremes.

The flagellar motor in bacteria consists of a rotor ~45 nm in diameter that spins at several hundred revolutions per second, surrounded and pushed by a ring of protein complexes anchored to the cell wall and powered by an ionic current across the cytoplasmic membrane (see the figure). It is connected to a propeller consisting of a helical filament that extends for many micrometers outside the cell. In *B. subtilis*, motility and matrix formation are linked by SmrR, a protein that upregulates expression of flagellar genes and down-regulates expression of matrix-forming genes. Deletion of the *smrR* gene causes cells to form biofilm-like aggregates (*5*).

Blair *et al.* used fluorescent labels to show that flagellar filaments do not rotate in these aggregates. Furthermore, these bacteria do not swim even in the absence of a gene that is needed for matrix formation. A search for mutations that allow swimming without *smrR* revealed the off-switch for rotation. EpsE, a putative glycosyltransferase protein involved in building biofilms. The *epsE* gene is not found with other flagellar genes, but in an operon that encodes the proteins that

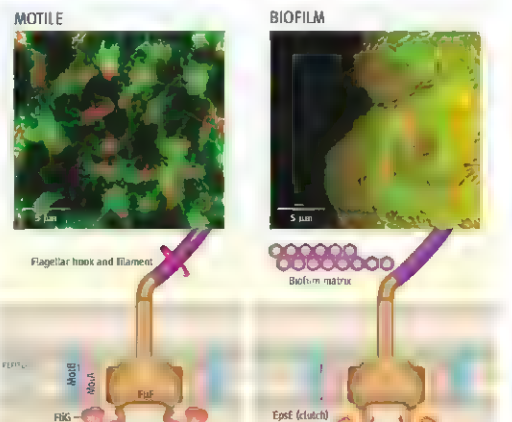

Motor works. A schematic of the *B. subtilis* rotary flagellar motor is shown. Motile cells are powered by interaction of the FliG protein with the MotA/B complex (which generates torque). The protein EpsE acts as a molecular clutch to disengage the rotary flagellar motor, leaving the flagellum intact but unpowered. This shuts down motility and facilitates biofilm formation. Fluorescence microscopy photos of *B. subtilis* show bacterial membranes in red and flagella in green, as described in (*4*). FliM and FliF are motor proteins.

CREDIT (PHOTO): BLAIR AND D'ASENZO

Department of Physics, Clarendon Lab, University of Oxford, Oxford OX1 3PU, UK. [2]Department of Biochemistry & Oxford Centre for Integrative Systems Biology, University of Oxford, Oxford OX1 3QU, UK. E-mail: rberry1@physics.ox.ac.uk

make the matrix and is repressed by SinR

How does EpsE work? A search for mutants that could swim even with EpsE expressed found several mutations in *flhG*, a gene distant from the matrix-encoding operon that codes for a protein involved in torque generation in the flagellar rotor. Induced expression of EpsE in *B. subtilis* stopped cell motility. Fluorescent-labeled EpsE localized at spots corresponding to individual motors, suggesting direct interaction with FlhG, but not in cells with the mutations rendering FlhG insensitive to EpsE.

To determine whether EpsE acts as a brake that locks the motor, or a clutch that leaves the rotor freely spinning, Blair *et al.* tethered bacteria to a substrate by their filaments and observed rotation of the cell bodies around single flagellar motors. Under the influence of EpsE, cells stopped spinning but continued to undergo free rotational Brownian motion, indicating a clutch mechanism.

The direct inhibition of motor rotation by EpsE represents a newly discovered control mechanism for bacterial swimming. Bacterial flagella are large protein complexes that require about 40 to 50 genes to assemble (*6*). Thus, the most obvious advantage of the EpsE mechanism over transcriptional control of flagellar genes is speed. In *B. subtilis*, only one protein, EpsE, needs to be expressed to stop the motor. Presumably, this is important if cells are to stay put in the early stages of biofilm formation. However, the advantages of a clutch over a brake mechanism are not so clear. Perhaps free rotation of flagella—or, alternatively, reduced motility during the transition to the EpsE-inhibited state—is important for the formation of well-structured biofilms (*7*). Or maybe a clutch is simply easier to make than a brake.

Whether this is a universal mechanism or a peculiarity of *B. subtilis* remains to be discovered, as do the details of how the clutch works and how it helps biofilm formation. More experiments like this are needed, not just to find genes and proteins, but to learn what they do and how.

References

1. K. P. Lemon, D. E. Higgins, R. Kolter, *J. Bacteriol.* **189**, 4418 (2007).
2. S. S. Branda, S. Vik, L. Friedman, R. Kolter, *Trends Microbiol.* **13**, 20 (2005).
3. R. Kolter, E. P. Greenberg, *Nature* **441**, 300 (2006).
4. K. M. Blair, L. Turner, J. T. Winkelman, H. C. Berg, D. B. Kearns, *Science* **320**, 1636 (2008).
5. D. B. Kearns, F. Chu, S. S. Branda, R. Kolter, R. Losick, *Mol. Microbiol.* **55**, 739 (2005).
6. R. M. Macnab, *Annu. Rev. Microbiol.* **57**, 77 (2003).
7. T. K. Wood, A. F. González Barrios, M. Herzberg, J. Lee, *Appl. Microbiol. Biotechnol.* **72**, 361 (2006).

10.1126/science.1160444

GEOCHEMISTRY

What Drives Iron Isotope Fractionation in Magma?

Unlike other metals, magmatic melting and recrystallization fractionate iron isotopes, possibly because of the different oxidation states of iron.

Stefan Weyer

Universität Frankfurt, Institut für Geowissenschaften, Altenhöfer Allee 1, 60431 Frankfurt, Germany. E-mail: stefan.weyer@em.uni-frankfurt.de

The isotope composition of natural material can vary, either through the decay of a radioactive parent that results in radiogenic ingrowth of a particular isotope, or as a product of chemical reactions driven by physical changes, for example, during the interactions between biosphere, hydrosphere, and rocks (*1*). Stable-isotope fractionation can reach levels of several percent for light elements, such as hydrogen, carbon, nitrogen, oxygen, or sulfur. However, the magnitude of isotope fractionation drastically decreases with the nuclear mass M (as $\sim 1/M^2$) and also with temperature. Accordingly, magmatic fractionation of (heavy) metal isotopes was long considered to be insignificant. Early studies on samples that formed at high temperatures, such as meteorites, used the isotopic composition of metals [such as iron (Fe), copper, and others] to detect heterogeneities from the origin of our solar system or to address processes of planetary accretion [see, for example, (*2*–*4*)]. However, the study by Teng *et al.* on page 1620 in this issue (*5*) strongly indicates that Fe isotope fractionation during magmatic differentiation needs to be considered when investigating planetary materials.

A remarkable range of Fe-isotope variations [on the order of ≈1 per mil (‰)] in high-temperature environments, such as Earth's mantle, was first observed by Williams *et al.* (*6*, *7*). Their findings could not be explained by the recycling of material into the mantle that had isotopically fractionated previously during low-temperature processes on Earth's surface. Rather, their results indicated that these isotopic variations in the mantle were produced by metasomatic processes, in which alteration is driven by interactions of the mantle with small amounts of melts or fluids.

Subsequently, Weyer *et al.* (*8*, *9*) observed that Fe appears to be isotopically lighter in Earth's mantle than in the crust, by ~0.1‰. Additionally, Weyer and Ionov (*10*) observed that in several suites of mantle rocks, Fe-isotope fractionation was coupled with the amount of melt that was extracted from these rocks.

These findings indicated that Fe isotopes can fractionate during partial melting in the mantle, at temperatures of 1200°C or higher (see the figure). However, because most mantle rocks that were brought to Earth's surface originate from the uppermost mantle, which is commonly modified by fluids and recycled material, it was still highly debated whether these isotopic differences between mantle and crust (and isotopic trends in the mantle) stem from partial melting or from metasomatic processes (*8*, *11*, *12*). This question is intriguing, because isotope fractionation during magmatic processes has not yet been observed for any other metal.

Teng *et al.* now provide convincing evidence that Fe isotopes fractionate during magmatic differentiation. Because mantle rocks in equilibrium with melt are difficult to find, these authors studied the opposite process, the fractional crystallization of olivine from a magma. They investigated the Fe-isotope composition of a suite of basalts from a lava lake in Hawaii and that of corresponding olivine grains that crystallized from the lava. They observed that Fe in basalts becomes isotopically heavier as more olivine has crystallized, and that olivines are always isotopically lighter than the coexisting basaltic melts from which they formed (see the figure).

Studies similar to the investigations of Teng *et al.* have been performed already for lighter metal isotope systems, such as lithium (Li) and magnesium (Mg) (*13*, *14*). However, no isotopic differences between basalts and olivine crystals were observed. Why do the isotopes of Fe fractionate during magmatic

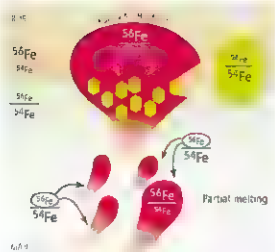

Fates of iron isotopes. Schematic of Fe-isotope fractionation during magmatic processes. During partial melting in the mantle, the heavy Fe isotopes preferentially enter the melt, resulting in high $^{56}Fe/^{54}Fe$ in melts and the crust, and low $^{56}Fe/^{54}Fe$ in the depleted mantle (the latter does not differ much from that of the bulk silicate Earth, for mass balance reasons). Likewise, light Fe isotopes preferentially enter olivine during fractional crystallization, resulting in low $^{56}Fe/^{54}Fe$ in the crystals and increasingly higher $^{56}Fe/^{54}Fe$ in the remaining melt. Fractional crystallization of magnetite has the opposite effect, however (15).

processes, when other metal ions do not? There is no definitive answer to this question yet. However, in contrast to Li and Mg, Fe occurs in two different oxidation states in basalts (Fe^{2+} and Fe^{3+}). Only Fe^{2+} fits into the olivine structure, whereas Fe^{3+} preferentially stays in the melt. Potentially, this different partitioning of Fe species leads to measurable fractionation of their isotopes. Future experimental studies may provide the answer to this question, and also resolve whether this isotope fractionation occurs as an equilibrium or kinetic process.

In addition, because olivine is the most abundant mineral in the upper mantle and is the major host for Fe, we can speculate that Fe-isotope fractionation during melting in the mantle must occur as well. Indeed, the direction of isotope fractionation between olivine and melt during fractional crystallization agrees with that earlier predicted to occur during partial melting (*8*–*10*); that is, olivine and mantle rocks are isotopically lighter than basalt.

These findings of magmatic Fe-isotope fractionation open new possibilities for studying magmatic processes on Earth and other planets. Future studies may link the small differences we are observing in the Fe-isotope composition of materials from different planets—for example, the apparently heavier Fe-isotope compositions of lunar and terrestrial basalts compared to those from the planets Mars and Vesta (*3*, *8*, *9*)—to their respective conditions during planetary differentiation.

References

1. H. C. Urey, *J. Chem. Soc.* **1947**, 562 (1947).
2. J. D. Muck, D. Ben Othman, J. A. Bartat, F. Albarede, *Geochim. Cosmochim. Acta* **67**, 143 (2003).
3. F. Poitrasson, A. Halliday, D. Lee, S. Levasseur, N. Teutsch, *Earth Planet. Sci. Lett.* **223**, 253 (2004).
4. X.-K. Zhu, Y. Guo, R. K. O'Nions, E. D. Young, H. D. Ash, *Nature* **412**, 311 (2001).
5. F.-Z. Teng, N. Caughran, R. T. Helz, *Science* **320**, 1620 (2008).
6. H. Williams *et al.*, *Science* **304**, 1656 (2004).
7. H. Williams *et al.*, *Earth Planet. Sci. Lett.* **235**, 435 (2005).
8. S. Weyer *et al.*, *Earth Planet. Sci. Lett.* **256**, 638 (2007).
9. S. Weyer *et al.*, *Earth Planet. Sci. Lett.* **240**, 251 (2005).
10. S. Weyer, D. A. Ionov, *Earth Planet. Sci. Lett.* **259**, 119 (2007).
11. B. L. Beard, C. M. Johnson, *Earth Planet. Sci. Lett.* **256**, 633 (2007).
12. R. Schoenberg, F. von Blanckenburg, *Earth Planet. Sci. Lett.* **252**, 342 (2006).
13. F. Z. Teng, M. Wadhwa, R. T. Helz, *Earth Planet. Sci. Lett.* **261**, 84 (2007).
14. P. B. Tomascak, F. Tera, R. T. Helz, R. J. Walker, *Geochim. Cosmochim. Acta* **63**, 907 (1999).
15. A. Shahar, E. D. Young, C. E. Manning, *Earth Planet. Sci. Lett.* **268**, 330 (2008).

10.1126/science.1160204

APPLIED PHYSICS

Diamond for Quantum Computing

Optically active defects in diamonds are promising candidates for the building blocks of quantum computers.

Steven Prawer and Andrew D. Greentree

For the technologist seeking to build devices that take advantage of the quantum mechanical properties of coherence and entanglement, diamond looks to be the ideal material. Single-crystal diamond has long held allure as a gemstone, and its extreme electrical, optical, and mechanical properties have already found applications such as heat spreaders, optical windows, electrodes for electrochemistry, high-energy particle detectors, dosimeters, and biosensors. But it is in the quantum realm that diamond truly stands apart, its optical properties tailor-made for the fabrication of the building blocks of new quantum technologies. The optical centers in diamond offer access to isolated quantum systems that can be controlled at room temperature.

A color center is an impurity or defect in a crystal and is responsible for the colors of emeralds and rubies. The color center most used in diamond is the negatively charged nitrogen vacancy (NV) center. These optically active centers, consisting of a substitutional nitrogen atom next to a missing carbon atom (see the figure, left panel), are so bright that they can be detected individually with conventional microscopy. Because the ground state shines more brightly than the excited state, the state of the NV center can be read out. Resonant microwave pulses allow full quantum control of the state of the center.

These properties have enabled the construction of the most basic building block of a quantum processor, the quantum bit or qubit that is operable at room temperature. This is revolutionary in terms of solid-state quantum computing, where the usual temperature scales being discussed are fractions of a kelvin. The time required to manipulate the state of the qubit is brief (tens of nanoseconds), and the measured room-temperature decoherence rate is measured to be 0.35 ms (*1*), meaning that some 10^4 operations can be performed before decoherence takes over and the state is lost. Demonstrations of multiqubit couplings (albeit in a nonscalable design) (*1*–*3*) show promise for building small quantum memories and other few-qubit protocols.

When a single atom deexcites, it emits a single photon, and these photons can be used for a number of applications including quantum metrology, imaging, and ultrasecure communications using quantum key distribution (QKD). The NV centers in diamond mimic these single atoms, displaying photostable

School of Physics, University of Melbourne, Melbourne, Victoria 3010, Australia. E-mail: sprawer@unimelb.edu.au; a.greentree@unimelb.edu.au

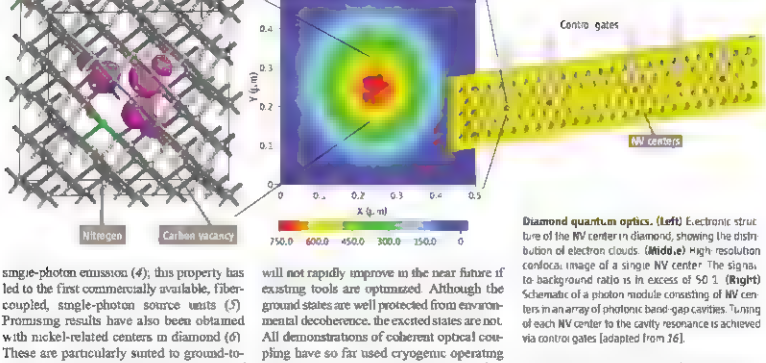

Diamond quantum optics. (Left) Electronic structure of the NV center in diamond, showing the distribution of electron clouds. **(Middle)** High-resolution confocal image of a single NV center. The signal-to-background ratio is in excess of 50:1. **(Right)** Schematic of a photon module consisting of NV centers in an array of photonic band-gap cavities. Tuning of each NV center to the cavity resonance is achieved via control gates [adapted from *16*].

single-photon emission (*4*); this property has led to the first commercially available, fiber-coupled, single-photon source units (*5*). Promising results have also been obtained with nickel-related centers in diamond (*6*). These are particularly suited to ground-to-satellite secure communications because of their longer wavelength. There are many other optical centers in diamond, and the race to find the "best" center is on.

Given these demonstrations of quantum-state readout, coherent manipulation, and quantum storage, why have devices not moved beyond single-photon sources? In part, the toolkit required to engineer diamond devices is in its infancy. The well-established techniques for silicon cannot be directly applied to diamond because of its hardness and chemical inertness. One approach to solving these issues is to grow chemical vapor–deposited diamond onto etchable substrates to leave behind the required structure (*7*). Another is to use a combination of ion implantation to graphitize the diamond (making it etchable) and then use a focused ion beam, laser ablation, or other milling methods to sculpt features into diamond (*8*).

The other challenge is to effectively couple light from the diamond to other solid-state photonic structures. Strong coupling enhances photon collection efficiency and provides a mechanism to control and tune the optical transitions (*9*). Optical coupling is also essential for scalability because it allows for long-range coupling between qubits (*10*). Considerable progress has been made in techniques for fabricating thin, single-crystal diamond membranes (*8*), whispering-gallery mode resonators (*11*), and photonic band-gap microcavities (*12*). However, the quality factor is still very far from what is required for scalable devices. Still, there seems to be no reason to believe that fabrication techniques will not rapidly improve in the near future if existing tools are optimized. Although the ground states are well protected from environmental decoherence, the excited states are not. All demonstrations of coherent optical coupling have so far used cryogenic operating conditions (*13*, *14*). Scalability may therefore preclude room-temperature operation of a diamond quantum computer.

One problem with using diamond is the lack of a reliable supply of materials that are perfect enough for quantum technologies. Progress has been made in the manufacture of single diamond crystals by chemical vapor deposition techniques. The background concentrations of nitrogen and boron (potential sources of decoherence) have been reduced to less than one part per billion (*15*), with dislocation densities far lower than that of natural diamond. The availability of material of such purity and perfection will enable practical quantum devices.

At present, fabrication of single qubits is very difficult. How then can we seriously propose building a large-scale qubit device, where every element is identical? One idea (championed by Ray Beausoleil of Hewlett Packard) is to follow strategies used when solid-state devices were not as perfect as they are now—that is, to incorporate a defect-tolerance approach. Diamond can incorporate defect-tolerant methodologies because the color centers can be individually characterized optically. The approach would be to make a large number of generic atom-cavity systems and expect that most will fail as qubits. When one is identified as functional, it is used as a component in the overall quantum computer. This approach builds scalability into the design at the outset and should lead to larger arrays of operational qubits.

Opinions of the viability of quantum computing have fluctuated between outlandish optimism and outlandish pessimism. Given what we know now about the challenges of scaling up quantum processors, it appears unlikely that we will see a large-scale quantum computer in the next 10 years. But the beauty of diamond for quantum information processing is that there are applications based on coherent quantum mechanics in few-qubit devices right now. These include entangled-state microscopy, teleportation, and quantum games. With ready access to genuine multiparticle entanglement, it is clear that new applications will also be found. Applications at the few qubit level are necessary to build a commercial pathway between today's demonstrations and massively entangled quantum computers. Diamond therefore seems ideal as a bridge because of its bright single centers and the rapidly emerging nanofabrication toolkit.

References

1. T. Gaebel *et al.*, *Nat. Phys.* **2**, 408 (2006).
2. R. Hanson *et al.*, *Phys. Rev. Lett.* **97**, 087601 (2006).
3. M. V. Gurudev Dutt *et al.*, *Science* **316**, 1312 (2007).
4. C. Kurtsiefer, S. Mayer, P. Zarda, H. Weinfurter, *Phys. Rev. Lett.* **85**, 290 (2000).
5. Quantum Communications Victoria (http://qcvictoria.com)
6. E. Wu *et al.*, *New J. Phys.* **9**, 434 (2007).
7. J. W. Baldwin *et al.*, *Diamond Relat. Mater.* **15**, 2061 (2006).
8. P. Olivero *et al.*, *Adv. Mater.* **17**, 2427 (2005).
9. Ph. Tamarat *et al.*, *Phys. Rev. Lett.* **97**, 083002 (2006).
10. S. C. Benjamin *et al.*, *New J. Phys.* **8**, 141 (2006).
11. C. F. Wang *et al.*, *Appl. Phys. Lett.* **90**, 081110 (2007).
12. C. F. Wang *et al.*, *Appl. Phys. Lett.* **91**, 201112 (2007).
13. C. Santori *et al.*, *Phys. Rev. Lett.* **97**, 247401 (2006).
14. A. Batalov *et al.*, *Phys. Rev. Lett.* **100**, 077401 (2008).
15. J. Isberg *et al.*, *Science* **297**, 1670 (2002).
16. S. J. Devitt *et al.*, *Phys. Rev. A* **76**, 052312 (2007).

10.1126/science.1158340

RETROSPECTIVE

John Archibald Wheeler (1911–2008)

The deep insights and far-reaching speculations of a theoretical physicist inspired generations of students

Kip S. Thorne

John Archibald Wheeler, one of the great theoretical physicists of the 20th century, died on 13 April, aged 96. I was his student, and I owe much of my scientific personality, style, and accomplishments to him, as do more than 100 other physicists whom he personally mentored. Our love and respect for Johnny (as his wife, Janette, told us we could call him after we got our doctorates) was enormous.

Wheeler was a Pied Piper among physicists. He identified deep issues, often beyond the frontiers of knowledge, and through his lectures, writings, and personal conversations, exhorted us to pursue them. The prime example in his years at Princeton University (1938 to 1976) was the issue of what happens to a star that implodes under the pull of its own gravity—the "issue of the final state," as Wheeler called it—and the implications of the final state for the unknown laws of quantum gravity, which Wheeler called the "fiery marriage of quantum mechanics and general relativity." His final-state exhortations played a major role in catalyzing black hole research and fostering early attempts to quantize gravity. Similarly, at the University of Texas (1976 to 1987), his exhortations about the role of observers in fashioning reality via collapse of the quantum wave function helped to reignite interest in quantum measurements and contributed to the birth of quantum-information science.

Many of Wheeler's visionary ideas appeared crazy at first, but, as Richard Feynman once told me, "if you unwrap his layers of craziness, like unwrapping the layers of an onion, at the core you will often find a kernel of very deep truth." His ideas were often "just crazy enough to be right" (a phrase he sometimes used). For example, Wheeler's insight, in the early 1940s, that a positron can be viewed as an electron traveling backward in time, played a key role in Feynman's invention of "Feynman diagrams" for computing quantum processes. In the late 1960s and early 1970s, Wheeler speculated that the laws of physics were created in the big bang along with matter, space, and time, and he exhorted scientists to discover the principles that governed which of all possible physical laws actually arose. This seemingly crazy idea was a quarter century before its time. In modern string theory, there is an enormous number of possible vacuum states that could have emerged from the big bang, each with its own set of physical laws, and string theorists are seeking the principles governing our Universe's choice.

Wheeler's often unconventional vision of nature was grounded in reality through the principle of radical conservatism, which he acquired from Niels Bohr. Be conservative by sticking to well-established physical principles, but probe them by exposing their most radical conclusions.

Wheeler was just as adept at carrying out concrete, complex analyses as he was at speculating beyond the frontiers of knowledge. In 1939, just weeks after Frisch and Meitner postulated nuclear fission, Wheeler, with Niels Bohr, used a liquid-drop model of the atomic nucleus to explain fission quantitatively and to compute which isotopes will undergo fission when bombarded by slow neutrons. He was the scientist liaison for the world's first production nuclear reactor in Hanford, Washington, which created the ^{239}Pu for the atomic bomb that brought World War II to an end by devastating Nagasaki, and he had a crucial impact on the reactor's design. In the early 1950s, Wheeler assembled and led a team that contributed crucially to the design for the first thermonuclear explosion, based on new insights of Ulam and Teller. Calculations by Wheeler's team convinced a previously skeptical Robert Oppenheimer that a hydrogen bomb was feasible.

After World War II, when Oppenheimer and others agonized over their personal roles in unleashing nuclear devastation on Nagasaki and Hiroshima, Wheeler had no such regrets. Instead, he agonized over the many millions of lives, both soldiers and civilians (including that of his brother Joe), that might have been saved if he had pressed to build the bomb sooner, so its devastation would end the war a year earlier.

Although superficially formal, Johnny Wheeler had a mischievous side. At a banquet in the Carlsberg Castle in Copenhagen in 1971, he lit and threw a string of firecrackers behind his chair, creating momentary havoc among the diners, nobody but he and those of us sitting beside him knew he was the culprit, nor did they know the reason: to celebrate his 60th birthday. Johnny's colleagues have long wondered whether, when coining the phrase "a black hole has no hair," he knew its scatological interpretation. His wife indicated to me that he did know; she disapproved of his "penchant for purple prose."

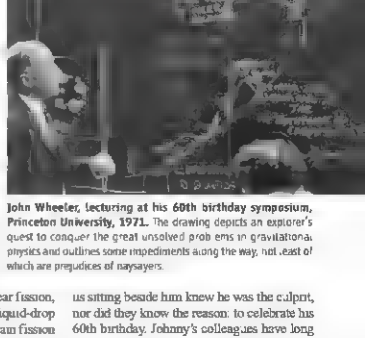

John Wheeler, lecturing at his 60th birthday symposium, Princeton University, 1971. The drawing depicts an explorer's quest to conquer the great unsolved problems in gravitational physics and outlines some impediments along the way, not least of which are prejudices of naysayers.

Perhaps Wheeler's greatest contribution to science was through the students he mentored: about 60 Ph.D. students, a comparable number of undergraduates, and nearly as many postdoctoral students. In his Nobel lecture, Feynman stressed how the inspirations that he derived from discussions with Wheeler led to his formulation of quantum electrodynamics. My own formulation of the hoop conjecture (that a black hole will form only when a mass is compressed into a region so small that a hoop of a certain size can be passed around it in all directions) arose from the research project that Wheeler gave to me on the day I first met him. Wheeler was full of beautiful ideas for research projects, and many of his students and his students' students launched their careers by exploiting those ideas.

Rarely did Wheeler join his students as a coauthor, even when all key ideas were his. He reasoned that, if his name appeared with theirs, readers would forget them and credit the work to him. He was loved and respected for his generosity and kindness, as well as for his vision and accomplishments.

California Institute of Technology, Pasadena, CA 91125, USA. E-mail: kip@tapir.caltech.edu

10.1126/science.1159820

Give knowledge

Special Gift Subscription Rate*

Professional $99 Postdoc Student $50

Give 51 issues of *Science* along with the same yearlong benefits of AAAS membership that you enjoy.

You'll give colleagues a career boost and students an academic leg-up. You'll intrigue and enlighten friends; educate and entertain family members. And you'll add new supporters for the AAAS international, public policy, education, and career programs that advance science and serve society.

Order online—Go to:

promo.aaas.org/giftmay2

or call 1-866-434-AAAS (2227)

When you give *Science*, you receive our popular AAAS shirt

Science
AAAS

*New members only. International orders will receive *Science* Digital edition. To place an order outside the U.S., go to promo.aaas.org/giftmay2

Policies Designed for Self-Interested Citizens May Undermine "The Moral Sentiments": Evidence from Economic Experiments

Samuel Bowles[1,2]

High-performance organizations and economies work on the basis not only of material interests but also of Adam Smith's "moral sentiments." Well-designed laws and public policies can harness self-interest for the common good. However, incentives that appeal to self-interest may fail when they undermine the moral values that lead people to act altruistically or in other public-spirited ways. Behavioral experiments reviewed here suggest that economic incentives may be counterproductive when they signal that selfishness is an appropriate response; constitute a learning environment through which over time people come to adopt more self-interested motivations, compromise the individual's sense of self-determination and thereby degrade intrinsic motivations; or convey a message of distrust, disrespect, and unfair intent. Many of these unintended effects of incentives occur because people act not only to acquire economic goods and services but also to constitute themselves as dignified, autonomous, and moral individuals. Good organizational and institutional design can channel the material interests for the achievement of social goals while also enhancing the contribution of the moral sentiments to the same ends.

David Hume (1711–1776), the Scottish philosopher and economist, cautioned legislators that constitutions and public policies should be designed for "knaves" motivated only by their "private interest" (*1*). Over the past century, economics, embracing Hume's axiom, has devised ingenious ways that taxes, subsidies, tournaments, auctions, and other incentives can be structured to induce self-regarding individuals to act in the common interest when market competition alone would fail to accomplish this (*2*, *3*). This past October, three of its leading practitioners—Leonid Hurwicz, Eric Maskin, and Roger Myerson—were awarded the Nobel Memorial Prize in Economic Sciences for their work in what is now called mechanism design. Dismissed by some as an arcane branch of applied mathematics, the field is, to the contrary, of immense practical importance for the public good: the invisible hand needs a helping hand.

But what if citizens are not knaves, or at least not all of them, all of the time? In this case, policies designed to harness self-interest to public ends may be counterproductive (*4*, *5*). As Bruno Frey warned, a constitution for knaves may produce knaves (*6*). A real-life experiment (*7*) provides an example.

In Haifa, at six day care centers, a fine was imposed on parents who were late picking up their children at the end of the day. Parents responded to the fine by doubling the fraction of time they arrived late. When after 12 weeks the fine was revoked, their enhanced tardiness persisted unabated. While other interpretations are possible, the counterproductive imposition of the fines illustrate a kind of negative synergy between economic incentives and moral behavior. The fine seems to have undermined the parents' sense of ethical obligation to avoid inconveniencing the teachers and led them to think of lateness as just another commodity they could purchase.

The example points to a shortcoming in the conventional economic approach to policy design. It overlooks the possibility that economic incentives may diminish ethical or other reasons for complying with social norms and contributing to the common good. Where this is the case, the kinds of incentives stressed by economists may have counterproductive effects. (By "incentives" without adjective, I mean those appealing to self-regarding preferences.)

The critical assumption in the conventional approach is not that other-regarding motives are absent but that policies that appeal to economic self-interest do not affect the salience of ethical, altruistic, and other social preferences. According to this view, the effects of material interests and "moral sentiments" on behavior are additive rather than interactive. This is called the assumption of separability; a mathematical formulation is provided in (*8*).

Incentives and Market Failures

When individuals do not take into account the effects of their actions on others (called external effects or spillovers), the result of private decentralized decision making will be inefficient in the sense that by implementing some other feasible outcome, at least one individual could be made better off without anyone being made worse off. These inefficient outcomes are termed market failures (environmental degradation or traffic congestion, for example). They would be avoided if people were held liable for the costs that their actions inflict on others (and were recompensed for the benefits conferred on others). What economists call complete contracts do just this. They eliminate the spillovers, internalizing the external effects by assigning claims and liabilities so that each actor "owns" all of the benefits and costs resulting from his or her actions, including those conferred or imposed on others.

Thus, if contracts were complete, the invisible hand would work: Self-interested individuals would implement outcomes that are efficient in the above sense (*9*). This is the economic alchemy by which entirely self-regarding individuals are induced to act as if they cared about the effects of their actions on others. Prices do the work of morals, recruiting shabby motives to elevated ends. A consequence, according to the philosopher David Gauthier, is that if contracts are complete, "morality has no application to market interaction under the conditions of perfect competition" (*10*).

Contracts are rarely complete, however, in part because information about the amount and quality of the good or service provided is either asymmetric or nonverifiable, that is, it is not known to both parties, or even if known it cannot be used in the courts to enforce a contract. As a result, market failures are not confined to the well-known cases of environmental spillovers but occur in the workaday exchanges essential to the functioning of a capitalist economy: labor markets and credit markets. Contractual incompleteness occurs in these cases because of the impossibility of writing an enforceable contract that specifies that the employee will work hard and well and the fact that credit contracts cannot be enforced if the borrower is broke (*11*). Contracts are also incomplete (or nonexistent) in team production processes and the voluntary provision of public goods such as neighborhood amenities or adherence to social norms.

The labor and credit market examples share a common structure: A principal (the employer or the lender) wishes to induce the agent (the employee or the borrower) to act in a way beneficial to the principal, but the conflict of interest between the two cannot be resolved by specifying the terms of a complete and enforceable contract. The de facto terms of the exchange are determined by the strategic interaction among the parties, not by the courts. The same problem arises when a farmer pays a share of his crop to the landowner. The problem common to these cases is that the agent does not own the results of his or her actions. The lender takes the loss if the

[1]Santa Fe Institute, 1399 Hyde Park Road, Santa Fe, NM 87501, USA. [2]Dipartimento di Economia Politica, Università degli Studi di Siena, Siena, Italy.
E-mail: samuel.bowles@gmail.com

borrower cannot repay because of the agent's choice of an overly risky project; the employer enjoys most of the benefits of the employee's hard work.

The task of the mechanism designer is to find a way to assign to each actor the entire benefits and costs (to themselves and to others) of his actions, thereby providing a surrogate for complete contracts. For example, assigning ownership of the land to the sharecropper (who would then own the entire crop) would accomplish this. Replacing sharecropping by a fixed rent that does not depend on how much is produced would do the same.

This emphasis on mechanisms to the exclusion of morals is new. Before the advent of economics in the 18th century, it was more common to appeal to civic virtues (fellow feeling toward one's neighbors, the work ethic, and the moral obligation to repay). These motives are hardly adequate to avoid market failures (especially among strangers in the global marketplace), but morals and other-regarding motives are essential to the performance of firms, communities, and other institutions. Examples include the payment of taxes [in the United States, far in excess of the amounts that would maximize one's expected income (*17*)] and the positive influence of good will toward management on employee effort (*13*). Behavioral experiments that model the voluntary provision of public goods and relationships between principals and agents show that substantial fractions of most populations adhere to moral rules, willingly give to others, and punish those who offend standards of appropriate behavior, even at a cost to themselves and with no expectation of material reward (*14*–*16*).

Thus, societies address market failures through some combination of incentive-based design and other-regarding motives (*9*). Likewise, organizations such as the Ford plant depicted in Diego Rivera's mural (Fig. 1) motivate their members in part by the carrots and sticks of incentives but also by appealing to other-regarding motives such as the desire to do a good job and a sense of reciprocal obligations among members of a firm. However, recent advances in experimental economics provide convincing evidence that the joint effect of these two kinds of motivation is not simply the sum of their effects considered separately.

The 41 experiments on which this review is based [listed with technical details in (*17*)] show that the separability assumption commonly fails. In a few cases, explicit incentives and ethical motives are complements, the former enhancing the salience of the latter. In most cases, though, separability fails in the opposite way: Incentives undermine ethical motives. As is standard in behavioral economics, most of the experiments were played anonymously for real (and often substantial) money stakes.

Four reasons have been suggested for the failure of the separability assumption: Incentives may frame a decision problem and thereby suggest self-interest as the appropriate behavior, or affect the long-term development of preferences, or compromise the individual's sense of autonomy, or convey information affecting behavior. These processes—termed framing, endogenous preferences, overdetermination, and the information content of incentives, respectively—often work jointly and sometimes with opposite effect. Experiments illustrating these four explanations follow.

Framing

Incentives are part of how a decision situation is represented and may signal appropriate behavior (*18*), as seems to have been the case for the Haifa parents, for example. Framing is also at work when simply using market terminology ("exchange") to describe an experiment reduces fair-minded behavior (*19*) or in which market-like competition "offers justifications for actions that in isolation would be unjustifiable" (*20*).

The frame-shifting effects of incentives may occur in cases of government-imposed incentives, too. Here is an example. Experimental subjects whose livelihoods depend on easily depleted forest resources in rural Colombia were asked by Cardenas and his colleagues to individually and anonymously choose how much to withdraw from a mutually beneficial common pool analogous to "the forest" (*21*). Payoffs were such that the level of withdrawal that maximized the gains of the group as a whole was substantially less than the level that maximized the gains of the individual acting singly. The experiment thus captured a common market failure in which self-interested actions by each would overexploit a common pool resource (the forest) and reduce the well-being of all.

Groups of subjects played eight rounds of this game without communication, withdrawing on average amounts that were about midway between the individually self-interested and the group-beneficial levels (Fig. 2). Their substantial deviation from the individually selfish level is a measure of the subjects' other-regarding or ethical values. The experimenters then changed the rules. In subsequent play, for some groups face-to-face communication was allowed (but there was no way to make binding promises). Groups in this "communication" treatment improved their performance, extracting less from the "forest," thereby deviating more from self-interest, and gaining higher benefits.

The other treatment precluded communication but simulated "government regulation." Withdrawals were not to exceed the announced

PHOTO COURTESY OF THE MUSEUM OF MODERN ART, NEW YORK

Fig. 1. Diego Rivera's mural of factory workers at Ford's River Rouge assembly plant (detail). Modern economies require cooperation toward common ends among countless individuals, often occurring as the result of both self-interested and ethical motives. Recent behavioral experiments show that organizational strategies may backfire if they rely solely on explicit economic incentives and seek to limit the options of group members.

group-optimum level, and subjects would be monitored and fined for overexploitation. The regulation reduced the level of withdrawal that would be chosen by an entirely selfish individual, but the expected fines were such that some overexploitation of the common pool remained the payoff maximizer's optimal choice. In this "regulation" treatment, subjects initially responded by restricting their withdrawals to close to the group optimum, but after two periods their behavior increasingly conformed to self-interest, and for the last three rounds their choices were almost entirely self-interested (Fig. 2), sacrificing only one fifth as much individual payoff to protect the "forest" as subjects in the communication treatment. The fine, although insufficient to enforce the social optimum, apparently all but extinguished the subjects' ethical predispositions that in the earlier rounds had induced them to withdraw much less than would maximize their own payoffs.

Endogenous Preferences

Incentives may also induce long-term change in motivations. Preferences are endogenous if one's experiences result in durable changes in motivations and hence a change in behavior in given situations. A number of experiments have documented durable learning effects (*22*, *23*). In these experiments, as in the case of the fines for tardiness at the Haifa day care centers, incentives induced more self-interested behavior, even after they were withdrawn. In the public goods experiment designed by Falkinger *et al.* (*23*), subjects who had experienced an incentive system that was very effective in increasing contributions to the public good later played the same game without the incentives: They contributed 26 percent less than subjects who had not been exposed to the incentives.

However, experiments of just a few hours duration are unlikely to uncover the causal mechanisms at work. This is because adopting new preferences is often a slow process more akin to acquiring an accent than to choosing an action in a game. The developmental processes involved typically include population-level effects such as conformism, schooling, religious instruction and other forms of socialization that are not readily captured in experiments. However, historical, anthropological, social, psychological, and other data (*3*) show that economic structures affect parents' child-rearing values, personality traits rewarded by higher grades in school, and other developmental influences. Thus, economies structured by differing incentives are likely to produce people with differing preferences (*24*).

Incentives change preferences because they affect key aspects of how we acquire our motivations. These effects include the fact that incentives influence both the range of alternative preferences to which one is exposed and the economic rewards and social status of those with preferences different from one's own (*11*). For example, if the relevant incentives allow the selfish to exploit the civic-minded, then the latter are less likely to be copied. Other effects are less obvious: A competitive market with complete contracts leaves little scope for acting on ethical, reciprocal, or generous preferences, even among those so inclined. Moreover, if such markets were, as Gardner says, morality-free zones, then nothing would be lost if people regarded markets as off limits for morality, other than the possibility that the moral dispensations claimed for the marketplace will be generalized to other arenas of life.

However, markets may have quite the opposite developmental impact. Behavior by subjects in experiments among hunter-gatherers, herders, farmers, and others in 15 small-scale societies in Africa, Asia, and Latin America (*24*) closely reflected the highly diverse economic livelihoods of the groups, consistent with the idea that developmental processes that affect adult behavior are linked to economic structure. We found that in anonymous experimental settings, individuals from the more market-integrated societies were also more fair-minded in that they made more generous offers to their experimental partners and more often chose to receive nothing rather than accept an unfair offer. A plausible explanation is that this kind of fair-mindedness is essential to the exchange process and that in market-oriented societies individuals engaging in mutually beneficial exchanges with strangers represent models of successful behavior who are then copied by others.

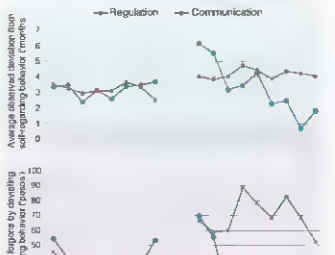

Fig. 2. Effects of social preferences with communication or fines. Shown are two measures of the salience of social preferences in an experiment replicating the problem of cooperation to protect an environmental resource (*21*). The top panel shows the average deviation (in months of exploitation of the forest) from the level that would have maximized the individual's material payoff, given what others in the group did. For example, in round 1 of stage I, both groups exploited the forest a little more than 3 months less than would have maximized their individual payoffs. Implementing the social optimum would have required deviating about 6-1/2 months from the self-interested response. The second measure is the income foregone by the individual by withdrawing less from the forest than would have maximized his income. The first eight rounds were the same treatment for both groups (no communication, no regulation), and there were no significant group differences in behavior by either measure. The groups diverged sharply in Stage II. In the communication treatment, subjects deviated from the self-interest optimum by an average of 4 or more months (top right), more than they had in the absence of communication, and at considerable cost to themselves (bottom right). In the regulation treatment, subjects initially conformed closely to the social optimum, but in successive rounds increasingly acted in an own-payoff-maximizing manner [Used by permission.]

Self-Determination

Where people derive pleasure from an action per se in the absence of other rewards, the introduction of explicit incentives may "overjustify" the activity and reduce the individual's sense of autonomy. The underlying psychological mechanism appears to be a fundamental desire for "feelings of competence and self-determination that are associated with intrinsically motivated behavior" (*25*). There is a substantial empirical literature on the psychology of intrinsic motivations (*26*, *27*), as well as nonexperimental studies in economics [surveyed in (*28*)]. Recent experiments by economists are consistent with this view.

For example, Falk and Kosfeld (*29*) explored the idea that "control aversion" may be a reason that incentives degrade performance. Experimental agents in a role similar to an employee chose a level of production that was costly to them and beneficial to the principal (the employer). The agent's choice effectively determined the distribution of gains between the two, with the agent's maximum payoff occurring if he produced nothing. Before the agent's decision, the principal could elect to leave the choice of the level of production completely to the agent's discretion or impose a lower bound on the agent's production (three bounds—low, medium, and high—were varied by the experimenter across treatments, the principal's choice was whether or not to impose it). The principal could infer that a self-regarding agent would perform at the lower bound and thus

that imposition of the bound would maximize the principal's payoffs.

In the experiment, however, agents chose a lower level of production when the principal imposed the bound. Apparently anticipating this response, fewer than a third of the principals opted for its imposition in the medium- or low-bound treatments. The minority of "untrusting" principals earned on average half of the profits of those who did not seek to control the agents' choice in the low bound treatment, and a third less in the medium-bound condition. In postplay interviews, most agents agreed with the statement that the imposition of the lower bound was a signal of distrust.

Control aversion and the desire for self-determination are not the only effects of the principal's seeking to bound the agent. The imposition of the minimum in this experiment gave the agents remarkably accurate information about the principals' beliefs concerning the agents. Those who imposed the bound had substantially lower expectations of the agents. Their consequent attempt to control the agents' choices induced over half of the agents (in all three treatments) to contribute minimally, thereby affirming the principals' pessimism. This illustrates our fourth reason that the separability assumption may fail.

Incentives Convey Information

Principals select incentives based on their own objectives and their beliefs about how well the agent will perform his task under each possible incentive. Thus, the incentives selected necessarily reveal information about the principal's preferences, the nature of the task, and his beliefs concerning the agent (*30*, *31*). The incentives selected may indicate that the principal is seeking to profit at the expense of the agent, or that the principal believes the agent to be otherwise not committed to performing well, or that the job is onerous, or, as we have seen, that he does not trust the agent.

This predicament for the principal is nicely illustrated in an experiment by Fehr and Rockenbach (*32*). German students in the role of "investor" chose a costly action benefiting the other player, the "trustee," who, knowing the investor's choice, could in turn provide a personally costly "back-transfer," returning a benefit to the investor. When the investor transferred money to the trustee, he also specified a desired level of the back-transfer. The experimenters implemented an incentive condition in which the investor had the option of declaring that he would impose a fine if the trustee's back-transfer were less than the desired amount. The investor could also decline the use of the fine, the choice of using or declining the fine option being taken before the trustee's decision. There was also a "trust" condition in which no such incentives were available to the investor.

The use of the fine reduced return transfers, whereas renouncing the fine when it was available increased return transfers (Fig. 3). Only one third of the investors renounced the fine, their payoffs were 90 per cent greater than the investors who threatened use of the fines. The authors' interpretation is that trusting elicited a positive reciprocal response that was extinguished by the threat of the fine. This was especially the case when it appeared that the intent of the fine was to impose an unfair outcome. Where the investor announced desired returns that would have shared the benefits equally, the use of the fines reduced back-transfers by only 8 percent. Where the announced desired back transfer would have allowed the investor to capture most of the benefits had the trustee complied, however, the reduction in back transfers was 38 percent.

The fact that incentives reveal that the principal is untrusting or self-aggrandizing helps explain a common pattern of experimental results. Incentives imposed by peers who do not stand to benefit personally do not compromise social preferences and are often synergistic with them. An example comes from a public goods experiment in which fellow group members have the opportunity to reduce their own payoffs in order to punish (reduce the payoffs of) others in their group once each member's contributions are revealed and in which group membership is shuffled so that a punisher cannot benefit from the target's response in subsequent periods. In contrast to the case where punishments are imposed by a principal who will benefit at the agent's expense if the agent responds positively, here there is a strong positive response by low contributors (*15*). The most plausible explanation of the effectiveness of peer punishment is that when punished, those who have contributed less than others feel shame, which they redress by contributing more subsequently (*33*). If instead those punished experience anger (if they have contributed more than others, for example), contributions may fall, and costly retaliatory punishment escalations result (*34*).

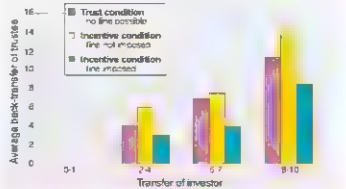

Fig. 3. Average trustee's back-transfer by level of investor's transfer (*32*). Larger investors' transfers are reciprocated by larger trustees' back-transfers, but the average back-transfer is least when the fine is imposed and greatest when the fine was available to the investor but was renounced. [Used by permission.]

Why Are Counterproductive Incentives Common?

We have seen that principals who understand that incentives may undermine social preferences that would otherwise contribute to the performance of the agent often forgo the use of explicit incentives and sanctions even in cases where the latter are feasible (*35*). Why then do we ever observe counterproductive incentives in practice?

An experiment by Fehr and Gächter [reported in (*36*)] with Swiss students suggests an answer. Even if incentives reduce the total gains associated with a project, their use may give the principal a sufficiently larger slice of the smaller pie to motivate the principal to use them. The experiment, similar to the Fehr and Rockenbach experiment above, was constructed so that had subjects responded optimally on the basis of self-regarding preferences, the total surplus (sum of payoffs of employer and employee) would have been more than twice as great under the incentive treatment as under the trust treatment. Negative synergy between the incentive and social preferences was so strong, however, that the total surplus was much higher in the trust treatment than when incentives were introduced. This was true even in those cases where principals offered exactly the kind of contract that a mechanism designer would recommend. Under these "optimal" contracts, profits were more than double those in the trust treatment, whereas the payoffs to employees were less than half. The incentive treatment allowed employers to save enough in wage costs to offset the reductions in work effort.

Thus, one of the reasons agents respond negatively to incentives—that they benefit the principal at the agent's expense—also explains why incentives may nonetheless be used by profit-maximizing principals, despite the fact that they shrink the pie. If a mutually acceptable division of the pie could be decided in advance (and enforced ex post) this problem would not arise, but such ex ante agreements are typically not feasible in real economies.

Why Moral Sentiments and Material Interests Are Not Separable

According to the conventional economic approach, individuals process raw materials and make exchanges so as to get something; the things acquired do not include one's moral standing or sense of having acted well. Behavior is not only acquisitive, however; it is also constitutive. People act also so as to be or to become a good person or one who is esteemed by others. When one's person itself is the raw material and its transformation or affirmation is the objective, the presence of explicit economic incentives may have unintended effects. The

individual who would give to charity so as to affirm his status as a generous person may find that even a small, material reward overjustifies his good deed and hence degrades its value as a signal (*37*).

Constitutive action appears to be at work also in the cases where incentives and morals work synergistically as complements. The rule of law and other institutional designs limit the more extreme forms of antisocial behavior and facilitate mutually beneficial interactions beyond the family. This may enhance the salience of social preferences by assuring people that those who conform to moral norms will not be exploited by their self-interested fellow citizens. This phenomenon may have been at work among the Hokkaido University subjects who cooperated more in a public goods experiment when assured that others who did not cooperate would be punished (*38*), despite the fact that this had no effect on the subjects' own material incentives. They apparently wanted to be cooperative but wished even more to avoid being the sucker who is exploited by defectors. Similar synergies occur in natural settings. Social norms support observance of traffic regulations, but these may unravel in the absence of state-imposed sanctions on flagrant violations.

The proximate reasons for nonseparability may reflect the fact that appeals to self-interest and to morality activate different cognitive and neurological processes, appeals to the former competing with the latter by a process of cognitive overload.

Discussion

Although standard in economics, reliance solely on self-interest in the design of policies has never won universal assent. Until recently, however, dissenting views, like Titmuss' (*39*) celebrated claim that paying for blood donations degrades the willingness to contribute, were thought to lack either empirical support or a coherent account of why separability might fail. But an experiment reported in (*40*) suggests that Titmuss may have been right, at least for women. Other experiments surveyed here provide additional evidence that material interests and moral sentiments are not separable in the sense required by the conventional economic approach to policy making. Economists, psychologists, and others, in part stimulated by these new empirical data, are well on their way to constructing an economic psychology of the interplay of self-regarding and other-regarding motivation that may eventually enlighten mechanism design and public policy.

Is there a message for policy-makers? There is nothing about mechanism design (or economics as a whole) that would preclude more realistic psychological assumptions. Where explicit incentives so strongly compromise social preferences that the effect is the opposite of that intended, the message is clear enough. Other means of affecting citizens' actions must be sought. However, where the effect of incentives is merely blunted rather than reversed, surprisingly, either greater or lesser use of economic incentives may be optimal (*8*). If the mechanism designer seeks to implement a target level of compliance (for example, that a given fraction of the population should be inoculated), greater use of the incentive is called for unless alternative means to the same end are available. However, lesser use of the incentive may be optimal in other cases, as the mechanism designer must weigh the value of additional contributions to the public good against the administrative costs, taking account of both the reduced effectiveness of the incentive and the fact that it reduces the utility that citizens experience from the act of contributing.

Policy-makers could learn valuable lessons, too, from experimental evidence that some mechanisms induce even the civic-minded to act as if they were selfish. Examples include anonymous competitive markets and the public goods game without opportunities for peers to monitor and punish free riders. Other mechanisms, such as the public goods game with peer punishment or opportunities for communication among participants, may induce the self-interested to act as if they were civic-minded. Thus, even for a population with a given distribution of self-regarding and other-regarding motives, small differences in institutional design may lead to very different outcomes at the societal level.

This suggests an extension of Hume's maxim about citizens as knaves and a challenge to the next generation of mechanism designers: Good policies and constitutions are those that support socially valued ends not only by harnessing self-ish preferences to public ends but also by evoking, cultivating, and empowering public-spirited motives. The modest tax on plastic grocery bags enacted in Ireland in 2002 that resulted in a 94 per cent decline in their use appears to have had just this effect (*41*): Carrying a plastic bag joined wearing a fur coat in the gallery of antisocial anachronisms.

References and Notes

1. D. Hume, *David Hume: The Philosophical Works*, T. H. Green, T. H. Grose, Eds. (Longmans, Green, and Co., London, 1898), pp. 117–118.
2. J. J. Laffont, E. Maskin, in *Advances in Economic Theory*, W. Hildenbrand, Ed. (Cambridge Univ. Press, Cambridge, 1982), pp. 31–92.
3. L. Hurwicz, in *Economic Institutions in a Dynamic Society: Search for a New Frontier*, T. Shiraishi, S. Ituno, Eds. (Macmillan, London, 1989).
4. A. O. Hirschman, *Econ. Philos.* **1**, 7 (1985).
5. S. Bowles, *J. Econ. Lit.* **36**, 75 (1998).
6. B. S. Frey, *Econ. J.* **107**, 1043 (1997).
7. M. Gneezy, A. Rustichini, *J. Legal Stud.* **29**, 1 (2000).
8. S. Bowles, S.-H. Hwang, *J. Public Econ.* **92**, 8 (2008).
9. K. J. Arrow, in *Frontiers of Quantitative Economics*, M. D. Intriligator, Ed. (North Holland, Amsterdam, 1971), pp. 3–23.
10. D. Gauthier, *Morals by Agreement* (Clarendon Press, Oxford, 1986), p. 93.
11. S. Bowles, *Microeconomics: Behavior, Institutions, and Evolution* (Princeton University Press, Princeton, NJ, 2004).
12. J. Andreoni, B. Brand, J. Feinstein, *J. Econ. Lit.* **36**, 818 (1998).
13. T. F. Bewley, *Why Wages Don't Fall During a Recession* (Harvard Univ. Press, Cambridge, MA, 1999).
14. E. Fehr, U. Fischbacher, *Nature* **425**, 785 (2003).
15. E. Fehr, S. Gaechter, *J. Econ. Perspect.* **14**, 159 (2000).
16. H. Gintis, S. Bowles, R. Boyd, E. Fehr (Eds. *Moral Sentiments and Material Interests. The Foundations of Cooperation in Economic Life* (MIT Press, Cambridge, MA, 2005).
17. Additional information about the studies reviewed here is available as supporting material on *Science* Online.
18. A. Tversky, D. Kahneman, *Science* **211**, 453 (1981).
19. E. Hoffman, K. McCabe, K. Shachat, V. L. Smith, *Games Econ. Behav.* **7**, 346 (1994).
20. A. Schotter, A. Weiss, I. Zapater, *J. Econ. Behav. Organ.* **31**, 37 (1996).
21. J. C. Cardenas, J. K. Stranlund, C. E. Willis, *World Dev.* **28**, 1719 (2000).
22. B. Irlenbusch, D. Sliwka, *IZA Discussion paper No. 1758*, http://ideas.repec.org/p/iza/izadps/dp1758.html (Institute for the Study of Labor, Bonn, 2005).
23. J. Falkinger, E. Fehr, S. Gaechter, R. Winter-Ebmer, *Am. Econ. Rev.* **90**, 247 (2000).
24. J. Henrich *et al.*, *Behav. Brain Sci.* **28**, 795 (2005).
25. E. L. Deci, *Intrinsic Motivation* (Plenum, New York, 1975).
26. J. Cameron, K. Banko, W. D. Pierce, *Behav. Anal.* **24**, 1 (2001).
27. E. L. Deci, R. Koestner, R. M. Ryan, *Psychol. Bull.* **125**, 627 (1999).
28. B. Frey, R. Jegen, *J. Econ. Surv.* **15**, 589 (2001).
29. A. Falk, M. Kosfeld, *Am. Econ. Rev.* **96**, 1611 (2006).
30. D. Sliwka, *Am. Econ. Rev.* **97**, 999 (2007).
31. R. Benabou, J. Tirole, *Rev. Econ. Stud.* **70**, 489 (2003).
32. E. Fehr, B. Rockenbach, *Nature* **422**, 137 (2003).
33. A. Hopfensitz, E. Reuben, *Tinbergen Institute Working Paper 05-075T*, www.tinbergen.nl/discussionpapers/05075.pdf (2006).
34. B. Herrmann, C. Thöni, S. Gächter, *Science* **319**, 1362 (2008).
35. M. Brown, A. Falk, E. Fehr, *Econometrica* **72**, 747 (2004).
36. E. Fehr, A. Falk, *Eur. Econ. Rev.* **46**, 687 (2002).
37. R. Benabou, J. Tirole, *Am. Econ. Rev.* **96**, 1652 (2006).
38. M. Shinada, T. Yamagishi, *Evol. Hum. Behav.* **28**, 330 (2007).
39. R. M. Titmuss, *The Gift Relationship: From Human Blood to Social Policy* (Pantheon, New York, 1971).
40. C. Mellström, M. Johannesson, *J. Eur. Econ. Assoc.* **6**, 4 (2008); available at http://gupea.ub.gu.se/dspace/handle/2077/2741.
41. E. Rosenthal, "Motivated by a Tax, Irish Spurn Plastic Bags," *New York Times*, 2 February 2008; www.nytimes.com/2008/02/02/world/europe/02bags.html.

42. The author declares no competing interests and would like to thank M. Alexander, J. C. Cardenas, J. Carpenter, C. Efferson, E. Fehr, M. Hauser, S. H. Hwang, S. Gaechter, H. Gintis, G. Loewenstein, K. McCabe, S. Polania, T. Taylor, and E. Wood for their contributions to this research and the Behavioral Sciences Program of the Santa Fe Institute, the Russell Sage Foundation, the University of Siena, the European Science Foundation, and the U.S. National Science Foundation for support of this work.

Supporting Online Material

www.sciencemag.org/cgi/content/full/320/5883/1605/DC1

Table S1

References

10.1126/science.1152110

Auxin Gradients Are Associated with Polarity Changes in Trees

Eric M. Kramer,[1]* Michael Lewandowski,[2] Satvik Beri,[1] Jessica Bernard,[2] Matthew Borkowski,[1] Michael H. Borkowski,[2] Laura Ann Burchfield,[2] Brenda Mathisen,[2] Jennifer Normanly[3]

Wood grain pattern is determined by the orientation of elongated fusiform initial cells in the vascular cambium, the cylinder of soft walled meristematic cells whose daughter cells differentiate to become new xylem and phloem (*1*). The orientation of the initials and the resulting grain pattern can remain approximately constant for the life of the tree, but the initials retain the ability to reorient in response to injury or other developmentally relevant events. This response is critical to the health of the tree because the grain direction is the principle direction of water and assimilates movement through the stem. Theories of wood grain patterning propose that the orienting signal is either mechanical strain in the cambium (*2*) or a concentration gradient of the plant hormone auxin in the plane of the cambium (*3*–*5*). We show that an auxin gradient exists in cambial tissue undergoing grain reorientation, following model predictions.

We conducted experiments on a stand of mature quaking aspen (*Populus tremuloides*) trees undergoing active secondary growth (*6*) (Fig. 1). Samples of cambial tissue were collected before and after the incision of a square wound in the cambium of the stem, and endogenous auxin content was measured with use of gas chromatography–mass spectrometry (GC-MS) (Fig. 1). Because auxin is actively transported down the stem, it accumulates in a zone (< 3 mm) above the wound and was depleted below the wound in a zone that expanded at the speed of transport (about 4 mm/hour). A concentration gradient was thus established below the lower corners of the wound (Fig. 1, 24 hours). Dissection of *P. tremuloides* knots showed that the grain rotated by ~ 0.5°/day in these zones, eventually rotating by more than 45° (*6*). Grain reorientation was slower in zones not immediately below the wound. Thus, lateral auxin gradients at the wound site are correlated with zones of cambial reorientation, supporting a role for auxin in grain patterning. The measured auxin concentrations agree with predictions derived from a computer model (*3*) of auxin transport through the cambrum (Fig. 1). Some excess auxin is apparent within 3 mm of the lower edge of the wound, perhaps because of a wound response (*7*). Above the wound, the accumulation zone seems too narrow to account for observed grain changes. However, a computer model that included feedback between the auxin distribution and grain orientation developed realistic grain patterns after several months of simulated development (*4*).

Experimental evidence for a dynamic auxin gradient during changes in plant cell polarity comes largely from auxin reporter-gene constructs, which may also respond to complex signaling and transcription networks (*8*–*10*). Our results demonstrate directly an endogenous auxin gradient associated with polarity changes

References and Notes

1. P. B. Larson, *The Vascular Cambium* (Springer Verlag, New York, 1994).
2. C. Mattheck, H. Kubler, *Wood: The Internal Optimization of Trees* (Springer-Verlag, New York, 1995).
3. E. M. Kramer, *J. Theor. Biol.* **216**, 147 (2002).
4. E. M. Kramer, M. H. Borkowski, *Trees (Berlin)* **18**, 493 (2004).
5. E. M. Kramer, *J. Plant Growth Regul.* **25**, 290 (2006).
6. Materials and methods are available on *Science* Online.
7. A. E. Sitrin, N. Hic, J. D. Cohen, T. J. Cook, *Plant Growth Regul.* **36**, 201 (2002).
8. E. Benkova *et al.*, *Cell* **115**, 591 (2003).
9. R. S. Smith *et al.*, *Proc. Natl. Acad. Sci. U.S.A.* **103**, 1301 (2006).
10. H. Jonsson *et al.*, *Proc. Natl. Acad. Sci. U.S.A.* **103**, 1633 (2006).

11. Supported in part by Simon's Rock College, National Research Initiative of the U.S. Department of Agriculture Cooperative State Research, Education, and Extension Service grant 2003-35303-13793 (to E.M.K.), and NSF grant 0517420 (to J.N.). We thank A. Jones, A. Davenport, and J. Segh DeNeo for technical assistance and T. Baskin and J. Cohen for discussions.

Supporting Online Material

www.sciencemag.org/cgi/content/full/320/5883/1610/DC1
Materials and Methods
Figs. S1 and S2
References

5 February 2008; accepted 22 April 2008
10.1126/science.1156130

[1]Physics Department, Bard College at Simon's Rock, Great Barrington, MA 01230, USA. [2]Centre for Plant Integrative Biology, University of Nottingham, Loughborough LE12 5RD, UK. [3]Department of Biochemistry and Molecular Biology, University of Massachusetts, Amherst, MA 01003, USA.

*To whom correspondence should be addressed. E-mail: ekramer@simons-rock.edu.

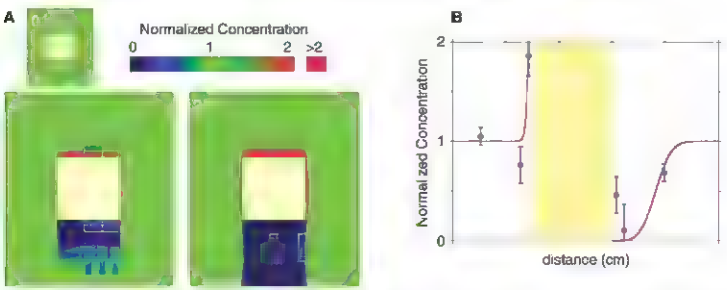

Fig. 1. (A) Measured redistribution of auxin near a 3-cm–by–3-cm square wound (beige) in the cambium of *Populus* trees. Wound occured at 0 hour. White rectangles enclose GC-MS values (data from eight experiments on five different trees), superimposed on the best fit computer model (details in (*5*)). Because auxin is actively transported downward through the cambium, auxin accumulates above the wound and becomes depleted below. All concentrations are normalized to the concentration before wounding. **(B)** Quantitative comparison of auxin concentration data and the computer model at 4 hours. Red line shows the model auxin concentration along a vertical line through the center of the wound. Blue dots show the mean auxin concentration measured within 1 cm of the vertical midline (error bars are ±SE, $n = 5$).

Strong Limit on a Variable Proton-to-Electron Mass Ratio from Molecules in the Distant Universe

Michael T. Murphy,[1]* Victor V. Flambaum,[2] Sébastien Muller,[3] Christian Henkel[4]

The Standard Model of particle physics assumes that the so-called fundamental constants are universal and unchanging. Absorption lines arising in molecular clouds along quasar sightlines offer a precise test for variations in the proton-to-electron mass ratio, μ, over cosmological time and distance scales. The inversion transitions of ammonia are particularly sensitive to μ as compared to molecular rotational transitions. Comparing the available ammonia spectra observed toward the quasar B0218+357 with new, high-quality rotational spectra, we present the first detailed measurement of μ with this technique, limiting relative deviations from the laboratory value to $|\Delta\mu/\mu| < 1.8 \times 10^{-6}$ (95% confidence level) at approximately half the universe's current age—the strongest astrophysical constraint to date. Higher-quality ammonia observations will reduce both the statistical and systematic uncertainties in these observations.

The Standard Model of particle physics assumes that the fundamental constants of nature (or, at least, their low-energy limits) are the same everywhere and at every epoch in the universe. However, it cannot itself justify this assumption, nor can it predict their values. Our confidence in their constancy stems from Earth bound laboratory experiments conducted over human time scales. Extrapolating to the entire universe seems unwise, especially considering that the physics driving the universe's accelerating expansion, labeled dark energy, is completely unknown. Nevertheless, the Earth-bound experiments achieve impressive precision. Time variations in the fine-structure constant, $\alpha = e^2/\hbar c$ (where e is the electron charge, $\hbar$ is Planck's constant h divided by 2π, and c is the speed of light), which measures the strength of electromagnetism, are limited to $\dot{\alpha}/\alpha = (-1.6 \pm 2.3) \times 10^{-17}$ year^{-1} ($\dot{\alpha}$, α's time derivative), whereas those in the proton-to-electron mass ratio, $\mu = m_p/m_e$ (effectively, the ratio of the strong and electroweak scales) are limited to $\dot{\mu}/\mu = (1.9 \pm 4.0) \times 10^{-15}$ year^{-1} ($\dot{\mu}$, μ's time derivative) (*1*). Still, more dramatic variations might have occurred over the 13- to 14-billion-year history of the universe, and the residual variations in our small spacetime region might remain undetectably small. It is therefore imperative to measure the constants over cosmological time and distance scales.

Variations in μ and/or α would manifest themselves as shifts in the transition energies of atoms and molecules. By comparing transition energies registered in spectra of astronomical objects with laboratory values, possible variations can, in principle, be probed over our entire observable universe and through most of its history. Because of the narrowness of the spectral features involved, absorption lines arising in gas clouds along lines of sight to background quasars are currently our most precise cosmological probes. For example, by comparing various heavy-element electromagnetic resonance transitions in optical quasar spectra, 5σ evidence has emerged for variations in α of ~5 parts in 10^6 at redshifts (z's) $0.2 < z < 4.2$ (*2*–*5*). Although a more recent statistical sample found no variation (*6*), errors in the analysis prevent reliable interpretation of those results (*7*, *8*), leaving open the possibility of a varying α.

Similarly, tentative (3σ) evidence for a fractional variation in μ of -20×10^{-6} has recently come from two quasar spectra containing many ultraviolet (UV) H_2 transitions at $z \sim 2.8$ (*9*, *10*). Comparison of UV heavy-element resonance lines and Hi 21-cm absorption is sensitive to $\alpha^2\mu$ and, assuming α to be constant, has yielded indirect null constraints on μ variation, albeit with slightly worse precision than the direct H_2 method (*11*).

An alternative method for measuring μ at high redshift, suggested recently by Flambaum and Kozlov (*12*), is to use the sensitivity to μ variation of the ammonia inversion transitions (*13*) near 24 GHz. A shift in their frequencies due to a varying μ can be discerned from the cosmological redshift by comparing them to transitions with lower sensitivity to μ. Good candidates for comparison are the rotational transitions of molecules such as CO, HCO^+, and HCN because (i) their transition frequencies depend mainly on μ and not on other fundamental quantities (such as α); (ii) they are simple molecules, commonly detected in the interstellar medium; and (iii) their rest frequencies (80 to 200 GHz) are not vastly dissimilar to the NH_3 transitions' frequencies (compared with UV and 21 cm absorption), thus

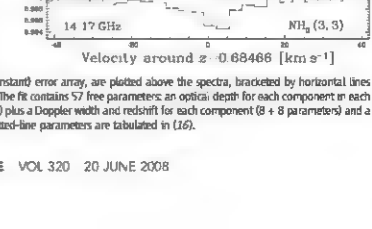

Fig. 1. Spectra of the molecular transitions used in this study, registered to a heliocentric velocity scale centered on $z = 0.68466$. The nominal observed frequencies are noted in each panel. The data, normalized by fits to their continua, are plotted as black histograms. Numbered tick marks above the spectra show the positions of velocity components in our fiducial eight-component fit (the solid line following the data). The HCN and NH_3 transitions have complex hyperfine structure reflected in each velocity component; the tick marks show the position of the strongest hyperfine component in LTE (*16*). Residuals between the fit and data, normalized by the (constant) error array, are plotted above the spectra, bracketed by horizontal lines representing the ±1σ level. The fit contains 57 free parameters: an optical depth for each component in each transition (5 × 8 parameters) plus a Doppler width and redshift for each component (8 + 8 parameters) and a single value of $\Delta\mu/\mu$. The fitted-line parameters are tabulated in (*16*).

[1]Centre for Astrophysics and Supercomputing, Swinburne University of Technology, Mail H39, Post Office Box 218, Victoria 3122, Australia. [2]School of Physics, University of New South Wales, Sydney, New South Wales 2052, Australia. [3]Academia Sinica Institute of Astronomy and Astrophysics, Post Office Box 23-141, Taipei, 106 Taiwan. [4]Max-Planck-Institut für Radioastronomie, Auf dem Hügel 69, 53121 Bonn, Germany

*To whom correspondence should be addressed. E-mail: mmurphy@swin.edu.au

reducing possible effects due to frequency-dependent spatial structure in the background quasar's emission.

For rotational and NH_3 inversion transitions, we may write the apparent change in velocity or redshift of an absorption line due to a variation in μ as

$$\frac{\Delta v}{c} = \frac{\Delta z}{1+z} = K_i \frac{\Delta\mu}{\mu} \qquad (1)$$

where K_i is the sensitivity of transition i to μ and $\Delta\mu/\mu \equiv (\mu_z - \mu_{lab})/\mu_{lab}$ for μ_{lab} and μ_z, the values of μ in the laboratory and absorption cloud at redshift z, respectively. All rotational transitions have $K_i = 1$, so comparing them with each other provides no constraint on $\Delta\mu/\mu$. However, the sensitivity of the NH_3 inversion transitions is strongly enhanced, $K_i \approx 4.46$ (*12*). That is, as μ varies, the NH_3 transitions shift relative to the rotational transitions.

Only one quasar absorption system displaying NH_3 absorption is currently known, that at $z = 0.68466$ toward quasar B0218+357. From z uncertainty estimates for NH_3, CO, HCO^+, and HCN in the literature (*12*), the precision achievable is crudely estimated to be $\delta(\Delta\mu/\mu) \approx 2 \times 10^{-6}$. However (*12*), a proper measurement of $\Delta\mu/\mu$ from NH_3 would require detailed simultaneous fits to all the molecular transitions, and significantly better precision may be possible. Here we make the first detailed measurement of μ using the NH_3 inversion transitions by comparison with HCO^+ and HCN rotational transitions.

The only published NH_3 absorption spectra are those for the $(J,K) = (1,1)$, $(2,2)$, and $(3,3)$ inversion transitions reported by (*14*) toward B0218+357, reproduced in Fig. 1. The channel spacing is 1.67 km s^{-1} for (1,1) and (2,2) and 3.3 km s^{-1} for (3,3). The spectra are normalized by a low-order fit to the quasar continuum. See (*14*) for observational and data reduction details. The signal-to-noise ratio (SNR) for the flux is very high, ~1000 per channel, but because <1% of the continuum is absorbed, the effective SNR for the optical depth is quite low.

HCO^+ and HCN(1-2) absorption toward B0218+357 was discovered more than a decade ago (*15*). New high-resolution (≈0.9 km s^{-1} per channel), high SNR (~100 per channel) observations of these lines were recently undertaken with the Plateau de Bure Interferometer in France (*16*). Figure 1 shows both spectra normalized by fits to the quasar continuum.

All spectra were registered to the heliocentric reference frame; possible errors in this procedure are discussed in (*16*) and shown to be negligible.

Spectra representing the 1σ uncertainty in normalized flux per channel were constructed for all the molecular spectra by calculating the root mean square (RMS) flux variations in the continuum portions of each transition. Because no large differences were observed on either side of the absorption for any transition, a simple constant-error model was adopted.

As Eq. 1 states, the signature of a varying μ would be a velocity shift between the rotational and NH_3 inversion transitions. Complicating the measurement of any shift is the velocity structure evident in Fig. 1. The profiles comprise absorption from many gas clouds, all associated with the absorbing galaxy but nevertheless moving at different velocities. The number and velocity distribution of these velocity components are unknown and must be determined from the data themselves. Each fitted velocity component is represented by a Gaussian profile parameterized by its optical depth, Doppler width, and redshift. The best-fitting parameter values are determined with a χ^2 minimization code, VPFIT (*17*), designed specifically for fitting quasar absorption lines. To determine the statistically preferred velocity structure, the best-fit (that is, minimized) values of χ^2 per degree of freedom, χ^2_ν, are compared for several fits with different velocity structures. That with the lowest χ^2_ν is taken as the fiducial one (similar to an F test used to discriminate between models).

Measuring $\Delta\mu/\mu$ requires the assumption that the velocity structure is the same in all transitions. This does not mean that the ratio of optical depths of corresponding velocity components in different transitions must be constant across the profile. Rather, it means that the number and velocity distribution of components are assumed to be the same in different transitions. We discuss this assumption below, but in practice the velocity structure was determined by tying together the redshifts of corresponding velocity components in different transitions. The high SNR rotational spectra clearly place the strongest constraints on the velocity structure, but the NH_3 spectra must be included to measure $\Delta\mu/\mu$. The Doppler widths of corresponding components were also tied together, effectively assuming a turbulent broadening mechanism.

Figure 1 shows the fiducial eight-component fit. The detailed hyperfine structure of the HCN(1-2) and NH_3 transitions is reflected in each velocity component. The relative hyperfine-level populations were fixed by assuming local thermodynamic equilibrium (LTE). The laboratory data used in the fits are tabulated in (*16*). Given this fit, determining $\Delta\mu/\mu$ is straightforward. A single additional free parameter is introduced for the entire absorption system, which shifts all the velocity components of each transition according to its K coefficient (Eq. 1). All parameters in the fit, including the single value of $\Delta\mu/\mu$, are varied by VPFIT to minimize χ^2. The best-fit value is $\Delta\mu/\mu = (+0.74 \pm 0.47) \times 10^{-6}$, corresponding to a (statistically insignificant) velocity shift between the NH_3 and rotational transitions of 0.77 ± 0.49 km s^{-1}. The 1σ error quoted here, formed from the diagonal terms of the final parameter covariance matrix, derives entirely from the photon statistics of the absorption spectra. A different (though intimately related) approach to determining $\Delta\mu/\mu$ and its error is discussed in (*16*); it provides the same result.

Fitting too few velocity components causes large systematic errors in such analyses (*8*). A reliable measurement of $\Delta\mu/\mu$ can be derived only from fits replicating all of the statistically significant structure in the absorption profiles. Therefore, the fiducial velocity structure must be the statistically preferred one and may be more complicated than that preferred by the human eye, especially when many transitions are fitted simultaneously. The simplest objective method to achieve this is demonstrated in Fig. 2, which shows the decrease in χ^2_ν as increasingly complex velocity structures are fitted. When the fit is

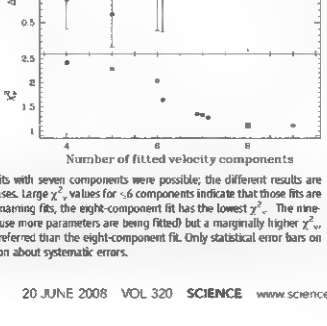

Fig. 2. Variation in $\Delta\mu/\mu$ and χ^2_ν per degree of freedom, χ^2_ν, of different velocity structures characterized by the number of fitted absorption components. χ^2_ν is defined as $\chi^2_\nu \equiv \sum_j^{N_d} (d_j - m(j))/\sigma_j^2$ for d_j, the j^{th} data value with variance σ_j^2 and model value $m(j)$. The sum is over all $N_d = 223$ data points; $\nu = N_d - N_{par}$ for N_{par} free model parameters. Our fiducial eight-component ($N_{par} = 57$) result is highlighted with square points. Different components were added to or removed from the fiducial fit to form each initial velocity structure, and VPFIT was run again to minimize χ^2 by varying all free parameters; results are displayed as solid circles. Two different initial fits with six components and three fits with seven components were possible; the different results are offset in the plot for clarity in these cases. Large χ^2_ν values for <6 components indicate that those fits are not statistically acceptable. Of the remaining fits, the eight-component fit has the lowest χ^2_ν. The nine-component fit has a smaller χ^2 (because more parameters are being fitted) but a marginally higher χ^2_ν, indicating that it is less statistically preferred than the eight-component fit. Only statistical error bars on $\Delta\mu/\mu$ are shown; see text for discussion about systematic errors.

too simple to adequately describe the data, quite different values of $\Delta\mu/\mu$ are found. On the other hand, the nine-component overfitted case provides a value and error very similar to those of the fiducial eight-component model.

The consistency of the velocity structures in the two highest SNR transitions, HCO^+ and HCN(1-2), was tested by fitting those transitions independently. Again, different fits with different velocity structures were compared to determine the statistically preferred one. Both transitions are best fit by velocity structures similar to that in Fig. 1 (*16*), providing some confidence that they can meaningfully be fitted simultaneously. These independent velocity structures were applied to the NH_3 transitions, and new values of $\Delta\mu/\mu$ were derived. When fitting only HCO^+(1-2) and NH_3, $\Delta\mu/\mu = (+0.67 \pm 0.51) \times 10^{-6}$; for HCN(1-2) and NH_3, $\Delta\mu/\mu = (+0.88 \pm 0.51) \times 10^{-6}$. Neither value substantially deviates from our fiducial one. The marginal increase in the 1σ error when using a single rotational transition indicates that the NH_3 spectra limit the statistical uncertainty.

To consider potential systematic uncertainties, it is important to recall our main assumption that the velocity components constituting the absorption profiles have the same redshifts in different transitions. Although the HCO^+ and HCN(1-2) velocity structures are evidently similar enough for measuring $\Delta\mu/\mu$, the NH_3 spectra have a SNR that is too low for a direct comparison. And because the observed frequencies of the NH_3 (~14-GHz) and rotational (~106-GHz) transitions are somewhat different, it is possible that, if the background source morphology is frequency-dependent, some NH_3 components might arise along slightly different sightlines from those components in the rotational profiles.

B0218+357 is at $z = 0.944$ BL Lac object (*18*) lensed by a nearly face-on Sa/Sab $z = 0.68$ galaxy (*19*) in which the absorption occurs. Two lensed images, A and B, separated by 334 milliarc sec, straddle the lensing galaxy's center, with image B much closer to the center. An Einstein ring with diameter ~300 milli–arc sec, centered near image B, has also been identified (*20*). B0218+357 itself has a core-jet morphology with an unresolved [$< 1 \times 1$ milli–arc sec or $< 7 \times 7$ pc (*21*)] flat spectrum core dominating the observed 8.4-GHz emission (*22*). The jet has a knotty structure extending over ~10 × 10 milli–arc sec and, like other jets, is expected to have a steep spectrum.

Various absorption lines have been detected in the $z = 0.68466$ absorber, from Hı 21 cm and OH below 2 GHz (in the rest frame) (*23*, *24*), through six H_2CO transitions at 5 to 150 GHz (*25*), to H_2O at 557 GHz (*26*), to name but a few. Furthermore, the molecular absorption arises only toward image A (*25*, *27*–*29*). The flat spectrum core should completely dominate at high frequencies; the fact that H_2CO and H_2O absorb most of the total high frequency continuum therefore implies that at least those transitions arise only toward the core. All the observed molecular transitions have consistent velocity structures (though most spectra have poorer resolution and/or SNR than those studied here). Thus, the most important velocity components in all transitions evidently arise toward image A's flat-spectrum, compact core (*14*, *29*).

Nevertheless, indirect evidence suggests that the molecular clouds do not completely cover the background source (*16*, *30*). If the covering fraction is different for the rotational and NH_3 transitions, some velocity components may appear in one and not the other. Similar problems may arise because some HCO^+ and HCN(1-2) velocity components may be optically thick (*16*). The spurious shifts in $\Delta\mu/\mu$ that these effects may cause are difficult to estimate in general, but in (*16*) we conduct several fits in which different combinations of NH_3 velocity components are removed, providing an estimate of $\pm 0.7 \times 10^{-6}$. Another potential systematic error is our assumption of LTE for the HCN(1-2) and NH_3 hyperfine-structure populations. Removing HCN(1-2) from the analysis barely changes the measured $\Delta\mu/\mu$. Removing different parts of the hyperfine structure from the NH_3 transitions results in maximum deviations of $\pm 0.3 \times 10^{-6}$ from our fiducial value of $\Delta\mu/\mu$ (*16*).

Combining these two potential systematic errors in quadrature, we obtain $\Delta\mu/\mu = (+0.74 \pm 0.47_{stat} \pm 0.76_{sys}) \times 10^{-6}$, providing no evidence for cosmological variations in μ. The NH_3 spectra currently set both the statistical (stat) and systematic (sys) errors. Although the SNR and resolution clearly directly determine the former, they also indirectly influence the latter. The velocity structure of higher-quality NH_3 spectra could be more directly compared with the rotational profiles, and limits on non-LTE hyperfine-structure anomalies could be constrained by the data themselves. That is, with improved NH_3 spectra, both the statistical and systematic error components can be improved. Nevertheless, until the NH_3 data are improved, our final result is a 2σ limit on variation in μ from this single absorber: $|\Delta\mu/\mu| < 1.8 \times 10^{-6}$. This corresponds to a shift of <1.9 km s^{-1} between the NH_3 and rotational transitions.

Our new value of $\Delta\mu/\mu$ seems inconsistent with the current tentative evidence for μ variation from H_2 absorption at $z \sim 2.8$, $\Delta\mu/\mu = (+24.4 \pm 5.9) \times 10^{-6}$ (*10*). However, reliable comparison is difficult because cosmological time and/or space variations in μ remain poorly constrained. Clearly, a statistical sample from both techniques, covering a wide redshift range and with detailed assessment of systematic effects, is highly desirable.

Assuming that μ varies linearly with time, our measurement corresponds to a drift of $\dot{\mu}/\mu = (-1.2 \pm 0.8_{stat} \pm 1.2_{sys}) \times 10^{-16}$ year^{-1}. However, this assumption is only a convenient means for comparison with current limits from laboratory atomic clocks, $\dot{\mu}/\mu = (-1.9 \pm 4.0) \times 10^{-16}$ year^{-1} (*1*); it is not motivated by any physical (necessarily un-tested) varying-μ theory.

With so few measurements of μ distributed throughout the universe, each new measurement is an invaluable test of the most basic—and theoretically unjustifiable—assumptions in the Standard Model: that the laws of physics are universal and unchanging. The precision demonstrated here highlights the importance of discovering many more molecular absorbers to further our knowledge of fundamental physics.

References and Notes

1. T. Rosenband *et al.*, *Science* **319**, 1808 (2008).
2. J. K. Webb, V. V. Flambaum, C. W. Churchill, M. J. Drinkwater, J. D. Barrow, *Phys. Rev. Lett.* **82**, 884 (1999).
3. M. T. Murphy *et al.*, *Mon. Not. R. Astron. Soc.* **327**, 1208 (2001).
4. M. T. Murphy, J. K. Webb, V. V. Flambaum, *Mon. Not. R. Astron. Soc.* **345**, 609 (2003).
5. M. T. Murphy *et al.*, *Lecture Notes Phys.* **648**, 131 (2004).
6. H. Chand, R. Srianand, P. Petitjean, B. Aracil, *Astron. Astrophys.* **417**, 853 (2004).
7. M. T. Murphy, J. K. Webb, V. V. Flambaum, *Phys. Rev. Lett.* **99**, 239001 (2007).
8. M. T. Murphy, J. K. Webb, V. V. Flambaum, *Mon. Not. R. Astron. Soc.* **384**, 1053 (2008).
9. A. Ivanchik *et al.*, *Astron. Astrophys.* **440**, 45 (2005).
10. E. Reinhold *et al.*, *Phys. Rev. Lett.* **96**, 151101 (2006).
11. P. Tzanavaris, M. T. Murphy, J. K. Webb, V. V. Flambaum, S. J. Curran, *Mon. Not. R. Astron. Soc.* **374**, 634 (2007).
12. V. V. Flambaum, M. G. Kozlov, *Phys. Rev. Lett.* **98**, 240801 (2007).
13. J. van Veldhoven *et al.*, *Eur. Phys. J. D* **33**, 337 (2004).
14. C. Henkel *et al.*, *Astron. Astrophys.* **440**, 893 (2005).
15. T. Wiklind, F. Combes, *Astron. Astrophys.* **299**, 382 (1995).
16. Materials and methods are available as supporting material on *Science* Online.
17. VPFIT is maintained by R. F. Carswell (see www.ast.cam.ac.uk/~rfc/vpfit.html).
18. J. G. Cohen, C. R. Lawrence, R. D. Blandford, *Astrophys. J.* **583**, 67 (2003).
19. T. York, N. Jackson, W. A. Browne, O. Wucknitz, J. E. Skelton, *Mon. Not. R. Astron. Soc.* **357**, 124 (2005).
20. A. R. Patnaik *et al.*, *Mon. Not. R. Astron. Soc.* **261**, 435 (1993).
21. Throughout we employ a standard cosmology, with Hubble constant $H_0 = 71$ km s^{-1} Mpc^{-1}, and matter and dark energy densities $\Omega_m = 0.27$ and $\Omega_\Lambda = 0.73$, respectively, whereby $z = 0.68466$ corresponds to a look-back time of 6.2 billion years (about half the age of the universe), with a linear angular scale of 7.1 pc milli–arc sec^{-1}.
22. A. D. Biggs *et al.*, *Mon. Not. R. Astron. Soc.* **338**, 599 (2003).
23. C. L. Carilli, M. P. Rupen, B. Yanny, *Astrophys. J.* **412**, 59 (1993).
24. N. Kanekar, J. N. Chengalur, A. G. de Bruyn, D. Narasimha, *Mon. Not. R. Astron. Soc.* **345**, 7 (2003).
25. N. Jethava, C. Henkel, K. M. Menten, C. L. Carilli, M. J. Reid, *Astron. Astrophys.* **472**, 435 (2007).
26. F. Combes, T. Wiklind, *Astrophys. J.* **486**, 79 (1997).
27. K. M. Menten, M. J. Reid, *Astrophys. J.* **465**, 99 (1996).
28. C. L. Carilli *et al.*, *Phys. Rev. Lett.* **85**, 5511 (2000).
29. S. Muller, M. Guelin, F. Combes, T. Wiklind, *Astron. Astrophys.* **468**, 53 (2007).
30. T. Wiklind, F. Combes, in *Highly Redshifted Radio Lines*, C. L. Carilli, S. J. E. Radford, K. M. Menten, G. I. Langston, Eds. vol. 156 of *ASP Conference Series* (Astronomical Society of the Pacific (ASP), San Francisco, 1999), pp. 202–209.

31. M. T. M. thanks the Australian Research Council for a Queen Elizabeth II Research Fellowship (DP0877998).

Supporting Online Material

www.sciencemag.org/cgi/content/full/320/5883/1611/DC1
Materials and Methods
Figs. S1 to S3
Tables S1 and S2
References and Notes

7 February 2008; accepted 22 May 2008
10.1126/science.1156352

Single-Cycle Nonlinear Optics

E. Goulielmakis,[2]* M. Schultze,[1] M. Hofstetter,[2] V. S. Yakovlev,[2] J. Gagnon,[2] M. Uiberacker,[2] A. L. Aquila,[3] E. M. Gullikson,[3] D. T. Attwood,[3] R. Kienberger,[2] F. Krausz,[1,2]* U. Kleineberg[2]*

Nonlinear optics plays a central role in the advancement of optical science and laser-based technologies. We report on the confinement of the nonlinear interaction of light with matter to a single wave cycle and demonstrate its utility for time-resolved and strong-field science. The electric field of 3.3-femtosecond, 0.72-micron laser pulses with a controlled and measured waveform ionizes atoms near the crests of the central wave cycle, with ionization being virtually switched off outside this interval. Isolated sub-100-attosecond pulses of extreme ultraviolet light (photon energy ~ 80 electron volts), containing ~0.5 nanojoule of energy, emerge from the interaction with a conversion efficiency of ~10^{-4}. These tools enable the study of the precision control of electron motion with light fields and electron-electron interactions with a resolution approaching the atomic unit of time (~24 attoseconds).

Nonlinear electron-light interactions driven by strong light fields of controlled wave form (*1*) have allowed for the control of electronic motion at light frequencies and the real time observation of electron dynamics inside and between atoms with ~100-as resolution (*2*–*7*). However, time-domain access to a number of fundamental processes, such as the intra-atomic energy transfer between electrons (resulting, for example, in shake-up) (*8*), the response of an atomic electron system to external influence (e.g., to ionizing radiation) (*9*) and its rearrangement after the sudden loss of one or more electrons (*10*), the charge transfer in biologically relevant molecules (*11*) and related changes in chemical reactivity (*12*) or because of nonadiabatic tunneling (*13*, *14*), would require (or benefit from) an improved temporal resolution.

We used waveform-controlled sub-1.5-cycle near-infrared (NIR) light to demonstrate the generation of robust, energetic, isolated sub-100-as pulses of extreme ultraviolet (XUV) radiation and their precise temporal characterization. Photoionization confined to a single wave cycle results in observables (such as high-harmonic photons and electrons emitted by above-threshold ionization) that can now be related to several distinguishable subcycle ionization events and subsequent electron trajectories with a known timing with respect to the driving field, whose strength and temporal evolution is accurately known (*3*). These circumstances provide ideal conditions for testing models of strong-field control of electron motion and electron-electron interactions.

The generation of attosecond pulses benefits from the abrupt onset of ionization within a single half-cycle, which minimizes the density of free electrons and, hence, the distortion of the driving wave and its dephasing with the generated harmonic wave. As a result, the coherent build-up of the harmonic emission over an extended propagation is maximized. In addition, the order-of-magnitude variation of the ionization probability between adjacent half-cycles creates unique conditions for single sub-100-as pulse emission without the need for sophisticated gating techniques (*3*, *15*, *16*).

On the measurement side, improved resolution results from three provisions: (i) shorter

[1]Max-Planck-Institut für Quantenoptik, Hans-Kopfermann-Strasse 1, D-85748 Garching, Germany. [2]Department für Physik, Ludwig-Maximilians-Universität, Am Coulombwall 1, D-85748 Garching. [3]Center for X-Ray Optics, Lawrence Berkeley National Laboratory, Berkeley, CA 94720, USA.

*To whom correspondence should be addressed. E-mail: elgo@mpq.mpg.de (E.G.); ferenc.krausz@lmu.de (F.K.); ulf.kleineberg@physik.uni-muenchen.de (U.K.)

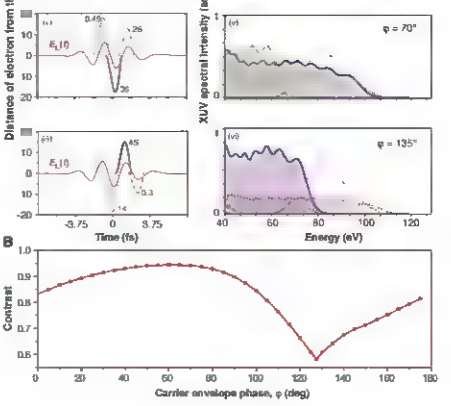

Fig. 1. Simulation of sub-femtosecond XUV emission from neon atoms ionized by a linearly polarized, sub-1.5-cycle, 720-nm laser field. E_0 and $\sigma_i(t)$ are inferred from best agreement between the modeled (*17*) and measured (Fig. 2) spectra and the streaking spectrogram (Fig. 3), respectively. The laser field liberates electrons near its most intense wave crests. **(A)** Classical trajectories of maximum return energy (left panels) and spectra of emerging XUV emission (right panels) are shown for waveforms consistent with $\sigma_i(t)$ inferred from Fig. 3 (correspondence established by colors and line style). The numbers in (i) to (iii) quantify, in units of 10^{-4}, the ionization probability and, hence, the squared modulus of the amplitude of the electron wave packets launched. This amplitude substantially dictates the intensity of XUV emission upon recollision. Contrast ionization probability in (i) to (iii) with the corresponding emission intensities in (iv) to (vi). The pink "dotted-line" emission is not visible in (iv) to (vi) because of the lower ionization probability (by two orders of magnitude) with respect to that resulting in the purple "solid-line" emission [see (iii)]. The gray dashed-and-dotted lines denote the band-pass used in our experiments (Fig. 5*2*). $\varphi = 70°$ and $\varphi = 135°$ yield highest contrast [see (B)] and highest XUV cutoff energy, respectively. arb.u., arbitrary units. **(B)** Contrast versus CE phase. Here, contrast is defined as the ratio of the energy of the main attosecond XUV pulse to the overall XUV emission energy transmitted through the bandpass [gray dashed-and-dotted lines in (A)].

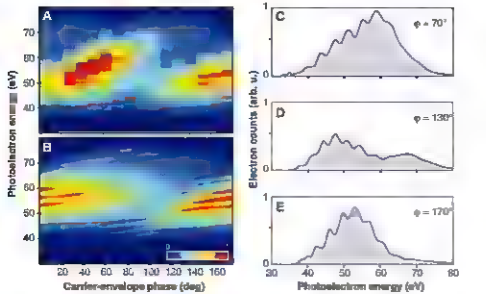

Fig. 2. Control of bandpass-filtered XUV emission with the waveform of monocycle light. Measured (**A**) and simulated (**B**) (*17*) photoelectron spectra versus CE phase, with the delay increased in steps of ~11° (π/16 rad). (**C** to **E**) Spectra measured at the CE phase setting closest to the values selected in Fig. 1A. The zero of the CE phase scale in (A) was set to yield the best agreement with the modeled spectra in (B).

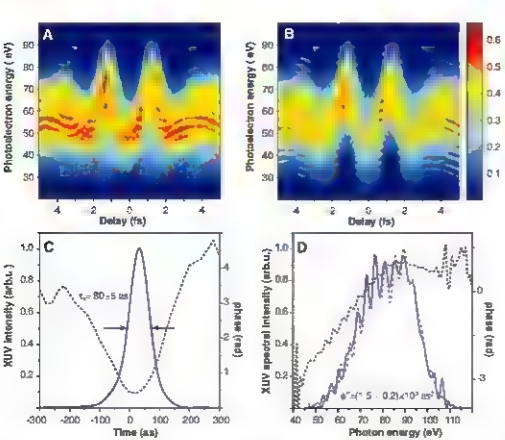

Fig. 3. Sub-100-as XUV pulse retrieval. (**A**) Measured ATR spectrogram compiled from 126 energy spectra of photoelectrons launched by an XUV pulse with a bandwidth of ~28 eV (FWHM) and recorded at delay settings increased in steps of 80 as. Here, a positive delay corresponds to the XUV pulse arriving before the NIR pulse. The high flux of the XUV source allows this spectrogram to be recorded within ~30 min. (**B**) ATR spectrogram reconstructed after ~10^3 iterations of the FROG algorithm (*17*). (**C**) Retrieved temporal intensity profile and spectral phase of the XUV pulse. The intrinsic chirp of the XUV emission (Fig. 4B) is almost fully compensated by a 300-nm-thick Zr foil introduced into the XUV beam between the attosecond source and the ATR measurement. Arrows indicate the temporal FWHM of the XUV pulse. (**D**) XUV spectra evaluated from the measurement of the XUV-generated photoelectron spectrum in the absence of the NIR streaking field (blue dashed line) and from the ATR retrieval (blue solid line). The black dotted line indicates the retrieved spectral phase.

XUV pulse duration, (ii) improved signal-to-noise (S/N) ratio due to the increased XUV photon flux, and (iii) stronger streaking before the onset of the NIR field–induced ionization in attosecond streaking (*Z*) or enhanced S/N ratio due to a reduced number of tunneling steps in attosecond tunneling spectroscopy (*14*).

Figure 1 summarizes results of the modeling of the single-cycle interaction of ionizing NIR radiation with an ensemble of neon atoms (*17*). In Fig. 1A, the left panels plot possible NIR electric waveforms, $E_L(t) = E_0 a_L(t) e^{-i(\omega_L t+\varphi)} + cc$ (where *cc* stands for complex conjugate) derived from our streaking measurements (as presented in the next sections) for different settings of the carrier-envelope (CE) phase, φ. Here, E_0 is the peak electric-field strength, $a_L(t)$ is the normalized complex amplitude envelope, and ω_L is the carrier frequency. The probability of ionization outside the central cycle is more than two orders of magnitude lower than that at the field maximum and hence is negligible.

The spectra of XUV emissions originating from the individual recollisions (*18*) are predicted to differ by tens of electron volts in cut-off energy and by up to orders of magnitude in intensity as a consequence of the single-cycle nature of the driving field. The strong variation of emission energies and intensities within a single wave cycle creates ideal conditions for isolated sub-100-as pulse generation. Indeed, filtering radiation with the bandpass depicted by the dashed-and-dotted line is predicted to isolate XUV radiation with more than 90% of its energy delivered in a single attosecond pulse for a range of CE phases as broad as $30° < \varphi < 90°$ (Fig. 1B). In contrast, with few-cycle–driven harmonic generation resulting in isolated subfemtosecond pulses over only a relatively narrow range of the CE phase near $\varphi \approx 0°$ (*3*), single-cycle excitation appears to permit robust isolated attosecond pulses for a variety of driver waveforms, ranging from near-cosine- to sine-shaped ones, owing to the order-of-magnitude variation of the ionization probability within a single wave cycle.

We used phase-controlled sub-1.5-cycle laser pulses centered at a wavelength of $\lambda_L = 2\pi c/\omega_L = 720$ nm (*19*) to generate XUV harmonics in a neon gas jet up to photon energies of ~110 eV (fig. S1). The emerging XUV pulse—following a spectral filtering through a bandpass (dashed-and-dotted line in Fig. 1A) introduced by metal foils and a Mo/Si multilayer mirror (fig. S2)—subsequently propagates, along with its NIR driver wave, through a second jet of neon atoms in which the XUV pulse ionizes the atoms in the presence of the NIR field. The freed electrons with initial momenta directed along the electric-field vector of the linearly polarized NIR field are collected and analyzed with time-of-flight spectrometry (*17*).

The variation of the measured photoelectron spectra versus CE phase shows good agreement with the predictions of our simulations (Fig. 2, A and B). Figure 2, C to E, shows plots of electron spectra corresponding to the CE phase

settings selected in Fig. 1A. Apart from a downshift by the ionization potential of neon (21.5 eV), they reveal close resemblance to the XUV spectra transmitted through the bandpass in Fig. 1A(v), (vi), and (iv), respectively. Figure 2C depicts the broadest filtered spectrum produced by a single recollision [full-line spectrum in Fig. 1A(vi)]. Emission from the same recollision dominates also in the spectrum shown in Fig. 2E, with this spectrum red-shifted and (upon transmission through the bandpass) correspondingly narrowed, as predicted in Fig. 1A(iv). The two humps of the spectrum plotted in Fig. 2D are indicative of contributions from two recollisions, in accordance with the "solid line" and "dotted line" contributions to the emission spectrum in Fig. 1A(vi).

Before measuring the XUV pulse, we optimized the generation process by "fine-tuning" the NIR laser peak intensity to achieve the broadest possible XUV spectrum transmitted through the bandpass in the range of CE phase settings where the contrast is maximized (50° – 80°, according to Fig. 1B) to generate a clean single pulse with the shortest possible duration. For the temporal characterization of the generated XUV supercontinuum, we shined the NIR field into the neon atoms ionized by the XUV pulse to implement the attosecond transient recorder (ATR) technique introduced in (*2*, *3*). The NIR field boosts or decreases the momenta of the photoelectrons, depending on their instant of release within the 2.4-fs period of the laser field, resulting in broadened and shifted (streaked) spectra of the electrons' final energy distribution. Figure 3A is a plot of a series of streaked spectra recorded versus delay between the XUV and NIR pulse, which we refer to as an ATR or streaking spectrogram. It is practically equivalent to the spectrogram obtained by frequency-resolved optical gating (FROG) (*20*), with the oscillating NIR field constituting an attosecond phase gate in the present case (*21*). As a consequence, a FROG retrieval algorithm (*22*) allows complete determination of both the (gated) XUV pulse and the (gating) NIR laser field (*17*). The reconstructed ATR spectrogram is plotted in Fig. 3B and reveals excellent agreement with the measured one.

The retrieved temporal intensity profile and phase of the XUV pulse are shown in Fig. 3C. The pulse duration of $\tau_x = 80 \pm 5$ as is close to its transform limit of 75 as, with a small positive chirp of $\phi'' = (1.5 \pm 0.2) \times 10^3$ as^2 being responsible for the deviation. As a further consistency check of the attosecond pulse retrieval, we compared the measured NIR field–free electron spectrum (dashed blue line in Fig. 3D) with the electron spectrum calculated from the retrieved attosecond pulse (solid line in Fig. 3D). Given that the pulse retrieval draws on streaked spectra that are strongly distorted with respect to the field-free one, the degree of agreement between the retrieved and directly measured spectrum provides yet another conclusive testimony of the reliability of the retrieved data.

The ATR retrieval algorithm indicates the presence of a satellite pulse accompanying the main attosecond pulse, containing ~1% of the energy of the main pulse. This amount of satellite is consistent with the depth of the experimentally observed modulation in the XUV spectrum (Fig. 3D). However, this result is inconsistent with our numerical modeling, which predicts a satellite energy content of some 6 to 7% for the optimum range of CE phase settings (Fig. 1B). From analysis of the streaked spectra recorded at the maximum of the NIR electric field (fig. S3), where the momentum of the electrons released by the main attosecond pulse and its satellite is shifted in opposite directions, we inferred a relative satellite energy of ~8%, which is in good agreement with the prediction of our modeling. As a consequence, the fringe visibility in the XUV spectrum is lower than was implied by the relative amplitude of the satellite pulse. The discrepancy may originate from a temporal jitter between the main pulse and the satellite pulse and/or from a different spatial amplitude distribution of the beams transporting the emission from the adjacent recollision events. The important lesson from these findings is that the fringe visibility in the XUV spectrum does not allow a reliable determination of the energy carried by the satellite(s) accompanying the main attosecond pulse.

The laser waveform evaluated from the ATR measurement is preserved between the location of the generation and measurement. Figure 4A illustrates the evaluated NIR waveform with electric-field amplitude corresponding to a peak intensity of $I_0 \approx (5.8 \pm 0.5) \times 10^{14}$ W/cm^2, as evaluated from the cut-off of our XUV spectra. The pulse duration [full width at half maximum (FWHM)] of 3.3 fs is in good agreement with the results of previous interferometric autocorrelation measurements (*19*), and the evaluated CE phase of ~50° is consistent with the optimum contrast according to our modeling (Fig. 1B).

Accurate knowledge of the attosecond XUV pulse parameters, the temporal evolution of the generating NIR field, and the emergence of the former from a single recollision permit one to perform precision tests of models of light-electron interactions underlying the ionization and subsequent attosecond pulse generation processes. As an example, we calculated the intrinsic spectral chirp (i.e., the variation of the group delay versus frequency) carried by the attosecond XUV pulse during its emergence from the chirp measured by the ATR and the known dispersion of the components traversed by the pulse on its way

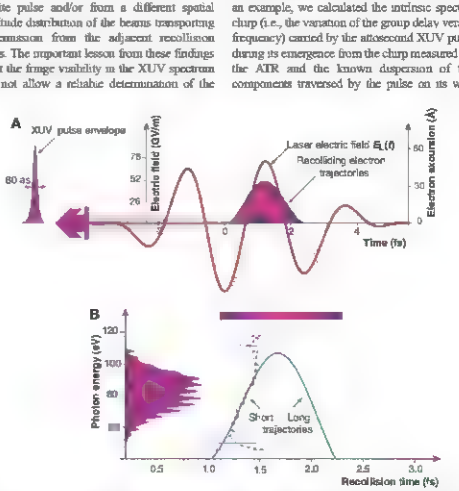

Fig. 4. (**A**) Retrieved electric field of the NIR laser pulse used for generating and measuring the attosecond XUV pulse shown in Fig. 3. The duration of the pulse (FWHM of the cycle-averaged intensity profile) is $\tau_L = 3.3$ fs, and the CE phase is evaluated as $\varphi \approx 50°$. The classical electron trajectories responsible for the emission of the filtered attosecond pulse are calculated with the plotted electric field and shown in the same panel. The color coding indicates the final return energy of the electrons. (**B**) Energy of the recolliding electron plus ionization potential (which is equal to the emitted XUV photon energy) versus recollision time evaluated from the classical trajectory analysis (solid green line), and emitted photon energy versus emission time (dashed purple line) inferred from the chirp of the measured attosecond pulse and the dispersion of the metal filter that the attosecond pulse passes through before the measurement. The basic idea for the graphical representation is borrowed from (*29*). Error bars indicate the uncertainty in the retrieved group delay.

from the source to the measurement (fig. S2). The result (purple dashed line in Fig. 4B) is compared with the intrinsic attosecond chirp (green solid line in Fig. 4B) calculated from a classical trajectory analysis (*23*, *24*). There is a notable discrepancy at the high-energy components of the wave packet, possibly because of quantum effects near cutoff. Nevertheless, the agreement with the attochirp resulting from short trajectories is stunning in the main part of the spectrum, where the S/N ratio is excellent. This agreement indicates the powerfulness of semiclassical modeling of strong-field interactions (*25*, *26*) and the negligible role of long trajectories in contributing to the XUV radiation in the far field (*27*).

In a similar way, the confinement of interaction between the ionizing field and the atom to a single wave cycle will permit accurate quantitative tests of theories of strong-field ionization. The sub-100-as XUV pulses emerging from the interaction with a flux greater than 10^{-1} photons/s—along with their monocycle NIR driver wave—will push the resolution limit of attosecond spectroscopy to the atomic unit of time (~24 as) and allow for the real-time observation of electron correlations, by means of streaking (*6*), time-of-flight (*14*), or absorption (*28*) spectroscopy.

References and Notes

1. A. Baltuška *et al.*, *Nature* **421**, 611 (2003).
2. R. Kienberger *et al.*, *Nature* **427**, 817 (2004).
3. E. Goulielmakis *et al.*, *Science* **305**, 1267 (2004).
4. M. F. Kling *et al.*, *Science* **312**, 246 (2006).
5. G. Sansone *et al.*, *Science* **314**, 443 (2006).
6. A. L. Cavalieri *et al.*, *Nature* **449**, 1029 (2007).
7. E. Goulielmakis *et al.*, *Science* **317**, 769 (2007).
8. S. Svanberg, B. Erlkyson, N. Martensson, G. Wendin, U. J. Gelius, *J. Electron Spectrosc. Relat. Phenom.* **47**, 327 (1988).
9. S. X. Hu, L. A. Collins, *Phys. Rev. Lett.* **96**, 073004 (2006).
10. J. Breidbach, L. S. Cederbaum, *Phys. Rev. Lett.* **94**, 033901 (2005).
11. A. I. Kuleff, J. Breidbach, L. S. Cederbaum, *J. Chem. Phys.* **123**, 044111 (2005).
12. F. Remacle, R. D. Levine, *Proc. Natl. Acad. Sci. U.S.A.* **103**, 6793 (2006).
13. G. Yudin, M. Y. Ivanov, *Phys. Rev. A* **64**, 035401 (2001).
14. M. Uiberacker *et al.*, *Nature* **446**, 627 (2007).
15. T. Pfeifer *et al.*, *Phys. Rev. Lett.* **97**, 163901 (2006).
16. Y. Oishi *et al.*, *Opt. Express* **14**, 7230 (2006).
17. See supporting material on *Science* Online.
18. C. A. Haworth *et al.*, *Nature Phys.* **3**, 52 (2007).
19. A. L. Cavalieri *et al.*, *New J. Phys.* **9**, 242 (2007).
20. R. Trebino, D. J. Kane, *J. Opt. Soc. Am. A* **10**, 1101 (1993).
21. Y. Mairesse, F. Quéré, *Phys. Rev. A* **71**, 011401(R) (2005).
22. D. J. Kane, G. Rodriguez, A. J. Taylor, T. S. Clement, *J. Opt. Soc. Am. B* **14**, 935 (1997).
23. P. Salières *et al.*, *Science* **292**, 902 (2001).
24. M. S. Yakovlev, A. Scrinzi, *Phys. Rev. Lett.* **91**, 153901 (2003).
25. P. B. Corkum, *Phys. Rev. Lett.* **71**, 1994 (1993).
26. K. J. Schafer, B. Yang, L. F. DiMauro, K. C. Kulander, *Phys. Rev. Lett.* **70**, 1599 (1993).
27. R. López-Martens *et al.*, *Phys. Rev. Lett.* **94**, 033001 (2005).
28. Z. H. Loh *et al.*, *Phys. Rev. Lett.* **98**, 143601 (2007).
29. K. Varju *et al.*, *Laser Phys.* **15**, 888 (2005).

30. Supported by the Max Planck Society and the Deutsche Forschungsgemeinschaft Cluster of Excellence Munich Centre for Advanced Photonics (www.munich-photonics.de). E.G. acknowledges a Marie-Curie fellowship (MEIF-CT-2005-024402) and a Marie-Curie Reintegration grant (MERG-CT-2007-208643). A.L.A. is supported by the NSF Extreme Ultraviolet Engineering Research Center. R.K. acknowledges support from the Sofia Kovalevskaya award of the Alexander von Humboldt Foundation.

Supporting Online Material

www.sciencemag.org/cgi/content/320/5883/1614/DC1
SOM Text
Figs. S1 to S4
References

27 March 2008; accepted 27 May 2008
10.1126/science.1157846

The Formation Conditions of Chondrules and Chondrites

C. M. O'D. Alexander,[1]* J. N. Grossman,[2] D. S. Ebel,[3] F. J. Ciesla[1]

Chondrules, which are roughly millimeter-sized silicate-rich spherules, dominate the most primitive meteorites, the chondrites. They formed as molten droplets and, judging from their abundances in chondrites, are the products of one of the most energetic processes that operated in the early inner solar system. The conditions and mechanism of chondrule formation remain poorly understood. Here we show that the abundance of the volatile element sodium remained relatively constant during chondrule formation. Prevention of the evaporation of sodium requires that chondrules formed in regions with much higher solid densities than predicted by known nebular concentration mechanisms. These regions would probably have been self-gravitating. Our model explains many other chemical characteristics of chondrules and also implies that chondrule and planetesimal formation were linked.

Chondrules make up ~20 to 80 volume % of most chondrites and formed at peak temperatures of ~1700 to 2100 K (*1*). Chondrules in the different chondrite groups have distinct physical and chemical properties (*2*), as well as distinct age ranges (*3*), indicating that they formed in relatively local environments via a process that operated at least periodically between ~3 and 4 million years after the formation of the solar system.

It was long thought that individual chondrules behaved as chemically closed systems during their formation, inheriting their compositions from their precursors (*4*, *5*). However, for likely cooling rates of 10 to 1000 K/hour (*1*) and at the low pressures (total pressure ≈ 10^{-6} to 10^{-3} bars) of the solar protoplanetary disk (nebula), experiments (*6*–*8*), natural analogs (*9*, *10*), and theoretical calculations (*11*, *12*) all show that there should be extensive evaporation of major and minor elements, in the order S > Na, K > Fe > Si > Mg.

Elements fractionations in chondrules are generally a function of volatility (*4*, *5*). If evaporation in the nebula produced the alkali metal and Fe fractionations, the more volatile elements (such as S) should be entirely absent, which they are not. In addition, the fractionated elements should exhibit large and systematic isotopic fractionations, which they do not (*13*).

Here we demonstrate that chondrules did indeed behave as essentially closed systems during melting, at least for elements with volatilities less than or equal to that of Na. We also propose a means of resolving the apparent conflict between this result and experimental and theoretical expectations that chondrules should have suffered considerable evaporation during formation. Our conclusions have implications for mechanisms of dust concentration in the solar nebula, for chondrule formation, and for planetesimal formation.

Chondrules are dominated by olivine [$(Mg,Fe)_2SiO_4$], pyroxene [$(Mg,Fe,Ca)SiO_3$], Fe-Ni metal, and quenched silicate melt (glass). Many of the more volatile elements (such as Na) can diffuse rapidly, particularly in melts and glasses. Therefore, it is possible that volatiles were completely lost when chondrules melted, and reentered the chondrules during cooling or even after solidification. However, Na clinopyroxene/glass ratios show that the Na contents of the final chondrule melts (now glass) had approximately their observed, relatively high abundances at temperatures of ~1600 to 1200 K (*14*–*16*).

Calculations suggest that chondrule melts could have been stabilized in the nebula by substantially enriching solids (chondrule precursors or other dust) relative to gas (*11*, *12*). This also substantially increases the condensation temperatures of even highly volatile elements such as S (*11*, *17*). Even in solid-enriched systems, there is an initial phase of evaporation when a chondrule melts, but subsequent chondrule/gas re-equilibration would erase any isotopic fractionations (*17*). If the enrichment of solids is high, little evaporation may be needed to reach chondrule/gas equilibrium, and the behavior of volatile elements during cooling would resemble closed-system behavior. However, even at a high total pressure of 10^{-3} bars, with a solids enrichment of 1000 relative to the solar composition, all the Na would evaporate at near-liquidus temperatures, and substantial recondensation only begins well below 1600 K (*11*). Locally enriching chondrule-sized or smaller solids by 1000 times

[1]Department of Terrestrial Magnetism, Carnegie Institution of Washington, Washington, DC 20015, USA. [2]U.S. Geological Survey, Reston, VA 20192, USA. [3]American Museum of Natural History, New York, NY 10024, USA.
*To whom correspondence should be addressed. E-mail: alexande@dtm.ciw.edu.

on substantial spatial scales would have been difficult to achieve in the nebula with known mechanisms (*17*), except perhaps if levels of turbulence were very low (*18*).

It is evident from the above that the behavior of Na during cooling can constrain the degree to which solids were enriched during chondrule formation. Olivine is the highest-temperature liquidus phase in chondrules and is predicted to crystallize throughout much of their supersolidus cooling (*11*). Olivine phenocrysts in chondrules are generally zoned in major and minor elements, demonstrating that olivine cores did not maintain equilibrium with the liquid during cooling. Na does partition into olivine, albeit at low levels. Therefore, if Na could be measured in them, olivine phenocrysts should record any changes in the Na content of their host chondrules as they crystallized.

We analyzed bulk, mineral, and glass compositions in 26 Semarkona (classified as a LL3.0) chondrules (Table 1) (*18*) with a range of types (IA, IAB and IIA-IIAB-IIB, where I = FeO-poor, II = FeO-rich, A = olivine-dominated, B = pyroxene-dominated, and AB = intermediate). In general, chondrule olivines exhibit pronounced normal zoning in major (Mg and Fe) and minor (Na, Cr, Mn, and Ca) elements that is consistent with expectations for crystallization from their bulk chondrule melts (*5*, *16*, *19*). Na can diffuse rapidly in some minerals and glasses at high temperature, but the fact that its zoning roughly parallels that of Cr, Mn, and Ca demonstrates its primary nature. In addition, the shapes of Na zoning profiles around Na- and Fe-poor relict olivine grains (unmelted precursors) (*20*, *21*) in type II chondrules are similar to or broader than those of Fe (*22*), suggesting that Na diffusion rates in these olivines were comparable to those of Fe. Except where grains are clearly relict, analyses of phenocrysts and microphenocrysts from the same chondrule fall on similar trends, but these trends commonly differ from chondrule to chondrule.

The simple observation of measurable Na in the cores of chondrule olivines (Fig. 1 and Table 1) (*18*) is contrary to predictions (Fig. 1), even in what has previously been considered a highly dust-enriched system (1000 times that of the solar composition) (*11*). To determine how much Na was present in the chondrule melts during olivine crystallization, it is necessary to know the Na olivine-melt distribution coefficient (K_D), measurements of which have yet to be published. However, clinopyroxene-glass partitioning demonstrates that the Na contents of the glass in the central regions of these chondrules were established before solidification (*14*–*16*). In olivine-normative chondrules, olivine was generally still on the liquidus at the onset of clinopyroxene crystallization [calculated with MELTS (*23*)]. Consequently, we can estimate the olivine-liquid K_D for Na at the end of crystallization for each chondrule as the ratio of the Na_2O contents of the last olivine to form (the most Na- and Fe-rich phenocryst rims and microphenocrysts) to that in the glass (rim K_Ds, Table 1). The rim K_Ds are fairly similar for all chondrules, implying no strong compositional dependence.

To determine whether bulk chondrule Na abundances were very different at liquidus

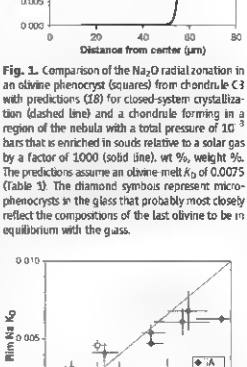

Fig. 1. Comparison of the Na_2O radial zonation in an olivine phenocryst (squares) from chondrule C3 with predictions (*18*) for closed-system crystallization (dashed line) and a chondrule forming in a region of the nebula with a total pressure of 10^{-3} bars that is enriched in solids relative to a solar gas by a factor of 1000 (solid line). wt %, weight %. The predictions assume an olivine-melt K_D of 0.0075 (Table 1). The diamond symbols represent microphenocrysts in the glass that probably most closely reflect the compositions of the last olivine to be in equilibrium with the glass.

Table 1. The petrologic types and estimated liquidus temperatures of the Semarkona chondrules studied, as well as the Mg number and Na olivine-melt K_Ds of the first (core) and last (rim) olivines to crystallize.

Chondrule	Type	Liquidus* (°C)	Core† Mg no.	Rim† Mg no.	Core§ K_D	Rim‖ K_D	Density¶ (g/m³)
C1	IIA	1680	0.898	0.699	0.0077(11)	0.0068(13)	17 to 311
C2	IIA	1652	0.888	0.796	0.0028(07)	0.0028(06)	12 to 194
C3	IIA	1658	0.898	0.716	0.0095(13)	0.0063(02)	14 to 251
C4	IIA	1702	0.905	0.771	0.0074(15)	0.0061(07)	33 to 476
C5	IIA	1646	0.792	0.722	0.015(02)	0.0053(09)	14 to 229
C6	IA‡#	1706	0.994	0.995	0.019(05)	0.0055(45)	91 to 2510
C7	IA	1716	0.996	0.994	0.0011(14)	0.0023(12)	51 to 1610
C8	AB‡	1752	0.994	0.994	0.0066(44)	0.0025(12)	118 to 3090
C9	IAB‡	1770	0.993	0.993	0.025(13)	0.0081(40)	198 to 5750
C10	IIA	1642		0.791		0 0061(08)	11 to 194
C11	A‡	1778	0.993	0.992	0.069(18)	0.0063(42)	388 to 9080
C13	IIAB	1582	0.846	0.647	0.0028(05)	0 0046(03)	3 to 60
C14	IIA	1672	0.909	0.675	0.0032(07)	0.0041(05)	16 to 260
C18	IIAB	1646	0.840	0.766	0.0031(06)	0.0020(02)	10 to 165
C19	IIAB	1630	0.936	0.888	0.0009(06)	0.0009(01)	6 to 117
C20	IIA	1718	0.923	0.795	0.0040(09)	0 0030(05)	32 to 526
C22	IIA	1678	0.910	0.688	0.0057(09)	0.0054(05)	15 to 273
C23	IIAB	1634	0.875	0.690	0.0014(06)	0 0031(04)	10 to 158
C27	IIAB	1674	0.875	0.780	0.0060(11)	0.0014(02)	14 to 259
C29	IIAB	1612	0.871	0.840	0.0009(05)	0.0003(01)	6 to 99
C31	IIAB	1630	0.849	0.696	0.0059(10)	0.0020(01)	7 to 128
C33	IIA#	1632	0.854	0.806	0.0024(06)	0.0027(01)	9 to 167
C34	IIAB	1554		0.738		0.0033(08)	2 to 43
C35	IIA	1580	0.835	0.745	0.0057(07)	0.0047(02)	4 to 72
C38	IIA	1704	0.866	0.813	0.0034(10)	0 0027(02)	30 to 534
C40	IB	1622	0.858		0.0056(20)		6 to 139

*Liquidus temperatures were estimated with MELTS (*23*). †Mg number is the atomic Mg/(Mg+Fe) number of the olivine. ‡The alkali metals in the glasses of these chondrules are radially zoned. The core glass compositions were used for the rim K_Ds and to calculate the initial bulk compositions. §The errors are based only on the uncertainty of the Na measurements in the olivine cores and a nominal 10% error in the bulk compositions. ‖The errors are based only on uncertainties in the measured olivine and glass compositions. ¶Upper and lower density limits assume that 90% of the Na remained condensed. The lower limit assumes a vapor in equilibrium with a silicate melt only. The upper limit assumes a vapor in equilibrium with silicate and pure Fe-metal melts. #All chondrules have porphyritic textures, except C6 and C33, which are barred.

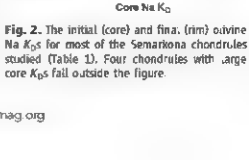

Fig. 2. The initial (core) and final (rim) olivine Na K_Ds for most of the Semarkona chondrules studied (Table 1). Four chondrules with large core K_Ds fall outside the figure.

temperatures, when olivine began to grow (~400 to 500 K above the clinopyroxene and final olivine crystallization temperatures), we calculated the apparent K_Ds for the cores of olivine grains. We did this for each chondrule, using their most Na- and Fe-poor core olivine compositions and their bulk Na content (core K_Ds, Table 1). Figure 2 compares the apparent core and rim K_Ds. Most chondrules fall close to the 1:1 line, as would be expected for closed system behavior. The notable exceptions, which all fall well to the right of the 1:1 line and out of the figure, are the three type IAs and chondrule C5, which have very high core K_Ds. We suspect that this is because they contain unrecognized relatively Na-rich relict cores. The good correspondence between core and rim K_Ds for most chondrules, which cover several hundred degrees of cooling, suggests that (i) they do not have strong temperature or compositional dependences, and (ii) the Na contents of most chondrules did not vary dramatically during cooling. This inference is supported by the subparallel Na, Cr, Mn, and Ca zoning profiles in most olivine phenocrysts. Some chondrules do have core K_Ds that, for the quoted errors, are significantly lower than the rim K_Ds, which could be indicative of some Na gain by the melt during cooling, although the differences are still much less than predicted by the most solids-enriched model of (*11*).

There are several potential sources of uncertainty in estimating the K_Ds that could not be quantified (*18*). There is also a range of K_Ds even for those chondrules that lie close to the 1:1 line. Some of this variation could be due to the gain or loss of Na after crystallization (*18*). Despite these concerns, because most chondrules fall close to the 1:1 line, we infer that to first order they were essentially closed systems for Na during crystallization.

There is some uncertainty about the nebular conditions during chondrule formation. To estimate the range of solids densities that would have been necessary for roughly closed-system behavior of Na at liquidus temperatures, we calculated the equilibrium vapor pressures over the bulk chondrule silicate melts alone as well as over the silicate melts in equilibrium with pure Fe metal (*18*). The solids densities were estimated by calculating, for a given temperature and equilibrium pressure of Na (P_{Na}), the density of solids required for 90% of the Na to remain condensed (Table 1). If the P_{H_2} was >10^{-7} bars during chondrule formation, it will increase the lower limits on the densities (*18*).

The ranges of solids densities in Table 1 are much higher than previously considered for chondrule formation. In principle, the required solids densities could be lowered if the oxygen fugacity (f_{O_2}) were enhanced. However, the f_{O_2} levels in the calculations of the lower limits were well above the iron-wüstite buffer and, therefore, almost certainly already too high because chondrules contain metal. The apparent absence of chondrules exhibiting clear evidence for the open-system behavior of Na or isotopic evidence for evaporation indicates that the chondrules in chondrites formed almost exclusively in such high-density regions. Either there was a remarkably efficient process for concentrating chondrule precursors in regions with high solids densities, or only chondrules that formed in high-density regions accreted into chondrites.

On the basis of the lack of isotopic fractionations in chondrules, it has been estimated that chondrule-forming regions were at least 150 to 6000 km in radius (*24*). At the minimum liquidus densities we calculated (typically >10 g/m^3), regions >4000 km in radius will be self-gravitating (*18*). Regions of this size and density should cool at rates that are consistent with those inferred for chondrules (*18*) and contain enough mass to produce a body of the size typically assumed for the chondrite parent asteroids (radius ~50 km, density ~3 g/cc). These observations raise the possibility that planetesimal formation and chondrule formation in high-density regions were linked. In any case, such high densities would promote the aggregation of larger objects that could then coalesce into asteroid-sized objects (*25*).

A close link between chondrule and planetesimal formation would explain how distinct chondrule populations were preserved in a turbulent nebula in which large-scale mixing would have occurred relatively rapidly. At near liquidus temperatures and inferred densities, there would be gas-mediated exchange between chondrules in close proximity to one another. The diversity of chondrule compositions would thus seem to be problematic, but equilibration time scales are poorly understood and would depend on vapor pressures, diffusion rates in the melts, and the magnitude of the initial compositional differences between chondrules. Even at equilibrium, differences in bulk chondrule compositions are possible to generate simply by varying the proportions of the equilibrium phases. The finite time scales of gaseous diffusion mean that if chondrule-forming regions were relatively large, microenvironments could exist within them (*24*). However, chondrite formation cannot have immediately followed chondrule formation, because at least some chondrules experienced multiple heating events (*2*), and the low-temperature matrix that cements chondrites must also be present before final assembly (*18*).

Shock (*26*) and current-sheet (*27*) heating models both predict thermal histories that are consistent with those inferred for chondrules. The solids densities we estimate are much higher than assumed in previous models (*26*, *27*) but are more consistent with shock heating than with current sheets. Over the range of previously explored solids densities, chondrule cooling rates after shock heating are predicted to increase with increasing solids density. It remains to be seen whether the calculated cooling rates at the densities we estimate are consistent with those inferred for real chondrules. If not, other heating mechanisms, such as lightning or planetesimal collisions, will have to be explored.

References and Notes

1. R. H. Hewins, R. C. Connolly Jr, G. E. Lofgren, G. Libourel, in *Chondrules and the Protoplanetary Disk*, A. N. Krot, E. R. D. Scott, B. Reipurth, Eds. (Astronomical Society of the Pacific, San Francisco, 2005), vol. 341, pp. 286–316.
2. R. H. Jones, J. N. Grossman, A. E. Rubin, in *Chondrules and the Protoplanetary Disk*, A. N. Krot, E. R. D. Scott, B. Reipurth, Eds. (Astronomical Society of the Pacific, San Francisco, 2005), vol. 341, pp. 251–285.
3. N. T. Kita *et al.*, in *Chondrules and the Protoplanetary Disk*, A. N. Krot, E. R. D. Scott, B. Reipurth, Eds. (Astronomical Society of the Pacific, San Francisco, 2005), vol. 341, pp. 558–587.
4. J. N. Grossman, J. T. Wasson, in *Chondrules and their Origins*, E. A. King, Ed. (Lunar and Planetary Institute, Houston, TX, 1983), pp. 88–121.
5. R. H. Jones, *Geochim. Cosmochim. Acta* **54**, 1785 (1990).
6. Y. Yu, R. H. Hewins, C. M. O'D. Alexander, J. Wang, *Geochim. Cosmochim. Acta* **67**, 773 (2003).
7. J. Wang, A. M. Davis, R. N. Clayton, T. K. Mayeda, A. Hashimoto, *Geochim. Cosmochim. Acta* **65**, 479 (2001).
8. B. Cohen, R. H. Hewins, C. M. O'D. Alexander, *Geochim. Cosmochim. Acta* **68**, 1661 (2004).
9. C. M. O'D. Alexander, S. Taylor, J. S. Delaney, P. Ma, G. F. Herzog, *Geochim. Cosmochim. Acta* **66**, 173 (2002).
10. S. Taylor *et al.*, *Geochim. Cosmochim. Acta* **69**, 2647 (2005).
11. D. S. Ebel, L. Grossman, *Geochim. Cosmochim. Acta* **64**, 339 (2000).
12. C. M. O'D. Alexander, *Geochim. Cosmochim. Acta* **68**, 3943 (2004).
13. A. M. Davis, C. M. O'D. Alexander, H. Nagahara, F. M. Richter, in *Chondrites and the Protoplanetary Disk*, A. N. Krot, E. R. D. Scott, B. Reipurth, Eds. (Astronomical Society of the Pacific, San Francisco, 2005), vol. 341, pp. 432–455.
14. C. M. O'D. Alexander, J. N. Grossman, *Meteorit. Planet. Sci.* **40**, 541 (2005).
15. G. Libourel, A. N. Krot, L. Tissandier, *Lunar Planet. Sci. XXXIV*, 1558 (abstr.) (2003).
16. R. H. Jones, *Geochim. Cosmochim. Acta* **58**, 5325 (1994).
17. J. M. Cuzzi, R. C. Hogan, J. M. Paque, A. R. Dobrovolskis, *Astrophys. J.* **546**, 496 (2001).
18. Materials and methods are available as supporting material on *Science* Online.
19. R. H. Jones, G. E. Lofgren, *Meteoritics* **28**, 213 (1993).
20. H. Nagahara, *Nature* **292**, 135 (1981).
21. R. H. Jones, in *Chondrules and the Protoplanetary Disk*, A. N. Krot, E. R. D. Scott, B. Reipurth, Eds. (Astronomical Society of the Pacific, San Francisco, 2005), vol. 341, pp. 849–872.
22. C. M. O'D. Alexander, J. N. Grossman, D. S. Ebel, F. J. Ciesla, *Science* **320**, 1617 (2008).
23. M. S. Ghiorso, R. O. Sack, *Contrib. Mineral. Petrol.* **119**, 197 (1995).
24. J. N. Cuzzi, C. M. O'D. Alexander, *Nature* **441**, 483 (2006).
25. A. Johansen *et al.*, *Nature* **448**, 1022 (2007).
26. S. J. Desch, F. J. Ciesla, ..., Hood, T. Nakamoto, in *Chondrites and the Protoplanetary Disk*, A. N. Krot, E. R. D. Scott, B. Reipurth, Eds. (Astronomical Society of the Pacific, San Francisco, 2005), vol. 341, pp. 849–872.
27. M. K. R. Joung, M. M. Mac Low, D. S. Ebel, *Astrophys. J.* **606**, 532 (2004).

28. This paper is dedicated to the memory of Robert Hutchison. J. Wuth and an anonymous reviewer greatly improved this manuscript. CA was partially supported by NASA Origins of Solar Systems grant NNG06GE39G, JG was partially supported by NASA Cosmochemistry grant NNH05AB65I, DE was partially supported by NASA Cosmochemistry grant NANG06GD89G, and FC was funded by a Department of Terrestrial Magnetism Carnegie Institution of Washington postdoctoral fellowship.

Supporting Online Material

www.sciencemag.org/cgi/content/full/320/5883/1617/DC1
Methods
Fig. S1
Tables S1 to S5
References

15 February 2008; accepted 14 May 2008
10.1126/science.1156561

Iron Isotope Fractionation During Magmatic Differentiation in Kilauea Iki Lava Lake

Fang-Zhen Teng,[1]*† Nicolas Dauphas,[1] Rosalind T. Helz[2]

Magmatic differentiation helps produce the chemical and petrographic diversity of terrestrial rocks. The extent to which magmatic differentiation fractionates nonradiogenic isotopes is uncertain for some elements. We report analyses of iron isotopes in basalts from Kilauea Iki lava lake, Hawaii. The iron isotopic compositions ($^{56}Fe/^{54}Fe$) of late-stage melt veins are 0.2 per mil (‰) greater than values for olivine cumulates. Olivine phenocrysts are up to 1.2‰ lighter than those of whole rocks. These results demonstrate that iron isotopes fractionate during magmatic differentiation at both whole-rock and crystal scales. This characteristic of iron relative to the characteristics of magnesium and lithium, for which no fractionation has been found, may be related to its complex redox chemistry in magmatic systems and makes iron a potential tool for studying planetary differentiation.

Studies of isotopic variations in terrestrial and extraterrestrial rocks can be used to identify the processes that govern planetary differentiation. For example, Fe isotopic compositions of lunar and terrestrial basalts are slightly heavier than those of chondrites, Mars, and Vesta; this has been ascribed to evaporation induced kinetic fractionation of Fe isotopes during the giant impact that formed the Moon (*1*). This interpretation assumes that the Fe isotopic composition of basalts is representative of the source composition (i.e., mantle), which is supported by isotopic studies of other elements like Li and Mg (*2*, *3*). Although studies of mantle peridotites have shown measurable Fe isotope fractionation during mantle melting (*4*, *5*), the effect of fractional crystallization on Fe isotopes remains uncertain (*6*–*10*). Many processes—such as partial melting, magma mixing, assimilation of country rocks, fractional crystallization, and late-stage fluid exsolution—can affect Fe isotope systematics of the magma before it reaches the surface. Isotopic variations may result from different processes, and it is difficult to identify the contributions of specific processes to the observed isotopic signatures.

To isolate and evaluate the influence of fractional crystallization, we worked on a set of well-characterized samples from Kilauea Iki lava lake, Hawaii. Kilauea Iki lava lake formed during the 1959 summit eruption of Kilauea volcano by filling a previously existing crater (Fig. 1). After the formation of a stable crust at the end of the eruption, the lava lake cooled and crystallized as a small, self-roofed, closed magma chamber surrounded on all sides by partially molten regions and extending outward to fully solidified rocks (*11*, *12*). It was drilled repeatedly from 1960 to 1988, resulting in almost 1200 m of drill cores. We analyzed two 1959 eruption samples (IKI-22 and IKI-58) and a variety of drill core samples, ranging from olivine-rich cumulates to andesitic segregation veins, to cover the whole spectrum of chemical compositions, mineralogies, and crystallization temperatures (*12*).

The $\delta^{56}Fe$ values ($\delta^{56}Fe = [(^{56}Fe/^{54}Fe)_{sample}/(^{56}Fe/^{54}Fe)_{IRMM-014} - 1] \times 1000$) of all the whole-rock samples vary inversely with MgO and total FeO contents (Fe_2O_3 and FeO calculated as FeO_{total}) and directly with $Fe^{3+}/\sum Fe$ ratios ($\sum Fe = Fe^{3+} + Fe^{2+}$) (Fig. 2). Olivine cumulates have high MgO contents [up to 26.87 weight percent (wt %)] and low $\delta^{56}Fe$ values (down to −0.03‰), whereas late-stage veins have low MgO contents (down to 2.37 wt %) and high $\delta^{56}Fe$ values (up to +0.22‰) (table S1). The Fe isotopic compositions of 42 olivine grains, separated from two drill core samples, display a larger Fe isotopic variation, ranging from −1.10 to +0.09‰ (Fig. 3). The variations are irrespective of the olivine crystal weight (table S2). The average $\delta^{56}Fe$ of these olivine grains is −0.22 ± 0.08‰ [95% confidence interval (CI)], which is significantly lower than that of the two whole rocks (i.e., +0.11 and +0.12‰).

The large chemical variations in Kilauea Iki lavas mainly resulted from posteruptive redistribution of olivine phenocrysts, followed by crystallization of pyroxene, plagioclase, and Fe-Ti oxide phases as the lava lake cooled (*11*). Both equilibrium (*7*, *8*, *13*, *14*) and kinetic (*15*–*17*) Fe isotope fractionation between minerals and melts could happen during fractional crystallization and produce the observed Fe isotopic variations in the lava lake.

During the process of isotope fractionation, Fe isotopic variations in the samples with MgO < 11 wt %, which mainly result from fractional crystal

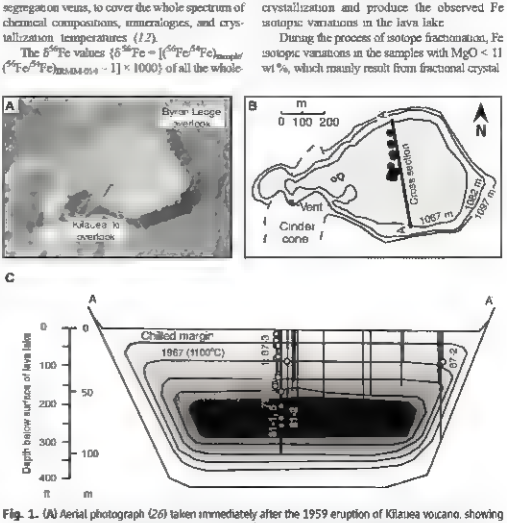

Fig. 1. (**A**) Aerial photograph (*26*) taken immediately after the 1959 eruption of Kilauea volcano, showing the surface of the newly formed Kilauea Iki lava lake. (**B**) Plan view of the posteruptive surface of Kilauea Iki lava lake. The black circles indicate locations of holes drilled between 1967 and 1988. Numbers on contour lines are elevations above sea level. (**C**) Cross section of Kilauea Iki lava lake with a vertical exaggeration of 2:1. The vertical lines show locations of drill holes or closely spaced clusters of drill holes, projected onto this cross section. The concentric zones show the limit of drillable crust and temperatures at different years. Only the drill holes that are labeled indicate where samples (white circles) came from in this study.

[1]Origins Laboratory, Department of the Geophysical Sciences and Enrico Fermi Institute, University of Chicago, 5734 South Ellis Avenue, Chicago, IL 60637, USA. [2]United States Geological Survey, Reston, VA 20192, USA.

*Present address: Isotope Laboratory, Department of Geosciences and Arkansas Center for Space and Planetary Sciences, University of Arkansas, 113 Ozark Hall, Fayetteville, AR 72701, USA.

†To whom correspondence should be addressed. E-mail: fteng@uark.edu

lization (*11*), can be modeled by Rayleigh fractionation with average crystal melt fractionation factors ($\Delta\delta^{56}$Fe) of −0.1 to −0.3‰ (Fig. 4). For a given δ^{56}Fe of the original melt of −0.1‰, the predicted δ^{56}Fe of the minerals are −0 to −0.2‰. These values, in turn, are used to model the compositions of samples with MgO > 11 wt %, which are composed of melt + olivine phenocrysts (*11*), by mixing the assumed composition of the most Mg-rich melt (δ^{56}Fe = +0.11‰) with that of the predicted olivine crystals (δ^{56}Fe = 0 to −0.2‰) (Fig. 4) (*12*).

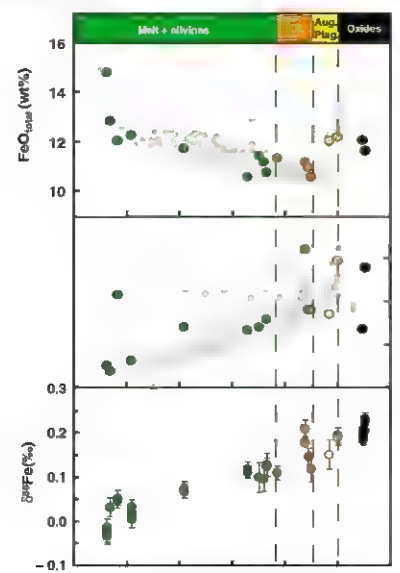

Fig. 2. Variations of FeO_{total}, $Fe^{3+}/\Sigma Fe$ ratios, and δ^{56}Fe values as a function of MgO contents in whole-rock samples. Samples with MgO > 11 wt % are melt + olivine phenocrysts, whereas those with MgO < 11 wt % reflect fractional crystallization of olivine (Ol), followed by augite (Aug.), plagioclase (Plag.), and Fe-Ti oxides (*11*). Gray circles represent all samples from Kilauea Iki lava lake (*27*). Error bars indicate 95% CI of the mean. Data from table S1.

Fig. 3. Iron isotopic compositions of olivine grains from Kilauea Iki lava lake. The curves are kernel density estimates with automatic bandwidth selection and have the same surface area. The dashed lines are the δ^{56}Fe values (+0.11 and +0.12‰) of those two whole rocks. Error bars indicate 95% CI of the mean. Data from tables S1 and S2.

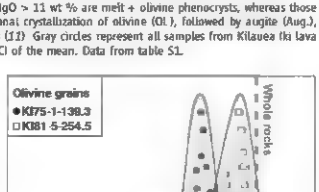

Although no experimentally calibrated equilibrium fractionation factor for olivine melt is currently available, the fractionation factors that fit the whole-rock data generally agree with theoretical calculations (*13*, *14*), experimental studies on fractionation of pyrrhotite and silicate melt (*7*), and fractionation of olivine and magnetite (*8*). These results are also consistent with the range of Fe isotope fractionation during mantle melting (*4*, *5*). However, olivine phenocrysts from the lava lake are highly varied and have δ^{56}Fe values well beyond the range defined by the equilibrium isotope fractionation model (Fig. 4). Segregation veins and some diapirs are known to have formed as the lake crystallized (*18*). The diapirs transferred olivines from the cumulate zone into differentiated liquid (*18*). These processes affected the whole column of "trash" and could have magnified the equilibrium fractionation of Fe isotopes in the olivine in a way that is analogous to isotope fractionation during chromatography (*19*). Different olivine grains in the lake might have experienced these processes to different extents and hence display different degrees of isotope fractionation.

Alternatively, significant high-temperature kinetic fractionation of Mg and Fe isotopes has been documented during thermal diffusion in silicate melts (*16*, *17*, *20*) and chemical diffusion between molten basalt and rhyolite (*16*, *20*). Substantial thermal gradients were observed in the lava lake throughout its crystallization history; the cumulate zone was hotter than the surrounding partially molten zone, and temperature gradients within the partially molten zone reached up to 65°C/m vertically (*21*). Because the hot end was always enriched with light isotopes during thermal diffusion experiments (*16*, *17*, *20*), these thermal gradients may have driven Fe diffusion and Fe isotope fractionation in both whole rocks and olivines, enriching the olivine cumulates in the light isotopes of Fe (and the light isotopes of Mg).

In addition to thermal diffusion, kinetic isotope fractionation can also happen by chemical diffusion. This could have happened during diffusion-limited crystal growth, where light isotopes can be supplied to the growing crystal at a faster rate than heavy isotopes resulting from differences in diffusivities (*15*, *22*). Fractionation could also have taken place during chemical re-equilibration of olivines in the course of cooling and crystallization of the lava lake. The olivines from samples quenched at lower temperature are more Fe-rich and show more scatter in composition than those from samples quenched at higher temperature (fig. S1) (*12*), which reflects re-equilibration of the olivines with evolving residual melts (*23*). Diffusion of Fe from the melt into the interior of the olivine phenocrysts should be associated with kinetic isotope fractionation, thereby enriching the partially equilibrated

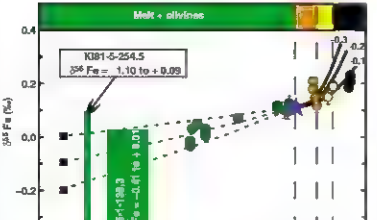

Fig. 4. Modeling of Fe isotopic variations during magmatic differentiation in Kilauea Iki lava lake (*12*). Solid lines represent calculated Fe isotopic compositions of residual melts during fractional crystallization by assuming a Rayleigh distillation process with average crystal-melt fractionation factors ($\Delta\delta^{56}Fe_{crystal\text{-}melt} \approx \delta^{56}Fe_{crystal} - \delta^{56}Fe_{melt}$) of −0.1, −0.2, and −0.3‰. Dashed horizontal lines represent calculated mixing lines between the most magnesian melt from the 1959 eruption (*23*) and the most magnesian olivines (MgO = 46.6 ± 1 wt % and $\delta^{56}Fe \approx 0$, −0.1, and −0.2‰ (black squares)). The blue star represents the most magnesian melt (MgO = 10.7 wt %; assumed $\delta^{56}Fe = 0.11‰$). The green bars represent the ranges of measured $\delta^{56}Fe$ and estimated MgO in olivine grains from two drill core samples (MgO = 33.6 to 39.8 wt % and 41.9 to 42.7 wt %; table S3). Sample crystallization sequences are the same as those in Fig. 2. Error bars indicate 95% CI of the mean.

olivines in the light isotopes of Fe (and the heavy isotopes of Mg) (*16*, *20*).

The extent of equilibrium isotope fractionation is mainly controlled by the relative mass difference between the isotopes, and more fractionation happens in isotopes with a larger relative mass difference (*14*, *24*). If the Fe isotope variation in the lava lake was produced by equilibrium isotope fractionation, Mg isotopes should show more significant fractionation than Fe isotopes because of their larger relative mass difference. Furthermore, kinetic isotope fractionation driven by thermal, and chemical diffusion should also result in larger fractionation in Mg isotopes as compared with that in Fe isotopes (*16*, *17*, *20*). The absence of Mg isotope fractionation in Kilauea Iki lavas may result from the low-precision isotopic analysis of Mg relative to Fe (e.g., 0.1 versus 0.04), which prevents the detection of Mg isotopic variation. More likely, the presence of Fe isotope fractionation and the absence of Mg isotope fractionation may reflect the influence of Fe oxidation states on kinetic or equilibrium isotope fractionation (as compared with those of Mg, two oxidation states of Fe exist in terrestrial magmatic systems) (*5*, *25*).

Our study suggests that, unlike Li and Mg isotopes (*2*, *3*), Fe isotopes fractionate during basaltic differentiation at both whole-rock and crystal scales. Mineral compositions should therefore be used to help interpret whole-rock basalt Fe isotopic data. The elevated $\delta^{56}Fe$ of crustal igneous rocks, which is more evolved than that in basalts, could be explained by fractional crystallization (*10*).

References and Notes

1. F. Poitrasson, A. N. Halliday, D. C. Lee, S. Levasseur, N. Teutsch, *Earth Planet. Sci. Lett.* **223**, 253 (2004).
2. F. Z. Teng, M. Wadhwa, R. T. Helz, *Earth Planet. Sci. Lett.* **261**, 84 (2007).
3. P. B. Tomascak, F. Tera, R. T. Helz, R. J. Walker, *Geochim. Cosmochim. Acta* **63**, 907 (1999).
4. S. Weyer, D. A. Ionov, *Earth Planet. Sci. Lett.* **259**, 119 (2007).
5. H. M. Williams *et al.*, *Earth Planet. Sci. Lett.* **235**, 435 (2005).
6. B. L. Beard *et al.*, *Chem. Geol.* **195**, 87 (2003).
7. J. A. Schuessler, R. Schoenberg, H. Behrens, F. von Blanckenburg, *Geochim. Cosmochim. Acta* **71**, 417 (2007).
8. A. Shahar, C. E. Manning, E. D. Young, *Earth Planet. Sci. Lett.* **268**, 330 (2008).
9. R. Schoenberg, F. von Blanckenburg, *Earth Planet. Sci. Lett.* **252**, 342 (2006).
10. F. Poitrasson, *Rev. Mineral. Geochem.* **62**, 289 (2006).
11. R. T. Helz, in *Magmatic Processes: Physicochemical Principles*, B. O. Mysen, Ed. (Geochemical Society, University Park, PA, 1987), vol. 1, pp. 241–258.
12. Materials, methods, data, and modeling details are available as supporting material on *Science* Online.
13. V. B. Polyakov, R. N. Clayton, J. Horita, S. D. Mineev, *Geochim. Cosmochim. Acta* **71**, 3833 (2007).
14. E. A. Schauble, in *Geochemistry of Non-Traditional Stable Isotopes*, C. M. Johnson, B. L. Beard, F. Albarede, Eds. (Mineralogical Society of America, Washington, DC, 2004), vol. 55, pp. 65–111.
15. M. Dauphas, O. Rouxel, *Mass Spectrom. Rev.* **25**, 515 (2006).
16. F. M. Richter, *Geochim. Cosmochim. Acta* **71**, A839 (2007).
17. F. Huang, C. C. Lundstrom, A. J. Ianno, *Geochim. Cosmochim. Acta* **71**, A422 (2007).
18. R. T. Helz, H. Kirschenbaum, J. W. Marinenko, *Geol. Soc. Am. Bull.* **101**, 578 (1989).
19. A. D. Anbar, J. E. Roe, J. Barling, K. H. Nealson, *Science* **288**, 126 (2000).
20. F. M. Richter, F. B. Watson, R. A. Mendybaev, F. Z. Teng, P. E. Janney, *Geochim. Cosmochim. Acta* **72**, 206 (2008).
21. R. T. Helz, C. R. Thornber, *Bull. Volcanol.* **49**, 651 (1987).
22. A. Jambon, *Geochim. Cosmochim. Acta* **44**, 1373 (1980).
23. R. T. Helz, *U.S. Geol. Surv. Prof. Pap.* **1350**, 691 (1987).
24. H. C. Urey, *J. Chem. Soc. (London)* **1947**, 562 (1947).
25. H. M. Williams *et al.*, *Science* **304**, 1656 (2004).
26. D. H. Richter, J. P. Eaton, K. J. Murata, W. U. Ault, H. L. Krivoy, *U.S. Geol. Surv. Prof. Pap.* **537-E**, 1 (1974).
27. R. T. Helz, H. Kirschenbaum, J. W. Marinenko, R. Qian, *U.S. Geol. Surv. Open-File Rep.* **94-684**, 1 (1994).
28. Discussions with S. Huang, A. T. Anderson Jr., F. M. Richter, M. Wadhwa, P. B. Tomascak, R. J. Walker, and A. Pourmand are appreciated. We thank three anonymous reviewers for constructive comments. This work was supported by a Packard Fellowship, the France-Chicago Center, and NASA through grant NNG06GG75G to N.D.

Supporting Online Material

www.sciencemag.org/cgi/content/full/320/5883/1620/DC1
SOM Text S1 to S5
Fig. S1
Tables S1 to S4
References

29 February 2008; accepted 12 May 2008
10.1126/science.1157166

Natural Variability of Greenland Climate, Vegetation, and Ice Volume During the Past Million Years

Anne de Vernal* and Claude Hillaire-Marcel

The response of the Greenland ice sheet to global warming is a source of concern notably because of its potential contribution to changes in the sea level. We demonstrated the natural vulnerability of the ice sheet by using pollen records from marine sediment off southwest Greenland that indicate important changes of the vegetation in Greenland over the past million years. The vegetation that developed over southern Greenland during the last interglacial period is consistent with modes experiments, suggesting a reduced volume of the Greenland ice sheet. Abundant spruce pollen indicates that boreal coniferous forest developed some 400,000 years ago during the "warm" interval of marine isotope stage 11, providing a time frame for the development and decline of boreal ecosystems over a nearly ice-free Greenland.

The potential for sea-level rise, caused by melting of the Greenland ice-sheet as surface air temperature increases, is considerable (*1*). Although there is evidence that the velocity of ice streams flowing into the ocean and the rate of thinning of the ice have increased recently (*2*, *3*), large uncertainties remain about the long-term stability of the ice sheet. The climate

and ice volume of Greenland seem to have varied considerably in the recent geological past, as shown by paleoecological data indicating a warmer regional climate and reduced ice volume during the last interglacial period (*4*) and by biogenic remains of coniferous trees from forests that grew on Greenland during Pliocene and early-to-mid-Pleistocene times some hundred thousands to million years ago (*5*, *6*). However, although the climate and ice sheet history of Greenland during the last climatic cycle are well documented by isotope and geochemical records from ice cores, which reveal high sensitivity to sea-surface conditions over the northern North Atlantic Ocean (*7*), very little is known about conditions preceding the onset of the last glaciation because of the lack of continuous direct records. On one hand, glacial activity on Greenland over millions of years is evidenced by ice-rafted debris in marine cores from continental margins (*8*), but the precise size of the Greenland ice sheet and its relative stability over time remain unknown. On the other hand, sedimentary outcrops from the Greenland coasts and near-shore marine sediment cores suggest the recurrence of relatively warm climatic conditions during the past (*5*, *6*, *9*), but the duration and timing of these phases remain uncertain. We used the pollen content of sediment cores from the Ocean Drilling Program (ODP) site 646 on the continental rise, off southern Greenland (Figs. 1 and 2), as an independent proxy for assessing the dominant type of vegetation and the timing of the last forested episodes. The stratigraphy of the cores was established from $\delta^{18}O$ on foraminifer shells (*10*), which permits correlation with the stack marine isotope stratigraphy of Lisiecki and Raymo (*11*) and the setting of a time scale (*12*) (fig. S1).

One difficulty in interpreting pollen assemblages from marine sediments is the identification of the vegetation source area because the pollen is necessarily exotic and derives from more or less long-distance transport. Two main transport mechanisms have to be taken into account: atmospheric transport by winds, and hydrodynamic transport through runoff, rivers, and marine currents. The long-distance atmospheric transport of pollen results in low concentrations with distorted assemblages characterized by an overrepresentation of *Pinus* pollen grains that show exceptional aerial dispersion properties (*13*). Along continental margins, detailed studies have shown that most of the pollen in marine sediments is due to fluvial inputs from adjacent lands, therefore allowing direct comparison with terrestrial palynostratigraphy (*14*). In the Labrador Sea, pollen analyses along a near-shore to offshore transect showed that atmospheric transport is accompanied with an asymptotic decrease in the concentration of pollen from the coastline and an increase in the relative proportion of

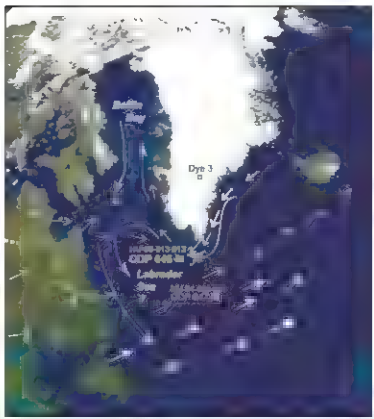

Fig. 1. Location of ODP site 646 (58°12.56 N, 48°22.15 W; water depth 3460 m) in the northern North Atlantic and of other coring sites referred to in the text: HU-90-013-013 (58°12.59 N, 48°22.40 W; water depth 3379 m); ODP site 647 (53.19.9 N, 45°14.7 W, water depth 3862 m); and HU-84-030-003 (53.19.8 N, 45°14.7 W, water depth 3771 m). The Dye 3 coring site, where spruce DNA was found, is indicated by a blue square (*6*). The white arrows correspond to the mean surface vector wind from June to September based on the 1968-to-1996 climatology [see the National Centers for Environmental Prediction/National Center for Atmospheric Research reanalysis (www.cdc.noaa.gov/cgi-bin/Composites/comp.pl)], available from the Earth System Research Laboratory Physical Science Division, of the National Oceanic and Atmospheric Administration (www.esrl.noaa.gov/psd/). The thin and thick white arrows correspond to wind speeds lower and higher than 2 m s^{-1}, respectively. The blue arrows schematically illustrate the surface ocean circulation pattern along the Greenland coast, in the Labrador Sea, and in Baffin Bay. The dashed green line corresponds to the present-day northern limit of the potential natural tree line or cold evergreen needle-leaf forest in Biome models (*27*).

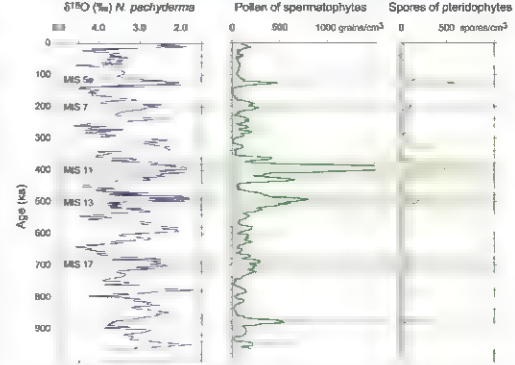

Fig. 2. Stratigraphy and chronology of the upper 76 m at ODP site 646 (58°12.56N, 48°22.15 W; water depth 3460 m) based on ^{18}O measurements in *Neogloboquadrina pachyderma* (*10*) and correlation with the stack curve LR04 of Lisiecki and Raymo (*11*). The abundance of pollen grains and spores of pteridophytes is expressed in concentration per cm^3 of sediments. Sedimentation rates are uniform and average 7.8 cm per ka, which permits the assumption that pollen concentrations are approximately proportional to fluxes (fig. S1) (*12*). The vertical gray bands correspond to modern values of concentrations, and the horizontal green bands correspond to phases with concentrations at least twice that of those recorded during the late Holocene.

[1]GEOTOP Geochemistry and Geodynamics Research Center–Université du Québec à Montréal, Case Postale 8888, succursale Centre-Ville, Montreal, Québec H3C 3P8, Canada.
*To whom correspondence should be addressed. E-mail: devernal.anne@uqam.ca

Pinus (*15*). Pliocene to recent pollen contents at offshore sites from the northwest North Atlantic (ODP site 647, core sample HU84-030-003) (Fig. 1), where mostly wind inputs can be recorded, are characterized by pollen fluxes lower than 0.5 grain cm^{-2} $year^{-1}$ and largely dominated by *Pinus* (*16*). The analyses of Arctic snow, Greenland ice, and pollen traps along the southern Greenland edge show an exotic component from boreal forests of North America, but illustrate that long-distance atmospheric transport is responsible for low inputs (*17*, *18*). Therefore, the large-amplitude variations in pollen content from the southern Greenland margin records at ODP site 646, with fluxes well above "modern" or Holocene (that is, the past 1., 500 years) values, can be interpreted as reflecting changes in hydrodynamic inputs from a relatively proximal source-vegetation located on southern Greenland (*12*). Further evidence for the prominence of proximal sources during interglacials is provided by the comparison of total pollen content to long-distance transported grains of *Pinus* (*12*)

The pollen record of the last million years at ODP site 646 shows important variations both in concentrations [thus fluxes, because sedimentation rates remained fairly constant in the study sequence (*12*)] and dominance of the main taxa (Figs. 2 and 3 and figs. S2 and S3) (*12*). Pollen concentrations vary by orders of magnitude, from less than 10 grains cm^{-3} to more than 10^5 grains cm^{-3}. In general, low concentrations are recorded during glacial stages. Minimum values (close to zero) characterize the marine isotope stage (MIS) 6, indicating very low fluxes from both long-distance and proximal sources, which is consistent with extensive development of the Laurentide and Greenland ice sheets (*9*). Higher concentrations are seen in interglacial sediments. The Holocene is characterized by concentrations of about 100 grains cm^{-3}. The assemblages include inputs from the boreal forest of southeastern Canada linked to predominant southwest-northeast summer winds, but show components (*12*) that are from more-proximal shrub-tundra vegetation.

Earlier interglacial stages record much higher pollen concentrations than the Holocene. Those of MIS 5e are five times higher, and the concentrations of pteridophytes spores are also higher. The assemblages are characterized by dominant *Alnus* and abundant spores of *Osmunda* (Fig. 3B and fig. S2). In core sample HU-90-013-013 collected near ODP site 646 (*19*), more detailed analyses of MIS 5e document the pollen succession (Fig. 4). A rapid increase of *Alnus* occurred during an early phase of MIS 5e characterized by high summer sea-surface temperatures, which suggests rapid development of shrub tundra after the ice retreat (*9*). The subsequent increase of *Osmunda* represents a unique event in the last million years. It coincides with maximum sea-surface temperatures in winter and suggests the development of dense fern vegetation over southern Greenland under climatic conditions not unlike those of the modern boreal forest, given the present distribution of the genus. *Osmunda* expanded possibly in a large geographical domain, because spores were identified at the base of ice cores drilled in the Agassiz ice cap (*20*). Toward the end of MIS 5e, pollen and spore influxes decreased concomitantly with the augmentation of herb percentages. This event corresponds to the first step toward higher $\delta^{18}O$ values in *Globigerina bulloides* and *Neogloboquadrina pachyderma*. It suggests a change to the herb tundra resulting from regional cooling at the onset of ice growth.

MIS 7, the penultimate interglacial period, differed from MIS 5e in many respects (Fig. 3C). Sea-surface temperatures never reached those of MIS 5e, and the pollen and spore content of sediment remained lower. Its pollen assemblages are characterized by dominant herb taxa (notably Poaceae and Cyperaceae), suggesting the development of tundra along southern Greenland coasts.

The MIS 11 interglacial is different than others because of its near 50,000-year duration [374 to 424 thousand years ago (ka) (*11*)]. At site 646, MIS 11 is also unique because of pollen concentrations one order of magnitude higher than those of the Holocene, the dominance of *Picea* spp., and the occurrence of *Abies* pollen grains (Figs. 2 and 3D and fig. S2). The dominance of *Picea* from the beginning to the end of the interglacial period suggests the presence of forest vegetation throughout the entire interval, at least over southern Greenland. The base of MIS 11 is marked by higher pro-

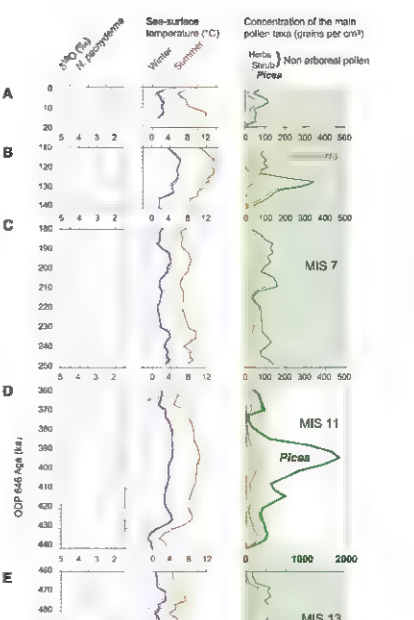

Fig. 3. (A to E) Stratigraphy, sea-surface temperatures, and concentration of dominant pollen and spore taxa during the present interglacial period [MIS 1 (A)], the last interglacial period [MIS 5e (B)], MIS 7 (C), MIS 11 (D), and MIS 13 (E). Sea-surface temperatures are estimated from dinocysts [the thin lines are best estimates from five modern analogs and the thick lines correspond to three-point running averages (*28*)]. Dinocyst assemblages were reported by de Vernal and Mudie (*29*). The modern sea-surface temperatures at ODP site 646 are 3.9 ± 0.7°C and 7.3 ± 1.1°C in winter and summer, respectively [data from the World Ocean Atlas, 2001 (*30*)]. Among pollen assemblages, herb taxa include mostly Poaceae, Cyperaceae, and Asteraceae. Shrub pollen is dominated by *Alnus* and *Betula* with the occasional occurrence of Salix and Ericaceae (fig. S2). *Pinus* has been excluded because of its overrepresentation due to long-distance atmospheric transport.

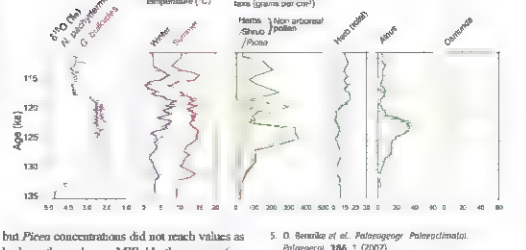

Fig. 4. Close-up on the stratigraphy of the last interglacial period (MIS 5e) from core sample HU-90-013-013, collected near ODP site 646. Shown are the isotope stratigraphy based on *Globigerina bulloides* and *Neogloboquadrina pachyderma* (*19*), the sea-surface temperatures estimated from dinocysts (*28*), and the concentration and percentages of the dominant pollen and spore taxa. The percentages of *Osmunda* were calculated from the pollen sum, excluding spores.

portions of shrub and herb pollen, indicating more open vegetation and a cooler climate, but *Picea* was probably already present regionally, taking into account the fact that its concentrations reached hundreds of grains per cm^3. The covariance of $\delta^{18}O$ in planktic foraminifers and of *Picea* concentrations suggests a synchronous ice retreat and early forest development, a maximum of *Picea* concentration when maximum sea-surface temperatures occurred, and a concomitant glacial onset and forest decline at the end of MIS 11. The development of spruce forest over Greenland probably indicates relatively mild conditions (*6*) and a substantial reduction of the Greenland ice sheet during the long MIS 11 interglacial period. However, precise paleoclimatic and paleoecological inferences from pollen or DNA are uncertain without knowing the species of conifer trees. The identification of *Picea* pollen grains down to the species level is difficult because of uniform morphological characteristics of the genus. Nevertheless, detailed microscopic examination suggests the occurrence of several species, among which *Picea abies* dominated (Fig. S4). In northern Europe and Fennoscandia, *Picea abies* is a common conifer tree of montane and boreal environments that often occurs at the tree limit and acted as a pioneer along emerging postglacial coasts (*21*). Growth of *Picea abies* is fostered by high July temperatures and cool and snowy winters, but has a low temperature threshold (2.6°C) for the initiation of bud and stem growth. *Picea abies* has adapted to survive severe climate, it can persist for hundreds of years by vegetative propagation. Therefore, its development, at least over southern Greenland during MIS 11, does not necessarily imply a zonal climate that was warmer than at present, because the northern tree limit and the *Picea abies* timberline occur now near the polar circle in Europe. However, it certainly indicates ice-free conditions over a large area of Greenland, and thus a much reduced ice-sheet volume, otherwise katabatic winds (*22*) would have restricted any forest development.

Before MIS 11, the pollen content was rarely less abundant than it was during the Holocene, thus suggesting vegetation that was generally as extensive as it is at present. Pollen was particularly abundant during MIS 13 (Figs. 2 and 3E), but *Picea* concentrations did not reach values as high as those during MIS 11, thus suggesting shrub-tundra–type vegetation.

In conclusion, although the pollen record from site 646 does not provide a direct picture of climate changes over Greenland, it yields important information that helps link fragmentary terrestrial records into a continuous sequence. Furthermore, the pollen record is as a proxy for the ice volume of Greenland in two ways. First, it provides information on pollen production, and thus on the vegetation density on adjacent land, which implies ice-free conditions. Second, it depends on the distance to site 646 from the source vegetation, which has been shorter during ice-free episodes in southern Greenland because of low relative sea levels that are a result of isostatic adjustment. A substantially reduced Greenland ice volume seems to have characterized MIS 5e, 11, and 13, as well as the Pliocene (*23*), indicating a long-term sensitivity of the Greenland ice sheet to warm temperatures. Among warm climate intervals of the last million years, MIS 11 stands out in terms of forest vegetation spreading over southern Greenland. Thus, if the melting of Greenland and other Arctic ice caps are assumed to have contributed to the equivalent of a 2.2- to 3.4-m-higher sea level during MIS 5e (*24*), we may assume that they contributed some more during MIS 11. The actual volume of the ice-sheet decline during these episodes is difficult to estimate, but it did occur under natural forcing with an atmospheric partial pressure of CO_2 ~280 parts per million by volume (*25*). During MIS 5e, particularly high summer insolation probably contributed to the Greenland ice melt (*4*), whereas the long duration of MIS 11 might explain the retreat of the ice sheet under an insolation pattern that is similar to that of the Holocene (*26*). The data presented here provide evidence of the vulnerability of the Greenland ice sheet to natural forcing and should increase concerns about its fate during the anticipated global warming.

References and Notes

1. J. A. Dowdeswell, *Science* **311**, 963 (2006).
2. E. Rignot, P. Kanagaratnam, *Science* **311**, 986 (2006).
3. S. B. Luthcke *et al.*, *Science* **314**, 1286 (2006).
4. R. S. W. Otto-Bliesner *et al.*, *Science* **311**, 1751 (2006).
5. O. Bennike *et al.*, *Palaeogeogr. Palaeoclimatol. Palaeoecol.* **186**, 1 (2002).
6. E. Willerslev *et al.*, *Science* **317**, 111 (2007).
7. K. Andersen *et al.*, *Nature* **431**, 147 (2004).
8. N. C. Lovan *et al.*, *Science* **264**, 952 (1994).
9. S. Funder *et al.*, *Quat. Sci. Rev.* **17**, 77 (1998).
10. A. E. Aksu, C. Hillaire-Marcel, P. Mudie, *Proceedings of the Ocean Drilling Program* **105B**, 689 (1989).
11. L. E. Lisiecki, M. E. Raymo, *Paleoceanography* **20**, PA1003, doi:10.1029/2004PA001071 (2005).
12. Material and methods are available as supporting material on *Science* Online.
13. L. E. Heusser, W. L. Balsam, *Quat. Res.* **7**, 45 (1977).
14. M. F. Sánchez Goñi, F. Eynaud, J. C. K. Andersen, N. J. Shackleton, *Earth Planet. Sci. Lett.* **171**, 123 (1999).
15. A. Rochon, A. de Vernal, *Can. J. Earth Sci.* **31**, 15 (1994).
16. C. Hillaire-Marcel, A. de Vernal, *Géographie physique et Quaternaire* **43**, 263 (1989).
17. J. C. Bourgeois, K. Gajewski, R. M. Koerner, *J. Geophys. Res.* **106** (D6), 5255 (2001).
18. D. D. Rousseau *et al.*, *Rev. Paleobot. Palyno.* **143**, 277 (2006).
19. C. Hillaire-Marcel, A. de Vernal, G. Bilodeau, A. J. Weaver, *Nature* **410**, 1073 (2001).
20. R. M. Koerner, J. Bourgeois, D. Fisher, *Ann. Glaciol.* **10**, 85 (1988).
21. T. Grosclaude, K. D. Bennett, *J. Biogeogr.* **31**, 1523 (2004).
22. A. G. Meesters, N. J. Bink, E. A. C. Henneken, H. F. Vugts, *F. Cannemeijer, Boundary-Layer Meteorol.* **85**, 475 (1997).
23. A. de Vernal, P. J. Mudie, *Proceedings of the Ocean Drilling Program* **105B**, 401 (1989).
24. J. T. Overpeck *et al.*, *Science* **311**, 1747 (2006).
25. U. Siegenthaler *et al.*, *Science* **310**, 1313 (2005).
26. A. Berger, M. F. Loutre, *Science* **297**, 1287 (2002).
27. Kaplan, J.O. *et al.*, *Journal of Geophysical Research* 108 (D19, 8171. doi:10.1029/2002JD002559 (2003).
28. A. de Vernal *et al.*, *Quat. Sci. Rev.* **24**, 897 (2005).
29. A. de Vernal, P. J. Mudie, in *Neogene and Quaternary Dinoflagellate Cysts and Acritarchs*, M. J. Head, J. H. Wrenn, Eds. (American Association of Stratigraphic Palynologists Foundation, College Station, TX, 1992), p. 329.
30. National Oceanographic Data Center, *World Ocean Database 2005, Scientific Data Set, Observed and Standard Level Oceanographic Data* (CD-ROM) (National Oceanic and Atmospheric Administration, Silver Spring, MD, 2001).

31. This study is a contribution of the Polar Climate Stability Network supported by the Canadian Foundation of Climate and Atmospheric Science. We also acknowledge financial support from the Natural Sciences and Engineering Research Council of Canada and the Fonds Québécois de Recherche sur les Sciences de la Nature et les Technologies.

Supporting Online Material

www.sciencemag.org/cgi/content/full/320/5883/1622/DC1
Materials and Methods
Figs. S1 to S4
References

10 December 2007; accepted 9 May 2008
10.1126/science.1153929

Elevation Changes in Antarctica Mainly Determined by Accumulation Variability

Michiel M. Helsen,[1]* Michiel R. van den Broeke,[1] Roderik S. W. van de Wal,[1] Willem Jan van de Berg,[1] Erik van Meijgaard,[2] Curt H. Davis,[3] Yonghong Li,[3] Ian Goodwin[4]†

Antarctic ice Sheet elevation changes, which are used to estimate changes in the mass of the interior regions, are caused by variations in the depth of the firn layer. We quantified the effects of temperature and accumulation variability on firn layer thickness by simulating the 1980–2004 Antarctic firn depth variability. For most of Antarctica, the magnitudes of firn depth changes were comparable to those of observed ice sheet elevation changes. The current satellite observational period (~15 years) is too short to neglect these fluctuations in firn depth when computing recent ice sheet mass changes. The amount of surface lowering in the Amundsen Sea Embayment revealed by satellite radar altimetry (1995–2003) was increased by including firn depth fluctuations, while a large area of the East Antarctic Ice Sheet slowly grew as a result of increased accumulation.

The Antarctic Ice Sheet is constantly adjusting its mass in response to changes in the accumulation of snow on its surface, which occur on centennial to millennial time scales (*1*), with a concomitant effect on global sea level. Although most coupled general circulation models predict the mass of the interior of the Antarctic Ice Sheet to grow in a warmer climate (*2*, *3*), no clear trend has been found there over the past half century (*3*, *4*). On the other hand, extensive areas in coastal Antarctica have recently suffered mass losses through acceleration of coastal glaciers (*5*–*7*). As a result, the latest intergovernmental Panel on Climate Change assessment estimates a net mass loss of Antarctic grounded ice of 76 ± 127 Gt year^{-1} (1993–2003; 1 Gt = 10^{12} kg), equivalent to 0.21 ± 0.35 mm year^{-1} sea level rise (*8*), with recent estimates showing losses increasing to as much as 196 ± 92 Gt year^{-1} in 2006 (*7*).

One way to estimate ice sheet mass change is through remote measurement of elevation changes (dH/dt) using satellite radar altimetry to determine volume change; this technique has often been applied with an assumption of constant ice sheet density (*9*–*11*). Most studies of the interior of the Antarctic Ice Sheet show extensive areas of slightly increasing elevation, typically by several centimeters per year, suggesting mass gain. However, the unknown depth and density of the firn complicates the conversion from dH/dt to mass change. The densification of firn is influenced by both accumulation rate and temperature, and the thickness of the firn layer therefore varies over time scales of days to millennia (*12*–*14*). Because the period of reliable satellite radar altimetry observations spans only about 15 years, firn depth changes driven by variability in temperature and accumulation may have a large influence on observed elevation trends (*15*). Temperature and accumulation anomalies are correlated in Antarctica and have counteracting effects on firn layer depth. Enhanced accumulation obviously favors firn layer thickening, but as these events coincide with higher than average temperatures, densification in the upper firn pack is enhanced, thus favoring thinning. Previous studies did account for temperature-driven variability of firn compaction (*9*), but in the absence of reliable snowfall time series over the Antarctic Ice Sheet, accumulation rate variability has not been considered in detail.

Here, we derived a corrected dH/dt signal that is free of interannual fluctuations in firn thickness. Our approach combines a firn densification model (*13*) with time series of accumulation and temperature. The firn densification model is forced at the upper boundary with the use of annual accumulation rates from ice cores of various lengths from three Antarctic regions (*16*–*19*), as well as values for skin temperature, solid precipitation, and sublimation from a regional climate model specifically adapted for the Antarctic region (RACMO2/ANT) (*19*, *20*). The regional climate model, in turn, is forced at its lateral boundaries with the use of European Centre for Medium-Range Weather Forecasts (ECMWF) reanalysis (ERA-40) and operational analyses. The forcing with ice core–derived accumulation is used to assess the influence of multidecadal to centennial firn depth variability at the ice core locations, whereas output from the regional climate model (1980–2004) yields interannual firn depth variability over the entire continent.

Relatively modest deviations from the long-term mean accumulation rate can cause large changes in firn depth, especially when the anomalies last for several years (Fig. 1). A critical parameter for our results is this mean accumulation rate that we assume to balance the vertical ice velocity below the firn layer (*19*). We call this the balance accumulation rate (A_b), and its value is estimated using average accumulation rate over the length of the available time series. The shorter the time series, the less valid this approximation is. In theory, the averaging period over which A_b should be calculated is determined by the response time of ice flow to a certain change in accumulation. The response time of an ice mass is inversely proportional to the ice velocity (*21*, *22*), and thus also to A_b. Both velocity (*22*) and A_b (*20*) vary by several orders of magnitude over the Antarctic Ice Sheet. As a consequence, response times vary from millennia (for the dry East Antarctic Plateau) down to several decades (in fast flowing drainage basins in West Antarctica).

To illustrate the effects of accumulation rate anomalies at different time scales on firn depth variability, Fig. 1B shows simulated firn depth anomalies using a synthetic time series of accumulation rate, keeping annual mean temperature constant (Fig. 1A). Clearly, firn depth changes are determined not by the actual sign of the accumulation trend, but by the period and sign of the accumulation anomaly. In this particular case, a 100-year cycle in accumulation rate dominates the resulting dH/dt pattern. The effect of a 25-year accumulation rate fluctuation is smaller and superimposed on the 100-year signal (Fig. 1B).

Forcing the firn model with accumulation rate time series from an ice core drilled in coastal Dronning Maud Land (DML) (Fig. 1, C and D) reveals that firn depth increased by as much as 4 m between 1850 and 1920, and subsequently fell again by the same amount after 1955, in response to a persisting negative accumulation anomaly. Only in the past two decades does firn depth increase again. In Wilkes Land (WL), using a stack of three ice cores (*19*), firn depth has been increasing during the past three to four decades because of above-average accumulation rates.

Comparing simulated firn depth time series with linear ice sheet surface elevation trends from the European Remote-Sensing satellite ERS-2 (Fig. 1D) illustrates the limited value of the short satellite time series (1995–2003) in identifying long-term dH/dt values. Simulated firn depth trends at the core sites compare well with ERS-2 dH/dt in DML and in WL, where elevation trends can thus be explained by changes in firn depth. This is not valid for West Antarctica (using a stack of four ice cores) (*19*), where simulated firn depth increases but elevation decreases. This is indicative of dynamic thinning due to the recent acceleration of coastal glaciers (*5*–*7*, *23*).

[1]Institute for Marine and Atmospheric Research, Utrecht University, 3584 CC Utrecht, Netherlands. [2]Royal Netherlands Meteorological Institute, 3732 GK De Bilt, Netherlands. [3]Department of Electrical and Computer Engineering, University of Missouri, Columbia, MO 65211, USA. [4]School of Environmental and Life Sciences, University of Newcastle, Callaghan, NSW 2308, Australia.

*To whom correspondence should be addressed. E-mail: m.m.helsen@uu.nl

†Present address: Climate Risk CoRE and Department of Physical Geography, Macquarie University, NSW 2109, Australia.

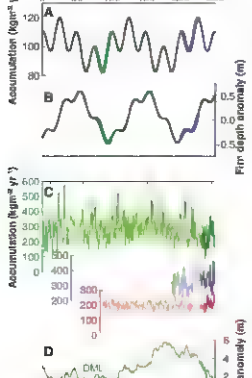

Fig. 1. Simulations of firn depth time series (**B** and **D**) using annual accumulation rate (**A** and **C**) as input data. A synthetic time series of accumulation rate (**A**) containing sinusoidal fluctuations around A_b = 100 kg m^{-2} year^{-1}, with periodicities of 25 and 100 years and each with an amplitude of 10 kg m^{-2} year^{-1}, results in firn depth changes (**B**) with a dominant signal on the 100-year time scale. Note the different response of firn depth within two 25-year periods (in green and blue), forced with accumulation time series that are identical in shape but not in their absolute value (A_{green} = 94 kg m^{-2} year^{-1}; A_{blue} = 106 kg m^{-2} year^{-1}). Time series of accumulation rate from ice cores (**C**) (*16*–*19*) show that irregular deviations from the long-term mean can result in firn depth changes of several meters (**D**). The light colors in (**C**) and (**D**) represent annual accumulation and resulting firn depth records from ice core accumulation data; darker colors are annual accumulation and firn depth records from RACMO2/ANT data (*19*). Observed ERS-2 elevation change trends over 1995–2003 are indicated as straight lines below the simulated firn depth time series; these agree well with firn depth simulations for WL and DML but disagree with West Antarctic firn depth anomalies. Note that the 25-year periods (colored) in (**B**) are conceptual analogs for the firn depth changes in DML and WL (**D**). Firn depth changes [in (**D**)] have been offset by ±2 m for clarity.

of skin temperature, solid precipitation, and sublimation at 6-hour intervals from the regional climate model RACMO2/ANT (*19*, *20*), so that we could correct for all variability < 25 years. For this experiment we used the 1980–2004 average accumulation rate ($A_{80\text{-}04}$) to estimate A_b, and as such we assumed that the ice sheet is in balance with $A_{80\text{-}04}$ (*19*). This period could be far too short to obtain a reliable estimate of A_b. However, ice budget calculations suggest that accumulation and outflow of the East Antarctic Ice Sheet are in near-balance (*7*). A deviation between A_b and $A_{80\text{-}04}$ will be reflected in a difference between simulated firn depth trend and observed dH/dt, and hence is due either to recent change in glacial flow velocity or to changes in accumulation rate on time scales larger than the RACMO2/ANT period.

In Antarctica, the effect of accumulation rate variability on firn depth by far outweighs the temperature effect (*19*). Consequently, the patterns in simulated firn depth trends over the ERS-2 observational period (1995–2003, Fig. 2A) mainly reflect the 1995–2003 accumulation anomaly (relative to $A_{80\text{-}04}$) (fig. S5). Areas with a positive accumulation anomaly and hence increasing firn depth are found in the Amundsen Sea Embayment (ASE), the Antarctic Peninsula (AP), DML, the Transantarctic Mountains (TM) along the Ross Ice Shelf, and the region east of the Amery Ice Shelf, whereas coastal WL and inland West Antarctica received less than average snowfall, resulting in a decrease in firn depth. The magnitude of simulated firn depth changes (Fig. 2A), −20 to +20 cm year^{-1}, is comparable to satellite-derived dH/dt values (*9*–*11*) (fig. S6). Figure 2A reveals that even during periods of insignificant trends in accumulation rate (*15*), accumulation variability can cause substantial ice sheet elevation changes.

Subtracting simulated firn depth changes (Fig. 2A) from satellite-derived dH/dt (fig. S6) results in an elevation change pattern that is corrected for firn depth variability (dH/dt_{corr}, Fig. 2B). A nonzero value of dH/dt_{corr} indicates an imbalance between $A_{80\text{-}04}$ and vertical ice velocity, but as indicated in Fig. 1, this does not necessarily mean that the ice sheet is out of balance on time scales longer than 25 years. It merely indicates that the 1980–2004 accumulation rate does not accurately represent A_b.

In Fig. 3, the different contributions of elevation change trends are summarized per drainage basin. An extensive error analysis is presented in (*19*). In West Antarctica, a recent positive accumulation anomaly over the ASE and AP has caused increasing firn depths in basins 14 to 19. However, ERS-2 dH/dt observations show a negative dH/dt in the ASE (basins 14 to 16) and in the AP (basin 18). Thus, the firn depth correction enhances the estimate of downward motion relative to the original ERS-2 data (Table 1). This has important implications for the estimation of ice sheet mass changes from dH/dt data (*19*).

The situation for western Palmer Land (PL, drainage basin 17) is different. The simulated firn depths have increased here as well, but they only explain half of the observed increase in surface height. It is likely that the onset of increased accumulation has occurred earlier than 1980, which implies that $A_{80\text{-}04}$ is an overestimate of A_b. This results in a large positive value of dH/dt_{corr} (Fig. 3), in agreement with other reconstructions of accumulation time series from this region (*24*, *25*).

Also in East Antarctica, large differences remain between the 1995–2003 firn depth trends and observed ice sheet elevation changes. In DML (basin 1), when corrected for the fact that firn depth increased during the period 1995–2003, a long-term thinning is found for the multidecadal time scale (Figs. 2B and 3). This is corroborated in Fig. 1D, with firn depth in DML decreasing during the second half the 20th century as the result of a negative accumulation anomaly. The simulated firn depth increase in DML (Fig. 2A) thus represents an overestimate of the observed dH/dt signal, because $A_{80\text{-}04} < A_b$. A conceptual analog for this situation is given by the green lines in Fig. 1, A and B. A negative accumulation anomaly results in a net 25-year negative firn depth trend, while a small elevation increase at the end of the period is visible. Note that these patterns occur without any long-term (<100-year) trend in accumulation.

The opposite situation is found in WL, East Antarctica (basin 6 and 7): Below-average accumulation during 1995–2003 (the satellite period) relative to 1980–2004 (the firn depth model period) causes a decreasing simulated firn depth in Fig. 2A, whereas a positive elevation change is observed. Values of dH/dt_{corr} therefore indicate ice sheet growth, which can be explained if $A_{80\text{-}04} > A_b$. The 25-year analog in Fig. 1, A and B, is outlined by the blue lines; variability within the 25-year period produces both increases and decreases in firn depth, while the dominant signal is a positive firn depth trend, given that the 25 year average accumulation exceeds A_b. Hence, positive dH/dt values in East Antarctica are not caused by a positive trend in accumulation over the period of observation, as suggested by (*10*), but instead by a positive accumulation anomaly over a longer (>25-year) time scale. This also agrees with increased continental average accumulation found for the period 1955–1999 (*3*). These results demonstrate that to confidently assess the mass budget of the Antarctic Ice Sheet from satellite dH/dt data, these observations first need to be further constrained and corrected by a firn densification model forced by independent data (e.g., accumulation time series from ice cores).

We have shown that even insignificant trends in accumulation can cause considerable ice sheet elevation changes. Removing the interannual

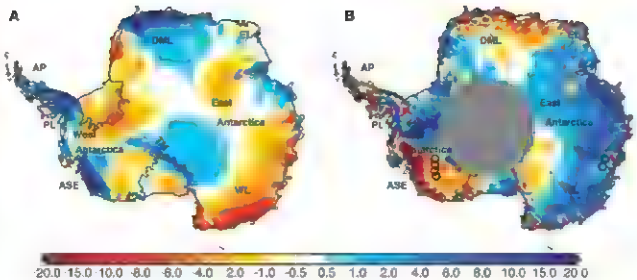

Fig. 2. (**A**) Simulated firn depth trends over the period 1995–2003. (**B**) Observed elevation change trends corrected for firn depth variability as derived from ERS-2 satellite altimetry data over the same period. Firn depth increases over DML, AP, ASE, and along the TM, whereas decreasing firn depths are observed over areas such as WL. The corrected elevation change pattern in (B) reveals a pattern of strongly decreasing ice sheet elevation over the ASE, moderate decreasing elevation over DML, and increasing elevation over a large part of East Antarctica. Black circles in (B) indicate ice core locations that are used in Fig. 1, thick line indicates edge of the grounded ice sheet; gray areas indicate ablation areas (A) and areas without reliable ERS-2 data (B). DML, Dronning Maud Land; EL, Enderby Land; AP, Antarctic Peninsula; PL, Palmer Land; ASE, Amundsen Sea Embayment; TM, Transantarctic Mountains; WL, Wilkes Land.

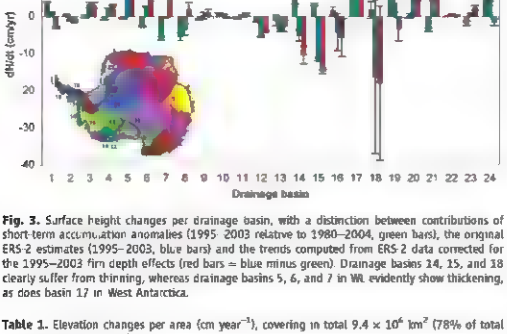

Fig. 3. Surface height changes per drainage basin, with a distinction between contributions of short-term accumulation anomalies (1995–2003 relative to 1980–2004, green bars), the original ERS-2 estimates (1995–2003, blue bars) and the trends computed from ERS-2 data corrected for the 1995–2003 firn depth effects (red bars = blue minus green). Drainage basins 14, 15, and 18 clearly suffer from thinning, whereas drainage basins 5, 6, and 7 in WL evidently show thickening, as does basin 17 in West Antarctica.

Table 1. Elevation changes per area (cm year^{-1}), covering in total 9.4 × 10^6 km^2 (78% of total grounded ice sheet area).

	Firn depth	Uncorrected ERS-2	Corrected ERS-2
ASE	3.5 ± 0.5	−9.2 ± 0.7	−12.7 ± 0.9
Rest of West Antarctica	0.6 ± 0.3	2.1 ± 0.8	1.6 ± 0.8
East Antarctica	−0.6 ± 0.1	1.8 ± 0.5	2.4 ± 0.5
Total	−0.2 ± 0.1	1.1 ± 0.5	1.3 ± 0.5

variability in firn depth from satellite radar altimetry data reveals strong dynamical thinning in the ASE. On the other hand, a large part of the East Antarctic Ice Sheet shows increasing elevation due to accumulation variability on time scales larger than 25 years. We conclude that accumulation variability over a wide range of time scales has a large influence on ice sheet elevation changes, and needs to be taken into account for the assessment of the Antarctic mass budget.

References and Notes

1. J. Oerlemans, *Nature* **290**, 770 (1981).
2. G. A. Meehl *et al.*, in *Climate Change 2007: The Physical Science Basis*, S. Solomon *et al.*, Eds. (Cambridge Univ. Press, Cambridge, 2007), pp. 747–845.
3. A. J. Monaghan, D. H. Bromwich, D. P. Schneider *Geophys. Res. Lett.* **35**, L07502 (2008).
4. A. J. Monaghan *et al.*, *Science* **313**, 827 (2006).
5. E. Rignot, R. H. Thomas, *Science* **297**, 1502 (2002).
6. R. H. Thomas *et al.*, *Science* **306**, 255 (2004); published online 23 September 2004 (10.1126/science.1099650)
7. E. Rignot *et al.*, *Nat. Geosci.* **1**, 106 (2008).
8. P. Lemke *et al.*, in *Climate Change 2007: The Physical Science Basis*, S. Solomon *et al.*, Eds. (Cambridge Univ. Press, Cambridge, 2007), pp. 337–383.
9. H. J. Zwally *et al.*, *J. Glaciol.* **51**, 509 (2005).
10. C. H. Davis, Y. Li, J. R. McConnell, M. M. Frey, E. Hanna, *Science* **308**, 1898 (2005); published online 19 May 2005 (10.1126/science.1110662).
11. D. J. Wingham, A. Shepherd, A. Muir, G. J. Marshall, *Philos. Trans. R. Soc. London Ser. A* **364**, 1627 (2006).
12. R. J. Arthern, D. J. Wingham, *Clim. Change* **40**, 605 (1998).
13. H. J. Zwally, J. C. J. *Glaciol.* **48**, 199 (2002).
14. J. Li, H. J. Zwally, J. C. Comiso, *Ann. Glaciol.* **46**, 8 (2007).
15. M. R. van den Broeke, W. J. van den Berg, E. van Meijgaard, *Geophys. Res. Lett.* **33**, L02505 (2006).
16. I. Goodwin, M. de Angelis, M. Pook, N. W. Young, *J. Geophys. Res.* **108**, 10.1029/2002JD002995 (2003).
17. M. Kaczmarska *et al.*, *Ann. Glaciol.* **39**, 339 (2004).
18. S. Kaspari *et al.*, *Ann. Glaciol.* **39**, 585 (2004).
19. See supporting material on Science Online.
20. W. J. van de Berg, M. R. van den Broeke, C. H. Reijmer E. van Meijgaard, *J. Geophys. Res.* **111**, D11104 (2006).
21. J. F. Nye, *Geophys. J. R. Astron. Soc.* **7**, 431 (1963).
22. J. L. Bamber, D. G. Vaughan, I. Joughin, *Science* **287**, 1248 (2000).
23. A. Shepherd, D. J. Wingham, J. A. D. Mansley, H. F. J. Corr, *Science* **291**, 862 (2001).
24. J. Turner, T. Lachlan-Cope, S. Colwell, G. J. Marshall, *Ann. Glaciol.* **41**, 85 (2005).
25. E. R. Thomas, G. J. Marshall, J. R. McConnell, *Geophys. Res. Lett.* **35**, L01706 (2008).

26. We thank M. Kaczmarska, S. Kaspari, and A. Monaghan for generously providing time series of accumulation rates, and three anonymous reviewers for their comments

that improved this manuscript. Supported by NWO's Netherlands Polar Programme (M.M.H., W.J.v.d.B.) and by NASA's Cryospheric Sciences Program (C.H.D., Y.-L.). ERS-2 radar altimeter data were provided by NASA Goddard Space Flight Center. All authors have discussed results and contributed to the manuscript. M.M.H. developed the firn densification model and integrated the results. M.M.H., M.R.v.d.B., and R.S.W.v.d.W. frequently discussed results. M.R.v.d.B., W.J.v.d.B., and E.v.M. contributed to RACMO2/ANT data. C.H.D. and Y.-L. analyzed elevation changes from ERS-2 data. I.G. contributed to accumulation records.

Supporting Online Material
www.sciencemag.org/cgi/content/full/1153894/DC1
Materials and Methods
Figs. S1 to S9
Table S1
References

7 December 2007; accepted 7 May 2008
Published online 29 May 2008.
10.1126/science.1153894
Include this information when citing this paper

Natural Selection Shapes Genome-Wide Patterns of Copy-Number Polymorphism in *Drosophila melanogaster*

J. J. Emerson,[1,2*†] Margarida Cardoso-Moreira,[1,3,4*†] Justin O. Borevitz,[1] Manyuan Long[1]

The role that natural selection plays in governing the locations and early evolution of copy-number mutations remains largely unexplored. We used high-density full-genome tiling arrays to create a fine-scale genomic map of copy-number polymorphisms (CNPs) in *Drosophila melanogaster*. We inferred a total of 2658 independent CNPs, 56% of which overlap genes. These include CNPs that are likely to be under positive selection, most notably high-frequency duplications encompassing toxin-response genes. The locations and frequencies of CNPs are strongly shaped by purifying selection, with deletions under stronger purifying selection than duplications. Among duplications, those overlapping exons or introns, as well as those falling on the X chromosome, seem to be subject to stronger purifying selection.

Differences in the numbers of copies of large DNA segments are an abundant source of genetic variation in humans (*1*, *2*), mice (*3*), and flies (*4*). Because CNPs can create new genes, change gene dosage, reshape gene structures, and/or modify the elements that regulate gene expression, understanding their evolution is at the very heart of understanding how such structural changes in the genome contribute to the phenotypic evolution of organisms (*5*–*7*).

A rigorous characterization of CNPs requires high resolution data unbiased with respect to genome annotation. We used tiling arrays covering the full euchromatic genome of *D. melanogaster* at a median density of one unique perfect match probe for every 36 base pairs (bp) (*8*, *9*) in 15 natural isofemale lines (table S1). We inferred copy number changes with a hidden Markov model (HMM) (*9*) that inferred the posterior probabilities for copy number by comparing DNA hybridization intensities between natural isolates and the reference genome strain. Training data for copy number changes were obtained via hybridization with a line known to contain a ~200-kb homozygous duplication and from a set of 52 validated homozygous deletions (*9*). The probabilities of mutation were parsed to make CNP calls (table S3).

Because tiling arrays are restricted to nonredundant regions in the reference genome, deletion and duplication are detected by the absence of nonredundant DNA and by the doubling of unique DNA, respectively. In principle, it is possible to confound unique duplications with multiple hit scenarios of deletion of ancestral duplications. However, the few CNPs that exhibited even weak signs of ancestral redundancy in either *D. simulans* or *D. yakuba* (109 CNPs) showed a site frequency spectrum (SFS) suggesting that the derived state cannot be a deletion [table S4, (*9*)]. Nevertheless, we excluded those events from our analyses.

In order to validate the CNP predictions, we performed polymerase chain reaction–based assays (*9*). For duplications, we obtained a false-positive rate of 14% and a false-negative rate of 16%. Notably, our assay can only amplify tandem duplications lying within several kilobases of each other, suggesting that the false-positive rate is overestimated. Conversely, the fact that we confirmed 86% of the duplications confirms that most CNPs form in tandem. For deletions, we obtained a false-positive rate of 47%. This high rate of falsely called deletions is in part due to the prevalence of multiple adjacent single-nucleotide polymorphisms (SNPs) in highly polymorphic regions of the *D. melanogaster* genome (*10*). We also obtained a false-negative rate of 18% for homozygous deletions and 32% for heterozygous deletions.

We detected 2658 unique CNPs among all 15 lines of *D. melanogaster*, with an average of 312 CNPs (SD = 31.9 CNPs), after adjusting for false positives. Except where noted, total mutation counts are corrected only for false positives. In total, CNPs comprise ~2% of the genome. The size distribution of CNPs was roughly exponential, with most being small variants (median, 336 bp) and few being larger variants (maximum size detected: 35 kb). The predicted and real CNP boundaries differ only by about one probe for duplications and about three probes for deletions (table S3). These data indicate that we were able to both detect

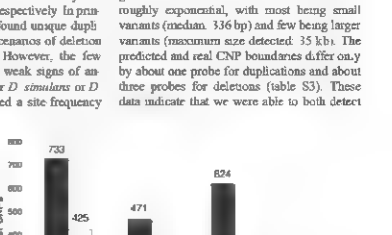

Fig. 1. Frequency of CNPs within different genomic contexts. The numbers of polymorphic duplications (black) and deletions (white) are shown for four mutually exclusive genomic contexts: intergenic (mutations between genes), intronic (mutations entirely within introns), exonic (mutations that overlap exons but not complete gene structures), and complete gene (mutations that overlap at least one complete gene structure, including UTRs).

[1]Department of Ecology and Evolution, University of Chicago, Chicago, IL 60637, USA. [2]Genomics Research Center, Academia Sinica, Taipei 115, Taiwan. [3]Graduate Program in Areas of Basic and Applied Biology, Universidade do Porto, Porto, Portugal. [4]Faculdade de Ciências, Universidade do Porto, Porto, Portugal.

*These authors contributed equally to this work.
†To whom correspondence should be addressed. E-mail: jje@uchicago.edu (J.J.E.); mmoreira@uchicago.edu (M.C.M.)

Table 1. Description of the CNP dataset: number of events, frequency of singletons (CNPs detected in only one population), and size. We assumed a false-positive rate of 14% for duplications and 47% for deletions. Size and frequency of singletons were determined with the raw data.

CNP type	Number of events		Size (bp)		Frequency of singletons
	Raw data	Corrected false positives	Median	Mean	
Duplications	2211	1901	367	1117	0.75
Deletions	1428	757	282	604	0.67

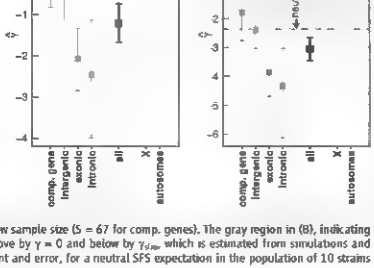

Fig. 2. Selection coefficients for polymorphic duplications with estimates obtained with the PRF-SFS methodology (*19*) are shown, both with and without incorporating ascertainment bias and error into the likelihood [(A) and (B) respectively]. Squares indicate the maximum likelihood estimates of γ (selection coefficient). Error bars indicate the 95% confidence interval ($\alpha > 0.05$ in a likelihood ratio test-ing framework) for the parameter γ. The upper bound was not plotted for complete (comp.) gene duplications because of low sample size (S = 67 for comp. genes). The gray region in (B), indicating neutrality, is bounded above by $\gamma = 0$ and below by $\gamma_{5\%}$, which is estimated from simulations and corrected for ascertainment and error, for a neutral SFS expectation in the population of 10 strains [section 7.1.1 in (*9*)].

small CNPs as well as estimate CNP boundaries with precision (table S4). Despite a smaller sample size and a smaller genome, this study detected more CNPs than a recent survey in humans [2658 detected here versus 1447 detected in (*2*)]. This discrepancy is likely explained by the denser genome coverage in this study. Our data suggest that humans harbor a class of CNPs that is much larger than anything observed in fruit flies and that recent mammalian studies may be neglecting most small scale variations.

Duplications outnumbered deletions 2.5:1 (Sign test P value $< 2.22 \times 10^{-16}$, Fig. 1) and were significantly larger (Wilcoxon rank sum test, P value $< 2.22 \times 10^{-16}$, Table 1). One mechanism thought to be an important contributor to tandem CNP formation—nonallelic homologous recombination—leads to either one gamete with a duplication and another with a complementary deletion or only one gamete carrying a deletion (*11*). Thus, nonallelic homologous recombination generates either an equal number of each mutation or an excess of deletions. Additionally, studies of insertion and deletion variation have shown a deletion bias in *D. melanogaster*, although the mutations' size (*12*) was considerably smaller than those examined here. The fact that we observed fewer deletions when either an equal number or an increased number of deletions was expected suggests that a large proportion of deletions are removed from the population by purifying selection. In this context, the dearth of deletions observed in our data, as well as the smaller size of the deleted variants, suggest that they are far more deleterious than duplications and that larger mutations are more deleterious than smaller ones.

Every region of the genome harbors at least low levels of CNPs. The median distance between two events was 12.6 kb (fig. S5). We found that pericentromeric regions were enriched in duplications, though not in deletions (fig. S5). Such regions are known to be rich in duplications (*13*). Redundancy results in a lower probe resolution in those regions, suggesting that our observation of increased levels of polymorphism was actually conservative. However, given the lower probe resolution in our work and the smaller size of deletions, we cannot assume that the absence of deletions in such regions is not artifactual. Pericentromeric regions are also characterized by extremely low rates of crossing-over, leading to a lower effective population size as a result of linkage (*14*). Therefore, the higher density of CNPs observed in these regions may be a consequence of the reduced effectiveness of selection in purging deleterious mutations (*14*). Alternatively, the mutation rate may simply be higher in such regions (*15*).

The genome distribution of CNPs varied significantly both between genome regions (i.e., coding versus noncoding) as well as between mutation types (i.e., duplication versus deletion) (Fig. 1). Duplications outnumbered deletions in all categories (all Sign test P values $< 1 \times 10^{-10}$). Deletions falling in coding regions represented a smaller proportion of all deletions as compared with duplications (Fig. 1, Fisher's exact test P value $< 2.2 \times 10^{-16}$).

Given the high incidence and widespread genomic distribution of CNPs, it is not surprising that 8 and 2% of genes were at least partially duplicated or deleted, respectively. Before correcting for false positives, we found 133 genes completely duplicated and 27 completely deleted (table S5). Among completely deleted genes, two have known, nonlethal mutant phenotypes (*16*). Tandem duplications of a sequence partially overlapping adjacent genes may create a chimera between them while leaving intact versions of both donor genes. We identified 92 CNPs that appear to be such chimeras. Curiously, 1.5 times as many duplications overlap the ends of genes than their starting points (Sign test P value = 0.0101), which is similar to the excess of transposable element insertions observed in 3′ untranslated regions (3′ UTRs) in *D. melanogaster* (*17*).

Taken together, the evidence above suggests that purifying selection eliminates a large fraction of standing CNP variation, especially deletions. Previous research on CNPs in humans (*1*) suggests that purifying selection may shape patterns of copy-number variation. Therefore, we tested selection on these variants in *D. melanogaster* by analyzing the distribution of allele frequencies (the SFS) [table S7 and fig. S8, (*18*)]. Purifying selection against deleterious mutations increases the fraction of rare variants, which is a common signature of natural selection. However, an excess of rare variants may also represent demographic processes such as population expansion, bottlenecks, or population structure (*19*). In order to quantify these effects, we sampled putatively neutral mutations. We collected ~600 synonymous SNPs from 46 loci located in all major chromosome arms in all 15 lines (*9*) and eliminated the effects of population structure (*9*, *20*). We then estimated demographic parameters for two models using a Poisson random fields–SFS (PRF-SFS) approach (*19*): (i) a two-epoch model to identify recent population expansions and (ii) a three-epoch model to identify bottlenecks (*21*–*23*). Because neither scenario rejected the neutral model ($P = 0.39$ and $P = 0.07$, respectively), we used the standard neutral model as the demographic null hypothesis (*9*). All SFS analyses were performed with raw CNP calls

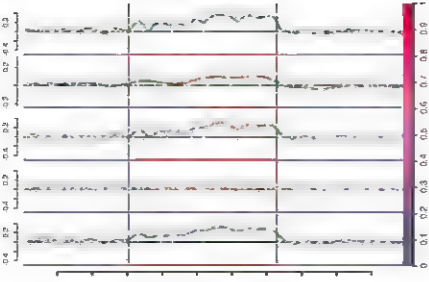

Fig. 3. Representation of a subset of 5 out of 15 individuals for the *Cyp6g1* polymorphism. The image in each row represents the log ratio of array intensities for the natural and reference lines as a function of genome position on chromosome 2R in kilobases. The green line is a smoothing spline for reference. The shading below each image indicates the posterior probability of duplication from the HMM, with red indicating a probability of 1 and blue indicating a probability of 0. The vertical lines indicate our boundary calls.

greater than 500 bp to restrict our inferences to mutations with smaller error rates, with error and bias corrected [as described in (*9*)].

We estimated γ, the scaled coefficient of natural selection (*9*, *19*). Our estimates show that natural selection is a pervasive force shaping the standing variation in *D. melanogaster* (Fig. 2). Notably, selection differentially influenced CNP evolution among different genomic features as well as among different chromosomes. We compared the patterns of variants between the different classes of variants: both correcting for bias and error and with no corrections. For inferences incorporating error and bias (Fig. 2A), we found that the intronic class exhibited the largest reduction in variation ($\gamma = -2.5$), although duplications within exons were only slightly less disfavored ($\gamma = -2.1$). We detected a significantly higher constraint in intronic than in intergenic regions ($\gamma = -0.34$). This observation contrasts with studies of nucleotide variation that found similar levels of constraint in both regions (*24*, *25*). This may be because introns are more strongly constrained by changes in size [e.g., for proper splicing (*26*, *27*)]. We hypothesize that duplications involving partial gene structures (the exonic and intronic classes) were the most strongly disfavored, because such mutations often result in the disruption of genes.

Notably, complete gene duplications showed the least constraint. Despite our conservative corrections for bias and error (*9*), we fail to reject neutrality. This unexpected observation is compatible with the hypothesis that full duplications are redundant. This result should, however, be interpreted with caution, because the synonymous SNPs that were used to parameterize the demographic model may be under weak purifying selection, potentially leading to an underestimate of the selection coefficient. Also, assuming a fixed selection coefficient may be wrong, because the set of complete gene duplications may include both advantageous and deleterious mutations.

We also found that the autosomes have higher selection coefficients than the X chromosome (Fig. 2). This observation is compatible with the following models: (i) duplicate mutations on the X chromosome are more deleterious than those on autosomes (X linked genes may be more sensitive to changes in dosage) and/or (ii) duplicate polymorphisms tend to be slightly deleterious and recessive.

We identified five duplications overlapping seven genes involved in the response to toxins. For example, a duplication encompassing *Cyp6g1* and *Cyp6g2* was present in 13 of the 15 lines. *Cyp6g1* confers resistance to DDT and is known to be under positive selection for increased gene product [Fig. 3, (*28*)]. Three other independent high-frequency duplication events overlap four other genes (*Ugt86Dj*, *Ugt86Dh*, *CG30438*, and *CG10170*) involved in the response to toxins, and we found another duplicate gene (*Ugt86Di*, in one line) involved in the response to toxins. These duplications are good candidates to be under positive selection.

Overall, we present compelling evidence that the regional patterns of duplicate and deletion variation showed strong evidence for the pervasive action of natural selection, both in their patterns of polymorphism and in their distribution in the genome. These conclusions provide a comprehensive picture of the polymorphic phase of copy number change.

References and Notes

1. L. Feuk, A. R. Carson, S. W. Scherer, *Nat. Rev. Genet.* **7**, 85 (2006).
2. R. Redon *et al.*, *Nature* **444**, 444 (2006).
3. T. A. Graubert *et al.*, *PLoS Genet.* **3**, e3 (2007).
4. E. B. Dopman, D. L. Hartl, *Proc. Natl. Acad. Sci. U.S.A.* **104**, 19920 (2007).
5. M. Long, E. Betrán, K. Thornton, W. Wang, *Nat. Rev. Genet.* **4**, 865 (2003).
6. S. P. Otto, P. Yong, *Adv. Genet.* **46**, 451 (2002).
7. F. A. Kondrashov, A. S. Kondrashov, *J. Theor. Biol.* **239**, 141 (2006).
8. F. Bilstar *et al.*, *Proc. Natl. Acad. Sci. U.S.A.* **102**, 15907 (2005).
9. Materials and methods are available as supporting material on *Science* Online.
10. J. O. Bonvitz *et al.*, *Genome Res.* **13**, 513 (2003).
11. D. J. Turner *et al.*, *Nat. Genet.* **40**, 90 (2008).
12. D. A. Petrov, E. R. Lozovskaya, D. L. Hartl, *Nature* **384**, 346 (1996).
13. A. S. Fiston-Lavier, D. Anxolabéhere, H. Quesneville, *Genome Res.* **17**, 1458 (2007).
14. L. Gordo, B. Charlesworth, *Curr. Biol.* **11**, 1684 (2001).
15. C. M. Bergman, H. Quesneville, D. Anxolabéhere, M. Ashburner, *Genome Biol.* **7**, R112 (2006).
16. M. Ashburner, R. Drysdale, *Development* **120**, 2077 (1994).
17. M. Ignatov, K. Lunkow, D. A. Petrov, C. M. Bergman, *BMC Biol.* **3**, 24 (2005).
18. B. Charlesworth, C. H. Langley, *Annu. Rev. Genet.* **23**, 251 (1989).
19. S. H. Williamson *et al.*, *Proc. Natl. Acad. Sci. U.S.A.* **102**, 7882 (2005).
20. J. K. Pritchard, M. Stephens, P. Donnelly, *Genetics* **155**, 945 (2000).
21. P. R. Haddrill, K. R. Thornton, B. Charlesworth, P. Andolfatto, *Genome Res.* **15**, 790 (2005).
22. N. Li, M. Stephens, *PLoS Genet.* **2**, e166 (2006).
23. J. E. Pool, C. F. Aquadro, *Genetics* **174**, 915 (2006).
24. P. Andolfatto, *Nature* **437**, 1149 (2005).
25. D. L. Halligan, P. D. Keightley, *Genome Res.* **16**, 875 (2006).
26. S. M. Mount *et al.*, *Nucleic Acids Res.* **20**, 4255 (1992).
27. M. Deutsch, M. Long, *Nucleic Acids Res.* **27**, 3219 (1999).
28. R. J. Daborn *et al.*, *Science* **297**, 2253 (2002).
29. J.L.T. was supported by an NSF Graduate Research Fellowship, an NSF Doctoral Dissertation Improvement Grant, and a Graduate Assistantships in Areas of National Need training grant. M.C.M. was supported by the Portuguese Foundation for Science and Technology (PDCT 2010, FSE). J.O.B. was supported by NIH R01GM074822. M.I. was supported by the Packard Fellowship for Science and Engineering, the NSF Career Award (MCB-0238168), and NIH (RO1GM065429-03A1 and 3R01GM074870-01A1). We thank J. Pool and M. . Wu for providing the lines used in the study; J. Byrnes, G. Coop, R. Hudson, J. Shapiro, K. Thornton, R. Arguello, M. Vibranovski, and other members of the M... laboratory for discussions; A. Boyko for PRF-SFS methodology and code; M. Noor for characterizing the hybridization properties of the tanning foci; and M. Y. . u, H. M. Sung, and J. Spofford for help with the manuscript. Assay information is deposited in the Gene Expression Omnibus database (accession number GSE11326), and sequence polymorphism information is deposited in the GenBank database (accession numbers EU706459 to EU707348).

Supporting Online Material

www.sciencemag.org/cgi/content/full/1158078/DC1
Materials and Methods
Figs. S1 to S8
Tables S1 to S7
References and Notes

20 March 2008; accepted 15 May 2008
Published online 5 June 2008.
10.1126/science.1158078
Include this information when citing this paper

Phylogeny-Aware Gap Placement Prevents Errors in Sequence Alignment and Evolutionary Analysis

Ari Löytynoja* and Nick Goldman

Genetic sequence alignment is the basis of many evolutionary and comparative studies, and errors in alignments lead to errors in the interpretation of evolutionary information in genomes. Traditional multiple sequence alignment methods disregard the phylogenetic implications of gap patterns that they create and infer systematically biased alignments with excess deletions and substitutions, too few insertions, and implausible insertion-deletion–event histories. We present a method that prevents these systematic errors by recognizing insertions and deletions as distinct evolutionary events. We show theoretically and practically that this improves the quality of sequence alignments and downstream analyses over a wide range of realistic alignment problems. These results suggest that insertions and sequence turnover are more common than is currently thought and challenge the conventional picture of sequence evolution and mechanisms of functional and structural changes.

New DNA sequencing methods permit quick and affordable exploration of genomic sequences of different organisms. Some of the greatest beneficiaries of the rapid increase of sequence data are comparative genomic studies that seek to provide increasingly accurate reconstruction of evolutionary histories of related genomes, e.g., to study functional and structural sequence changes leading to phenotypic differences between species (*1*–*4*). However, all sequence analyses that rely on evolutionary information require an accurate sequence alignment, i.e., the correct identification of homologous nucleotides or amino acids and the positioning of gaps indicating inserted and deleted sequence.

Alignment is still a highly error-prone step in comparative sequence analysis. Different multiple sequence alignment methods often lead to drastically different conclusions in both phylogenetic analyses and functional studies (supporting online material text), and alternative alignments of the same data can support entirely different mechanisms driving evolutionary and functional changes in sequences. As an example, a traditional alignment of HIV and SIV envelope glycoprotein gp120 (*5*) (Fig. 1A) has a familiar pattern of insertions and deletions squeezed compactly between conserved blocks of structurally important residues and suggests that part of the variable V2 region has a high amino acid–substitution rate and has shortened over time at a mutation hotspot where overlapping sites have been independently deleted in different evolutionary branches, some sites as many as eight times among the 23 sequences included. With an alignment method that considers the sequences' phylogeny and distinguishes insertions from deletions (*5*), the story is different. Instead of multiple point substitutions and loss of sequence, the region evolves through short insertions and deletions, allowing for rapid and radical changes in the coding sequence (Fig. 1B). The latter alignment, which suggests rapid turnover of sequence material instead of long ancestral sequences shrinking in length, provides a more convincing mechanism for the evolution of this region. Furthermore, its association of gap patterns with meaningful insertion and deletion events at the branches of the phylogenetic tree, i.e., specific points in the history of the sequences, allows a realistic reconstruction of the evolutionary process leading to the present-day sequences. In this example, the different implications of the alternative alignments for the mechanisms and time scale of sequence changes may be of medical importance for understanding the evolutionary dynamics of HIV (*6*), particularly in this protein region where insertions, deletions, and substitutions are associated with the efficiency of HIV entry, biological phenotype, and neutralizing antibody response (*7*–*11*).

Progressive algorithms (*12*–*15*), the multiple sequence alignment methods most widely used today, are based on backtracking the evolutionary process and building a multiple alignment from pairwise alignments between sequences and sequence alignments, performed in order of decreasing relatedness (Fig. 2) (supporting online material text). However, whereas insertion and deletion events are indistinguishable when comparing one pair of sequences, the two events differ greatly in progressive iteration of pairwise alignments. A gap for a deletion, with its associated penalty, is created only once, but a gap for an insertion has to be opened multiple times (Fig. 2, A and B). Simple iteration associates a full penalty with each of these gap-opening events, which leads to excessive penalization of single insertion events.

No alignment methods have previously implemented a precise solution to this problem, instead, heuristics to lower the penalty for opening gaps at positions already containing gaps have been used (*12*, *14*). Although these site-specific penalties reduce the high overall cost of single insertion events and encourage subsequent alignment iterations to correctly place their gaps at the same position, the approach fails when there are multiple nearby insertions and deletions and becomes systematically biased. By definition, inserted characters are not descendants of—and thus are not homologous with—any other insertions or ancestral characters, and should never align with anything (Fig. 2C, evolution). Progressive algorithms, however, always incorrectly align neighboring insertions in the same column if that is not explicitly prevented, the use of site-specific gap penalties, instead of preventing the incorrect matching of independent insertions, encourages it (Fig. 2C, site-specific alignment). Such "collapsed insertions" create incorrect homologies and, as the resulting gap pattern implies multiple independent deletions, give an impression of deletion hotspots where the overly long ancestral sequences are shortened (Fig. 2C, interpretation). In addition, the procedure also lowers the penalties at deletion sites where no further gaps are required, creating "gap magnets" that make nearby deletions coincide in subsequent stages of progressive iteration (Fig. 2D, evolution and site-specific alignment). Similarly to incorrectly aligned insertions, the clustering of deletions creates false homologies and gives an impression of deletion hotspots (Fig. 2D, interpretation).

We previously identified the problem of multiple penalization of insertions and reported a preliminary attempt to solve it (*16*). This uses a phylogeny-aware approach that "flags" the gaps made in previous alignments and, using evolutionary information from related sequences to indicate whether each gap has been created by an insertion or a deletion, permits their "reuse" for inserted characters without further penalty in the next stage of the progressive alignment (Fig. 2C, phylogeny aware alignment). In addition, information from closely related sequences can be used to infer sites as "permanent" insertions that cannot be matched in subsequent alignments (*5*), so that distinct insertion events are correctly kept separate even when they occur at exactly the same position. If related sequences indicate that a gap is caused by a deletion, flags are removed and no further free gaps at that position are permitted (Fig. 2D), and the effect is correctly targeted on insertions only.

To understand the type and magnitude of algorithm-based errors in traditional sequence

European Molecular Biology Laboratory—European Bioinformatics Institute, Wellcome Trust Genome Campus, Hinxton CB10 1SD, UK.

*To whom correspondence should be addressed. E-mail: ari@ebi.ac.uk

alignment methods, we compared the accuracy of different variants of the progressive algorithm, including our implementation of the new phylogeny-aware algorithm distinguishing insertions and deletions (as described above). We simulated synthetic DNA sequence data according to 16-, 32-, and 64-taxon symmetric trees using realistic evolutionary parameters, mimicking the evolution of genomic DNA without the structural and functional constraints expected in protein coding regions and so that the true alignments contained equal numbers of insertions and deletions (*5*). For the 16-taxon tree we set evolutionary relationships close, intermediate, and distant (Fig. 3, see color gradients), approximately representing comparisons of primates, primates and rodents, and mammals, respectively. Using the 32- and 64-taxon trees and the maximum species divergence of the close set, we assessed the effects of denser sampling (2X and 4X, respectively) of increasingly similar sequences (fig. S1). The sequences were aligned by using a set of published alignment software programs based on variants of the traditional progressive algorithm [CLUSTAL W (*12*), MAFFT (*15*), MUSCLE (*14*) and T-COFFEE (*13*)] and the phylogeny-aware algorithm [PRANK (*16*). we used the PRANK$_{+F}$ variant indicating "permanent" insertions (*5*)]. For each alignment, various statistics describing the inferred insertion-deletion processes and the accuracy of the solution were computed.

The alignments generated by the alternative methods vary greatly even for the closely related sequences. The methods implementing the traditional algorithm produce alignments with all the errors expected from a biased, nonphylogenetic handling of insertions and deletions. The failure to separate distinct, nearby insertions leads to underestimation of their true number (Fig. 3A) and overestimation of the number of deletions (Fig. 3B); this gives seriously incorrect estimates of the insertion rate/deletion rate ratio (Fig. 3C). Collapsed insertions and gap magnets create an impression of mutation hotspots where the same sequence sites are deleted multiple times [indicated by the "gap overlap" statistic (Fig. 3D)]. These problems make the alignments overly compact and are reflected in the proportion of alignment columns recovered entirely correctly (Fig. 3, E and F). In contrast to the traditional algorithm, the phylogeny-aware PRANK$_{+F}$ program is not systematically biased. It has slightly superior performance in terms of alignment length and proportion of correct columns but, crucially, it is unbiased with respect to insertions and deletions and has virtually no error in all the other measures of insertion and deletion parameters.

As distances between sequences increase, the greater numbers of insertions, deletions, and substitutions make the sequences more difficult to align. The proportion of columns correct is a very stringent measure of alignment accuracy, even under this measure, PRANK$_{+F}$ clearly performs best in response to increased sequence divergence (Fig. 3F, close-intermediate-distant). However, this masks much deeper underlying problems in the traditional algorithms, as can be clearly seen in the growth of the errors in all statistics describing the insertion-deletion processes (Fig. 3, A to E, close-intermediate-distant). In contrast, PRANK$_{+F}$, already more accurate for close sequences, shows superior performance as evolutionary distances increase and alignment becomes more difficult (Fig. 3, A to E, close-intermediate-distant). Although the correctness of individual insertions and deletions created decreases in more difficult alignments (table S1), the phylogeny aware method still suffers no systematic bias concerning the number of each type of event inferred.

As errors increase with greater evolutionary distances, the only way to improve alignments would seem to be to follow the practice widely used in phylogenetics, that is, to sample additional intermediate sequences (*17*–*19*), which increases the average sequence similarity. We find that this additional sequence information does not help the traditional methods.

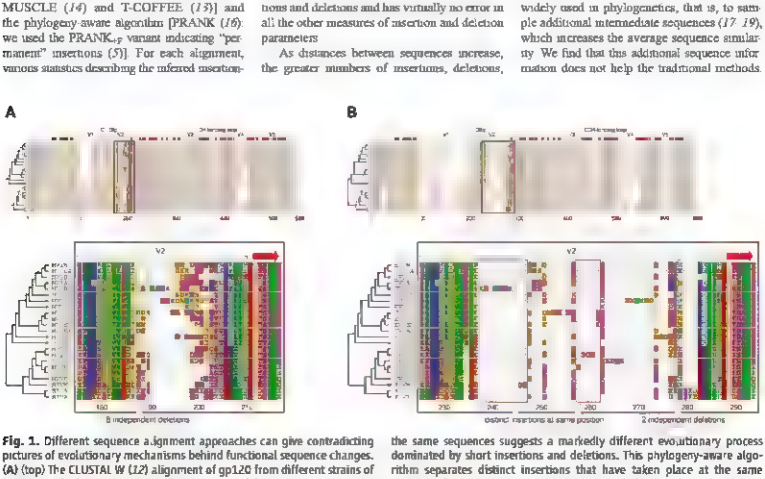

Fig. 1. Different sequence alignment approaches can give contradicting pictures of evolutionary mechanisms behind functional sequence changes. **(A)** (top) The CLUSTAL W (*12*) alignment of gp120 from different strains of human and simian immunodeficiency virus (*5*) represents a typical structural matching of protein sequences and clusters nearby alignment gaps in tight blocks. (bottom) The expanded fragment suggests that part of the V2 region evolves with a high rate of point substitutions and is shortened over evolutionary time by numerous overlapping deletions. For example, the pattern of gaps highlighted with a green box requires eight independent deletions, which have occurred in the lineages marked with green dots in the tree on the left. **(B)** (top) The PRANK$_{+F}$ (*5*) alignment of the same sequences suggests a markedly different evolutionary process dominated by short insertions and deletions. This phylogeny-aware algorithm separates distinct insertions that have taken place at the same positions (bottom: examples highlighted with blue and red boxes and dots) while permitting homologous sites to be deleted multiple times when the data support this (e.g., column highlighted in green). Alignment annotations indicate the V1 to V5 variable regions, C108g epitope, CD4-binding loop, N-linked glycosylation sites (residues N in bold white type), and α helices (blue blocks) and β strands (red blocks) of the known HIV-1 gp120 structure (*5*). Both alignments used the guide phylogeny generated by CLUSTAL W (left).

Instead, the additional sampling creates increasingly serious errors for all computed measures of accuracy (Fig. 3, A to F, close-2X 4X), very similar to the patterns observed with increasing evolutionary distance. This disappointing result is explained by the fact that both greater evolutionary distances and greater numbers of closely related sequences increase the total tree length, i.e., the evolutionary time spanned by the sequence sample. This increases the chances of sequences having insertions or deletions occurring at nearby positions. Algorithms ignoring phylogeny match these nearby insertions, and the use of site-specific, lowered gap penalties encourages nearby deletions to overlap even when sequence similarity may suggest the contrary, which creates gap patterns that are phylogenetically unreasonable. This error is avoided, however, by using phylogenetic information to distinguish insertions from deletions and by treating each mutation type appropriately. In contrast to all other methods tested, PRANK$_{+F}$ is able to use the additional data from denser sequence sampling to improve the accuracy of all estimates of parameters describing the insertion-deletion processes (Fig. 3, A to D, close-2X 4X).

Wong *et al.* (*20*) showed that alignment uncertainty is crucially important in subsequent genomic analyses, such as phylogeny inference and detection of positive selection. We have shown that incorrect handling of alignment gaps is a significant contributing factor to systematic alignment error. As a further simple, but fundamental, demonstration of the effects on downstream studies, we illustrate the effect on the inference of the branch lengths of the 16-taxon intermediate phylogenetic tree. Comparing branch length estimates based on the true alignments with those based on alignments generated using the different methods, we detected patterns of errors that are consistent with our alignment accuracy results. As our analysis predicts, artifactually compact alignments with incorrect insertions and deletions create erroneous mismatches between sequence sites and cause branch lengths to be overestimated. Estimates based on the most erroneous alignments depart most significantly from the true values, and errors increase in the deeper branches (Fig. 3G). Pairwise estimates of sequence divergence and estimates of substitution rates are similarly affected. Again, branch length estimates based on the PRANK$_{+F}$ alignments were the most accurate at all levels of sequence divergence.

Our analyses show that sequence alignment remains a challenging task, and alignments generated with methods based on the traditional progressive algorithm may lead to seriously incorrect conclusions in evolutionary and comparative studies. The main reason for their systematic error is disregard of the phylogenetic implications of gap patterns created—which is not corrected by considering alignment consistency (*13*) or using post alignment refinement (*14*, *15*)—and this error is intensified by methods that intentionally force gaps into tight blocks. Affected methods can be positively misleading and become increasingly confident of erroneous solutions as more sequences are included. It is not the progressive algorithm as such that is defective, rather, correct alignment requires that we take account of sequences' phylogeny, irrespective of alignment method used or data type, but the original implementations of the progressive algorithm

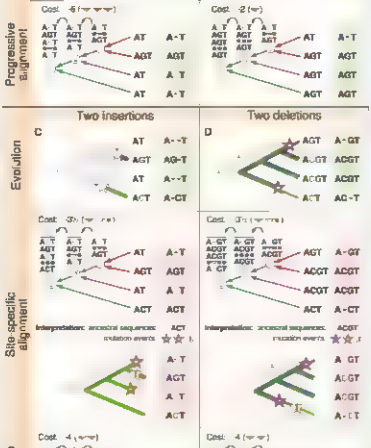

Fig. 2. Insertions and deletions are different in progressive sequence alignment. (**A**) Progressive algorithms build a multiple alignment from sequential pairwise alignments, and an insertion requires a new gap to be opened in each of them (①②③). Naïve iteration of pairwise alignment penalizes this single evolutionary event multiple times (orange triangles), giving an inappropriately high cost for the correct alignment. (**B**) A deletion is penalized only once (④, orange triangle). (**C**) A widely used "correction" for multiple penalization of insertions uses Site-specific gap penalties (gray bars) that lower the cost for reopening gaps (open triangles). With multiple nearby insertions, this encourages incorrect matching of independent events and collapses distinct insertions. Evolutionary interpretation of the incorrect alignment overestimates the substitution rate and lengths of ancestral sequences and indicates enrichment of deletions at one sequence position. The phylogeny-aware algorithm uses evolutionary information from a related sequence (⑤, green arrow) to confirm the earlier event as an insertion and, by marking it as permanent and preventing that site from being matched in later alignments (⑥, red flag), correctly places the second insertion in a column of its own and recovers the correct homology. (**D**) Site-specific lowered gap penalties create gap magnets that induce nearby deletions to coincide, also resulting in an incorrect alignment. Evolutionary interpretation again overestimates the substitution rate and indicates multiple deletions at one sequence position. The phylogeny-aware algorithm considers the earlier event (③) a deletion, removes the flag that allows for a free gap (⑦); and handles the second deletion correctly (⑧)

have a flaw that has gone unnoticed as long as different methods have been consistent in the error they create.

That such a significant error has passed undetected may be explained by the alignment field's historical focus on proteins, where these biases tend to be manifested in less-constrained regions such as loops (compare Fig. 1). Alignments with insertions and deletions squeezed compactly between conserved blocks may suffice for, and even be preferred by, some molecular biologists working with proteins. We have shown, however, that these patterns are, in fact, imposed by systematic biases in alignment algorithms, even in cases where they are incorrect and, indeed, phylogenetically unreasonable. We contend that algorithms that impose gap patterns like those found in structural alignments of proteins are inappropriate for the increasingly widespread analysis of genomic DNA and are likely to cause error when the resulting alignments are used for evolutionary inferences.

We believe that alignment methods specifically designed for evolutionary analyses will give a very different picture of the mechanisms of sequence evolution and show sequence turnover through short insertions and deletions as a more frequent and important phenomenon. This raises interesting questions of the true evolution of variable sequences such as promoter regions, non-coding DNA, and exposed coil regions in proteins. Do they predominantly evolve through point substitutions, or are those dissimilar regions just incorrectly aligned non-homologous sequences? To resolve that, we need more sequence data and alignment methods that can really benefit from the additional information. The resulting alignments may be fragmented by many gaps and may not be as visually beautiful as the traditional alignments, but if they represent correct homology, we have to get used to them.

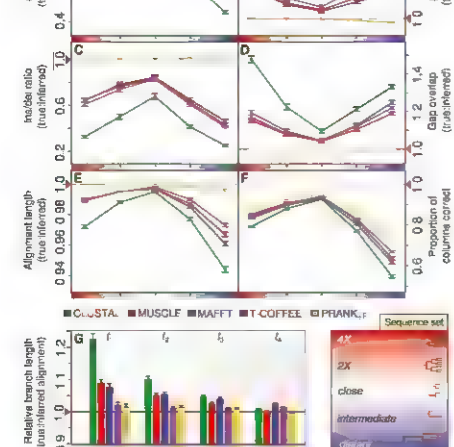

Fig. 3. Alignment accuracy errors are reduced by a phylogeny-aware algorithm. (**A** to **F**) Errors from traditional alignment methods grow with increasing evolutionary distances and more difficult alignments (close-intermediate-distant, white to blue gradient) and also with a denser sequence sampling and increasingly similar sequences (close-2X-4X, white to red gradient). The phylogeny-aware method PRANK$_{+F}$ is less biased by greater distances and, in contrast to other methods, improves in accuracy with additional sequence data. Alignment statistics for the five multiple sequence alignment methods are number of (**A**) insertions and (**B**) deletions, (**C**) insertion/deletion ratio, (**D**) gap overlap, (**E**) total length of the alignment, and (**F**) proportion of columns correctly recovered. (**G**) Inferred branch lengths at different depths in the tree (t_1 – t_4) for the intermediate sets indicate that alignment errors lead to overestimated branch lengths, with PRANK$_{+F}$ giving the most accurate estimates across the whole range of depths. All measures in (A) to (G) are shown relative to those inferred from the true alignment, and values closer to 1 are more correct. Vertical bars show means and 95% confidence intervals.

References and Notes

1. R. A. Gibbs *et al.*, *Nature* **428**, 493 (2004).
2. Rhesus Macaque Genome Sequencing and Analysis Consortium, *Science* **316**, 222 (2007).
3. The ENCODE Project Consortium, *Nature* **447**, 799 (2007).
4. A. Stark *et al.*, *Nature* **450**, 219 (2007).
5. Materials and methods are available as supporting material on *Science* Online.
6. A. Rambaut, D. Posada, K. Crandall, E. Holmes, *Nat. Rev. Genet.* **5**, 52 (2004).
7. M. Sullivan, M. Thali, C. Furman, D. Ho, J. Sodroski, *J. Virol.* **67**, 3674 (1993).
8. R. Myati *et al.*, *J. Virol.* **69**, 5723 (1995).
9. M. Jansson *et al.*, *AIDS Res. Hum. Retroviruses* **17**, 1405 (2001).
10. S. D. Frost *et al.*, *Proc. Natl. Acad. Sci. U.S.A.* **102**, 18514 (2005).
11. M. Sagar, X. Wu, S. Lee, J. Overbaugh, *J. Virol.* **80**, 9586 (2006).
12. J. D. Thompson, D. G. Higgins, T. J. Gibson, *Nucleic Acids Res.* **22**, 4673 (1994).
13. C. Notredame, D. G. Higgins, J. Heringa, *J. Mol. Biol.* **302**, 205 (2000).
14. R. C. Edgar, *BMC Bioinformat.* **5**, 113 (2004).
15. K. Katoh, K. Kuma, H. Toh, T. Miyata, *Nucleic Acids Res.* **33**, 511 (2005).
16. A. Loytynoja, N. Goldman, *Proc. Natl. Acad. Sci. U.S.A.* **102**, 10557 (2005).
17. D. D. Pollock, D. J. Zwickl, J. A. McGuire, D. M. Hillis, *Syst. Biol.* **51**, 664 (2002).
18. M. S. Rosenberg, S. Kumar, *Syst. Biol.* **52**, 119 (2003).
19. M. S. Rosenberg, *BMC Bioinformat.* **6**, 278 (2005).
20. K. M. Wong, M. A. Suchard, J. P. Huelsenbeck, *Science* **319**, 473 (2008).

21. This work was funded in part by a Wellcome Trust Programme Grant (GR078968). We thank N. Goldman for many suggestions that improved the manuscript.

Supporting Online Material

www.sciencemag.org/cgi/content/full/320/5883/1632/DC1
Materials and Methods
SOM Text
Figs. S1
Table S1
References

28 March 2008; accepted 15 May 2008
10.1126/science.1158395

A Molecular Clutch Disables Flagella in the *Bacillus subtilis* Biofilm

Kris M. Blair,[1] Linda Turner,[2] Jared T. Winkelman,[1] Howard C. Berg,[2,3] Daniel B. Kearns[1]*

Biofilms are multicellular aggregates of sessile bacteria encased by an extracellular matrix and are important medically as a source of drug-resistant microbes. In *Bacillus subtilis*, we found that an operon required for biofilm matrix biosynthesis also encoded an inhibitor of motility, EpsE. EpsE arrested flagellar rotation in a manner similar to that of a clutch, by disengaging motor force-generating elements in cells embedded in the biofilm matrix. The clutch is a simple, rapid, and potentially reversible form of motility control.

Many bacteria in the environment live either as motile planktonic individuals or within sessile multicellular groups called biofilms (*1*). Planktonic cells are motile owing to the presence of rotating flagella, molecular machines assembled from nearly 30 proteins (*2*). A motor, located at the base of each flagellum, uses the proton motive force to power rotation of an extracellular helical filament and propel the bacterium through the environment (*3*). In contrast, cells within a biofilm are nonmotile and aggregated by an extracellular matrix composed of secreted macromolecules (*4*). Motility and matrix synthesis are often coordinately and oppositely regulated.

In *Bacillus subtilis*, motility and biofilm formation are alternately controlled by the DNA binding transcription factor SinR (*5*). SinR represses the transcription of genes that encode the structural components of the biofilm including the *eps* operon that encodes enzymes that synthesize the matrix extracellular polysaccharide (EPS) (*6*). Cells with mutations in *sinR* constitutively derepress the *eps* genes, overproduce the matrix, and grow in sticky aggregates. We investigated why *sinR* mutants are also nonmotile (Fig. 1A).

SinR has no appreciable effect on the expression of genes required for flagellar motility (*7*). We considered the possibility that cells with mutations in *sinR* assembled flagella that were obscured by an excess of EPS and severe cell aggregation. To detect flagella within cell aggregates, we genetically altered the flagellar filament protein, Hag (*8*), such that the filament could be labeled with a fluorescent probe (Hag^{T209C}) (Fig. 1B and fig. S1). Flagella colocalized with the cell membrane in the *sinR* mutant but were undetected when EPS biosynthesis and cell aggregation were abolished by introduction of an *epsH* mutation (Fig. 1, C and D). Nonetheless, the *sinR epsH* double mutant remained nonmotile (*sinR epsH*) (Fig. 1, A and D). Thus, the *sinR* mutant synthesized flagella that were concealed by the biofilm EPS matrix, and the flagella were also nonfunctional.

To ascertain how SinR regulates flagellar function, we genetically selected for second-site *sor* (suppressor of *sinR*) mutations that restored motility in the absence of SinR and EpsH. Eighteen spontaneous *sor* suppressor mutant strains were independently isolated, and nine of the suppressors contained mutations in the gene *epsE* (formerly *yveO*), encoding EpsE, a putative family II glycosyltransferase (*9*) (fig. S2). An artificially constructed in frame markerless deletion of *epsE* restored motility to the *sinR epsH* mutant (*ΔepsE sinR epsH*) (Fig. 1, A and E), and motility inhibition was complemented when the *epsE* gene was cloned directly downstream of the native P_{eps} promoter and integrated at an ectopic locus (*ΔepsE* ($epsE^+$) *sinR epsH*) (Fig. 1A). The *epsE* gene is a member of the *eps* operon, the transcription of which is directly repressed by SinR. Thus, cells with mutations in *sinR* are nonmotile as a result of constitutive EpsE derepression.

To determine whether EpsE was sufficient to inhibit motility, we fused the *epsE* gene to an isopropyl β-D-thiogalactopyranoside (IPTG)-inducible $P_{hyperspank}$ promoter and integrated the fusion at an ectopic locus (*amyE*) of an otherwise wild-type strain (*amyE*::$P_{hyperspank}$-*epsE*). In the absence of induction, cells were vigorously motile (movie S1), and fluorescent staining of the Hag^{T209C}-modified filament revealed a blur of rapidly rotating flagella (movie S2). After 40 min of induction, EpsE completely inhibited cell motility (movie S3), and paralyzed flagella were clearly visible on the surface of the nonmotile cells (movie S4). Motility was similarly inhibited by an induced allele of EpsE for which a highly conserved glycosyltransferase active-site aspartate residue (*10*) was mutated to an alanine

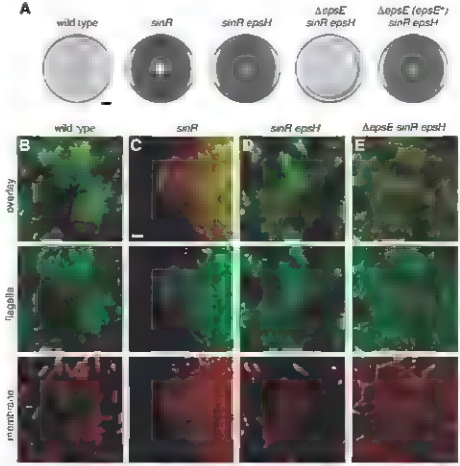

Fig. 1. EpsE is an inhibitor of motility. (**A**) Circles are top views of swarm agar Petri plates. Plates inoculated with wild-type (3610), *sinR* (DS859), *sinR epsH* (DS1674), *ΔepsE sinR epsH* (DS2946), and *ΔepsE* (*epsE*$^+$) *sinR epsH* (DS3844) were filmed against a black background such that zones of bacterial colonization appear white and uncolonized agar appears black. Motility defects are indicated as small zones of colonization. Bar, 1 cm. (**B** to **E**) Wild-type (DS1916), *sinR* (DS2198), *sinR epsH* (DS2179), and *ΔepsE sinR epsH* (DS3843) strains expressing the Hag^{T209C} construct were stained for membranes (false-colored red) and flagella (false-colored green). Bar, 2 μm.

[1]Department of Biology, Indiana University, Bloomington, IN 47405, USA. [2]Rowland Institute at Harvard, Cambridge, MA 02142, USA. [3]Department of Molecular and Cellular Biology, Harvard University, Cambridge, MA 02138, USA.
*To whom correspondence should be addressed. E-mail: dbkearns@indiana.edu.

(*amyE*::$P_{hyperspank}$-*epsE*^{D244}). Thus, EpsE is sufficient to inhibit motility and does so by arresting flagellar rotation. Furthermore, the mechanism by which EpsE inhibits the flagellum is apparently unrelated to its putative enzymatic activity.

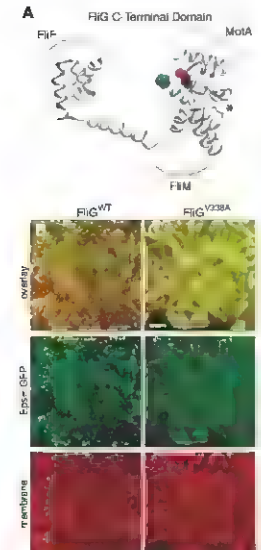

Fig. 2. EpsE interacts with the flagellar rotor. (**A**) The sites of missense mutations generated from *sorE* alleles (fig. S3) were mapped onto the published structure of FliG from *T. maritima* (*24*): Ala^{264} (blue, corresponding to *B. subtilis* FliG^{A267}), Gly^{267} (red, corresponding to *B. subtilis* FliG^{V270G}), and Leu^{300} (green, corresponding to *B. subtilis* FliG^{L303}). The final amino acid altered by *sorE*-class mutations FliG^{V338A} and FliG^{V338G} does not appear on the structure because the most C-terminal residue that is ordered and visible is Arg^{327} (indicated by an asterisk). The surfaces of FliG predicted to interact with FliF, MotA, and FliM are indicated by curved lines. (**B** and **C**) A strain expressing the wild-type allele of FliG (FliG^{WT}, DS2989) or *sorE10* allele of FliG (FliG^{V338A}, DS3004) was doubly mutated for *sinR* and *ΔepsE* with a complementing EpsE-GFP construct integrated at an ectopic locus. Membranes were stained with FM4-64 and false-colored in red ("Membrane"). GFP signals were false-colored in green ("EpsE-GFP"). Bar, 2 μm. Enlarged images of each panel are shown in fig. S7.

To identify the target with which EpsE interacted to inhibit flagellar rotation, we selected for spontaneous *sorE* mutations (suppressors of redundant EpsE) in the downstream cellular target that could render motility insusceptible to inhibition by EpsE. To reduce the possibility that rescue of motility mutations would disrupt the *epsE* gene itself, we expressed two copies of *epsE* on the chromosome: one at the native site by derepression due to mutation of *sinR*, and the other at the ectopic *amyE* site by induction with IPTG (*amyE*::$P_{hyperspank}$-*epsE*). The *epsH* gene was mutated to eliminate EPS production that might confound mutant recovery. Twelve motile *sorE* suppressor strains were isolated from the nonmotile parent, and all 12 suppressors contained missense mutations in *fliG*.

The *fliG* gene encodes a protein that is 32% identical to the flagellar motor component FliG of *Escherichia coli*. FliG subunits polymerize into a wheel-like rotor attached to the flagellar basal body and transduce the energy of proton flux through the MotA-MotB proton channel into the rotational energy of the flagellum (*11*–*13*). The 12 different suppressors were mutated in four different residues within the C-terminal domain of FliG specifically required for torque generation (fig. S3) (*14*, *15*). Three of the four residues localized to a common surface when mapped onto the three-dimensional structure of FliG from *Thermotoga maritima* (Fig. 2A). The fourth residue, the C terminus of FliG, fell in an eight-amino acid disordered domain that might occupy a groove in the protein and potentially position the C-terminal residue near the other three suppressor sites. The surface of FliG containing the altered residues is not occluded by known interactions with the flagellum components FliF, MotA, or FliM and is a candidate site for interaction with EpsE (*16*–*18*).

To investigate whether EpsE inhibited motility through interaction with FliG, we determined the subcellular localization of EpsE translationally fused to the green fluorescent protein (GFP) and expressed under the control of the native P_{epsE} promoter. In cells with the *sinR* mutation, the EpsE-GFP construct was fully able to inhibit motility and when visualized by fluorescence microscopy, the EpsE-GFP fusion localized as puncta that were associated with the cell membrane, reminiscent of the sites of flagellar basal bodies (Fig. 2B). EpsE failed to localize as puncta in the presence of the FliG alleles that rendered the flagellum insusceptible to inhibition by EpsE (Fig. 2C and fig. S4). Thus, punctate localization of EpsE was required to inhibit motility. EpsE and FliG interacted in vivo, and EpsE puncta represented sites of flagellar basal bodies.

When EpsE interacts with FliG, it may cause a deflection of the FliG C-terminal domain, alter FliG interaction with MotA, and inhibit flagellar rotation in a manner similar to that of a brake or a clutch (*19*, *20*). As a brake, EpsE would jam the rotor and immobilize the flagellum. As a clutch, EpsE would disengage the rotor from the power source, but the flagellum would still be free to rotate. To distinguish these models, we tethered *B. subtilis* cells by a single flagellum and measured flagellar rotation by the counter-rotation of the cell body (*21*). Tethered motile cells rotated at a rate of about one revolution in 5 s (Fig. 3). When EpsE was induced, cell rotation was reduced but not abolished and resembled that of cells failing to express the MotA-MotB proton channel that provides the power for flagellum rotation (Fig. 3). The rotation of cells either un-

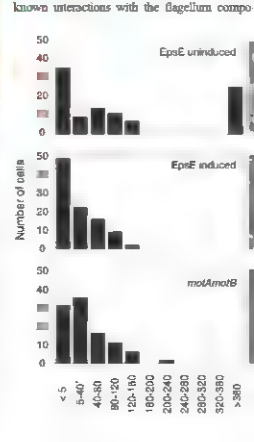

Fig. 3. When EpsE is expressed, flagella behave as though they are unpowered. Cells were tethered to microscope slides by sheared flagellar stubs, and cell rotation was monitored by video microscopy. The behavior of cells in a particular field was not uniform, and therefore 100 cells were chosen at random for motion analysis. (**Left**) The histograms indicate the number of cells that rotated through the indicated angle of rotation during a 90-s interval for "EpsE uninduced" (DS3317), "EpsE induced" (DS3317 induced with 2 mM IPTG for 2.5 hours before observation), and "*motAmotB*" (DS3318) cells. (**Right**) Each image is a time-lapse composite of a sample field corresponding to the histogram immediately to its left. Parts of the cell that are stationary are black. The range of motion that a cell travels through is depicted as a time-lapse composite and is shown in white. Bar, 10 μm.

duced for EpsE or lacking *motA* and *motB* was consistent with a calculated root mean square angular deviation of ~80° in 90 s for a *B. subtilis* cell tethered by an unpowered flagellum freely rotating by Brownian motion (supporting online material). In contrast, the angular deviation is much less, ~3°, for an *E. coli* cell tethered by an immobilized flagellum (*22*). Thus, EpsE acted as a clutch, when EpsE was induced, the flagella behaved as though they were unpowered rather than immobilized.

The biological function of the clutch appears to be related to the *B. subtilis* biofilm because *epsE* is encoded within the 15-gene *eps* operon that promotes the biosynthesis of the biofilm EPS and is repressed by SinR, the master regulator of biofilm formation. Therefore, control of a single locus ensures that cells become immobilized concomitant with biofilm formation (fig. S5A). In wild-type cells, trapped flagella and punctа of EpsE were observed within biofilm aggregates, and the cells within the aggregates were sessile (fig. S6 and movie S5). Cells expressing the $FliG^{V338A}$ clutch-unsusceptible allele formed aggregates, but the cells writhed within the confines of the matrix (movie S6). We hypothesize that the clutch helps to stabilize biofilms in the environment and acts as a fail safe mechanism to ensure that flagella do not rotate while the cells are bound by EPS

The bacterial flagellum, powered by a motor that generates 1400 pN nm of torque, can rotate at a frequency of greater than 100 Hz (*23*). EpsE disabled this powerful biological motor when associated with a flagellar basal body and, in a manner similar to that of a clutch, disengaged the drive train from the power source (fig. S5B) Clutch control of flagellar function has distinct advantages over transcriptional control of flagellar gene expression for regulating motility. Some bacteria, such as *E. coli* and *B. subtilis*, have many flagella per cell. The flagellum is an elaborate, durable, energetically expensive, molecular machine and simply turning off de novo flagellum synthesis does not necessarily arrest motility. Once flagellar gene expression is inactivated, multiple rounds of cell division may be required to segregate preexisting flagella to extinction in daughter cells. In contrast, the clutch requires the synthesis of only a single protein to inhibit motility. Furthermore, if biofilm formation is prematurely aborted, flagella once disabled by the clutch might be reactivated, allowing cells to bypass fresh investment in flagellar synthesis Whereas flagellum expression and assembly are complex and slow, clutch control is simple, rapid, and potentially reversible.

References and Notes

1. R. Kolter, P. Greenberg, *Nature* **441**, 300 (2006)
2. R. M. Macnab, *Annu. Rev. Microbiol.* **57**, 77 (2003).
3. H. C. Berg, *Annu. Rev. Biochem.* **72**, 19 (2003).
4. S. S. Branda, S. Vik, L. Friedman, R. Kolter, *Trends Microbiol.* **13**, 20 (2005).
5. D. B. Kearns, F. Chu, S. S. Branda, R. Kolter, R. Losick, *Mol. Microbiol.* **55**, 739 (2005).
6. S. S. Branda, J. F. González-Pastor, S. Ben-Yehuda, R. Losick, R. Kolter, *Proc. Natl. Acad. Sci. U.S.A.* **98**, 11621 (2001).
7. F. Chu, D. B. Kearns, S. S. Branda, R. Kolter, R. Losick, *Mol. Microbiol.* **59**, 1216 (2006).
8. E. R. LaVallie, M. L. Stahl, *J. Bacteriol.* **171**, 3043 (1989).
9. P. M. Coutinho, E. Deleury, G. J. Davies, B. Henrissat, *J. Mol. Biol.* **328**, 307 (2003).
10. C. Gardner Schweder, A. C. Jellouch, R. A. Gerwick *J. Biol. Chem.* **275**, 31407 (2000).
11. D. F. Blair, H. C. Berg, *Cell* **60**, 439 (1990).
12. S. A. Lloyd, H. Tang, X. Wang, S. Billings, D. F. Blair *J. Bacteriol.* **178**, 223 (1996).
13. D. R. Thomas, N. R. Francis, C. Xu, D. J. DeRosier *J. Bacteriol.* **188**, 7039 (2006).
14. V. M. Irikura, M. Kihara, S. Yamaguchi, H. Sockett, R. M. Macnab, *J. Bacteriol.* **175**, 802 (1993).
15. S. A. Lloyd, D. F. Blair *J. Mol. Biol.* **266**, 733 (1997).
16. D. L. Maryknoss, S. A. Schmidt, H. C. Berg, *J. Mol. Biol.* **256**, 564 (1996).
17. J. Zhou, S. A. Lloyd, D. F. Blair *Proc. Natl. Acad. Sci. U.S.A.* **95**, 6436 (1998).
18. P. N. Brown, M. Terrazas, K. Paul, D. F. Blair, *J. Bacteriol.* **189**, 305 (2007).
19. S. Kojima, D. F. Blair *Biochemistry* **40**, 13041 (2001).
20. Y. Hashimoto, N. Hashimoto, S. Yamaguchi, S. ., Akawa, *J. Bacteriol.* **189**, 5153 (2007)
21. S. M. Block, D. F. Blair, H. C. Berg, *Nature* **338**, 514 (1989).
22. S. M. Block, D. F. Blair, H. C. Berg, *Cytometry* **12**, 492 (1991).
23. N. C. Darnton, L. Turner, S. Rojevsky, H. C. Berg, *J. Bacteriol.* **189**, 1756 (2007)
24. P. N. Brown, C. P. Hill, D. F. Blair, *EMBO J.* **21**, 3225 (2002)
25. We thank N. Darnton, G. Gliakas, B. Holdenweng, A. Camp, Y. le Breton, S. Michaels, S. Muthupadhyay, G. Ordal, and D. Radmer for reagents, constructs, and technical assistance. We thank S. Ben Yehuda, D. Blair, C. Fergus, D. Higgins, P. Levin, R. Losick, S. Muthupadhyay and D. Radmer for insightful discussions and critical comments on the manuscript. This work was supported by N.H. grant AI065540 (to H.C.B.) and NSF grant MCB-0721187 (to D.B.K.).

Supporting Online Material

www.sciencemag.org/cgi/content/full/320/5883/1636/DC1
Materials and Methods
SOM Text
Figs. S1 to S7
Tables S1 to S3
References
Movies S1 to S6

17 March 2008; accepted 22 April 2008
10.1126/science.1157877

Tuned Responses of Astrocytes and Their Influence on Hemodynamic Signals in the Visual Cortex

James Schummers,* Hongbo Yu,* Mriganka Sur†

Astrocytes have long been thought to act as a support network for neurons, with little role in information representation or processing. We used two-photon imaging of calcium signals in the ferret visual cortex in vivo to discover that astrocytes, like neurons, respond to visual stimuli, with distinct spatial receptive fields and sharp tuning to visual stimulus features including orientation and spatial frequency. The stimulus-feature preferences of astrocytes were exquisitely mapped across the cortical surface, in close register with neuronal maps. The spatially restricted stimulus-specific component of the intrinsic hemodynamic mapping signal was highly sensitive to astrocyte activation, indicating that astrocytes have a key role in coupling neuronal organization to mapping signals critical for noninvasive brain imaging. Furthermore, blocking astrocyte glutamate transporters influenced the magnitude and duration of adjacent visually driven neuronal responses.

Though astrocytes are the major class of nonneuronal cell in the brain (*1*), their role in brain function is unresolved. Evidence has accumulated for an active role of astrocytes in brain function (*1*–*3*). Astrocytes are closely apposed to many central synapses (*4*, *5*) and can respond to a number of neurotransmitters, including glutamate (*6*), by increases in intracellular calcium. In turn, astrocytes release glutamate and other neuroactive substances (*7*–*10*) that affect neuronal activity (*11*) and can modulate synaptic strength (*10*, *12*, *13*). Astrocytes contact vascular networks and can potentially influence the cerebral microcirculation (*14*–*16*), which has led to the proposal that astrocytes might support indirect, hemodynamic imaging of neuronal activity (*17*, *18*). Despite these in vitro studies, however, little is known about the behavior of astrocytes in vivo Pioneering studies have demonstrated that astrocytes do respond to neural activity in vivo (*19*–*21*), but fundamental questions about the relationship between neuronal networks, astrocytes, and hemodynamic responses remain unsolved.

The precise orderly mapping of orientation preference in the visual cortex of higher mammals provides a model system with which to study these interactions. The synaptic input near pinwheel centers is nearly untuned (*22*), yet individual neurons are sharply tuned because of nonlinear filtering of inputs (*23*) and are organized on a scale of less than 50 μm (*24*). Do astrocyte responses passively follow the untuned

Picower Institute for Learning and Memory, Department of Brain and Cognitive Sciences, Massachusetts Institute of Technology, Cambridge, MA 02139, USA.

*These authors contributed equally to this work
†To whom correspondence should be addressed. E-mail: msur@mit.edu

inputs, or do they show similar tuning and maps as do their neighboring neurons? Is the spatial resolution of astrocyte activation sufficient to support hemodynamic mapping methods? If so, what influence do astrocytes have on hemodynamic mapping signals? We addressed these issues by performing parallel two-photon calcium imaging of neurons and astrocytes and optical imaging of blood volume changes in a single, well-characterized model system. We investigated the visual tuning and mapping of astrocytes, along with their influence on hemodynamic signals and neuronal responses, in the primary visual cortex (V1) of ferrets by loading cells with the fluorescent calcium indicator Oregon Green Bapta (OGB1) (*25*, *26*) and the specific astrocyte marker sulforhodamine101 (SR101) (*20*) and using two-photon imaging to simultaneously monitor the visual activity of neurons and that of neighboring astrocytes (*27*) (movie S1).

Our first finding is that astrocytes in the visual cortex respond to visual stimuli with robust increases in calcium concentration. Fig. 1A (left panel) shows double labeling of a 50-by-50-μm square patch of cortex, 120 μm below the pial surface containing neurons and an astrocyte. Fig. 1B shows the responses of the two cells circled in Fig. 1A to a visual stimulus consisting of a drifting grating. The neuron (blue trace) shows a fluorescence increase of close to 10%, which begins at the time of stimulus onset and lasts throughout the duration of the stimulus presentation. The astrocyte response (red trace) also exhibits a stimulus-locked calcium increase, which is delayed roughly 3 to 4 s from stimulus onset (movie S2). Whereas calcium increases in neurons result from spiking activity (*28*, *29*), astrocyte responses are attributable to a delayed release of calcium from internal stores (*30*). The existence of visually evoked calcium responses in astrocytes led us to ask whether astrocytes have spatially restricted receptive fields, similar to those found in neurons in the visual cortex. We tested the spatial extent of stimuli eliciting astrocyte responses by presenting vertical or horizontal bars moving sequentially across visual space. Astrocytes responded to stimuli over a similar region of space as neighboring neurons (Fig. 1C). Both the location of maximal response and the extent of the receptive field were comparable in the *x* and *y* dimensions of space. Contour plots of responses show that nearby neurons and astrocytes have largely overlapping receptive fields (Fig. 1D).

We next examined whether astrocytes have other receptive field characteristics found in neurons. We first tested orientation tuning with drifting gratings of different orientations. Fig. 1E shows plots of the responses of an astrocyte and a neuron to the presentation of drifting gratings of six orientations, spanning 180° at 30° intervals. The neuron (blue trace in Fig. 1E, middle panels) shows a visual response to a narrow range of orientations, as was expected from previous studies using calcium imaging or direct measurement of firing rate (*24*, *31*, *32*). The tuning curve (below) is typical of neurons in ferret V1 (*33*, *34*). The astrocyte (red trace) also has clear orientation tuning (Fig. 1E, right panels). Furthermore, the preferred orientation of the astrocyte is very

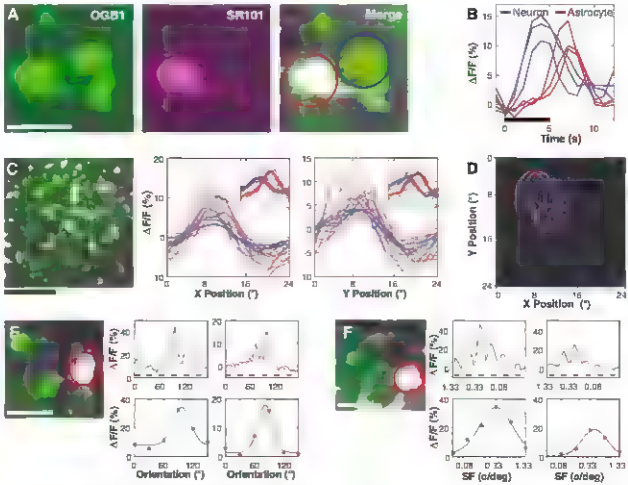

Fig. 1. Astrocytes have robust visual responses, spatially restricted receptive fields, and stimulus-feature selectivity. (**A**) Double labeling of a patch of cortex 120 μm below the pial surface. From left to right, the panels show cells loaded with the calcium indicator OGB1, astrocyte marker SR101, and merged OGB1 and SR101. Scale bar, 25 μm. (**B**) Time course of visually evoked responses (Δ*F*/*F*) in the neuron (blue) and astrocyte (red) outlined in the right panel of (A). The stimulus consists of three trials of a drifting grating presented for 5 s (indicated by the thick black bar). (**C**) Measurements of receptive-field location and extent in a population of neurons and astrocytes, labeled green and purple, respectively, in the merged image at left. Responses of neurons (blue) and astrocytes (red) to vertical (center panel) and horizontal (right panel) bars swept periodically across the receptive field. Each trace plots the cycle-averaged response for one cell. Scale bar, 100 μm. (Insets) Raw responses as a function of time, before aligning the astrocyte and neuron responses by subtracting a constant delay from the astrocyte responses. (Insets) *x* axis, time (0 to 18 s); *y* axis, Δ*F*/*F* (−10 to 20%). (**D**) Contour plots of the half-maximal response to *x* and *y* bars for a subset of neurons and astrocytes. Receptive fields of astrocytes are indicated in red; those of neurons are shown in blue. (**E**) Responses of a neuron (blue circle) and an astrocyte (red circle) to drifting gratings of varying orientation. Scale bar, 25 μm. (Right) Top panels show the responses to six orientations evenly spaced between 0° and 180° as a function of time, as orientation is systematically changed. Stimuli lasting 5 s (dashed lines) are alternated with 5-s blank periods. Bottom panels show the tuning curves computed from the responses above and the Gaussian fits to the curves. (**F**) Responses of a neuron and an astrocyte (both circled in left panel) to gratings of varying spatial frequency. Scale bar, 25 μm. (Right) Responses, in a format similar to that in (E). Spatial frequencies were presented in decreasing order, from 1.33 to 0.04 cycles per degree. Tuning curves were fit with a Gaussian function and are plotted as a function of increasing spatial frequency.

similar to that of the nearby neurons, suggesting that there may be spatial alignment of orientation preference between neurons and astrocytes. We also measured the responses of astrocytes to gratings varying in spatial frequency. The neuron in Fig. 1F (middle panels) shows spatial-frequency tuning typical of visual cortical neurons in ferret V1 (*35*). The astrocyte is also selective for spatial frequency (Fig. 1F, right panels).

We then analyzed the tuning characteristics of astrocytes in more detail. We made OGB1 injections into orientation domains, thus labeling a population of cells with a relatively homogeneous orientation preference, and subsequently obtained high-resolution tuning curves with stimulus sampling at 10° intervals. Astrocytes were even more sharply tuned for orientation than neurons (Fig. 2A). On average, neurons responded to a stimulus 20° from the preferred—roughly half as much as to the preferred orientation—whereas astrocytes responded only minimally, if at all. We fitted the tuning curves [calculated from fractional change in fluorescence (F); $\Delta F/F$] with a Gaussian function to quantify differences in tuning. There was a significant difference in tuning width, which is apparent in the overlaid tuning curves (Fig. 2B)

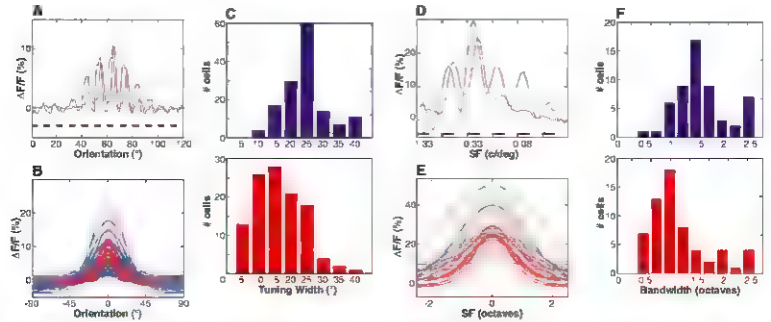

Fig. 2. Astrocytes have sharper orientation and spatial-frequency tuning than neurons. **(A)** Average stimulus-evoked response of a population of neurons (blue, n = 80 neurons) and astrocytes (red, n = 69 astrocytes) from the same regions of the visual cortex to gratings of different orientations. The response of each cell was aligned to its preferred orientation before averaging. The stimulus presentation time for each orientation is indicated by the short black horizontal bars; the display was blank in the intervening intervals. **(B)** Overlaid Gaussian fits to the tuning curves of all neurons (blue, n = 80) and astrocytes (red, n = 69). **(C)** Population histograms of the orientation tuning width, measured as half width at half height, pooled from three ferrets. Top, neurons (n = 143); bottom, astrocytes (n = 113). **(D)** Average stimulus-evoked response of a population of adjacent neurons (blue, n = 13) and astrocytes (red, n = 17) to gratings of varying spatial frequency. The stimulus presentation time for each spatial frequency is indicated by the black horizontal bars; the display was blank in the intervening intervals. **(E)** Overlaid Gaussian fits to the tuning curves of all neurons (blue, n = 13) and astrocytes (red, n = 17). **(F)** Population histograms of the spatial-frequency tuning width, measured as half width at half height, pooled from three ferrets. Top, neurons (n = 49); bottom, astrocytes (n = 47).

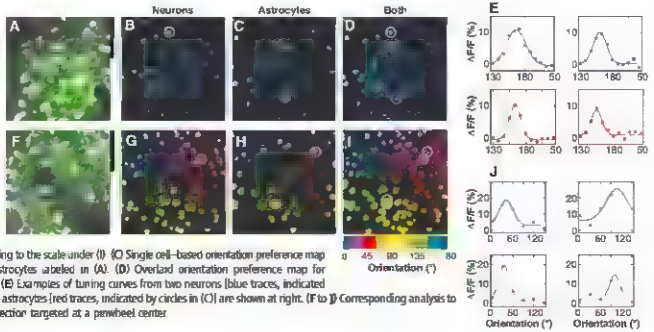

Fig. 3. Astrocyte and neuronal-orientation preference is mapped precisely across the cortical surface. **(A)** Merged image of SR101 and OGB1 label in a 250-by-250–μm patch of cortex 120 μm below the pial surface. **(B)** Single cell–based orientation preference map for the population of neurons labeled in (A). Orientation preference was determined by Gaussian fits to the data and is coded according to the scale under (I). **(C)** Single cell–based orientation preference map for the population of astrocytes labeled in (A). **(D)** Overlaid orientation preference map for neurons and astrocytes. **(E)** Examples of tuning curves from two neurons [blue traces, indicated by circles in (B)] and two astrocytes [red traces, indicated by circles in (C)] are shown at right. **(F** to **J)** Corresponding analysis to (A to E) for a second injection targeted at a pinwheel center.

and in the histograms of half width at half height (Fig. 2C; mean tuning width of neurons, 24.9°; n = 143 cells from three ferrets, mean tuning width of astrocytes, 16.4°; n = 113 cells from three ferrets. $P < 0.01$, t test).

Next, we quantitatively examined the tuning of astrocyte responses to spatial frequency and compared them with adjacent neurons. Astrocytes were more sharply tuned for spatial frequency than neurons (Fig. 2, D to F). On average, neurons responded to a much broader range of spatial frequencies, especially in the lower frequency range. The tuning bandwidth of astrocytes (0.8 octaves) was significantly narrower than that of neurons (1.5 octaves, $P < 0.01$, t test, n = 49 neurons, 47 astrocytes from three ferrets). Furthermore, the preferred response features tended to be clustered, such that groups of nearby neurons and astrocytes have similar preferred orientations (see also below) and spatial frequencies (fig. S1), though with a range of tuning widths.

Neuronal receptive-field tuning preferences are organized into two-dimensional maps across V1 (*36*–*40*). We thus asked if the receptive field properties of astrocytes are organized in a similar manner. Two-photon imaging is well suited to the mapping of cellular activity at single-cell resolution (*24*, *25*, *32*). We could therefore simultaneously image the spatial arrangement of neuronal and astrocytic orientation tuning over 250-by 250-μm expanses of the cortex (Fig. 3A). We first analyzed the cellular organization of tuning in an orientation domain, where there is a relatively uniform neuronal preferred orientation. An orientation map of individ-

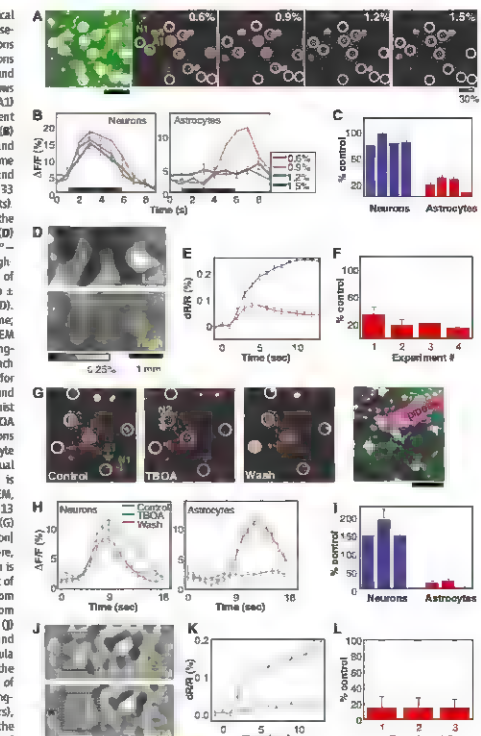

Fig. 4. Astrocyte calcium responses and the intrinsic optical signal are selectively affected by specific blockers. **(A)** Dose-dependent effect of isoflurane on the responses of neurons and astrocytes. The response amplitude of a field of neurons and astrocytes at different isoflurane levels (0.6, 0.9, 1.2, and 1.5%) is shown. White circles indicate astrocytes, and arrows indicate a representative neuron (N1) and astrocyte (A1) whose time course of visual responses under different isoflurane levels is shown in fig. S5. Scale bar, 50 μm. **(B)** Mean response time courses of the neurons (n = 8) and astrocytes (n = 11) from the field of view in (A). Stimulus time is indicated by the black bar. **(C)** Average neuron and astrocyte response suppression by high isoflurane (n = 33 neurons from four ferrets and 44 astrocytes from four ferrets). Each bar shows data from a single animal and depicts the response level under high isoflurane relative to low. **(D)** Example of intrinsic-signal optical imaging differential (0° – 90°) maps, computed from 4 to 13 s, during low- and high-isoflurane conditions. **(E)** Plots of the time course of reflectance change (dR/R, where R is reflectance) (mean ± SEM, indicated by error bars) in the example shown in (D). Stimulus was turned on at time 0 s. Blue line, low isoflurane; red line, high isoflurane. Each line shows the average ± SEM of five traces under each condition. **(F)** Summary of mapping-signal suppression by high isoflurane from four ferrets. Each bar shows data from a single animal. **(G)** Magnitude map for visually driven responses in a field of cells before, during, and after application of the glutamate transporter antagonist TBOA. Astrocytes are circled in white. The position of the TBOA pipette and dual-labeling of astrocytes (white) and neurons (green) are shown in far right panel. Arrows mark an astrocyte (A1) and two neurons (N1 and N2) whose time course of visual responses before, during, and after TBOA application is shown in fig. S6. Scale bar, 50 μm. **(H)** Mean (± SEM, indicated by error bars) responses of a population of 13 astrocytes and 25 neurons from the same experiment as in (G). (G) shows a zoomed-in portion of the entire imaged region to a continuously changing orientation stimulus before, during, and after TBOA application. The response duration is prolonged during TBOA application. **(I)** Summary bar plot of the effect of TBOA on astrocyte and neuron responses from three experiments (67 neurons and 32 astrocytes from three ferrets). Each bar shows data from a single animal. **(J)** Differential intrinsic-signal maps (0° – 90°) before and during TBOA application. TBOA was applied from a cannula positioned at the asterisk. Dotted boxes indicate the portion of the map used to calculate the time course of the mapping signal in (K). **(K)** Time course of the mapping-signal magnitude (mean ± SEM, indicated by error bars), calculated from the portion of the map indicated by the rectangle in the top panel of (J). **(L)** Summary bar plot of the mean (± SEM, indicated by error bars) suppression of the mapping signal by TBOA from three ferrets. Each bar shows data from a single animal. Error bars throughout the figure indicate SEM.

ual cells demonstrates that the spatial organization of neuronal orientation preference (Fig. 3B) and the organization of orientation preference in the interposed population of astrocytes (Fig. 3C) closely match each other (Fig. 3D). Examples of $\Delta F/F$ tuning curves of two neurons and two astrocytes are plotted in Fig. 3E. Quantitative analysis of the rate of change and scatter demonstrates that the spatial organization of astrocyte and neuron orientation tuning was indistinguishable within an orientation domain (fig. S2).

Orientation tuning of neurons in V1 is organized with high precision, at the level of individual neurons (*24*). We were interested to know whether the preferred orientation of astrocytes has a similar degree of organization. To further test the spatial resolution of astrocyte-orientation mapping, we made injections of OGB1 in pinwheel centers and orientation fractures, which are locations in the orientation map where preferred orientation changes dramatically on a short spatial scale (<50 μm). The single cell–based neuron maps closely match orientation maps obtained with optical imaging of intrinsic signals (fig. S3). The example in Fig. 3, F to J, demonstrates that the astrocyte-orientation map was just as precise as that of neurons. The single cell–based orientation map of neurons is shown in Fig. 3G (movie S3). The pinwheel center was remarkably distinct, there was no overlap of orientation preferences across the pinwheel center. The same holds true for astrocytes (Fig. 3H). The overlay of the two maps (Fig. 3I) shows that the alignment of the pinwheel center was matched perfectly. Quantitative analyses demonstrate that the orientation preference of astrocyte responses was mapped just as precisely as that of neuronal responses (fig. S2). Thus, there is a remarkable degree of specificity in the mechanisms responsible for generating and mapping orientation tuning in astrocytes. This is particularly notable, given that the presynaptic activity in the neuropil surrounding a pinwheel is very poorly tuned (fig. S4). In contrast to some situations in vitro where astrocyte activity has been associated with "calcium waves" that propagate through large networks of interconnected cells (*41*), our data demonstrate that, in vivo, astrocytes behave relatively independently of each other. Each astrocyte is sharply tuned for orientation, and two astrocytes only tens of microns apart can respond to orthogonal stimulus orientations.

The sharp tuning of astrocytes suggests the possibility that a high level of local neuronal activity is necessary to elicit astrocyte responses. In support of this hypothesis, we found that small changes in isoflurane concentration, over a narrow range of concentrations around ~1%, produce a modest reduction of neuronal responses but a dramatic reduction of astrocyte responses (Fig. 4, A to C). Fig. 4A shows the magnitude map for a field of neurons and astrocytes at different concentrations of isoflurane. The responses of astrocytes (circled in white) were reduced in a dose-dependent manner, with a sharp fall-off between 0.9 and 1.2% (fig. S5). The average reduction in astrocyte responses under high isoflurane (>1%) compared with low (<1%) was 77 ± 14% (44 astrocytes from four ferrets, $P < 0.001$ comparing individual animals, *t* test), whereas neuronal responses were only reduced by 16 ± 8% (33 neurons from four ferrets, $P < 0.001$, *t* test) (Fig. 4C).

We have taken advantage of the differential sensitivity of astrocytes and neurons to isoflurane to directly probe the role of astrocytes in translating neuronal-orientation maps into hemodynamic maps. Astrocyte activity leads to vasodilation in vitro (*14*, *16*, *42*, *43*) and in vivo (*15*, *16*). However, the spatial scale of astrocyte-mediated neurovascular coupling is unknown, and this is a critical factor for functional imaging of orientation maps. Spatial blurring of hemodynamic signals would lead to systematic errors of optically imaged orientation maps (*44*), whereas we find that the optical map matches the neuronal map nearly perfectly (fig. S3). To address the role of astrocytes in the ability to image high-resolution orientation maps with intrinsic signals, we performed optical imaging under identical conditions as our two-photon experiments. We used green (546-nm) light, which emphasizes changes in blood volume (*45*), and measured the mapping signal from orthogonal stimulus orientations. Concentrations of isoflurane that preferentially reduce astrocyte responses led to a large reduction in the differential orientation maps, with an average mapping-signal reduction of 77 ± 9% (Fig. 4, D to F; four ferrets; $P < 0.001$, *t* test). Thus, the ability to reliably measure the pinwheel structure of orientation maps with hemodynamic imaging (fig. S3) is probably due to the highly localized engagement of astrocytes by neuronal activity.

One potential concern about these results is that neuronal activity is also reduced, though modestly, by isoflurane, which could possibly lead to direct reduction of the blood-volume response (*46*–*48*). We therefore sought a means to block astrocyte responses without interfering with neuronal synaptic transmission. One mechanism to trigger astrocyte responses is the activation of glutamate transporters (*49*, *50*). Astrocyte glutamate transporters provide the major mechanism for glutamate clearance from the synaptic cleft, and their activity tightly regulates the amplitude and kinetics of synaptic transmission in vitro (*51*). Fig. 4G shows the response magnitudes of a field of neurons and astrocytes before, during, and after application of the glutamate transporter antagonist DL-threo-β-benzyloxyaspartate (TBOA) via a visualized pipette. The responses of astrocytes (circled in white) were clearly and significantly reduced (Fig. 4, H and I; 88 ± 10% reduction, 32 astrocytes from three ferrets, $P < 0.001$, *t* test). The responses of neurons were increased to a lesser extent (58 ± 25% increase, 67 neurons from three ferrets, $P < 0.001$, *t* test), and some neurons that were unresponsive in the control condition became measurably responsive during TBOA application (Fig. 4G and fig. S6). Furthermore, neuronal responses were prolonged during TBOA application (Fig. 4H), consistent with an increase in glutamate availability at synapses because it is not cleared by astrocyte transporters. These data demonstrate a key role for astrocytes in regulating the strength and time course of neuronal responses to incoming synaptic inputs.

Having demonstrated that TBOA is an effective means to silence astrocytes without any potential confound from reducing neuronal responses, we next tested the effects of TBOA on stimulus-specific blood-volume responses with optical imaging. TBOA reduced these signals to <20% of control (n = three ferrets, $P < 0.001$, *t* test, Fig. 4, J to L)—a notable effect, given that neuronal responses are actually increased during TBOA application. The orientation-selective mapping signals from intrinsic-signal imaging were reduced to a similar extent as those of the astrocyte calcium responses (by 85 ± 2%, mean of three ferrets, Fig. 4L).

We have demonstrated the visual response properties and detailed organization of astrocytes in the visual cortex. Astrocytes exhibit robust calcium responses to visual stimuli that are dependent on stimulus features and have many of the receptive-field characteristics of neurons. In particular, they have well-defined spatial receptive fields, orientation tuning, and spatial-frequency tuning. What's more, astrocytes are more sharply tuned for orientation and spatial frequency than neurons. Additionally, the orientation preference of astrocytes is exquisitely mapped across the cortex at single-cell resolution, in close register with the neuronal-orientation preference map. This suggests that, in vivo, astrocytes do not necessarily function as a broadly interconnected network [as has been suggested by some in vitro studies (*41*, *52*)], but rather that each astrocyte interacts quasi-independently with a small number of neurons surrounding it. Future work will be necessary to determine whether groups of astrocytes with similar response properties form distinct syncytia. Furthermore, astrocyte calcium responses are a critical step in local hemodynamic regulation, as is commonly measured with intrinsic-signal optical imaging and blood oxygen level–dependent functional magnetic resonance imaging.

Our findings indicate that the spatial scale of synaptic interactions between neurons and astrocytes is extremely precise. In orientation domains, where the presynaptic inputs are highly orientation selective (fig. S4) (*22*, *23*), it is not surprising that astrocytes and neurons have similar orientation tuning. However, at orientation pinwheels, where the inputs are almost untuned (fig. S4) (*22*, *23*) but neurons are sharply tuned because of a combination of the spike threshold and balanced inhibition (*23*), astrocytes surprisingly have similar orientation preference

as their neighboring neurons, and their tuning is even sharper. There are several potential explanations for the sharp tuning of astrocyte responses. Astrocyte visual responses probably arise from the presynaptic activity of afferent and/or recurrent inputs at synapses with closely abutting astrocytic processes. An important basis for astrocyte calcium responses in the ferret visual cortex is the binding of glutamate to astrocyte glutamate transporters. Though the signaling pathway is not fully known, it is feasible that the depolarization caused by the transporter current triggers calcium influx in astrocytes via voltage-dependent calcium channels or by the release of calcium from intracellular stores (*53*). It is possible that threshold levels of presynaptic activity need to be crossed to activate glutamate transporters on astrocytes, such a threshold could, in principle, account for sharper astrocyte tuning. Our data showing that increased isoflurane leads to small decreases in neuronal responses but large decreases in astrocyte responses supports this hypothesis. However, alternative interpretations are also possible. Astrocytes may sample presynaptic activity over a smaller spatial scale than neurons (and thus from a smaller region within a feature map), leading to sharper tuning. It is also possible that astrocytes may not sample uniformly from synapses within their anatomical span. If they had a higher proportion of processes or a higher density of receptors/transporters at the strongest synapses, this could effectively increase their response selectivity. Regardless of the mechanism, however, the sharp response tuning of astrocytes and their precise mapping, combined with their highly selective vascular effects, probably contributes critically to the ability of hemodynamic imaging methods to obtain valid measures of neuronal activity.

It is worth noting that the functional contribution of astrocytes includes the regulation of neuronal response magnitude and duration. In vitro studies demonstrate that astrocytes release glutamate upon activation (*7*–*10*), are closely apposed structurally to spines (*4*, *5*), and influence synaptic strength between neurons (*10*, *12*, *13*). This suggests that they may also influence temporal dynamics of neuronal responses during adaptation or learning in vivo (*54*–*56*).

References and Notes

1. M. Nedergaard, B. Ransom, S. A. Goldman, *Trends Neurosci.* **26**, 523 (2003).
2. R. D. Fields, B. Stevens-Graham, *Science* **298**, 556 (2002).
3. A. Volterra, J. Meldolesi, *Nat. Rev. Neurosci.* **6**, 626 (2005).
4. M. Haber, L. Zhou, K. K. Murai, *J. Neurosci.* **26**, 8881 (2006).
5. K. Ventura, K. M. Harris, *J. Neurosci.* **19**, 6897 (1999).
6. J. T. Porter, K. D. McCarthy, *J. Neurosci.* **16**, 5073 (1996).
7. A. Araque, N. Li, R. T. Doyle, P. G. Haydon, *J. Neurosci.* **20**, 666 (2000).
8. L. Hertz, H. R. Zielke, *Trends Neurosci.* **27**, 735 (2004).
9. V. Montana, Y. Ni, V. Sunjara, X. Hua, V. Parpura, *J. Neurosci.* **24**, 2633 (2004).
10. J. M. Zhang *et al.*, *Neuron* **40**, 971 (2003).
11. E. A. Newman, *Trends Neurosci.* **26**, 536 (2003).
12. J. Kang, L. Jiang, S. A. Goldman, M. Nedergaard, *Nat. Neurosci.* **1**, 683 (1998).
13. N. Kang, J. Xu, Q. Xu, M. Nedergaard, J. Kang, *J. Neurophysiol.* **94**, 4121 (2005).
14. S. J. Mulligan, B. A. MacVicar, *Nature* **431**, 195 (2004).
15. T. Takano *et al.*, *Nat. Neurosci.* **9**, 260 (2006).
16. M. Zonta *et al.*, *Nat. Neurosci.* **6**, 43 (2003).
17. D. R. Harder, M. J. Alkayed, A. R. Lange, D. Gebremedhin, R. J. Roman, *Stroke* **29**, 229 (1998).
18. P. G. Haydon, G. Carmignoto, *Physiol. Rev.* **86**, 1009 (2006).
19. H. Hirase, L. Qian, P. Barthó, G. Buzsáki, *PLoS Biol.* **2**, E96 (2004).
20. A. Wunderlich, F. Kirchhoff, J. M. Kerr, F. Helmchen, *Nat. Methods* **1**, 31 (2004).
21. X. Wang *et al.*, *Nat. Neurosci.* **9**, 816 (2006).
22. J. Schummers, J. Marino, M. Sur, *Neuron* **36**, 969 (2002).
23. J. Marino *et al.*, *Nat. Neurosci.* **8**, 194 (2005).
24. K. Ohki *et al.*, *Nature* **442**, 925 (2006).
25. F. Helmchen, W. Denk, *Nat. Methods* **2**, 932 (2005).
26. C. Stosiek, O. Garaschuk, K. Holthoff, A. Konnerth, *Proc. Natl. Acad. Sci. U.S.A.* **100**, 7319 (2003).
27. Materials and methods are available as supporting material on Science Online.
28. J. M. Kerr, D. Greenberg, F. Helmchen, *Proc. Natl. Acad. Sci. U.S.A.* **102**, 14063 (2005).
29. D. Somers, A. Majewska, M. Nelson, *Methods* **18**, 215 (1999).
30. G. Perea, A. Araque, *J. Neurosci.* **25**, 2192 (2005).
31. D. H. Hubel, T. N. Wiesel, *J. Physiol.* **160**, 106 (1962).
32. K. Ohki, S. Chung, Y. H. Ch'ng, P. Kara, R. C. Reid, *Nature* **433**, 597 (2005).
33. H. J. Alitto, W. M. Usrey, *J. Neurophysiol.* **91**, 2797 (2004).
34. B. Chapman, M. P. Stryker, *J. Neurosci.* **13**, 5251 (1993).
35. G. F. Buzás, D. Thompson, C. King, J. Smyth, D. J. Tolhurst, *Eur. J. Neurosci.* **10**, 265 (1998).
36. A. Basole, F. White, D. Fitzpatrick, *Nature* **423**, 986 (2003).
37. Bonhoeffer, A. Grinvald, *Nature* **353**, 429 (1991).
38. M. Hübener, D. Shoham, A. Grinvald, Bonhoeffer, *J. Neurosci.* **17**, 9270 (1997).
39. M. P. Issa, C. Trepel, M. P. Stryker, *J. Neurosci.* **20**, 8504 (2000).
40. H. Yu, B. J. Farley, D. Z. Jin, M. Sur, *Neuron* **47**, 267 (2005).
41. A. H. Cornell-Bell, S. M. Finkbeiner, M. S. Cooper, S. J. Smith, *Science* **247**, 470 (1990).
42. J. A. Filosa, A. D. Bonev, M. T. Nelson, *Circ. Res.* **95**, e73 (2004).
43. M. R. Metea, E. A. Newman, *J. Neurosci.* **26**, 2862 (2006).
44. J. R. Pohmann, D. Granquist-Fraser, R. J. Wood, E. L. Schwartz, *Proc. Natl. Acad. Sci. U.S.A.* **102**, 4158 (2005).
45. R. D. Frostig, E. E. Lieke, D. Y. Ts'o, A. Grinvald, *Proc. Natl. Acad. Sci. U.S.A.* **87**, 6082 (1990).
46. D. Attwell, C. Iadecola, *Trends Neurosci.* **25**, 621 (2002).
47. B. Cauli *et al.*, *J. Neurosci.* **24**, 8940 (2004).
48. A. Rancillac *et al.*, *J. Neurosci.* **26**, 6997 (2006).
49. D. De Saint Jan, G. L. Westbrook, *J. Neurosci.* **25**, 2917 (2005).
50. H. Gurden, N. Uchida, Z. F. Mainen, *Neuron* **52**, 335 (2006).
51. C. M. Anderson, R. A. Swanson, *Glia* **32**, 1 (2000).
52. J. W. Dam, A. Cherniavsky, S. J. Smith, *Neuron* **8**, 429 (1992).
53. A. Verkhratsky, R. K. Orkland, H. Kettenmann, *Physiol. Rev.* **78**, 99 (1998).
54. V. Dragoi, C. Rivadulla, M. Sur, *Nature* **411**, 80 (2001).
55. T. O. Sharpee *et al.*, *Nature* **439**, 936 (2006).
56. J. Schummers, J. Sharma, M. Sur, *Prog. Brain Res.* **149**, 65 (2005).
57. We thank A. Majewska for initial and ongoing assistance with two-photon microscopy and helpful comments on a draft of the paper. This work was supported by grants from the NIH and the Simons Foundation (to M.S.).

Supporting Online Material

www.sciencemag.org/cgi/content/full/320/5883/1638/DC1
Materials and Methods
Figs. S1 to S6
Movies S1 to S3

5 February 2008; accepted 25 April 2008
10.1126/science.1156120

Proliferating Cells Express mRNAs with Shortened 3′ Untranslated Regions and Fewer MicroRNA Target Sites

Rickard Sandberg,[1,2]† Joel R. Neilson,[2]* Arup Sarma,[3] Phillip A. Sharp,[1,2]‡ Christopher B. Burge[1]‡

Messenger RNA (mRNA) stability, localization, and translation are largely determined by sequences in the 3′ untranslated region (3′UTR). We found a conserved increase in expression of mRNAs terminating at upstream polyadenylation sites after activation of primary murine CD4$^+$ T lymphocytes. This program, resulting in shorter 3′UTRs, is a characteristic of gene expression during immune cell activation and correlates with proliferation across diverse cell types and tissues. Forced expression of full-length 3′UTRs conferred reduced protein expression. In some cases the reduction in protein expression could be reversed by deletion of predicted microRNA target sites in the variably included region. Our data indicate that gene expression is coordinately regulated, such that states of increased proliferation are associated with widespread reductions in the 3′UTR-based regulatory capacity of mRNAs.

The 3′ untranslated region (3′UTR) of mRNA has known functions in the stability, localization, and translation of mRNA (*1*). These roles are mediated by interactions with regulatory proteins and RNAs, including microRNAs (miRNAs) (*2*). About half of mammalian genes use alternative cleavage and polyadenylation (APA) to generate multiple mRNA isoforms differing in their 3′UTRs (*3*–*5*). However, the extent to which differential expression of these isoforms is used to regulate mRNA and protein levels in cellular proliferation and differentiation programs is poorly understood.

T lymphocyte activation is central to the immune response, and much is known about the associated gene expression and regulation (*6*).

[1]Department of Biology, Massachusetts Institute of Technology, Cambridge, MA 02139, USA. [2]Koch Institute for Integrative Cancer Research, Massachusetts Institute of Technology, Cambridge, MA 02139, USA. [3]Department of Electrical Engineering and Computer Science, Massachusetts Institute of Technology, Cambridge, MA 02139, USA.

*These authors contributed equally to this work
†Present address: Department of Cell and Molecular Biology, Karolinska Institutet, 171 77 Stockholm, Sweden.
‡To whom correspondence should be addressed. E-mail: sharppa@mit.edu (P.A.S.); cburge@mit.edu (C.B.B.)

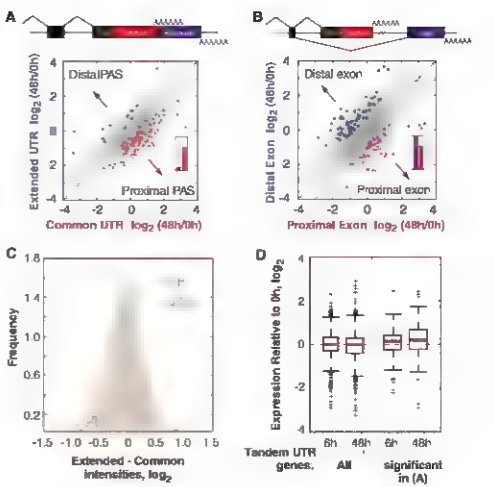

Fig. 1. Reduced relative expression of extended 3′UTR regions 48 hours after T lymphocyte activation. **(A)** Scatterplot of common and extended UTR region expression of tandem APA genes in resting and stimulated (48 hours) T lymphocytes. Significantly increased expression of isoforms resulting from usage of distal PAS (blue) or proximal PAS (red) ($P < 0.02$, 20% false discovery rate) are colored. Inset: Direction of change (13 distal, 86 proximal; $P < 2.3 \times 10^{-16}$, binomial test). **(B)** Relative expression of mutually exclusive 3′ exons in resting and stimulated (48 hours) T lymphocytes. Significant events ($P < 0.0031$, 5% FDR) and inset are as in (A). **(C)** Expression of common versus extended 3′UTR regions in resting (0 hours, $n = 1768$) versus activated (48 hours, $n = 1761$) cells. Difference $P < 6.6 \times 10^{-19}$, t test. **(D)** Relative expression (activated/resting) of all tandem UTR genes and in the set of significant events from (A) after stimulation.

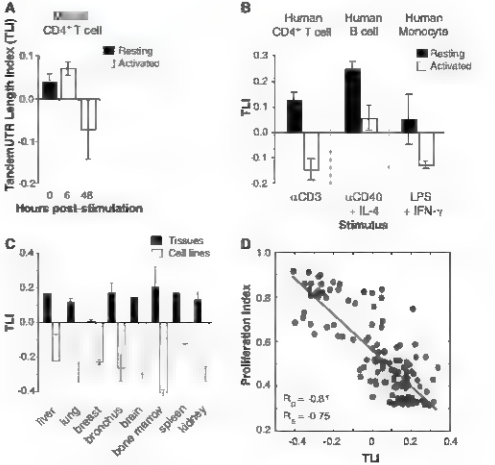

Fig. 2. Reduced expression of extended 3′UTR regions is widespread, conserved to humans, and correlated with proliferation. **(A)** TLI analysis of murine CD4+ T lymphocytes stimulated with anti-CD3/anti-28 beads (this study). **(B)** TLI values from human CD4+ T cells, B cells, and monocytes activated for 30 hours with the indicated stimulus. **(C)** TLI values of cultured cancer cell lines and of matched normal tissues. **(D)** Correlation of TLI with proliferation index across a panel of 135 different tissues and samples (R_p = Pearson; R_s = Spearman correlations, both $P < 10^{-16}$). Data in (A) to (D) are means ± SD of 2 to 33 repicates (table S8).

Earlier work demonstrated that APA is regulated in activated T cells (*4*, *7*, *8*). To provide a better understanding of how APA is used in a dynamic gene expression program, we performed a global analysis of alternative 3′UTR isoforms during T cell activation. We developed a method for probe level alternative transcript analysis (PLATA) that uses variation in hybridization of individual oligonucleotide probes on Affymetrix Mouse Exon 1.0 ST microarrays. This platform was used to compare transcripts in resting primary murine T cells expressing CD4 ($CD4^+$) to cells stimulated through the T cell antigen receptor (TCR) for 6 or 48 hours (figs. S1 to S4 and tables S1 to S4).

APA occurs in both a splicing-independent form [multiple polyadenylation sites (PASs) in a terminal exon, here called tandem UTRs] and a splicing-dependent form (mutually exclusive terminal exons, here called 3′ exon switching), diagrammed in Fig. 1A and Fig. 1B, respectively (*4*). These classes were considered separately in stimulated and resting cells. We first compared the relative expression of the common 3′UTR regions (between stop codon and first or "proximal" PAS) and of the extended 3′UTR regions (between proximal PAS and second, "distal" PAS) of 1190 genes with expressed sequence tag (EST)–supported tandem UTRs and then compared the relative expression of mutually exclusive 3′ exons for 1991 genes (Fig. 1, A and B, figs. S5 and S6, and tables S5 and S6). Patterns of splicing-independent and splicing-dependent APA events in stimulated cells were markedly different. Statistically significant 3′ exon switching events were observed at both early (n = 89; fig. S6) and late (n = 203, Fig. 1B and table S6) stages of activation, but statistically significant changes in tandem UTR events were observed only at late stages of activation (n = 99; Fig. 1A and fig. S6). Proximal-to-distal and distal-to-proximal 3′ exon switching were similarly represented (Fig. 1B, inset, fig. S6, inset, 143 versus 149 overall). However, 86% of changes in genes with tandem UTRs occurred in the direction of decreased expression of the extended 3′UTR region (Fig. 1A, inset). Changes in isoform expression estimated by PLATA were confirmed by quantitative reverse transcription polymerase chain reaction (fig. S4D and table S7). Genes with significantly reduced relative expression of extended 3′UTR regions had an average factor of 2.2 reduction in expression of extended region probes relative to common region probes. Because probes querying the common 3′UTR region assess the aggregate expression of both isoforms, this value underestimates changes in APA isoform expression. Increased relative expression of shorter isoforms derived from tandem UTR-containing genes was independently validated by Northern analysis (fig. S4E). A comprehensive analysis of all genes with tandem UTRs expressed at 48 hours revealed a highly significant ($P < 6.6 \times 10^{-19}$, t test) reduction in extended 3′UTR expression at late stages of T lymphocyte activation (Fig. 1C and fig. S6). This reduction was not associated with significant changes in median gene expression (assessed by common region probes), although median expression of genes with highly significant UTR changes was slightly increased in activated cells (Fig. 1D).

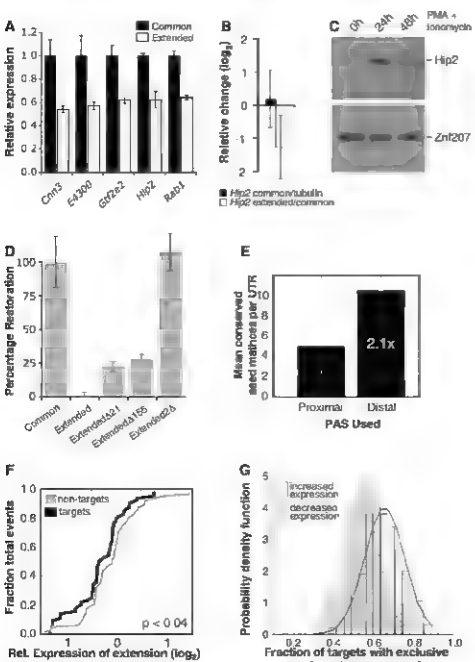

Fig. 3. Differential protein expression conferred by extended 3′UTR regions and analysis of miRNA seed matches. (**A**) Luciferase activity in stimulated primary murine T lymphocytes transfected with reporter constructs encoding common and extended 3′UTR isoforms of indicated genes (*Cnn3*, acidic calponin 3, *E4300* putative phosphodiesterase, *Gtf2e2*, General transcription factor II E, polypeptide 2, *Hip2*, Huntingtin-interacting protein 2; *Rab1*, Ras-associated protein Rab1). (**B**) Mean expression ± SD of common transcript expression and relative 3′UTR expression of the *Hip2* transcript at 48 hours after stimulation. (**C**) Immunoblot of Hip2 protein in resting and stimulated (24 and 48 hours) primary $CD4^+$ T cells. Znf207 serves as a loading control. (**D**) Percentage restoration of luciferase activity in stimulated primary murine T lymphocytes transfected with the indicated reporter constructs (fig. S9). (**E**) Mean number of conserved 3′UTR miRNA seed matches in proximal and distal PAS isoforms of genes with tandem APA sites. (**F**) Cumulative density plot of mean relative expression of extended regions ($\log_2$) for conserved targets (n = 64) and nontargets (n = 64) of activation- and proliferation-associated miRNAs (*miR-155*, *miR-17-92* cluster) at 48 hours after stimulation. (**G**) Distribution of fraction of mRNA targets lost for each miRNA upon shift from distal to proximal PAS in genes with tandem UTRs that increase or decrease in expression 48 hours after stimulation. Data in (A) and (D) are means ± SD of triplicate measurements and are representative of three or four independent experiments.

To determine whether the apparent global decrease in relative expression of extended UTR isoforms was unique to late stages of murine $CD4^+$ T lymphocyte activation, we developed a tandem UTR length index (TLI) that assesses aggregate expression of extended 3′UTR regions relative to overall gene expression levels (fig. S7 and table S9). In our mouse $CD4^+$ T cell data, TLI changed very little at 6 hours after stimulation but showed a marked decrease at 48 hours (Fig. 2A). Analysis of array data from human T lymphocytes stimulated through the TCR revealed that decreased relative expression of distal PAS isoforms in tandem UTR genes is conserved between mouse and human (Fig. 2B). TLI also decreased after stimulation of human B cells with anti-CD40 and interleukin-4, and stimulation of human monocytes with lipopolysaccharide and interferon-γ (Fig. 2B and fig. S8A). Thus, a global decrease in relative expression of distal 3′UTRs occurs after activation of several immune cell types with a variety of activating or proliferative stimuli.

Analysis of a broader panel of human and mouse tissues revealed tissue-based usage of APA isoforms, in agreement with previous studies (*3*, *5*) (fig. S8B). TLI values from cell lines were consistently lower than for the normal tissue type from which the line was derived (Fig. 2C). Given that cultured cell lines have been selected for rapid proliferation, and that activation of hematopoietic cells is often associated with a marked increase in proliferation rate, these observations suggested that decreased relative expression of distal PAS isoforms might be generally associated with cellular proliferation. To address this hypothesis, we developed a proliferation index (PI), a gene expression–based measure of cellular proliferation (see SOM text). Analysis of array data over hundreds of individual samples revealed a strong negative correlation between PI and TLI ($P < 10^{-20}$), indicating that reduced relative expression of distal PAS isoforms is broadly associated with cellular proliferation (Fig. 2D).

Common and full-length 3′UTRs from several tandem APA genes were fused to a luciferase reporter this enabled us to assess how different 3′UTR isoforms influence protein expression. To isolate the effects of the UTR on protein expression from effects on efficiency of polyadenylation, we used a heterologous SV40 PAS to terminate both transcripts. Use of the SV40 PAS in the full-length transcript was ensured by deletion of the sequence encoding the proximal PAS (fig. S9A). In all cases tested, the full-length UTR reporter yielded significantly lower luciferase activity in stimulated primary T cells than did the construct containing only the common UTR region ($P < 0.01$ by two-tailed t test, Fig. 3A). Thus, sequences within the extended UTR regions of tandem UTR genes commonly reduced protein output, likely by affecting mRNA stability and/or translation.

The extended 3′UTR region of one tested gene, *Hip2*, contains conserved seed matches to miR-21 and miR-155, both of which are expressed in activated mouse T cells (*9*, *10*). Overall *Hip2* transcript expression was very similar between naïve and activated T lymphocytes; however, upon activation, relative expression of the extended UTR region decreased while protein levels increased substantially (Fig. 3, B and C). This pattern is consistent with a model in which elimination of the extended region of the *Hip2* 3′UTR in activated T cells releases this transcript from negative regulation by *miR-21* and *miR-155*. In luciferase assays, whereas deletion of either miRNA seed match in the full-length construct resulted in a modest increase in expression, elimination of both sites restored luciferase expression to levels indistinguishable from those observed with the shorter UTR (Fig. 3D). We conclude that in activated T lymphocytes, the extended region of the *Hip2* 3′UTR confers reduced protein expression, and that the miR-21 and miR-155 seed matches within this region contribute to this regulation.

In agreement with previous studies (*11*), we found that extended UTR regions contained slightly higher numbers of conserved miRNA seed matches than common regions (Fig. 3E), but no single target site was significantly enriched in extended regions. However, the set of genes containing conserved seed matches to proliferation-associated T cell miRNAs (*miR-155* and the oncogenic *miR-17-92* cluster) exhibited significantly reduced expression of the distal PAS isoform relative to nontargets ($P < 0.05$, Fig. 3F) in stimulated T cells, where expression of these miRNAs is increased (*9*) (fig. S10). Furthermore, tandem APA genes whose overall transcript expression increased after activation were more likely to be targeted exclusively in their extended UTR region by miRNAs than tandem APA genes whose expression decreased (Fig. 3G, $P = 3.2 \times 10^{-4}$, t test). Taken together, these data are consistent with a model in which reduced expression of distal PAS isoforms in genes up-regulated after activation results in reduced potential for targeting by proliferation-associated negative regulatory factors.

Comparisons of tissue-specific EST libraries have been used to catalog genes with APA and to identify motifs enriched around the PASs of these genes (*3*, *5*, *11*, *12*). However, to our knowledge, a widespread pattern of directed changes in 3′UTR isoform expression has not been previously described as part of a gene expression program. The observed pattern of decreased relative expression of longer mRNA isoforms could result from a systematic shift in APA or from preferential destabilization of longer mRNA isoforms. The available evidence tends to support regulated APA as being more important; for example, a stability-based mechanism would predict a significant decrease in mean expression of genes with altered 3′UTR isoform expression after activation, but no general decrease was observed (Fig. 1D), and Northern blots (fig. S4) generally showed increased expression of the shorter isoform, which is more consistent with APA regulation. However, our data do not conclusively distinguish between these two mechanisms.

Stimulation of B lymphocytes, T cells, and monocytes results in increased protein expression of the general polyadenylation factor Cstf-64, which plays a role in increased usage of "weaker" upstream PASs in certain 3′ exon switching events in these cell types (*7*, *13*–*16*). Because Cstf-64 protein expression is also increased as cultured fibroblasts initiate proliferative programs (*13*), one could imagine that this factor might function as a "master regulator" of PAS selection controlling all of the events that we observe. However, given that immunoglobulin μ heavy chain PAS selection can be functionally uncoupled from both proliferation and Cstf-64 protein levels in the B cell model (*13*), and that tandem UTR events respond very differently from 3′ exon switching events in this study, it is likely that additional factors are involved (*17*–*20*).

The general association of the program of increased relative expression of shorter 3′UTR isoforms with states of higher proliferation may indicate that UTR-based mRNA regulation plays distinct roles in the regulatory networks of nonproliferating or slowly proliferating cells as compared to actively proliferating cells. It is tempting to speculate that in some cases a shift toward expression of proximal PAS isoforms may be required to evade regulation that would otherwise restrict cell cycle progression. Both of these ideas are consistent with the observation that global down-regulation of mRNA expression is observed in human cancers (*21*) and promotes cellular transformation and tumorigenesis (*22*).

References and Notes

1. M. J. Moore *Science* **309**, 1514 (2005).
2. D. P. Bartel, C. Z. Chen, *Nat. Rev. Genet.* **5**, 396 (2004).
3. E. Beaudoing, D. Gautheret, *Genome Res.* **11**, 1520 (2001).
4. G. Edwalds-Gilbert, K. J. Veraldi, C. Milcarek, *Nucleic Acids Res.* **25**, 2547 (1997).
5. H. Zhang, J. Y. Lee, B. Tian, *Genome Biol.* **6**, R100 (2005).
6. G. R. Crabtree *Science* **243**, 355 (1989).
7. S. Chevrier *et al.*, *Immunity* **30**, 261 (1999).
8. D. A. Pearce, K. Nishio, M. Benjamin, J. A. Lipple *Gene* **150**, 251 (1994).
9. S. Mantchev *et al.*, *Genome Biol.* **8**, R71 (2005).
10. H. Wu *et al.*, *PLoS ONE* **2**, e1020 (2007).
11. M. Legendre, W. Ritchie, F. Lopez, D. Gautheret, *PLoS Comput. Biol.* **2**, e43 (2006).
12. T. Arai, F. Lopez, W. Ritchie, P. Benech, D. Gautheret *BMC Genomics* **7**, 189 (2006).
13. K. Martincic *et al.*, *Proc. Natl. Acad. Sci. U.S.A.* **95**, 2095 (1998).
14. S. A. Shell, C. Hesse, S. M. Morris Jr., C. Milcarek, *J. Biol. Chem.* **280**, 39950 (2005).
15. Y. Takagaki, R. E. Seipelt, M. L. Peterson, J. L. Manley, *Cell* **87**, 941 (1996).
16. Y. Takagaki, J. L. Manley *Mol. Cell* **2**, 761 (1998).
17. K. M. Brown, G. M. Gilmartin, *Mol. Cell* **12**, 1467 (2003).
18. V. Quesada, R. Macdonald, C. Dean, G. G. Simpson, *EMBO J.* **22**, 3142 (2003).

19. G. G. Simpson, P. P. Dijkwel, V. Quesada, I. Henderson, C. Dean, *Cell* **113**, 777 (2003).
20. K. L. Veraldi *et al.*, *Mol. Cell. Biol.* **21**, 228 (2001).
21. J. Lu *et al.*, *Nature* **435**, 834 (2005).
22. M. S. Kumar, J. Lu, K. L. Mercer, T. R. Golub, T. Jacks, *Nat. Genet.* **39**, 673 (2007).
23. We thank members of the Burge and Sharp labs as well as M. Winslow, K. Cante-Barrett, and O. Larsson. Supported by the Knut and Alice Wallenberg Foundation (R.S.); the Cancer Research Institute (L.R.M.); the Gina De Felice and Robert M. Lefkowitz (1995) Fund (A.S.); U.S. Public Health Service grant RO1-GM34277 and National Cancer Institute grants PO1-CA42063 and (T.J.) AI056900 (P.A.S.); Cancer Center Support (core) grant P30-CA14051 from the National Cancer Institute; and National Human Genome Research Institute grant R01-HG002439 (C.B.B.). Array data have been deposited in Gene Expression Omnibus Accession number GSE10666.

Supporting Online Material
www.sciencemag.org/cgi/content/full/320/5883/1643/DC1
Materials and Methods
SOM Text
Figs. S1 to S10
Tables S1 to S10
References

18 January 2008; accepted 19 May 2008
10.1126/science.1155398

Evolution of Mammals and Their Gut Microbes

Ruth E. Ley,[1] Micah Hamady,[2] Catherine Lozupone,[1,3] Peter J. Turnbaugh,[1] Rob Roy Ramey,[4] J. Stephen Bircher,[5] Michael L. Schlegel,[6] Tammy A. Tucker,[6] Mark D. Schrenzel,[6] Rob Knight,[3] Jeffrey I. Gordon[1]*

Mammals are metagenomic in that they are composed of not only their own gene complements but also those of all of their associated microbes. To understand the coevolution of the mammals and their indigenous microbial communities, we conducted a network-based analysis of bacterial 16*S* ribosomal RNA gene sequences from the fecal microbiota of humans and 59 other mammalian species living in two zoos and in the wild. The results indicate that host diet and phylogeny both influence bacterial diversity, which increases from carnivory to omnivory to herbivory; that bacterial communities codiversified with their hosts, and that the gut microbiota of humans living a modern life-style is typical of omnivorous primates.

Our "metagenome" is a composite of *Homo sapiens* genes and genes present in the genomes of the trillions of microbes that colonize our adult bodies (*1*). The vast majority of these microbes live in our distal guts. "Our" microbial genomes (microbiomes) encode metabolic functions that we have not had to evolve wholly on our own, including the ability to extract energy and nutrients from our diet. It is unclear how distinctively human our gut microbiota is, or how modern *H. sapiens*' ability to construct a wide range of diets has affected our gut microbial ecology. Here, we address two general questions concerning the evolution of mammals: How do diet and host phylogeny shape mammalian microbiota? When a mammalian species acquires a new dietary niche, how does its gut microbiota relate to the microbiota of its close relatives?

The acquisition of a new diet is a fundamental driver for the evolution of new species. Coevolution, the reciprocal adaptations occurring between interacting species (*2*), produces physiological changes that are often recorded in fossil remains. For instance, although mammals made their first appearance on the world stage in the Jurassic (~160 million years ago (Ma)), most modern species arose during the Quaternary [1.8 Ma to the present (*3*)], when C4 grasslands (dominated by plants that use for photosynthesis the Hatch-Slack cycle rather than the Calvin cycle typical of C3 plants) expanded in response to a fall in atmospheric CO_2 levels and/or climate changes (*4–6*). The switch to a C4 plant–dominated diet led to selection for herbivores with high-crowned teeth (*7*, *8*) and longer gut retention times necessary for the digestion of lower quality forage (*9*). However, these adaptations may not suffice for the exploitation of a new dietary niche. The community of microbes in the gut constitutes a potentially critical yet unexplored component of diet-driven speciation.

Because we cannot interrogate extinct gut microbiotas directly, past evolutionary processes can only be inferred from comparative analyses of extant mammalian gut microbial communities. Therefore, we analyzed the fecal microbial communities of 106 individual mammals representing 60 species from 13 taxonomic orders, including 17 nonhuman primates. To isolate the effects of phylogeny and diet, we included multiple samples from many of the mammalian species, as well as species that had unusual diets compared to their close phylogenetic relatives. For example, the majority of the nonhuman primate species studied were omnivores (12 of 17), but the leaf-eating (folivorous) East Angolan colobus, Eastern black-and-white colobus, Douc langur, and François langur were also sampled. In addition, the herbivorous giant panda and red panda were included from the Carnivora. Most animals were housed at the San Diego Zoo and the San Diego Zoo's Wild Animal Park ($n = 15$) or the St. Louis Zoo ($n = 56$). Others were examined in the wild ($n = 29$) or domesticated ($n = 6$; table S1). To test the reproducibility of host species–associated gut microbiotas and to gauge the effects of animal provenance, we represented mammalian species by multiple individuals from multiple locales where possible, and chose wild animals to match captive animals. We generated a data set of >20,000 16*S* rRNA gene sequences, for comparison of the human, primate, and nonprimate mammalian gut microbiotas (*10*), the 106 samples also included published fecal bacterial 16*S* rRNA sequences (>3000) from wild African gorilla (*11*), Holstein cattle (*12*), Wistar rats (*13*), and healthy humans of both sexes, ranging in age from 27 to 94, living on three continents and including a strict vegetarian (*14–18*) (table S1).

We used network-based analyses to map gut microbial community composition and structure onto mammalian phylogeny and diet, thereby complementing phylogeny-based microbial community comparisons. These analyses were used to bin 16*S* rRNA gene sequences into operational taxonomic units (OTUs) and to display microbial genera partitioning across hosts. Genus-level OTUs (sets of sequences with ≥96% identity) and animal hosts were designated as nodes in a bipartite network, in which OTUs are connected to the hosts in which their sequences were found (Fig. 1A). To cluster the OTUs and hosts in this network, we used the stochastic spring-embedded algorithm, as implemented in Cytoscape 2.5.2 (*19*), where nodes act as physical objects that repel each other, and connections act as a spring with a spring constant and a resting length; the nodes are organized in a way that minimizes forces in the network.

The ensemble of sequences in this study provides an overarching view of the mammal gut microbiota. We detected members of 17 phyla (divisions) of Bacteria (*10*). The majority of sequences belong to the Firmicutes [65.7% of 19,548 classified sequences (*10*)] and to the Bacteroidetes (16.3%), these phyla were previously shown to constitute the majority of sampled human (and mouse) gut-associated phylotypes (*10*, *20*). The other phyla represented were the Proteobacteria (8.8% of all sequences collected, 85% in the Gamma subdivision), Actinobacteria (4.7%), Verrucomicrobia (2.2%), Fusobacteria (0.67%), Spirochaetes (0.46%), DSS1 (0.35%), Fibrobacteres (0.13%), TM7 (0.13%), deep-

[1]Center for Genome Sciences, Washington University School of Medicine, St. Louis, MO 63108, USA. [2]Department of Computer Science, University of Colorado, Boulder, CO 80309, USA. [3]Department of Chemistry and Biochemistry, University of Colorado, Boulder, CO 80309, USA. [4]Wildlife Science International, Inc., Nederland, CO 80466, USA. [5]St. Louis Zoological Park, St. Louis, MO 63110, USA. [6]Zoological Society of San Diego, San Diego, CA 92112, USA.
*To whom correspondence should be addressed. E-mail: jgordon@wustl.edu

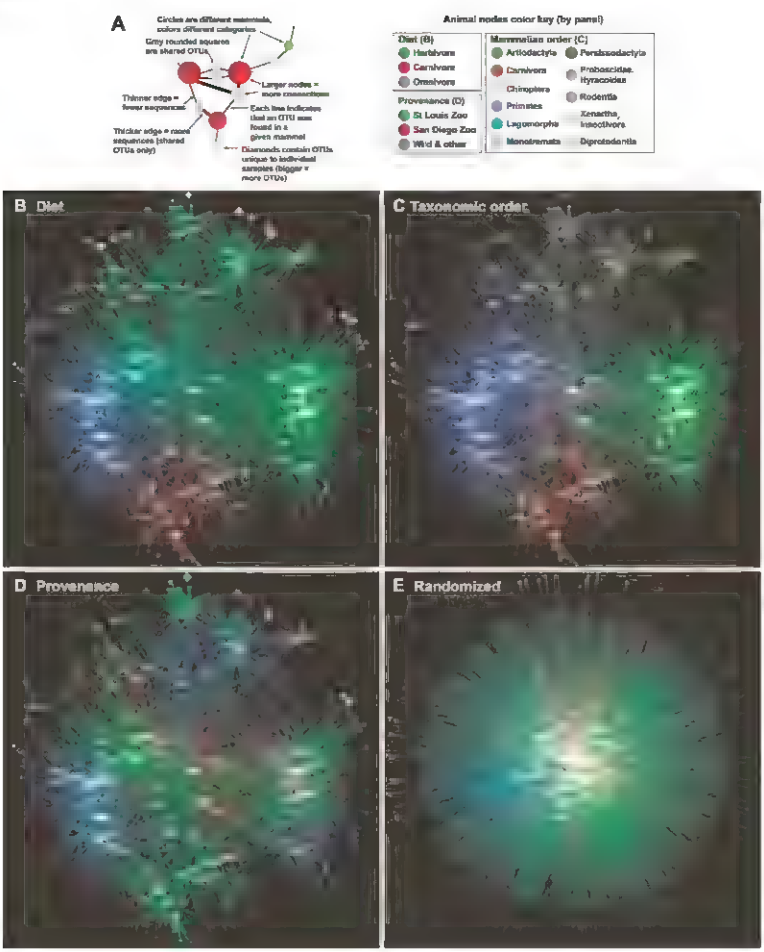
A
Circles are different mammals, colors different categories
Grey rounded squares are shared OTUs
Larger nodes = more connections
Thinner edge = fewer sequences
Each line indicates that an OTU was found in a given mammal
Thicker edge = more sequences (shared OTUs only)
Diamonds contain OTUs unique to individual samples (bigger = more OTUs)
Animal nodes color key (by panel)
Diet (B)
Herbivore
Carnivore
Omnivore
Provenance (D)
St Louis Zoo
San Diego Zoo
Wild & other
Mammalian order (C)
Artiodactyla
Carnivora
Chiroptera
Primates
Lagomorpha
Monotremata
Perissodactyla
Proboscidae, Hyracoidea
Rodentia
Xenarthra, Insectivora
Diprotodontia
B Diet
C Taxonomic order
D Provenance
E Randomized

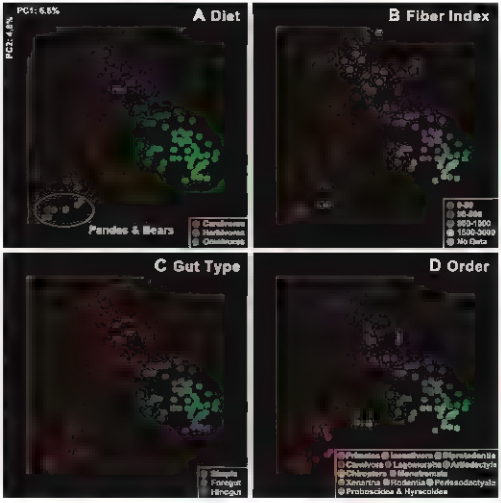

Fig. 2. Mammalian fecal bacterial communities clustered using principal coordinates analysis (PCoA) of the UniFrac metric matrix. PC1 and PC2 are plotted on x and y axes. Each circle corresponds to a fecal sample colored according to (**A**) diet, (**B**) diet fiber index, (**C**) gut morphology/physiology, and (**D**) host taxonomic order. The same data (samples) are shown in each panel. The percentage of the variation explained by the plotted principal coordinates is indicated on the axes.

rooting Cyanobacteria [0.10%; these are not chloroplasts (*20*)], Planctomycetes (0.08%), Deferribacteres (0.05%), Lentisphaerae (0.04%), and Chloroflexi, SR1, and Deinococcus-Thermus (all 0.005%). We were unable to assign 1985 16S rRNA gene sequences that passed a chimera-checking algorithm (*21*) to known phyla on the basis of BLAST searches against the Greengenes database (*22*) and the Ribosomal Database Project taxonomy annotations (*23*). Of the phyla that were detected, only Firmicutes were found in all samples (fig. S1). However, each mammalian host harbored OTUs (96% sequence identity) not observed in any other sample (at this level of sampling, on average, 56% and 62% of OTUs were unique within a sample and species, respectively; table S1).

The network-based analyses disclosed that overall, the fecal microbial communities of same-species (conspecific) hosts were more similar to each other than to those of different host species. Host nodes were significantly more connected within than between species (G test for independence, $G = 11.9$, $P = 0.0005$, Fig. 1B). Shown in fig. S2 is a tree-based analysis where similarity is defined using the UniFrac metric: this metric is based on the degree to which individual communities share branch length on a common (master) phylogenetic tree constructed from all 16S rRNA sequences from all communities being compared (*24*, *25*). The results are consistent with the network-based analysis: that is, they show that UniFrac distances are smaller within conspecific hosts than between conspecific hosts ($P < 0.005$ by one-tailed t test, confirmed by matrix permutation and corrected for multiple comparisons).

The impact of host species on community composition is most evident when considering conspecific hosts living separately, because cohousing may confound any species effect. For example, the two Hamadryas baboons clustered together (fig. S2), although one is from Namibia and the other from the St. Louis Zoo; similarly, the red pandas housed in different zoos clustered together. All 16 human samples also clustered together. Nonetheless, some conspecifics with different origins did not cluster (e.g., the two Western lowland gorillas), which suggests that diet and other environmental exposures ["legacy effects" (*26*)] play roles in addition to host phylogeny (taxonomic order).

The clustering by diet (herbivore, omnivore, and carnivore) was highly significant in both the tree-based (fig. S2) and network-based analyses (Fig. 1B). In the network-based analysis, host nodes are significantly more connected to other host nodes from the same diet group ($G = 115.8$, $P = 5.1 \times 10^{-27}$) (*10*). Similarly, hosts within the same taxonomic order are more connected in the network to hosts within the same order (Fig. 1C; $G = 356$; $P = 2.1 \times 10^{-75}$). Likewise, UniFrac-based principal coordinates analysis (PCoA) showed clustering by diet (Fig. 2, A and B) and by taxonomic order (Fig. 2D). (UniFrac distances are smaller for within versus between diet categories, and for within versus between orders, $P < 0.005$.) There was no significant clustering according to the provenance of the animals (including humans) in either the network- or UniFrac-based analyses ($P > 0.05$ for both, Fig. 1D and fig. S2, respectively), nor in a randomized network (Fig. 1E).

Classification of the mammals into herbivore, omnivore, and carnivore groups was based on diet records and natural history. Heavy use

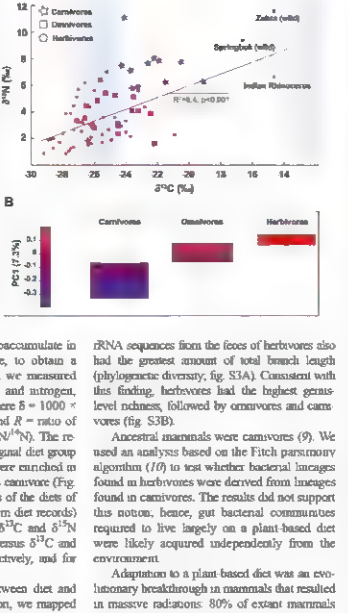

Fig. 3. Markers of trophic level mapped onto the variance in fecal microbial community diversity. (**A**) Stable isotope values for C and N plotted for each fecal sample, presented according to diet group. Symbols are colored according to their PC1 value; PC1 is the first principal coordinate of the PCoA of the unweighted UniFrac metric. $\delta^{13}C$ ranges for C3 and C4 plants [per mil (‰)] are highlighted in blue. R^2 is for $\delta^{13}C$ versus $\delta^{15}N$. (**B**) Box plots are shown for the three diet groups (central line is the mean; box outline equals 1 SD; the bar denotes 2 SD; circles are outliers). The majority of fecal $\delta^{13}C$ values are intermediate between the average for C4 plants (~ 12.5‰) and C3 plants (~26.7‰).

topes of carbon and nitrogen bioaccumulate in the food chain (*27*). Therefore, to obtain a more objective marker of diet, we measured stable isotope ratios of carbon and nitrogen, $\delta^{13}C$ and $\delta^{15}N$, in the feces (where $\delta = 1000 \times [(R_{sample} - R_{standard})/R_{standard}]$ and R = ratio of atom percentages $^{13}C/^{12}C$ and $^{15}N/^{14}N$). The results were consistent with the original diet group classification. Heavy isotopes were enriched in the order herbivore < omnivore < carnivore (Fig. 3A). The protein and fat contents of the diets of animals in captivity (obtained from diet records) were positively correlated with $\delta^{13}C$ and $\delta^{15}N$ fecal values (R^2 values for fat versus $\delta^{13}C$ and $\delta^{15}N$ were 0.51 and 0.45, respectively, and for protein, 0.36 and 0.38).

To test for a direct link between diet and microbial community composition, we mapped stable isotope values onto the coordinates that explained the largest proportion of the variance in the microbial communities, as determined by PCoA of the UniFrac distances between hosts (Fig. 3B). Principal coordinate 1 (PC1) separates carnivores from herbivores and omnivores (mean is significantly lower for carnivores than herbivores, which are equivalent to omnivores; $F_{80,2} = 9.9$, $P < 0.001$) and is also correlated with $\delta^{13}C$ and $\delta^{15}N$ values (multiple regression $R^2 = 0.25$, $F_{80,2} = 12.7$, $P < 0.001$). Together, these results support an association between microbial community membership and diet, and provide an independent validation of the dietary clustering observed in the network diagrams that is free of bias in assigning hosts to one of the three diet categories.

Underlying the correlation between bacterial community composition and diet is the partitioning of bacterial phyla among hosts according to diet. Herbivore microbiotas contained the most phyla (14), carnivores contained the fewest (6), and omnivores were intermediate (12) (fig. S1). Phylogenetic trees constructed from 16S rRNA sequences from the feces of herbivores also had the greatest amount of total branch length (phylogenetic diversity; fig. S3A). Consistent with this finding, herbivores had the highest genus-level richness, followed by omnivores and carnivores (fig. S3B).

Ancestral mammals were carnivores (*9*). We used an analysis based on the Fitch parsimony algorithm (*10*) to test whether bacterial lineages found in herbivores were derived from lineages found in carnivores. The results did not support this notion; hence, gut bacterial communities required to live largely on a plant-based diet were likely acquired independently from the environment.

Adaptation to a plant-based diet was an evolutionary breakthrough in mammals that resulted in massive radiations: 80% of extant mammals are herbivores, and herbivory is present in most mammalian lineages (*9*). To access the more complex carbohydrates present in plants, such as cellulose and resistant starches, disparate mammalian lineages lengthened gut retention times to accommodate bacterial fermentation; this occurred via enlargement of the foregut or hindgut (*9*). We found that herbivores clustered into two groups that corresponded generally to foregut fermenters and hindgut fermenters. The foregut-fermenting sheep, kangaroo, okapi, giraffe, and cattle clustered together to form herbivore group 1 in fig. S2, whereas the hindgut fermenting elephant, horse, rhinoceros, capybara, mole rat, and gorilla clustered together in herbivore group 2. The strong impact of gut morphology on bacterial community composition is also evident in PCoA of the UniFrac data: Herbivores separate into foregut and hindgut groups, and omnivores separate into hindgut fermenters and those with simple guts (Fig. 2, C and D).

Differences between the fecal communities of foregut and hindgut fermenters are likely due to host digestive physiology. In foregut fermenters, the digesta is moved into the equivalent of the monogastric stomach after fermentation, so that part of the microbiota is also digested; in hindgut fermenters, the fermentative microbes are more likely to be excreted in the feces. Fermentation requires microbial interactions such as cross feeding and interspecies hydrogen transfer (*28*). Our results suggest that as mammals underwent convergent evolution in the morphological adaptations of their guts to herbivory, their microbiota arrived at similar compositional configurations in unrelated hosts with similar gut structures.

The diet outliers in our study were folivores. Despite their herbivorous diet, red and giant pandas have simple guts, cluster with other carnivores, and have carnivore-like levels of phylogenetic diversity (figs. S2 and S3). In folivorous primates, the simple gut has evolved pouches for fermentation of recalcitrant plant material (*9*). The fecal microbiota of the two colobus monkeys and the François langur cluster together by UniFrac with the three pig species (Red River hog, Visayan warty pig, babirusa) and the flying fox, baboon, chimpanzee, gorilla, and orangutan, forming a phylogenetically mixed group whose diets include a large component of plant material. This cluster occupies an intermediate position between other primates and herbivorous foregut fermenters in fig. S2. This observation suggests that the colobus monkeys and the François langur harbor microbial lineages typical of omnivores but have a greater representation of the lineages driving the breakdown of a plant-based diet. Such host-level selection of specific members of a microbiota has been demonstrated under laboratory conditions by reciprocal transplantations of gut microbiota from one host species to germ-free recipients of a different species. Groups of bacteria were expanded or contracted in the recipient host to resemble its "normal" microbiota through a process that may have been influenced by diet (*26*).

Coevolution has been hypothesized to occur in animal species whose parental care enables vertical transmission of whole gut communities, and where the properties of the community as a whole confer a fitness advantage to the host (*29*). Although coevolution has been inferred from observations of bacterial host specificity (*30*), these observations could also be explained by dietary preference. Therefore, we searched for evidence of codiversification, a special case of coevolution (*3*) that would be manifest in this case by a clustering of fecal microbial communities that mirrors the mammalian phylogeny. A UniFrac analysis was performed recursively (*10*) on the entire mammalian fecal bacterial tree, using a procedure that had the effect of asking whether the bacterial lineages stemming from each tree node mirrored the mammalian phylogeny (*31*). The results were compared to those using a randomized version of the mammalian phylogeny. The patterns of community similarity matched the mammal phylogeny more often than would

be expected if no codiversification had occurred (fig. S4, $P = 1.79 \times 10^{-11}$, $t = 6.73$, $df = 88$).

Although mammalian gut microbes are highly adapted to life in this body habitat, and many lineages are extremely rare outside of it (*29*), they appear to be fairly promiscuous between hosts. This could account for the spectacular success of mammals and herbivores in particular. Acquiring a gut microbiota was not a constraint, and morphological and behavioral adaptations were likely far more restrictive. One implication of this work is that the tolerance of the immune system to gut microbes is a basal trait in mammal evolution.

The global success of humans is based in part on our ability to control the variety and amount of food available using agriculture and cookery. These capabilities have not appreciably affected the major bacterial lineages that constitute our gut microbiota. As noted above, fecal samples from unrelated healthy human samples cluster with other omnivores (Fig. 1 and fig. S2), with interpersonal differences (UniFrac distances) being significantly smaller than the distances between humans and all other mammalian species ($G = -47.7$, $P < 0.005$, $n = 106$). Although our interpersonal differences appear to be smaller than interspecies differences among mammals, deeper sampling and analysis will be required to circumscribe the gut microbial diversity inherent to humans. This is one of the early goals of the recently initiated international human microbiome project (*1*).

References and Notes

1. P. J. Turnbaugh *et al.*, *Nature* **449**, 804 (2007).
2. M. A. Nowak, *Curr. Biol.* **16**, R264 (2006).
3. A. M. Cotter *Philos. Trans. R. Soc. London Ser. B* **359**, 221 (2004).
4. M. Pagani, J. C. Zachos, K. H. Freeman, B. Tipple, S. Bohaty, *Science* **309**, 600 (2005); published online 16 June 2005 (10.1126/science.1110063).
5. Y. Huang *et al.*, *Science* **293**, 1647 (2001).
6. T. E. Cerling *et al.*, *Nature* **389**, 153 (1997).
7. B. J. MacFadden, *Trends Ecol. Evol.* **20**, 355 (2005).
8. T. E. Cerling, J. R. Ehleringer, J. M. Harris, *Philos. Trans. R. Soc. London Ser. B* **353**, 159 (1998).
9. C. Stevens, I. Hume, *Comparative Physiology of the Vertebrate Digestive System* (Cambridge Univ. Press, Cambridge, ed. 2, 2004).
10. See supporting material on *Science* Online.
11. J. C. Frey *et al.*, *Appl. Environ. Microbiol.* **72**, 3788 (2006).
12. Y. Urushiyama, H. Hayashi, M. Sakamoto, H. Kobashi, Y. Benno, *Biosci. Biotechnol. Biochem.* **69**, 1793 (2005).
13. S. P. Brooks, M. McAllister, M. Sandoz, M. L. Kalmokoff, *Can. J. Microbiol.* **49**, 589 (2003).
14. P. B. Eckburg *et al.*, *Science* **308**, 1635 (2005); published online 14 April 2005 (10.1126/science.1110591).
15. R. E. Ley, P. J. Turnbaugh, S. Klein, J. I. Gordon, *Nature* **444**, 1022 (2006).
16. H. Hayashi, M. Sakamoto, Y. Benno, *Microbiol. Immunol.* **46**, 535 (2002).
17. H. Hayashi, M. Sakamoto, Y. Benno, *Microbiol. Immunol.* **46**, 819 (2002).
18. H. Hayashi, M. Sakamoto, M. Kitahara, Y. Benno, *Microbiol. Immunol.* **47**, 557 (2003).
19. P. Shannon *et al.*, *Genome Res.* **13**, 2498 (2003).
20. R. E. Ley *et al.*, *Proc. Natl. Acad. Sci. U.S.A.* **102**, 11070 (2005).
21. T. Huber, G. Faulkner, P. Hugenholtz, *Bioinformatics* **20**, 2317 (2004).
22. T. Z. DeSantis *et al.*, *Appl. Environ. Microbiol.* **72**, 5069 (2006).
23. Q. Wang, G. M. Garrity, J. M. Tiedje, J. R. Cole *Appl. Environ. Microbiol.* **73**, 5261 (2007).
24. C. Lozupone, M. Hamady, R. Knight, *BMC Bioinform.* **7**, 371 (2006).
25. C. Lozupone, R. Knight, *Appl. Environ. Microbiol.* **71**, 8228 (2005).
26. J. F. Rawls, M. A. Mahowald, R. E. Ley, J. I. Gordon, *Cell* **127**, 423 (2006).
27. P. L. Koch, M. L. Fogel, N. Tuross, in *Stable Isotopes in Ecology and Environmental Science*, K. Lajtha, R. H. Michener, Eds. (Blackwell, Oxford, 1994).
28. J. B. Russell, J. L. Rychlik, *Science* **292**, 1119 (2001).
29. R. E. Ley, D. A. Peterson, J. I. Gordon, *Cell* **124**, 837 (2006).
30. L. DeFilippis-Jensen, M. McFall-Ngai, D. A. Relman, *Nature* **449**, 811 (2007).
31. J. Armesen *et al. Proc. Natl. Acad. Sci. U.S.A.* **99**, 8151 (2002).

32. We thank S. Wagoner for superb technical assistance. L. Fulton, R. Fulton, K. Delehaunty, and our other colleagues in the Washington University Genome Sequencing Center for assistance with 16S rRNA gene sequencing; and the Namibian Ministry of Environment and Tourism. Supported by NIH grants DK78669, DK70977 and DK30292 the W. M. Keck Foundation, the Ellison Medical Foundation, and NIH Molecular Biophysics Training Program grant T32GM065103 (M.H.). Sequences (EU458134 to EU475873 and EU771093 to EU779492) were deposited in GenBank.

Supporting Online Material

www.sciencemag.org/cgi/content/full/1155725/DC1
Materials and Methods
Figs. S1 to S14
Table S1
References

28 January 2008; accepted 15 May 2008
Published online 22 May 2008;
10.1126/science.1155725
Include this information when citing this paper

Ankyrin Repeat Proteins Comprise a Diverse Family of Bacterial Type IV Effectors

Xiaoxiao Pan,[1] Anja Lührmann,[2]* Ayano Satoh,[2]* Michelle A. Laskowski-Arce,[1]† Craig R. Roy[2]‡

Specialized secretion systems are used by many bacteria to deliver effector proteins into host cells that can either mimic or disrupt the function of eukaryotic factors. We found that the intracellular pathogens *Legionella pneumophila* and *Coxiella burnetii* use a type IV secretion system to deliver into eukaryotic cells a large number of different bacterial proteins containing ankyrin repeat homology domains called Anks. The *L. pneumophila* AnkX protein prevented microtubule-dependent vesicular transport to interfere with fusion of the *L. pneumophila*–containing vacuole with late endosomes after infection of macrophages, which demonstrates that Ank proteins have effector functions important for bacterial infection of eukaryotic host cells.

Type IV secretion systems (TFSSs) are molecular machines used by Gram-negative bacteria for protein transfer into recipient cells (*1*). Many bacterial pathogens and endosymbionts use TFSSs to regulate host processes important for survival and replication (*2*), and several of these organisms have a large number of genes encoding proteins with multiple ankyrin repeat homology domains (ARHDs) (*3*–*7*). Infrequently encountered in bacterial proteins but common in eukaryotic proteins, ARHDs form molecular scaffolds that mediate protein-protein interactions (*8*). An *Anaplasma phagocytophilum* protein containing multiple ARHDs called AnkA (*9*) and several ARHD proteins in strains of *Wolbachia* (*10*, *11*) have been proposed to be delivered into host cells by a TFSS (*12*); however, whether Ank proteins are bona fide TFSS effectors has not been established.

Legionella pneumophila and *Coxiella burnetii* are both intracellular pathogens that encode several proteins containing ARHDs and a TFSS called Dot/Icm (*3*–*7*). To test whether ARHD proteins are TFSS substrates, we measured host cell translocation of four *L. pneumophila* Ank proteins fused to a calmodulin-dependent adenylate cyclase reporter (Cya), using the *L. pneumophila* effector RalF as a positive control (*13*, *14*). These four Ank proteins were delivered into mammalian cells as indicated by a >10-fold increase in adenosine 3′,5′-monophosphate (cAMP) following infection (Fig. 1A). No cAMP increase was observed when the Cya-Ank proteins were produced in the *L. pneumophila* Δ*dotA* mutant lacking a functional TFSS, which indicates that the Dot/Icm system is required for Ank protein delivery into host cells. Thirteen different *C. burnetii* proteins with ARHDs were tested for translocation with the Cya assay. Genetic ma-

[1]Section of Microbial Pathogenesis, Yale University School of Medicine, 295 Congress Avenue, New Haven, CT 06536, USA. [2]Department of Cell Biology, Yale University School of Medicine, 333 Cedar Street, New Haven, CT 06520, USA.
*These authors contributed equally to this work.
†Present address: University of Texas Southwestern Medical Center, 6000 Harry Hines Boulevard, NA5.124, Dallas, TX 75390, USA.
‡To whom correspondence should be addressed. E-mail: craig.roy@yale.edu.

manipulation of the obligate intracellular pathogen *C. burnetii* is not currently possible, but the *C. burnetii* and *L. pneumophila* Dot/Icm systems are functionally similar (*15*, *16*), which suggests that *L. pneumophila* will deliver *C. burnetii* Dot/Icm substrates into host cells. *C. burnetii* AnkA, AnkB, AnkF, and AnkG fusion proteins were efficiently translocated into host cells by a process requiring the *L. pneumophila* Dot/Icm system (Fig. 1B). The AnkE, AnkH, AnkI, and AnkM proteins were delivered less efficiently (Fig. 1B). Specific Ank-encoding RNA transcripts were expressed during *C. burnetii* infection (Fig. 1C), which suggests that protein products should be available for delivery into host cells by the *C. burnetii* Dot/Icm system.

An antibody generated against AnkF confirmed that this protein was secreted during *C. burnetii* infection of mammalian cells (Fig. 1D), whereas the *C. burnetii* translation factor EF-Ts was not and remained associated with bacteria in the pellet. The amount of secreted AnkF diminished over time after treatment with the bacterial protein synthesis inhibitor chloramphenicol, which did not measurably affect levels of AnkF associated with bacterial cells (Fig. 1D). The short half life of secreted AnkF revealed by chloramphenicol treatment could be the result of proteasome-mediated degradation of this protein was translocated into the host cytosol. Indeed, inhibition of the host proteasome with MG132 prevented degradation of secreted AnkF in the chloramphenicol treated cells (Fig. 1E), which indicated that secreted AnkF was located in the host cytoso.

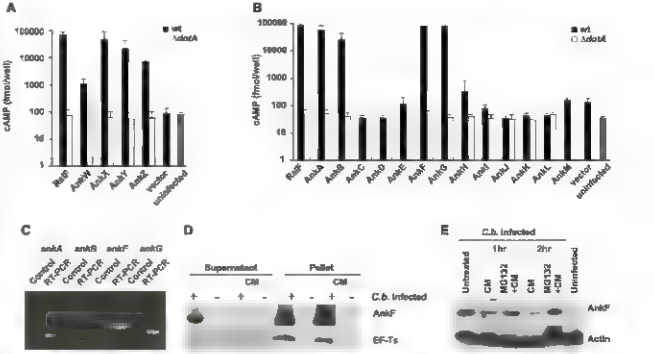

Fig. 1. Type IV translocation of bacterial Ank proteins (**A** and **B**) Translocation of Cya-Ank fusion proteins derived from *L. pneumophila* (**A**) or *C. burnetii* (**B**) into a stable Chinese hamster ovary (CHO) cell line producing the FcγRII receptor (CHO FcγRII cells) was determined. Results are means ± SD from three independent wells. (**C**) Reverse transcription polymerase chain reaction (RT-PCR) analysis of RNA isolated from *C. burnetii*–infected CHO FcγRII cells. The reverse transcription reaction was omitted in the control lanes to test for DNA contamination. (**D**) Identification of AnkF and EF-Ts in the indicated fractions isolated from human foreskin fibroblasts that were uninfected (–) or infected (+) with *C. burnetii* and either incubated with chloramphenicol (CM) or left untreated. Similar results were obtained from two independent experiments. (**E**) Identification of secreted AnkF in soluble fractions from human foreskin fibroblasts infected with *C. burnetii* that were incubated with chloramphenicol either in the presence or absence of the proteasome inhibitor MG132 as indicated for either 1 hour or 2 hours. Controls include untreated cells infected with *C. burnetii*, uninfected cells, and actin immunoblots to measure protein loading. Similar results were obtained from two independent experiments.

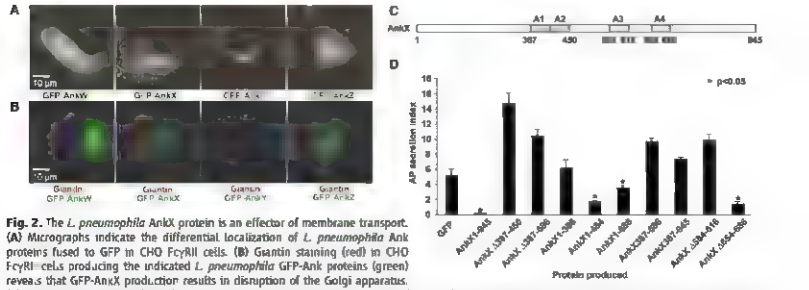

Fig. 2. The *L. pneumophila* AnkX protein is an effector of membrane transport. (**A**) Micrographs indicate the differential localization of *L. pneumophila* Ank proteins fused to GFP in CHO FcγRII cells. (**B**) Giantin staining (red) in CHO FcγRII cells producing the indicated *L. pneumophila* GFP-Ank proteins (green) reveals that GFP-AnkX production results in disruption of the Golgi apparatus. (**C**) Amino acid positions (below) and the location of four predicted ARMDs (A1to A4) are indicated in the schematic representation of the AnkX protein. (**D**) Secretion of alkaline phosphatase (AP) by CHO FcγRII cells producing GFP or the AnkX proteins indicated was measured. The AP index represents the ratio of secreted AP to the amount of AP that remained cell-associated. Data are the average ± SD from three independent samples. Asterisks indicate the samples where the secretion of AP was significantly lower than from GFP-producing cells in an unpaired Student's *t* test.

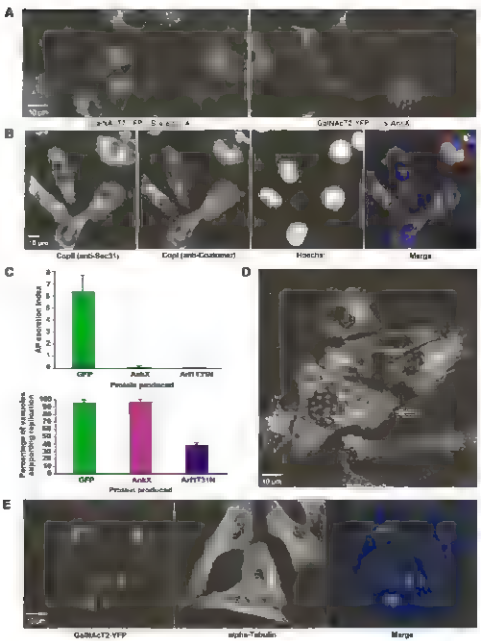

Fig. 3. AnkX interferes with minus end–directed transport of vesicles on microtubules. (**A**) GalNAc-T2-YFP localization in cells treated with BFA or injected with purified AnkX. (**B**) CopI and CopII localization in NRK cells injected with purified AnkX (asterisk) indicate that Golgi disruption does not affect the recruitment of both coat proteins to ER exit site vesicles. (**C**) CHO FcγRII cells were transfected with plasmids encoding the proteins indicated (Top) AnkX production and Arf1T31N production inhibited AP secretion to similar levels. (Bottom) AnkX production does not affect the efficiency by which *L. pneumophila* forms vacuoles that support replication in CHO FcγRII cells but production of Arf1T31N does. Data are the average ± SD from three independent samples. (**D**) Micrograph of Alexa 488–labeled transferrin in cells. The arrow indicates the location of a cell injected with AnkX. (**E**) GalNAc-T2-YFP (green) localization and microtubules (α-tubulin–specific antibody, blue) in cells microinjected with purified AnkX (asterisk).

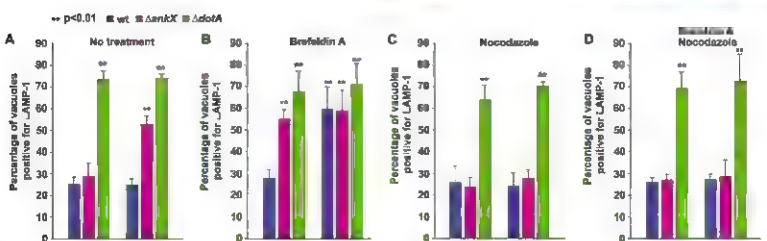

Fig. 4. AnkX prevents microtubule-dependent endocytic maturation of vacuoles containing *L. pneumophila*. (**A**) Mouse bone marrow–derived macrophages were infected with the either wild-type *L. pneumophila* (blue), the Δ*dotA* mutant (green), or the Δ*ankX* mutant (pink) for 0.5 hour or 2 hours as indicated, and the percentage of LAMP1-positive vacuoles for each was determined. Data are the average ± SD from three independent experiments where at least 50 different vacuoles in different cells were assessed. Asterisks represent data that showed significant difference from control (wild type, 0.5 hour) in an unpaired Student's *t* test. (**B** to **D**) The same assay described in (A) was conducted to examine the effects resulting from disrupting secretory transport using BFA (C), disrupting microtubules using nocodazole (C), or addition of both BFA and nocodazole (D).

Thus, multiple *C. burnetii* Ank proteins are substrates of the Dot/Icm system, and AnkF is delivered into host cells during *C. burnetii* infection.

The four translocated *L. pneumophila* Anks were fused to green fluorescent protein (GFP) and ectopically produced in mammalian cells to address whether these proteins have effector functions. Each of the four Ank proteins showed a different pattern of subcellular localization in mammalian cells, which suggested that these proteins have different targets and distinct functions (Fig. 2A). Extensive fragmentation of the Golgi apparatus was observed in cells producing GFP-AnkX, which correlated with a significant defect in the release of secreted alkaline phosphatase (AP) into the tissue culture medium (Fig. 2, B and D). GFP-AnkX deletion derivatives revealed that ARHDs and the amino-terminal region of AnkX were both required for disrupting secretory transport (Fig. 2, C and D).

Effectors translocated by the Dot/Icm system have predicted roles in blocking fusion of the *L. pneumophila*-containing vacuole with late endosomes and in promoting vacuole fusion with endoplasmic reticulum (ER)–derived vesicles (*17*). To determine whether AnkX is an effector that controls membrane transport, we further investigated the process of AnkX-mediated dispersion of the Golgi apparatus in mammalian cells by time-lapse microscopy. AnkX protein was microinjected into cells producing the resident Golgi enzyme *N*-acetylgalactosaminyltransferase 2 fused to yellow fluorescent protein (GalNAc-T2 YFP). Compared with control cells treated with brefeldin A (BFA) (movie S1), which stimulated retrograde transport of Golgi membranes and cargo back to the ER, microinjected AnkX protein resulted in dispersal of GalNAc-T2 YFP into peripheral vesicles formed during Golgi fragmentation, with no apparent delivery back to the ER (Fig. 3A and movie S2). Thus, the AnkX activity more closely mimicked fragmentation of the Golgi that occurs during mitosis (movie S2, cells marked "M"), when transport of vesicles from the ER to the Golgi is blocked.

The CopI and CopII coat proteins control initial events important for ER vesicle transport to the Golgi apparatus and colocalize on early secretory vesicles (*18*). CopI and CopII staining revealed no defects in the morphology of vesicles at ER exit sites in AnkX injected cells (Fig. 3B), which suggests that AnkX does not affect this early stage in vesicle production from the ER. Interfering with vesicle production from ER exit sites by production of the guanosine diphosphate (GDP)–locked Arf1T31N protein blocked AP secretion and reduced *L. pneumophila* replication in mammalian cells (Fig. 3C). AnkX production blocked AP secretion, but did not interfere with *L. pneumophila* replication (Fig. 3C). Thus, AnkX disrupts secretory transport after vesicles have exited the ER.

To address whether AnkX specifically prevented the transport of early secretory vesicles, we followed endocytic transport of transferrin in cells microinjected with AnkX protein (movie S3). In neighboring cells that were not injected with AnkX, fluorescently labeled transferrin was internalized and transported to perinuclear sorting compartments (Fig. 3D). In AnkX injected cells, however, transferrin remained in peripheral endosomes that enlarged over time (movie S3 and Fig 3D). The effects of AnkX resembled what occurs when cells are treated with the drug nocodazole (*19*–*21*), which depolymerizes microtubules. However, tubulin staining in cells microinjected with AnkX revealed no morphological defects in microtubules (Fig. 3E), which indicates that AnkX interfered with microtubule-dependent transport of vesicles without affecting the organization of the microtubule network.

Because microtubule-dependent transport is important for early to late endosome maturation (*19*–*21*), trafficking of wild-type *L. pneumophila* was compared with that of isogenic Δ*dotA* and Δ*ankX* mutants to determine whether AnkX was important for *L. pneumophila* evasion of endocytic maturation. The majority of vacuoles containing wild-type *L. pneumophila* evaded fusion with lysosomal-associated membrane protein (LAMP1)–positive late endosomes at 30 min and 2 hours post infection, whereas vacuoles containing the *L. pneumophila* Δ*dotA* mutant acquired LAMP1 within the first 30 min of infection (Fig. 4A). Most vacuoles containing the *L. pneumophila* Δ*ankX* mutant were LAMP1 negative at 30 min (Fig. 4A); however, there was a significant increase at 2 hours in the number of LAMP1 positive vacuoles containing the Δ*ankX* mutant. When remodeling of the *L. pneumophila*–containing vacuole by ER-derived vesicles was prevented by treating cells with BFA, there was a significant increase in the number of LAMP1 positive vacuoles containing *L. pneumophila* Δ*ankX* mutants compared with the wild type at 30 min post infection (Fig. 4B). The defect in avoiding LAMP1 acquisition for vacuoles containing the Δ*ankX* mutant was suppressed when the microtubule network was destabilized by nocodazole treatment (Fig. 4, C and D). By contrast, vacuoles containing the *L. pneumophila* Δ*dotA* mutant acquired LAMP1 rapidly in nocodazole-treated cells. Thus, microtubule depolymerization had a specific effect that restored the ability of the Δ*ankX* mutant to efficiently avoid endocytic maturation, which indicates that interfering with microtubule-dependent vesicle transport mimics a virulence activity mediated by the AnkX protein during infection.

The *L. pneumophila* and *C. burnetii* Ank proteins represent a large and diverse family of proteins containing ARHDs that we determined to be translocated into eukaryotic cells by pathogen-associated TFSSs. As seen in eukaryotic proteins, the prediction is that these bacterial proteins will have diverse cellular functions that are achieved by targeting different host factors through ARHD-dependent interactions. Finding that the *L. pneumophila* AnkX protein interferes with microtubule-dependent vesicular transport demonstrates that Ank proteins have effector functions. In addition to preventing endocytic maturation of the pathogen-occupied vacuole, AnkX interfered with transport of ER-derived vesicles generated at peripheral ER exit sites, an activity that will facilitate recruitment of early secretory vesicles to the vacuole and aid in construction of the specialized organelle that supports *L. pneumophila* replication (fig. S1).

References and Notes

1. P. J. Christie, K. Atmakuri, V. Krishnamoorthy, S. Jakubowski, E. Cascales, *Annu. Rev. Microbiol.* **59**, 451 (2005).
2. S. Backert, T. F. Meyer, *Curr. Opin. Microbiol.* **9**, 207 (2006).
3. E. A. McGrave, S. L. O'Neill, *Curr. Opin. Microbiol.* **7**, 67 (2004).
4. H. Ogata *et al.*, *Ann. N.Y. Acad. Sci.* **1063**, 26 (2005).
5. R. Seshadri *et al.*, *Proc. Natl. Acad. Sci. U.S.A.* **100**, 5455 (2003).
6. C. Cazalet *et al.*, *Nat. Genet.* **36**, 1165 (2004).
7. M. Chien *et al.*, *Science* **305**, 1966 (2004).
8. L. K. Mosser, T. J. Cammett, D. C. Desrosiers, Z. Y. Peng, *Protein Sci.* **13**, 2435 (2004).
9. J. Park, K. J. Kim, K. S. Choi, D. J. Grab, J. S. Dumler, *Cell. Microbiol.* **6**, 743 (2004).
10. C. Ivarie-Ormaetxe, G. R. Burkie, M. Riegler, S. L. O'Neill, *J. Bacteriol.* **187**, 5136 (2005).
11. T. Walker *et al.*, *BMC Biol.* **5**, 39 (2007).
12. M. Lin, A. den Dulk-Ras, P. J. Hooykaas, Y. Rikihisa, *Cell. Microbiol.* **9**, 2644 (2007).
13. Materials and methods are available as supporting material on *Science* Online.
14. H. Haga *et al.*, *Proc. Natl. Acad. Sci. U.S.A.* **102**, 826 (2005).
15. D. S. Zamboni, S. McGrath, M. Rabinovitch, C. R. Roy, *Mol. Microbiol.* **49**, 965 (2003).
16. T. Zusman, G. Yerushalmi, G. Segal, *Infect. Immun.* **71**, 3714 (2003).
17. S. Khana, C. R. Roy *Trends Microbiol.* **15**, 372 (2007).
18. S. J. Scales, R. Pepperkok, T. E. Kreis, *Cell* **90**, 1137 (1997).
19. J. S. Gaitz, A. W. Wolkoff, P. M. Novikoff, R. J. Stockert, *Proc. Natl. Acad. Sci. U.S.A.* **89**, 7026 (1992).
20. F. Ardeiza, M. Errasa, G. Griffiths, J. Gruenberg, *J. Cell Biol.* **123**, 1373 (1993).
21. O. J. Driskell, A. Mironov, V. J. Allan, P. G. Woodman, *Nat. Cell Biol.* **9**, 113 (2007).
22. Authors contribution: X.P., A.S., and M.S. performed research. A.S. conducted studies on the *C. burnetii* Anks. A.S. conducted the AnkX microinjection studies. X.P., A.S., and C.R. analyzed results and wrote the manuscript. We thank G. Warren, F. Gorelick, R. Heinzen, and J. Samuel for reagents. Supported by NIH grants AI041699 and AI064559 to C.R. AG030401 and GM060919 to A.S., and Brown-Coxe and Deutsche Forschungsgemeinschaft postdoctoral fellowships to A.S.

Supporting Online Material

www.sciencemag.org/cgi/content/full/320/5883/1651/DC1
Materials and Methods
Fig. S1
Tables S1 and S2
References
Movies S1 to S3

23 March 2008; accepted 23 May 2008
10.1126/science.1158160

Bora and the Kinase Aurora A Cooperatively Activate the Kinase Plk1 and Control Mitotic Entry

Akiko Seki,[1] Judith A. Coppinger,[2] Chang-Young Jang,[1] John R. Yates III,[2] Guowei Fang[1]*

A central question in the study of cell proliferation is, what controls cell-cycle transitions? Although the accumulation of mitotic cyclins drives the transition from the G_2 phase to the M phase in embryonic cells, the trigger for mitotic entry in somatic cells remains unknown. We report that the synergistic action of Bora and the kinase Aurora A (Aur-A) controls the G_2-M transition. Bora accumulates in the G_2 phase and promotes Aur-A–mediated activation of Polo-like kinase 1 (Plk1), leading to the activation of cyclin-dependent kinase 1 and mitotic entry. Mechanistically, Bora interacts with Plk1 and controls the accessibility of its activation loop for phosphorylation and activation by Aur-A. Thus, Bora and Aur-A control mitotic entry, which provides a mechanism for one of the most important yet ill-defined events in the cell cycle.

Entry into mitosis is controlled by the activation of cyclin-dependent kinase 1 (Cdk1), whose activity is regulated directly by mitotic cyclins and phosphatase Cdc25 (*1*) and indirectly by Polo-like kinase 1 (Plk1) and Aurora A (Aur-A) (*2*–*4*). Plk1, Cdc25, and Cdk1 form a feedback loop and positively regulate each other's activity (*1*). A fundamental question in the study of cell-cycle regulation is, what activates this feedback loop? Activation of Plk1 is probably an initiating event (*5*, *6*), because Plk1, through phosphorylation, activates Cdc25 (*5*, *7*) and downregulates Wee1 (*8*), a kinase inhibitory to Cdk1, and because Plk1 can be activated in the absence of the feedback loop (*9*, *10*).

The Plk1 activity is tightly controlled in the cell cycle (*11*). During mitosis, Plk1 is phosphorylated by an unknown kinase on a threonine residue (Thr^{210} in Plk1 and Thr^{201} in Plk1, the *Xenopus* homolog of Plk1) in its activation loop (T loop), and this phosphorylation is required for its activity (*5*, *11*–*14*). Plk1 consists of an N-terminal kinase domain and a C-terminal Polo-box domain (PBD). The PBD binds to a protein motif that contains a phosphorylated serine or threonine residue, and this binding promotes phosphorylation of the bound protein by Plk1 (*15*, *16*). The activity of Plk1 is also regulated by its own conformation, because the PBD interacts with the kinase domain and suppresses its activity when Thr^{210} is not phosphorylated in interphase cells (*14*, *17*). This inhibitory interaction is absent in mitotic Plk1 that has been phosphorylated on Thr^{210} (*17*). We report that a Plk1 interacting protein, Bora, accumulates in the G_2 phase and relieves the autoinhibition by the PBD in Plk1. Furthermore, Aur-A is a physiological Plk1 kinase, which phosphorylates Thr^{210} in the Plk1-Bora complex and activates Plk1 at the G_2-M transition.

We determined the kinetics of Plk1 accumulation and activation in HeLa S3 cells that were synchronously released from a cell-cycle arrest at the G_1-S boundary (Fig. 1) (*18*). Although Plk1 accumulated early in the G_2 phase [6 hours after release (TT6)], active Plk1 phosphorylated on Thr^{210} (Plk1 T210-P) was only detectable late in G_2 (TT9), right before mitosis, which is consistent with the measurement of the Plk1 activity (Fig. 1, A and B). Thus, accumulation of Plk1 is not sufficient for mitotic entry, and Plk1 activity is under active regulation. Active Aur-A phosphorylated on Thr^{288} was detected before Plk1 T210-P (Fig. 1A), suggesting that Aur-A may act upstream of Plk1.

To identify the trigger for the activation of Plk1 at the G_2-M transition, we focused on human genes whose transcription is increased in G_2 (*19*). We analyzed the function of these genes during mitotic entry by decreasing their expression in cells with small interfering RNAs (siRNAs) (*18*) and identified a regulator for the G_2-M transition, FLJ22624, whose *Drosophila* homolog, dBora, participates in asymmetric cell division (*20*).

Depletion of Bora in HeLa cells synchronously released from the G_1-S boundary did not affect the progression from G_1 to S and then to G_2, but delayed entry into mitosis (Fig. 2, A to C, and fig. S1), a phenotype similar to that of cells depleted of Plk1 (fig. S2) (*3*, *4*, *10*). Depletion of Bora did not affect the accumulation of cyclin B, Plk1, or Aur-A at the G_2-M transition, but delayed the activation of Cdk1 and the degradation of Wee1 (Fig. 2D). Bora appears to control the activation of Plk1, because depletion of Bora delayed the phosphorylation of Plk1 T210 and the activation of its kinase activity (Fig. 2, D and E). This effect was specific to Plk1, as depletion of Bora only marginally affected the activation of Aur-A phosphorylated on Thr^{288} (Fig. 2D).

Lack of phosphorylation on Plk1 T210 appears to be the cause of the cell-cycle delay, not a consequence of a change in the cell-cycle profile, because depletion of Bora in cells with cell-cycle profiles similar to those of control cells also resulted in lower levels of Plk1 T210-P (Fig. 2, F and G). On the other hand, ectopic expression of green fluorescent protein (GFP)–Bora increased the amounts of Plk1 T210-P, both in asynchronous cells and in prometaphase cells (fig. S3, A and B). Thus, Bora controls the activation of Plk1 and

[1]Department of Biological Sciences, Stanford University, Stanford, CA 94305–5020, USA. [2]Department of Chemical Physiology, The Scripps Research Institute, La Jolla, CA 92037, USA.

*To whom correspondence should be addressed. E-mail: gwfang@stanford.edu.

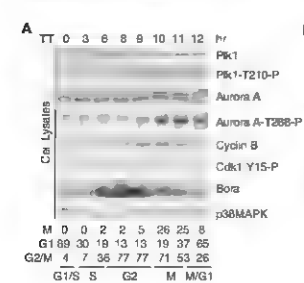

Fig. 1. Regulated activation of Plk1 at the G_2-M transition. (**A** and **B**) HeLa S3 cells were synchronized at the G_1-S boundary by a double-thymidine arrest (TT) (*18*), released into fresh media, and harvested at the indicated times (*18*). Cell-cycle stages were determined by means of fluorescence-activated cell sorting (FACS), and levels of indicated proteins were analyzed by Western blotting (**A**). Cdk1 Y15-P represents the inactive Cdk1 phosphorylated on Tyr15, and p38MAPK serves as a loading control. Plk1 was immunopurified (IP) from cell lysates and blotted for Plk1 and Bora or assayed for its kinase activity with the use of casein as a substrate (**B**).

entry into mitosis by promoting phosphorylation of Thr[210] (1).

To understand the mechanism of Bora function, we purified Bora-associated proteins from G_2 cells. Mass spectrometric analysis identified Plk1 as a major Bora-interacting protein (fig. S4A). Next, we examined Bora expression and its interaction with Plk1 in the cell cycle. Amounts of Bora peaked in G_2 (TT8 to TT9), but gradually decreased once cells entered mitosis (TT10 to TT12) (Fig. 1A) (*21*). Plk1 and Bora immunoprecipitated with each other, and the Bora-Plk1 complex peaked in G_2 (TT8 to TT9) (Fig. 1B and fig. S4B). Although Plk1 T210-P and its kinase activity peaked in mitosis (TT10 to TT11) (Fig. 1, A and B), Bora had already associated with active Plk1 T210-P in G_2 cells (TT8 to TT9) (fig. S4B). Bora interacts with Plk1 in a phosphorylation-independent manner, and recombinant Bora interacted with Plk1 and Plx1 in vitro (fig. S4, C to F).

The highly conserved sequence around Thr[210] in the Plk1 T loop fits the consensus site that is phosphorylated by Aur-A (fig. S5A) (*22*), a kinase required for mitotic entry (*2*). Aur-A directly phosphorylated Plx1 in vitro, and this phosphorylation was enhanced by Bora (Fig. 3A and fig. S5, B to E). This enhancement of Plx1 phosphorylation appears not to be the result of a general stimulation of Aur-A by Bora, as measured by the activity of Aur-A toward histone H3.

We analyzed the effect of Aur-A and Bora on Plk1 activity in vitro. Myc-Plk1 was expressed and affinity-purified from 293 cells and recombinant glutathione *S*-transferase (GST)–Plk1 from asynchronous *Sf9* cells. Although Bora alone had no effect on Plk1 activation and Aur A alone enhanced Plk1 activity to some extent, Bora and Aur-A together synergistically stimulated the Plk1 activity seven- to ninefold (Fig. 3B and fig. S5, B and F). Bora greatly stimulated the phosphorylation of the T loop in Plk1, suggesting that binding of Bora may control the accessibility of Plk1 Thr210 to Aur-A.

Aur-A– and Bora-mediated phosphorylation and activation of Plk1 are conserved evolutionarily, because inactive *Xenopus* Plx1 purified from asynchronous *Sf9* cells was efficiently phosphorylated on Thr[201] by purified Aur-A and became activated, but only in the presence of Bora (Fig. 3C and fig. S5, B, E, and G to J). However, active Plx1 that had been purified from mitotic *Sf9* cells already had Thr[201] phosphorylated, and the presence of Bora and Aur A neither enhanced Plx1 T201-P nor stimulated its kinase activity (Fig. 3D). Dephosphorylation of active Plx1 by λ-phosphatase (λPPase) allowed efficient activation of Plx1 by Bora and Aur-A.

This activation of Plx1 is mediated through phosphorylation of Plx1 Thr201, because Bora and Aur-A failed to stimulate the kinase activity of the Plx1-T201D mutant, even after its dephosphorylation (Fig. 3E). Consistent with this, Bora did not enhance the phosphorylation of the Plx1 T201D protein by Aur A (Fig. 3F), indicating that the enhancement in the wild-type Plx1 resulted from specific phosphorylation on Thr[201] (compare Fig. 3F with Fig. 3A).

To understand the structural basis of the Bora-mediated activation of Plk1, we analyzed interactions between Plk1 and Bora. Both the Plk1 kinase domain (amino acids 13 to 345) (Plk1 K) and the PBD domain (amino acids 352 to 603) (Plk1 PBD) directly associated with Bora (fig. S4, F to I). The PBD interacted with both the N- and C-terminal domains of Bora, and the association between the PBD and Bora was phosphorylation-independent. Consistent with this, the phosphopeptide-binding site in the PBD is not required for the activation of Plx1 by Bora and Aur-A (fig. S5K).

We analyzed the effect of Bora and Aur-A on the kinase domain of Plk1 (Myc Plk1 K). Myc-Plk1-K was phosphorylated on Thr[210] by Aur-A, independent of Bora (Fig. 3G). This was con-

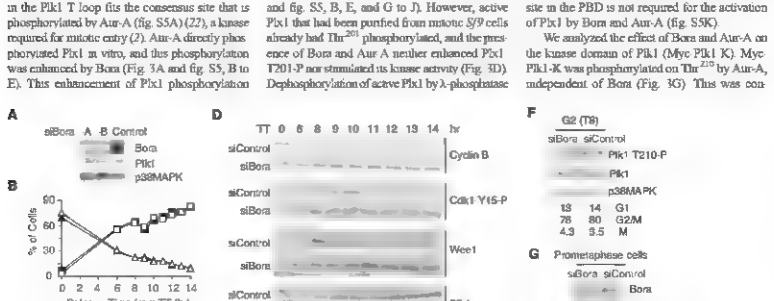

Fig. 2. Control of mitotic entry by Bora. (**A**) HeLa cells were control-transfected or transfected with two siRNAs against Bora (siBora-A and -B). Depletion efficiency was determined by Western blotting. (**B** to **E**) HeLa cells were synchronized to the G_1-S boundary by a double-thymidine treatment and transfected with siRNAs during the second thymidine arrest (*18*). Cells were released and Taxol was added at 9 hours after release to prevent mitotic exit. The cell-cycle profile was analyzed by FACS ((**B**) and (**C**)) and by Western blotting (**D**). Plk1 was immunopurified and assayed for its kinase activity (**E**). Solid symbols, siControl; open symbols, siBora-A, triangles, G_1 phase; squares, G2 phase and M phase; and circles, M phase. (**F** and **G**) HeLa cells were transfected, synchronized by a single-thymidine arrest, and harvested at 8 hours after release (T8) (**F**), or were synchronized by a thymidine-nocodazole arrest and harvested as prometaphase cells (**G**). The cell-cycle profile was determined by FACS, and the indicated proteins were assayed by Western blotting. Partial synchronization in (**F**) enriched G_2 cells and generated cells of similar cell-cycle profile between siControl and siBora.

sistent with the fact that, in the absence of the PBD, Thr^{210} is solvent-accessible in the Plk1 K atomic structure (*23*). Thus, Bora apparently controls the accessibility of Thr^{210} in the full length Plk1, in which the PBD interacts with and inhibits the kinase domain (*17*). Bora still contributed to the activation of Myc-Plk1 K to some extent (Fig. 3G), probably through its direct interaction with Plk1 K. Therefore, Bora regulates the activation of Plk1 through both T210-P–dependent and -independent mechanisms.

To analyze the role of Aur-A in the activation of Plk1 in vivo, we depleted Aur-A in cells synchronously progressing through the cell cycle (Fig. 4, A and B). Depletion of Aur-A prevented phosphorylation of Plk1 T210 and delayed mitotic entry (Fig. 4, A and B, and fig. S6), even though both Plk1 and Bora were expressed in depleted cells. On the other hand, ectopic expression of Aur-A stimulated Plk1 T210-P, and this effect was dependent on the Aur-A activity and the presence of Bora (Fig. 4C and fig. S3C). Similarly, ectopic expression of Bora also promoted Plk1 T210-P in G_2 cells in an Aur-A–dependent manner (Fig. 4D). We conclude that Aur-A appears to control the activation of Plk1 through phosphorylation of Thr^{210} in vivo.

dBora and *Drosophila* Aur-A (dAur-A) have been characterized to act in a genetic pathway required for asymmetric division of sensory cells (*20*). Although it has been reported that dBora interacts with dAur-A when both proteins are overexpressed in culture cells (*20*), human Bora did not coimmunoprecipitate with Aur-A when they were expressed at their physiological levels (fig. S4B). We find that Plk1 binds to Bora and is the target of regulation by Bora in mammalian cells (Fig. 1 and fig. S4). When Plx1 and histone H3 were incubated together, Bora specifically stimulated Aur A–mediated phosphorylation of Plx1-T201, not of histone H3 or Plx1 T201D (Fig. 3 and fig. S5). Furthermore, depletion of Bora in vivo reduced the activity of Plk1 not Aur-A (Fig. 2, D, E, and G). These observations point to a difference in function of Bora in human versus *Drosophila* cells.

Phosphorylation of Plk1 T210 and Plx1 T201 is required for mitotic entry (*6*, *24*). Although a *Xenopus* Plx1 kinase, xPlk1, phosphorylates and activates Plx1 in vitro (*24*), xPlk1 acts downstream of Plx1 and is not the trigger for mitotic entry (*6*, *26*). We found that Bora and Aur-A function cooperatively to activate Plk1 for mitotic entry (Fig. 4E). The accessibility to Thr^{210} in its unphosphorylated state is blocked by the PBD in interphase cells (*17*). Induction of Bora in G_2 and its subsequent binding to Plk1 increases the accessibility of Plk1 T210, which overrides the autoinhibition by the PBD and promotes the phosphorylation of Plk1 T210 by Aur-A. Active Plk1 then initiates the Plk1-Cdc25-Cdk1 positive feedback loop for mitotic entry. Consistent with Aur-A and Plk1 acting upstream of Cdk1, inhibition of Cdk1 did not affect or only weakly reduced the activating phosphorylation of Aur-A and Plk1 in G_2 and in mitosis (fig. S7). On the other hand, activation of Plk1 and Aur-A mutually depend on each other in both G_2 and mitosis (Fig. 4B and figs. S2C and S7), indicating that these two kinases form a positive feedback loop for mitotic entry. Our discovery of the Aur-A– and Bora-mediated activation of Plk1 is part of this loop (Fig. 4E).

In mitosis, active Plk1 with Thr^{210}-P binds to its substrates that have been phosphorylated on a PBD-recognition motif, and this binding further activates Plk1 (*15*). We found that a phosphorylated PBD-recognition peptide (P peptide) (*15*) only enhanced the kinase activity of active Plx1 T201-P, but not inactive Plx1 T201 (fig. S8, A to F). Furthermore, incubation of active Plx1, first with P peptide and then with Bora, prevented the enhancement of the Plx1 activity by P peptide (fig. S8, G and H). Thus, Bora competes against P peptide in the regulation of Plk1.

Bora appears to have a dual role in regulating Plk1 activity in the cell cycle. In G_2, Bora acts as

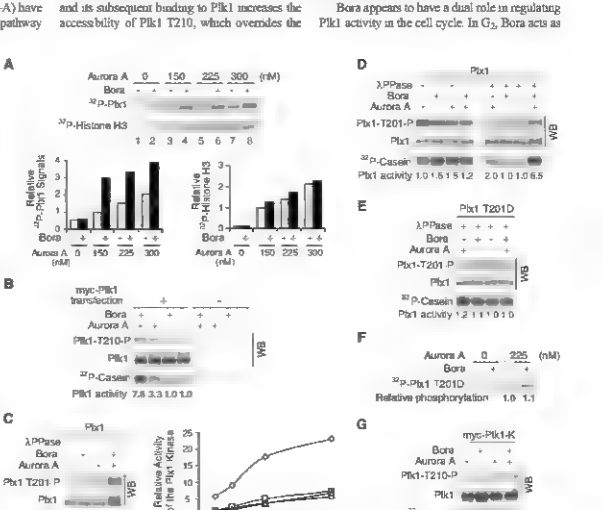

Fig. 3. Activation of Plx1 by Bora and Aur-A. (**A**) Plx1 and histone H3 were mixed together and then incubated with Aur-A, maltose-binding protein (MBP)–Bora/MBP, and radioactive adenosine triphosphate for 60 min (*18*). ^{32}P incorporation into Plx1 and histone H3 was plotted after being normalized to their respective samples in lane 3 (**B** and **G**) Myc-Plk1 and Myc-Plk1-K were expressed in 293 cells, immunopurified, and incubated with or without recombinant Aur-A and MBP-Bora/MBP (*18*). Myc-Plk1/Myc-Plk1-K beads were then washed to remove Aur-A and analyzed by Western blotting (WB) or assayed for the Plk1 activity, with casein as a substrate. (**C** to **E**) Recombinant Plx1 and Plx1 T201D were sequentially incubated with or without λPPase, with EGTA (to stop the λPPase reaction), and then with or without recombinant Aur-A and MBP-Bora/MBP. Plx1/Plx1 T201D were then analyzed by Western blotting or immunopurified to assay for the Plk1 activity (*18*). Plx1 (inactive) (C) and Plx1 T201D (E) were purified from asynchronous *Sf9* cells, whereas active Plx1 (D) was purified from okadaic-acid–treated mitotic *Sf9* cells (*7*). In a separate experiment in (C), the kinetics of the Plx1 activity were analyzed and plotted after normalizing all the samples to that of –Bora/–Aur-A at the 15-min time point. Diamonds, +Bora/+Aur-A; squares, –Bora/+Aur-A; circles, +Bora/–Aur-A; triangles, –Bora/–Aur-A. (**F**) Phosphorylation of recombinant Plx1-T201D by Aur-A, as described in (A).

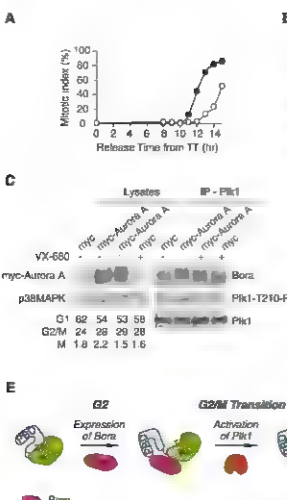

Fig. 4. Control of activation of Plk1 by Aur-A. (**A** and **B**) HeLa cells were synchronized at the G_1-S boundary by a double-thymidine treatment and transfected with siControl (solid symbols) or siAur-A (open symbols) during the second thymidine arrest. Cells were released and Taxol was added at 9 hours after release. The cell-cycle profile was determined by FACS (A) and by Western blotting (B). (**C** and **D**) HeLa cells were transfected with Myc-Aur-A/Myc (C) or with GFP-Bora/GFP (D) and synchronized by a single-thymidine treatment. At 7 (D) or 8.5 (C) hours after release, cells were treated with 1 μM VX-680, a small molecule inhibitor of Aur-A, and harvested 1 hour later. The cell-cycle profile was determined by FACS, and the indicated proteins were analyzed by Western blotting of either total cell lysates or Plk1 immunoprecipitates (IP). (**E**) A summary of the regulation of Plk1 by Bora and Aur-A in the cell cycle.

an activator to allow access of Plk1 Thr^{210} by Aur A. In mitosis, Bora, through direct binding to Plk1, interferes with the further activation of Plk1 by phosphorylated substrates. This inhibitory effect of Bora is relieved by its mitotic destruction mediated through a ubiquitin-proteasome pathway ubiquitin ligase in a Plk1-dependent manner (*21*). Thus, Bora activates Plk1 at the G_2-M transition, and active Plk1 then phosphorylates Bora and promotes its degradation in mitosis (Fig. 4E) (*21*). Phosphorylation of mitotic Plk1 on Thr^{210} appears to be maintained by Aur-A, primarily through a Bora-independent mechanism (Fig. 2G and fig. S7A), because active Plk1 is no longer in an autoinhibitory conformation in mitosis (*17*). In summary, the identification of the Aur-A–Bora-Plk1 regulatory circuit in mammalian cells elucidates a key mechanism in cell-cycle regulation.

References and Notes

1. A. W. Murray, *Cell* **116**, 221 (2004).
2. T. Hirota *et al.*, *Cell* **114**, 585 (2003).
3. P. Lénart *et al.*, *Curr. Biol.* **17**, 304 (2007).
4. D. W. Hansen, A. V. Lokker, K. H. Ban, P. K. Jackson, *Mol. Biol. Cell* **15**, 5623 (2004).
5. Y. W. Qian, E. Erikson, J. L. Maller, *Mol. Cell. Biol.* **19**, 8625 (1999).
6. J. Lin, J. L. Maller, *Oncogene* **24**, 238 (2005).
7. A. Kumagai, W. G. Dunphy, *Science* **273**, 1377 (1996).
8. N. Watanabe *et al.*, *Proc. Natl. Acad. Sci. U.S.A.* **101**, 4419 (2004).
9. X. Liu, S. Yan, T. Zhou, Y. Terada, R. L. Erikson, *Oncogene* **23**, 763 (2004).
10. Y. W. Qian, E. Erikson, P. E. Taieb, J. L. Maller, *Mol. Biol. Cell* **12**, 1791 (2001).
11. F. A. Barr, H. H. Sillje, E. A. Nigg, *Nat. Rev. Mol. Cell Biol.* **5**, 429 (2004).
12. O. Kelm, M. Wind, W. D. Lehmann, E. A. Nigg, *J. Biol. Chem.* **277**, 25247 (2002).
13. Y. J. Jang, S. Ma, Y. Terada, R. L. Erikson, *J. Biol. Chem.* **277**, 44115 (2002).
14. K. S. Lee, R. L. Erikson, *Mol. Cell. Biol.* **17**, 3408 (1997).
15. A. E. Elia *et al.*, *Cell* **115**, 83 (2003).
16. A. E. Elia, L. C. Cantley, M. B. Yaffe, *Science* **299**, 1228 (2003).
17. Y. J. Jang, C. Y. Lin, S. Ma, R. L. Erikson, *Proc. Natl. Acad. Sci. U.S.A.* **99**, 1984 (2002).
18. Materials and methods are available as supporting material on *Science* Online.
19. M. L. Whitfield *et al.*, *Mol. Biol. Cell* **13**, 1977 (2002).
20. A. Hutterer *et al.*, *Dev. Cell* **11**, 147 (2006).
21. A. Seki *et al.*, *J. Cell Biol.* **181**, 65 (2008).
22. S. Ferrari *et al.*, *Biochem. J.* **390**, 293 (2005).
23. M. Kothe *et al.*, *Biochemistry* **46**, 5960 (2007).
24. M. A. van Vugt, R. H. Medema, *Oncogene* **24**, 2844 (2005).
25. Y. W. Qian, E. Erikson, J. L. Maller, *Science* **282**, 1701 (1998).
26. E. Erikson, T. A. Haystead, Y. W. Qian, J. L. Maller, *J. Biol. Chem.* **279**, 32219 (2004).
27. We thank J. Maller (University of Colorado) for baculoviruses expressing Plk1 and its mutants; M. Cyert (Stanford University) for comments on the manuscript; H. Do for technical assistance; and members of the Fang lab for discussions. This work was supported by a Burroughs Wellcome Career Award in Biomedical Research (G.F.) and grants from NIH (GM062852 to G.F. and H(079842 and RR11823-10 to J.Y.).

Supporting Online Material

www.sciencemag.org/cgi/content/full/320/5883/1655/DC1
Materials and Methods
Figs. S1 to S8
References

6 March 2008; accepted 21 May 2008
10.1126/science.1157425

New Products Focus: Gene Expression

PCR Plates

The twin.tec real-time polymerase chain reaction (PCR) plates offer researchers the ability to significantly improve real time PCR data. The plates feature titanium oxide, which gives the reaction chambers a bright white, opaque color. This material results in up to a 10-fold increase in reflection of fluorescence, providing better data for applications such as low volume quantitative PCR. White wells also significantly reduce interfering background fluorescence and lead to increased homogeneity of replicates and reproducible results.

Eppendorf North America
For information 800-645-3050
www.eppendorfna.com

Cell-Based Assays

The xCELLigence system provides dynamic, real-time cell-based assays without the use of labels. The assays provide valuable data that traditional end-point analysis can't, leading to faster assay development and improved attrition rates. The assays offer several throughput options, from 16 to 576 (6 x 96) wells run simultaneously.

Roche Applied Science
For information 800-262-4911
www.roche.com

Whole Genome Amplification

The BioHelix Rapisome primase based Whole Genome Amplification (pWGA) system makes use of a primase to synthesize primers onsite, generating multiple initiation sites for random, whole genome amplification. Unlike conventional WGA products, the Rapisome pWGA Kit takes advantage of a natural cellular system to deliver faster, isothermal DNA amplification without the need for heat denaturation and synthetic primers. The kit's advantages include a one-step process, high efficiency in amplifying circular DNA, and speed—the reaction can be completed in an hour.

BioHelix
For information 866-800-5458
www.biohelix.com

Cells for Cloning

The Clean Genome *E. coli* and competent cells are suitable for most cloning applications. They offer superior genomic stability because of the removal of all mobile insertion sequence elements. The Clean Genome *E. coli* is the only insertion sequence–free *E. coli* strain available. The absence of mobile elements eliminates the danger of undesirable insertion sequence transposition into your clone and reduces the mutation rate of the strain itself. The competent cells increase success in cloning difficult or "unclonable" genes by eliminating cloning artifacts due to insertion-sequence transposition and minimizing plasmid rearrangement.

Scarab Genomics
For information 608-257-1624
www.scarabgenomics.com

Portable Gel Documentation System

The CSL MicroDoc is an ultracompact, portable gel documentation system that incorporates an eight inch screen and a 1 GB flash card. The system produces high quality images because of its integral 16-bit charge coupled device camera, which provides resolution to 8.0 megapixels. The system can be used either completely independent of a computer or connected to and controlled by a computer via a USB connection. Images can be captured from agarose or other fluorescent gels, colorimetric gels, autoradiography film, and blotting membranes. The system includes a 55-mm ethidium bromide filter with a built-in safety switch so the ultraviolet transilluminator is turned off when the door is open. Files can be saved in a variety of formats.

Cleaver Scientific, Ltd.
For information +44 (0) 1788-565 300
www.cleaverscientific.com

Angiogenesis Assays

The most established tests used to analyze new blood vessel formation in vitro are the "tube formation" and the "sprouting" assays. In both, the formation of new blood vessels is simulated on a gel matrix. The µ Slide Angiogenesis is a new carrier for angiogenesis assays with a "well-in-a-well" structure that drastically reduces the amount of matrix material needed and solves the classic meniscus problems. The miniaturized system of the inner well requires only 10 µl of matrix. The unique geometry of the slide places the cells that need to be imaged in the same focal plane, which strongly improves the imaging quality of the assays.

Integrated BioDiagnostics (ibidi)
For information +49-(0)89-52 38-80-30
www.ibidi.com

Virus Purification Kits

New Fast Trap Virus Purification and Concentration Kits include one for adenovirus purification and one for lentivirus purification. Purifying viruses after propagation in host cells is a critical step toward using the viruses as vectors for genetic modification of target cells. The kit contains all the components to accommodate the entire virus purification workflow. The Fast Trap kits provide more reliable, faster results than traditional methods because they incorporate Millipore's Steriflip filter unit, an easy-to-use format featuring a new anion exchange membrane that binds and elutes viruses. The vacuum-based, closed-system purification kits are quick, easy, and safe to operate with a turnaround time of less than two hours, compared with two days with traditional purification techniques.

Millipore
For information 800-548-7853
www.millipore.com

Electronically submit your new product description or product literature information! Go to **www.sciencemag.org/products/newproducts.dtl** for more information.

Newly offered instrumentation, apparatus, and laboratory materials of interest to researchers in all disciplines in academic, industrial, and governmental organizations are featured in this space. Emphasis is given to purpose, chief characteristics, and availability of products and materials. Endorsement by *Science* or AAAS of any products or materials mentioned is not implied. Additional information may be obtained from the manufacturer or supplier.

POSITIONS OPEN

TWO POSTDOCTORAL POSITIONS
Available in Enzymology and Molecular and Structural Biology of Coagulation Proteins
UCLA/Orthopaedic Hospital
Department of Orthopaedic Surgery

We are seeking two Postdoctoral Fellows to contribute to studies on molecular biology, enzymology, and structural biology of the tissue factor initiated blood coagulation. Applicants should have a recent Ph.D awardees who are highly motivated and energetic. In addition to participating in the existing research Program, the candidates will be strongly encouraged to develop complementary research objectives that lead to independent funding. Applicants should have strong enzymology, molecular, and structural biology background or willingness to learn these techniques rapidly. The stipend provided for each position will be commensurate with the candidate's education and experience.

Send cover letter, curriculum vitae including bibliography, and names of three references to:

S. Paul Bajaj, Ph.D.
University of California at Los Angeles
22-53 Rehab, Mail Code 179522
Los Angeles, CA 90095
E-mail: pbajaj@mednet.ucla.edu

Wenzhou Medical College, a rapid up-rising comprehensive health university located in China's most dynamic economic area, Wenzhou, Zhejiang, is looking for several leading scientists in biomedical sciences at the rank of **ASSISTANT, ASSOCIATE, or FULL PROFESSOR** in the newly established Institute of Genome Medicine. Applicants should have a doctoral degree in sciences and demonstrated excellent record in integration of basic and translational research. Expertise in genetics, epigenetics, biostatistics, pathogenesis, bioinformatics, and/or molecular biology will be a plus. The College will provide an excellent startup package and state-of-the-art research facility. Salary will be highly competitive, commensurate with experience. The College also offers a comprehensive fringe benefit package including medical care and retirement, plus housing benefits. Interested applicants please send full resume, copies of academic credentials, a publication list, and/or abstracts of selected published papers to **Ms. Wang Xiangmei (e-mail: wxm@wmu.net)** and **Dr. Sun Zhong sheng (e-mail: zssunss@yahoo.com).**

POSTDOCTORAL POSITIONS
Howard Hughes Medical Institute

My laboratory seeks to understand, on the molecular level, the mechanism of translation and translation control by cryo-electron microscopy of functional ribosome complexes, both in bacteria and eukaryotes. Several Postdoctoral positions (both Howard Hughes Medical Institute and NIH are available. Background should be in one of the following areas: ribosome biochemistry, RNA, computer modeling, or image processing. The new electron microscopy (EM) facility at Columbia Medical Center will comprise FEI F30 (Polara) and F20 instruments. In addition, access is available to the EM facilities of the New York Structural Biology Center.

Please send curriculum vitae and the names of three references to **Tomubarn Barnce (e-mail: tb2319@columbia.edu; fax: 212 305 9500).**

HHMI offers excellent salaries and benefits. HHMI is an Equal Opportunity Employer

---

POSTDOCTORAL FELLOWSHIPS (duration of two to three years) available in the laboratory of **Professor J. Lindsay Whitton,** Department of Immunology and Microbial Science, the Scripps Research Institute, La Jolla, California, United States. Projects will focus on the regulation of T cell responses to virus infection, and on coxsackievirus pathogenesis and immunology. Applicants should send detailed curriculum vitae, with names of three referees, to **e-mail: lwhitton@scripps.edu.** To receive acknowledgement of application delivery, ensure that the e-mail subject line is: Whitton PD Fellowship 2008

CONTINUED ON PAGE

EMINENT SCHOLAR POSITION
ASSOCIATE PROFESSOR/PROFESSOR
Department of Pharmacology, Physiology, and Toxicology
Marshall University Joan C. Edwards School of Medicine

Applications are invited for an Eminent Scholar at the Associate Professor or Professor level for a tenure-track faculty position in the Department of Pharmacology, Physiology, and Toxicology at the Marshall University Joan C. Edwards School of Medicine in Huntington, West Virginia. Applicants should have an active, nationally funded research program in an area complementary to current department research activities. Currently, faculty members in the Department are conducting research in the areas of cardiovascular disease, endocrine disorders, cancer, neuroscience, and toxicology. Eminent Scholars is a West Virginia state-funded program to recruit productive senior faculty to the state's two Research Universities. The position comes with a competitive salary and a substantial startup package. Applicants should send curriculum vitae, statement of research interests and funding sources, and the names and contact information for at least three references to: **Dr. Todd L. Green, Chair of the Search Committee, Department of Pharmacology, Physiology and Toxicology, Joan C. Edwards School of Medicine, Marshall University, One John Marshall Drive, Huntington, WV 25755,** or via e-mail: green@marshall.edu, or fax: **304-696-7391.** Applications will be accepted until the position is filled. *Marshall University is an Equal Opportunity Affirmative Action Employer. Women and minorities are strongly encouraged to apply.*

BAYLOR COLLEGE of MEDICINE
Department of Molecular and Cellular Biology
POSTDOCTORAL POSITIONS are immediately available in our internationally known research group, which is focused toward understanding the molecular, cellular, and physiological principles of nuclear receptor signaling in normal target cells and endocrine cancers. Successful applicants will utilize state-of-the-art technologies (i.e. established mouse models, lentiviral-mediated gene transfer microarray, and proteomics) to address important questions concerning nuclear receptor and coregulator function in normal physiological processes and disease states, such as breast and endometrial cancer. Applicants with a strong background in molecular biology and in using animal systems are encouraged to apply. Salaries will be at the upper competitive end of the national norm. Applicants should have received their Ph.D and/or M.D within the past one to two years and, if necessary, *be eligible for an appropriate U.S. visa.*

Current curriculum vitae, a brief statement describing prior research and future research goals, and three letters of recommendation (all required before interview, should be sent to: **Dr. John F. Lydon, Department of Molecular and Cellular Biology, Baylor College of Medicine, One Baylor Plaza, Houston, TX 77030-3498; fax: 713 798 2970;** or e-mail: **jlydon@bcm.tmc.edu.**

ENVIRONMENTAL SCIENTIST
Conduct environment inspections and soil and groundwater sampling. Compile and analyze derived data. Support operation of remediation system. Write risk assessments, prepare reports, and manage database. Required: B.S. in environmental engineering or environmental science, or foreign equivalent. Forty hours/week. Job/interview site: Irvine, California. Fax curriculum vitae to **GeoTrans, Incorporated, Human Resources, fax: 240-864-8008.**

Stiftung Mercator

Mercator
Research Group

RUHR-UNIVERSITÄT BOCHUM

Stiftung Mercator is one of Germany's leading foundations. It aims to [illegible] international opportunities in schools [illegible] and [illegible] Mercator [illegible] combine [illegible] open-mindedness and tolerance through intercultural encounters, encouraging the [illegible] knowledge of culture. The foundation provides a platform for new ideas to enable people – regardless of their national, cultural or social background – [illegible] and make the most of the opportunities available [illegible] approach to its work.

[illegible] with the Ruhr area, the home of its founding [illegible]

Ruhr University Bochum invites applications for the positions of three Young Professors (W2) to constitute a Mercator Research Group on the "Structure of Memory"

Understanding the mechanisms underlying memory is perhaps the greatest challenge facing modern neuroscientists. Fostering excellence in research, Stiftung Mercator (www.stiftung-mercator.de) intends to establish a novel research group on the topic of semantic and episodic memory that integrates the areas of neuroscience, cognitive psychology, medicine, neurobiology and philosophy.

Animal brain imaging, coupled with innovative animal models of learning, and electrophysiology will be integrated with philosophy of mind to attain a new understanding of the structures, mechanisms and theory of memory – an approach that extends beyond the traditional borders of the neurosciences. These young professors will spearhead this initiative and form an independent research group supplied with state-of-the-art infrastructure and funds. They will be accompanied by a senior scientific researcher (one per year), of their choosing, who through his/her extensive experience can act as a mentor and adviser for the independent research of the young professors.

Professorship 1
The Functional Architecture of Memory
The main focus of this research unit will be the analysis of the functional organisation and interaction mechanisms of structures relevant for semantic and episodic like memory formation in the brains of lower mammals. The development of innovative animal models at the behavioural level that can be combined with experiments in high resolution in vivo brain imaging analysis of memory processing will comprise a key element of the research strategy.

Professorship 2
The Neurobiology of Memory
This research unit will integrate electrophysiological approaches up to the single cell level with brain imaging strategies to address the neurobiological basis of memory. Comparative analysis through brain imaging in lower mammals and/or primates can be part of this goal. Investigations of the role of synaptic plasticity and network plasticity in semantic and episodic like memory formation and the investigation of affected structures using animal brain imaging in vivo will comprise a key component of research.

Professorship 3
The Theory of Memory
This research unit will have its origins in the area of the philosophy of mind. Its goal will be to develop an integrative theory of experience-dependent cognitive processes. The unit will work theoretically but will have strong interdisciplinary relations in the area of neuroscience, particularly in the area of human brain imaging. It will work closely with the young professors within the "Structure of Memory" programme but also with further neuroscientists on campus.

The research programme will be supported with funding of ca. 7 million Euro over a six year period. A newly acquired 7 Tesla magnetic resonance spectroscope for in vivo animal analysis will be provided for the research work of these projects. An on-site 1.5 Tesla brain imaging unit for primate or human studies will also be available on campus. Extensive facilities for animal electrophysiology as well as all further aspects of neuroscience are well established at Ruhr University. The research groups will be based at the Center for Synergic Neurosciences of Ruhr University Bochum. Further details can be viewed at www.ruhr.de/cnn, or by contacting Prof. Onur Güntürkün, Prof. Denise Manahan-Vaughan or Prof. Albert Newen at Ruhr University Bochum.

The Mercator Young Professorships will be appointed at the W2 Professor level for an initial period of six years (starting date early 2009). The professorships are particularly targeted at young neuroscientists at an early stage of their careers, but who have reached a qualification profile that enables research independence. Successful candidates will be integrated into the transdisciplinary neuroscience landscape of Ruhr University. For the two empirical young professors proven track records in the area of innovative neuroscience research is required. The candidates for the position in the philosophy of mind should have a proven track record of relevant interdisciplinary papers in peer-reviewed journals.

Ruhr-Universität Bochum [illegible] is one of Germany's leading research universities. The University draws its scholarly strengths from both the diversity [illegible] and the [illegible] of a single coherent campus: the Life Sciences, the Arts and Sciences, Engineering, the Social Sciences and the Humanities. The highly dynamic setting enables national and international students and researchers to work closely together in studying, teaching and research, and across traditional boundaries. [illegible] and demographic [illegible] with [illegible] students and 4,700 staff, the University is a vital institution [illegible] and [illegible] in [illegible] Athens, Metropolis Ruhr.

Ruhr University Bochum is committed to equal opportunity in employment and gender equality in its working environment. To increase equal gender distribution in all job categories and at all levels, we strongly encourage applications from qualified women. Female applicants will be given preferential consideration when their level of qualification, competence and professional achievements equals that of male candidates, unless arguments based on the personal background of a male co-applicant prevail. Applications from appropriately qualified handicapped persons are also encouraged.

Applications, including a curriculum vitae, a list of publications, a statement of research interests, and a research concept, must be sent electronically by 15th September 2008 to: Prof. Dr. Elmar W. Weiler, Rector of Ruhr-University Bochum, re: Mercator Research Group "Structure of Memory", Ruhr-Universität Bochum, D – 44780 Bochum, e-mail: rektor@ruhr.de. Potential candidates will be invited to participate in a scientific colloquium 30th October – 2nd November 2008. Further information can be found at www.ruhr.de/rmg.

NIDDK NATIONAL INSTITUTE OF DIABETES AND DIGESTIVE AND KIDNEY DISEASES

New Research Initiative – Fatty Liver Disease & Obesity - Tenure Track Position

The Liver Diseases Branch of the National Institute of Diabetes and Digestive and Kidney Diseases (NIDDK), National Institutes of Health (NIH) invites applications for one tenure track position from scientists interested in basic and/or clinical research involving non-alcoholic fatty liver disease and metabolic syndrome. Specific areas of research interest include pathogenesis and mechanism of metabolic derangement in non-alcoholic fatty liver disease and its pathophysiologic link to inflammation, insulin resistance, metabolic syndrome and obesity. Priority will be given to applicants at the Assistant Professor level in traditional universities or those finishing their post-doctoral fellowship positions. The applicant must have a proven record of accomplishments and will be expected to propose and pursue an independent research program in one of these fields. The position offers unparalleled opportunities for interdisciplinary collaboration within NIDDK and throughout NIH.

The Liver Diseases Branch of NIDDK is located on the main intramural campus of the NIH in Bethesda, Maryland, a suburb of Washington, D.C.

Interested applicants should send a Curriculum Vitae and list of publications, copies of three major publications, a summary of research accomplishments, a plan for future research, and two letters of recommendation (preferred but not required) to **Ms. Michelle Whitley, Search Committee, Liver Diseases Branch, NIDDK, Building 10-9B16, NIH, Bethesda, MD, 20892-1800. Application deadline: September 15, 2008**

fectious Diseases • Dengue Fever • Hepatitis C • Ecoli • Plague • Immunolo
ncer • Research • Malaria • STDs • Chlamydia • HIV/AIDS • Smallpox • Airbo
rgy • Infection • Immune • Cancer • Cells • Vaccine • Toxic
st • Bacteria • Virus • Genetics • Medicine • Drug
n • Science • Molecular • STDs • Antibiotics

NIAID

NATIONAL INSTITUTE OF ALLERGY AND INFECTIOUS DISEASES

ANNOUNCING THE NIAID INDEPENDENT SCHOLARS PROGRAM

Offering early career opportunities for creative, independent research at the National Institutes of Health

The National Institute of Allergy and Infectious Diseases (NIAID), a component of the National Institutes of Health (NIH), created the NIAID Independent Scholars Program to help exceptional young Ph.D.s establish cutting-edge, independent research programs within the mentoring framework of an NIAID laboratory.

The program aims to develop recent Ph.D.s into the next generation of leaders in immunology and infectious disease research. Unlike conventional postdoctoral programs, the NIAID Independent Scholars Program offers a direct and immediate path to independence.

PROGRAM BENEFITS

Scholars accepted to the program will have the opportunity to:

- Develop an independent research program within an NIAID laboratory with salary and research support directly from the Office of the NIAID Scientific Director.
- Focus on highly creative, cutting-edge research.
- Receive mentoring from senior colleagues in all aspects of leading an independent research group.
- Access the outstanding research resources and facilities at NIH.
- Acquire the skills necessary to compete for tenure-track positions.

ELIGIBILITY

Applicants to the NIAID Independent Scholars Program should have completed or be near completion of a Ph.D. thesis. Applicants with significant postdoctoral experience will not be considered.

DEADLINE: September [illegible]

The NIAID Independent Scholars Program is seeking the best of the best.
For instructions on how to apply, visit the Scholars Program Web site at
[illegible]

Department of Health and Human Services
National Institutes of Health
National Institute of Allergy and Infectious Diseases
Proud to be Equal Opportunity Employers

MICHIGAN STATE UNIVERSITY

CHAIRPERSON, DEPARTMENT OF HORTICULTURE

Position. The Michigan State University College of Agriculture and Natural Resources invites applications for Chairperson of the Department of Horticulture. The full-time, annual appointment position is open to candidates who meet the requirement for tenure at the rank of full professor in the Department of Horticulture.

Department: The Department of Horticulture is a flagship unit in a top-ranked College of Agriculture and Natural Resources that is highly supportive of the plant sciences. Areas of research, extension, and teaching include plant breeding, genetics and biotechnology, developmental and environmental physiology, production systems for fruit, vegetable, floriculture and ornamental crops including integrated crop management, sustainable, and organic systems, marketing, post-harvest handling and physiology, value-added natural products, landscape design, management and environmental stewardship, and international agriculture. The department has excellent laboratory, growth chamber, greenhouse, garden, and on- and off-campus farm facilities.

Responsibilities: The chairperson of Horticulture serves as the chief administrative officer, and provides leadership in teaching, research, extension, outreach, and international activities. The successful candidate must possess vision for long-range planning and leadership, advance departmental missions, and promote national and international prominence. The chair must communicate effectively with faculty, students, staff, and administration; promote professional development; foster diversity; serve as an advocate for the department; maintain effective liaisons with external clientele and facilitate external funding.

Qualifications: Applicants must have an earned doctorate in plant sciences or related fields and a national/international reputation for excellence in teaching, research, extension, outreach, or international activities in their discipline. Applicants must possess a vision for the future of horticultural disciplines, demonstrated leadership ability, and strong interpersonal, communication, and administrative skills.

Salary: Competitive and commensurate with professional experience.

Application Procedure: Please submit a cover letter, statement of administrative philosophy and vision for the future, curriculum vitae, and contact information for five references to: **Dr. Rebecca Grumet, Search Committee Chair, Dept. Horticulture, Michigan State Univ., East Lansing, MI 48824, grumet@msu.edu, Tel: 517-355-5191 x 1431; Fax: 517-353-0890**. Applications will be accepted until August 15, 2008, or a suitable candidate is selected. Additional information and the complete position announcement, may be obtained from: **http://www.hrt.msu.edu** and **http://www.msu.edu/chairsearch.htm**, or by contacting **Ms. Lorri Busick, busick@msu.edu, Tel: 517-355-5191 x 1363, Fax: 517-355-0749.**

MSU is committed to achieving excellence through cultural diversity. The University actively encourages applications and/or nominations of women, persons of color, veterans and persons with disabilities.

MSU IS AN AFFIRMATIVE ACTION, EQUAL OPPORTUNITY EMPLOYER

Bioinformatics Scientist in Taiwan

The Institute of Plant and Microbial Biology, Academia Sinica, Taipei, Taiwan enthusiastically invites applications for the position of a non-tenure tracked Assistant/Associate Research Specialist position in Bioinformatics. We are looking for a highly motivated bioinformatics scientist who will be responsible for providing bioinformatics expertise in the areas of data mining, data integration, and bioinformatics training. PhD in biochemistry/molecular biology/biotechnology/bioinformatics, with 2+ years of bioinformatics experience is required. Knowledge of the up-to-date bioinformatics tools and databases for sequence and structural analysis is required. Familiarity with languages like PERL, OGI, HTML and mySQL is also needed. Experience in statistical analysis and expression data analysis is a plus. For details of the Institute and Academia Sinica, please visit the website at **http://apmb.sinica.edu.tw/**. The application folder should include curriculum vitae and a working plan. The application folder and at least three letters of recommendation should be sent to Dr. Shih-Long Tu, Institute of Plant and Microbial Biology, Academia Sinica, 128 Sec. 2, Academia Rd, Nankang, Taipei, Taiwan 11529, FAX: (886)2 2782-7954, e-mail: **tsl@gate.sinica.edu.tw**. The review of applications will start on Aug. 15, 2008.

THE UNIVERSITY OF HONG KONG

in collaboration with

OCEAN PARK CONSERVATION FOUNDATION HONG KONG

Founded in 1911, The University of Hong Kong is committed to the highest international standards of excellence in teaching and research, and has been at the international forefront of academic scholarship for many years. Of a number of recent indicators of the University's performance, one is its ranking at 18 among the top 200 universities in the world by the UK's *Times Higher Education Supplement*. The University has a comprehensive range of study programmes and research disciplines, with 20,000 undergraduate and postgraduate students from 90 countries, and a complement of 1,900 academic members of staff, many of whom are internationally renowned.

Building on Hong Kong's international status and its mission to serve China, the University offers an intellectually-stimulating and culturally-rich academic environment, with attractive remuneration packages.

Tenure-Track Associate Professor/Assistant Professor
In Aquatic Mammal Ecology and Conservation
(Ref.: RF-2007/2008-599)

Applications are invited for appointment as Associate Professor/Assistant Professor in The Swire Institute of Marine Science, Faculty of Science from July 1, 2008 or as soon as possible thereafter, on a three-year fixed term contract, with consideration for tenure after satisfactory completion of a second three-year contract.

Applicants should possess a Ph.D. degree with a strong background and publication record in the field of aquatic mammal ecology and conservation. The appointee is expected to develop a vigorous and independent research program and have a commitment to excellence in undergraduate and graduate teaching. A track record of publications in international journals is essential. Research start-up funds will be available.

The appointee will be based at The Swire Institute of Marine Science, information about which can be found at http://www.hku.hk/swma/index.htm. He/She will also act as a Research Advisor to Ocean Park Conservation Foundation Hong Kong and contribute to their research, conservation and education programmes. Details about Ocean Park Conservation Foundation Hong Kong can be found at http://www.opcf.org.hk/eng/index.asp.

A highly competitive salary commensurate with qualifications and experience will be offered. The appointment will attract a contract-end gratuity and University contributions to a retirement benefits scheme, totaling up to 15% of basic salary, as well as leave, and medical/dental benefits. Housing benefits will be provided as applicable.

For enquiries of the existing research activities and the specific job requirements, please write to Dr. Gray A. Williams, Honorary Director (e-mail: hrshwga@hkucc.hku.hk). **Further particulars and application forms** (CV and names/tel) can be obtained at: https://www.hkuhr.applicant.cc or from: The Appointments Unit (Senior), Human Resource Section, Registry, The University of Hong Kong, Hong Kong (fax: (852) 2540 6735 or 2559 2058, e-mail: senrapp@hkucc.hku.hk). **Closes August 28, 2008**. Candidates who are not contacted within 4 months of the closing date may consider their applications unsuccessful.

The University is an equal opportunity employer and is committed to a No-Smoking Policy.

SWISS VACCINE RESEARCH INSTITUTE

The Swiss Vaccine Research Institute is seeking qualified applicants for Group Leader (Assistant Professor) positions in vaccine research. The ideal candidate is less than 40 years of age with previous postdoctoral experience. The successful applicants are expected to develop a junior research group and an independent research program. The research program is funded by the Swiss Vaccine Research Institute for up to four years.

The Swiss Vaccine Research Institute encourages applications from female and minority scientists.

For consideration a candidate must send a statement of research interests, curriculum vitae including e-mail address, list of publications, and three letters of recommendation to: **elena.nicod@chuv.ch** or mail complete application package to:

Search Committee
c/o Elena Nicod
Swiss Vaccine Research Institute
Centre Hospitalier Universitaire Vaudois
Division of Immunology and Allergy
Rue du Bugnon 46, 1011 Lausanne
Switzerland
www.swissvaccineresearch.ch

The Novo Nordisk Foundation

Center for Protein Research

The Novo Nordisk Foundation Center for Protein Research, located in central Copenhagen, is currently being established at the Faculty of Health Sciences, University of Copenhagen, to promote basic and applied discovery research on human proteins of medical relevance. The establishment of the center announced in April 2007 has been made possible by a donation of 125 million USD from the Novo Nordisk Foundation, **www.novonordiskfonden.dk**. The center, which operates as a charitable organization, has already secured world-class capabilities in protein expression and purification, proteomics and protein related systems biology. Our goal is to establish the center as the leader in protein focused research, and thus we are now seeking exceptionally talented and innovative scientists to further strengthen our team.

The center – **covering 4,500 m² and opening early in 2009** – will have research programs in the areas of disease systems biology, proteomics, high throughput protein production, chemical biology, protein focused disease biology and protein therapeutics. The center will also contribute to translational research within medicine and provide fundamental insights for drug discovery and development.

For additional information and details, see **www.cpr.ku.dk**

Research Directors and Group Leaders

We are now seeking excellent scientists to further strengthen our research capabilities – internationally renowned and established as well as promising younger scientists. Successful candidates will establish research groups carrying out independent research of highest scientific impact and standard as well as work with us on integrated projects. Currently, the center management team consists of Dr. Michael Sundström (Managing Director), Professor Matthias Mann (Research Director, Proteomics) and Professor Soren Brunak (Research Director, Disease Systems Biology).

The successful candidates should have an excellent track record, international reputation and documented abilities. We will prioritize applicants who have protein focused experience in relation to human health and disease – such as signaling pathways, metabolism, protein degradation and aggregation as well as analysis of post-translational modifications. Our goal is to establish a highly integrated research environment, thus collaborative interest is essential. In addition, your vision on how the unique environment and resources at the center will benefit your research projects will be of particular interest to us. Successful candidates will be offered generous start-up packages and competitive salaries.

Are you interested in becoming a Research Director or Group Leader at the center? Please send a letter of interest, including a brief CV/biography as well as a summary of planned future research to michael.sundstrom@cpr.ku.dk preferably before Sept 1st 2008.

COLUMBIA UNIVERSITY

College of Physicians and Surgeons

Columbia University seeks to hire a Chairperson for the Department of Biochemistry and Molecular Biophysics. The successful applicant will have demonstrated a commitment to creative research, made scholarly contributions in a field within the basic or biomedical sciences, and have an interest in leading a group of highly accomplished investigators. New areas of scientific investigation and innovative pedagogical approaches are encouraged.

The Department consists of 17 full-time faculty members whose primary research spans the range of biochemistry, molecular biophysics, developmental biology, neurobiology, structural biology, and molecular biophysics. The Department maintains interactive and collaborative research programs among its members and with investigators in other Departments in the basic biomedical and clinical sciences at the Columbia University Medical Center and in other Departments on the Arts and Sciences Campus of Columbia University.

The Department is responsible for teaching courses in the graduate program and for teaching aspects of biochemistry and molecular biophysics in the medical curriculum. All members of the Department maintain independently funded research programs.

Interested persons should send their CV's and statements of interest to **Dr Andrew R. Marks, Chair, Biochemistry and Molecular Biophysics Search Committee, Box 22, 630 West 168th Street, New York, NY 10032.** Additional information is available at **http://biochemistry.hs.columbia.edu.**

Columbia University is an Equal Opportunity/ Affirmative Action Employer

GRADUATE PROGRAM

International Max Planck Research School

PhD Program in
Structure and Function of Biological Membranes

Max Planck Institute of Biophysics
Max Planck Institute of Brain Research
Goethe University

Frankfurt am Main, Germany

Several PhD fellowships are available in the International Max Planck Research School in Frankfurt. The two Max Planck institutes and research groups at Frankfurt University offer a unique environment for the study of biological membranes and membrane proteins. PhD opportunities exist in internationally leading laboratories in the areas of membrane protein structure determination, membrane biochemistry, molecular biology, and functional studies by electrophysiological and spectroscopic methods, computational biophysics and structural bioinformatics, as well as studies of whole membranes, cells and organelles.

Highly qualified candidates with degrees in biochemistry, chemistry, physics, biology, medicine or related subjects are invited to apply for the next round of admission in November 2008. Application forms can be downloaded from the website of the Research School at www.mpibp-frankfurt.mpg.de/research-school. Completed application forms and two letters of reference should arrive no later than **31 July 2008.**

For further details please contact:

Dr. Janet Vonck
MPI of Biophysics
Max-von-Laue-Str. 3
D-60438 Frankfurt am Main
Germany
Tel. +49+69-6303-3004/3001
Fax: +49+69-6303-3002
E-mail: Research.School@mpibp-frankfurt.mpg.de

INVESTIGATOR, CUTANEOUS BIOLOGY

Department of Dermatology

The Department of Dermatology at Weill Cornell Medical College is recruiting for an investigator in cutaneous biology at the Assistant or Associate Professor level. We are seeking outstanding candidates working at the intersection of immunology and cancer biology with relevance to the skin. A successful candidate will be highly motivated and will have a strong independent research program or demonstrate the potential to develop and maintain a strong and independent research program. Applicants must hold an appropriate doctoral degree (M.D., Ph.D. or M.D./Ph.D.).

The Department of Dermatology has strong ongoing research programs in immunology, neuroimmunology, cancer biology and tissue repair. Weill Cornell Medical College is located adjacent to Rockefeller University and Memorial Sloan-Kettering Cancer Institute. These three institutions have world renowned programs in immunology, molecular biology, cancer biology, pharmacology, as well as many other areas of research offering extremely rich opportunities for collaboration.

Applicants should submit a copy of their curriculum vitae and a letter describing their academic interests to:

Richard D. Granstein, M.D.
Department of Dermatology
WEILL CORNELL MEDICAL COLLEGE
1305 York Avenue, 9th Floor
New York, NY 10021
Email to rdgranst@med.cornell.edu

EOE/AA/E/V

www.med.cornell.edu/jobs

Faculty Positions at
National Institute of Science Education and Research (NISER)
Bhubaneswar, India

The National Institute of Science Education and Research (NISER) has been set up at Bhubaneswar by the Department of Atomic Energy of the Government of India to be a unique institution of its kind pursuing undergraduate and post-graduate education in science combined with frontline research. NISER is being set up in a sprawling 300 acre campus about 3 km from Khurda Road Railway Station on the outskirts of Bhubaneswar overlooking Barunei Hills. It will be a fully residential campus with modern living amenities including children's school and health centre. Presently NISER operates from the campus of Institute of Physics at Bhubaneswar.

NISER invites applications from extremely motivated Indian scientists with a high-profile research agenda and a flair for teaching (especially at the undergraduate level) for faculty positions at various levels in Biology, Chemistry, Mathematics and Physics. For details visit the website **http://niser.iopb.res.in/careers**. The applications containing CV, list of publications, statement of purpose and research programme and a list of at least three referees may be sent by e-mail to **careers@niser.iopb.res.in**, marking "Faculty in (branch)" in the subject field (branch being one of the disciplines mentioned above). There is no time limit for sending the application but the applications received will be taken up for consideration at regular intervals. Candidates are advised to request the Referees to send their letters of recommendations directly to NISER at the above e-mail address.

Marie-Curie Doctoral and Post-doctoral Fellowships in Enzyme Engineering

UNIVERSITY OF CAMBRIDGE

One pre- and one post-doctoral position is available from 1 September 2008 at MedImmune's Cambridge (UK) site to work on enzyme engineering and protease-based therapeutics. This will exploit the expertise of MedImmune in ribosome and phage display, as well as high-throughput screening to evolve *in vitro* and characterise pharmacologically engineered proteases to specific protein targets of high therapeutic interest. The work will be carried out in the Technology group at MedImmune UK headed by Dr. Lutz Jermutus. The project will be collaborative with Dr. Florian Hollfelder at Cambridge University and is embedded in a European Research Training Network on Directed Evolution of Functional Proteins (ENEFP) that provides a special training programme in protein engineering methods involving novel display methods. Further information can be obtained at www.bio.cam.ac.uk/enefp

Post-doctoral applicants should have a Ph.D. in biochemistry or related areas and a strong research record. Pre-doctoral applicants should have a first class degree. Specific skills in preparing and handling large libraries for directed evolution including molecular modelling, enzymology, protein selection techniques (such as colony screening, display methods, protein-protein interaction studies) and familiarity with molecular biology techniques are advantageous.

Please see http://ec.europa.eu/research/marie-curie-actions/ for application criteria. Applications should contain a CV, full list of publications and the names and addresses of two referees submitted online quoting reference 127 at: www.medimmunecambridge.com/home/careers_@_cat

MedImmune is an Equal Opportunities Employer. We seek to empower each individual, and respect the diverse cultures, perspectives, skills and experiences within our workplace

MedImmune

Deputy Director – Science
Advanced Light Source, LBNL

LBNL is a world leader in science and engineering research, with 11 Nobel Prize recipients over the past 75 years, and 59 present members of the National Academy of Sciences. LBNL conducts unclassified research across a wide range of scientific disciplines, and is host to four national user facilities. Learn more at http://www.lbl.gov/.

The Advanced Light Source (ALS) at Lawrence Berkeley National Laboratory (LBNL) is seeking a Deputy Director – Science. As a member of ALS senior management, the Deputy Director will support the ALS Director in formulating and implementing scientific policy; in interactions with the scientific community in overseeing synchrotron user issues, and in joint management of scientific groups. The Deputy Director will have responsibility for identifying new scientific opportunities and overseeing review processes, and will play a leading role in strategic planning. Additionally, the Deputy Director will work to assure that the facility supports the best science consistent with available resources, acts as the scientific representative of the ALS, and play a key role in the future of photon science at LBNL.

The ALS is a national user facility and one of the world's brightest sources of ultraviolet and soft x-ray beams. To learn more about the ALS, visit **http://www-als.lbl.gov/**

Qualifications:

- Ph.D. and a record of outstanding scientific contributions
- International reputation for leadership in a scientific field associated with synchrotron-related research
- Experience with broad scientific programs
- Demonstrated capability for evaluating scientific proposals and identifying resources to compete research projects
- Demonstrated skills in management of a diverse group or organization in a research context
- Demonstrated ability to effectively interact with technical and administrative staff, funding agencies, university faculty, and students

Please apply at **http://jobs.lbl.gov/** and enter **21867** in the search field.

LBNL is an AA/EEO employer committed to the development of a safe and diverse workforce.

Applicants are invited for a **tenure track faculty position at the assistant or associate professor level in the Department of Pharmaceutical Sciences, College of Pharmacy**, Western University of Health Sciences. Rank and salary will commensurate with qualifications and experience.

Candidates must possess a Ph.D. in Pharmacology or a closely related field with postdoctoral training. The successful candidate will be expected to establish an independent research program leading to extramural funding. Research focus may be in any pharmacology related area. In addition to research, candidates must be highly motivated to excel in teaching in the professional pharmacy (Pharm.D.) program, with the ability to teach antimicrobial pharmacology, as well as other pharmacology related topics. The College of Pharmacy provides competitive salary and startup funds. Applicants must possess strong communication skills (written and spoken).

The review of applications will begin immediately and continue until the position is filled. To be considered for this position, applicants should submit (1) a letter of intent, (2) curriculum vitae, (3) teaching and research statement, and (4) arrange to have three letters of reference sent (email preferred) to: **Dr. Kabir Lutfy, Chair of Search Committee. Department of Pharmaceutical Sciences, College of Pharmacy, Western University of Health Sciences, 309 East Second Street, Pomona, CA 91766** (email: **klutfy@westernu.edu**).

Western University **http://www.westernu.edu/** is a vibrant and growing graduate health professions university with programs in Allied Health, Graduate Nursing, Osteopathic Medicine, Pharmacy and Veterinary Medicine. New programs in Dentistry, Optometry, Podiatry, and Graduate College of Biomedical Sciences will be added by fall 2009. The University's core values promote the discipline of learning and the art of caring in an environment that supports excellence in its faculty, staff and students.

Western University of Health Sciences is an Equal Opportunity Affirmative Action Employer and actively seeks applications from women and minorities

---

The Faculty of Science of the University of Fribourg/Switzerland (Adolphe Merkle Institute)

invites applications for a

Full Professor in Polymer Chemistry

The selected candidate must have an outstanding record of successful independent research in synthetic macromolecular or biomacromolecular chemistry and a well-documented strong interest in materials development and materials applications. She/He is expected to develop an internationally recognized research program in the field of polymer and hybrid (nano)materials and should furthermore contribute, in English, to the teaching program of the Faculty at Master and Graduate School level, preferably in a new specialized Master program on Materials and Nanoscience. The chair belongs to the newly founded Adolphe Merkle Institute (AMI), an interdisciplinary institute devoted to pure and applied nanoscience that offers outstanding facilities and competitive start-up funds. Collaboration in research and teaching is expected within the Institute and with other groups at the Faculty.

More information about the position, the application procedure (deadline **31.08.2008**) as well as the Adolphe Merkle Institute are available at **www.unifr.ch/science/positions**

SCHOOL OF MEDICINE

INDIANA UNIVERSITY

FACULTY POSITIONS

The Herman B. Wells Center for Pediatric Research and the Department of Pediatrics, Indiana University School of Medicine (IUSM), are seeking applications for several tenure track/tenured faculty positions at the Assistant/Associate Professor level positions in the area of diabetes research. This search begins a vigorous commitment to expand upon and develop a world-class pediatric basic diabetes research program within the Wells Center, and is supported in part by a major gift from the Eli Lilly and Company Foundation. There are currently thirty-two principal investigators in the Wells Center, and NIH funded areas include: reproductive and neuro-endocrinology, developmental pulmonary physiology, immunology, cardiovascular developmental biology, fetal and neonatal metabolic physiology, hematopoiesis, stem cell biology, myeloid biology and gene regulation, gene therapy, and DNA repair. Transgenic and gene targeting facilities and a mass spectrometry core facility are available on-site. The Wells Center occupies 65,000 sq. ft. of research space and will continue to expand in the forthcoming years.

Candidates with research interests in any area of diabetes, including islet biology or development, stem cell biology, insulin action, or diabetic complications are invited to apply. Successful applicants are expected to develop a strong, independent extramurally funded research program and participate in training students and fellows and engage in research interactions with the clinical diabetes program. Highly competitive salary, startup funds, and space will be provided. Applicants must have a PhD and/or MD degree (or equivalent degrees), post-doctoral research experience, and clear evidence of research productivity. The search committee will begin considering applications immediately and on an on-going basis until positions are filled. Applicants should submit a curriculum vitae, summary of past accomplishments and future plans, and names and email addresses of three references electronically to inlem@iupui.edu, or by mail to: **Raghu G. Mirmira, MD, PhD, c/o Shari Upchurch, Wells Center for Pediatric Research, Indiana University School of Medicine, 635 Barnhill Drive Room 2031, Indianapolis, IN 46202. Fax: 317-278-8944.**

Indiana University is an EEO/AA Employer M/F/D

Vice-Chair for Research/Open Rank

The Department of Anesthesiology, University of Texas Health Science Center at San Antonio, Texas (UTHSCSA) invites nominations and applications for the position of Vice-Chair for Research (VCR). As the chief research officer for the department, the VCR is responsible for implementation of the research vision, the overall management of departmental research activities, and the administration of sponsored research. The VCR will engage in multidisciplinary collaboration within UTHSCSA—a Clinical and Translational Science Award (CTSA) grantee—and its affiliated institutions.

Qualifications for this position include an M.D., M.D.-Ph.D., or Ph.D. degree in an appropriate field of study. The successful candidate will have a national/international reputation as a distinguished scientist with an outstanding record of research accomplishments, a proven track record of directing a research enterprise, outstanding communication skills as evidenced by an ability to mentor junior faculty, scientists, residents, and students. The candidate must be a critical and strategic thinker and a visionary leader who can develop and enhance the research enterprise, and one who can demonstrate expertise in crafting interdisciplinary proposals and negotiating multi-faceted awards. One or more currently funded NIH grant(s) and experience in translational research is highly desirable. Given the excellent research infrastructure in neurobiology at UTHSCSA, research experience in pain medicine would be a plus.

For more information, please visit our website at **www.anesthesia.uthscsa.com**. To apply or nominate a candidate for the position of Vice-Chair for Research, Department of Anesthesiology, U.T. Health Science Center at San Antonio, please submit a current CV, supporting documents, and names and addresses of five references to: **J. Jeffrey Andrews, M.D., Chair, Department of Anesthesiology – MSC 7838, U.T. Health Science Center at San Antonio, 7703 Floyd Curl Drive, San Antonio, TX 78229.**

All faculty appointments are designated as security sensitive positions. The University of Texas Health Science Center at San Antonio is an Equal Employment Opportunity/Affirmative Action Employer.

UNIL Université de Lausanne | live knowledge

THE FACULTY OF BIOLOGY AND MEDICINE OF THE UNIVERSITY OF LAUSANNE INVITES APPLICATIONS FOR THE POSITION OF

ASSISTANT (TENURE TRACK) OR ASSOCIATE PROFESSOR IN PLANT EVOLUTION

All areas of plant evolution will be considered and research programs taking an experimental approach are particularly welcome.

The position will be in the Department of Ecology and Evolution (http://www.unil.ch/dee) which has a long track record of excellence in research.
A generous start-up package and state-of-the-art research infrastructure will be available within an environment which favors collaborations.

The successful candidate is expected to develop an internationally recognized research program funded by external sources. Teaching duties include an undergraduate class in botany.
The appointee will supervise Masters and PhD students and participate to other training activities of the Department (http://www.unil.ch/bec & http://www.unil.ch/ee).
The job description is available on the Web at the address www.unil.ch/fbm/page2295_fr.html. For further information, contact ian.sanders@unil.ch or jerome.goudet@unil.ch.

Applications, including a curriculum vitae with a complete list of publications in which the five most significant are identified, a brief statement of research program and teaching philosophy, and the names of three referees, should be sent by August 22nd, 2008 to Prof. Patrick Francioli, Dean of the Faculty of Biology and Medicine, University of Lausanne, Rue du Bugnon 21, CH-1005 Lausanne, Switzerland.

The University of Lausanne wishes to promote the access of women to academic careers and encourages applications from women

EXECUTIVE DIRECTOR for UNESCO REGIONAL CENTRE FOR BIOTECHNOLOGY TRAINING & EDUCATION

Department of Biotechnology, Ministry of Science & Technology Government of India is in quest of a vibrant leader to spearhead establishment and manage thereafter the UNESCO Regional Centre for Biotechnology Training & Education, an autonomous institution and a part of Interdisciplinary Life Sciences Cluster located in Faridabad (40 minutes drive from New Delhi) in the National Capital Region. The position offers a unique opportunity to provide strong and visionary leadership to the new centre

The picturesque location of the Centre will be in the academic and research ambience of a Life Science cluster including the Translational Health Science Technology Institute (in collaboration with MIT, USA) the National Institute of Immunology, Technology Platforms a Vaccine Development Centre, a Molecular Diagnostics Centre, and Animal Research Facilities. The UNESCO Centre will provide opportunities for seamless co-operation with the other centres of the cluster and renowned institutions like All India Institute of Medical Sciences, Indian Institute of Technology, International Centre for Genetic Engineering & Biotechnology National Brain Research Centre

The Centre's mission is to provide world class interdisciplinary education and training in Life Sciences and to carry out research programmes of global quality with M.Sc., Ph. D, MD Ph. D courses in gap areas in the region e.g. Biomedical Engineering Nano Biotechnology Synthetic Biology; Molecular Cell Biology; Molecular Breeding, Genomics, Drug Discovery; Clinical Pharmacology and Pharmacogenomics

The activities of this Centre will be governed and monitored through a Board of Governors with participation of stakeholders The National Institute of Immunology will provide administrative support for the initial period and lab space for the selected candidate in the interim phase

Professional Requirements

Qualifications

- Ph.D, MD or equivalent degree and excellent track record with peer reviewed publications
- Global network of scientific contacts in the field of biotechnology
- Ability to command respect of the academic and the user communities across the domain of biological sciences through personal achievements in research and standing in the field

Experience

- Competences in managing research groups and interdisciplinary projects in areas of science, engineering, biomedical research.
- Demonstrated ability to translate scientific results into innovative applied technologies and new ventures;
- Networking with global institutions, industries and governmental agencies.

Skills

- A creative personality with strong leadership and managerial skills with efficiency and probity
- Effective cross talks with cluster partners,
- Expert communication skills to develop strong links with academic world
- Capacity for lateral thinking for finding new approaches to multidisciplinary research, education & training for value addition to the Centre's programmes.

Compensation

Salary, allowances and other perks will be same as that applicable to the highest executive level in the Government of India

Applications should include curriculum vitae, incorporating research experience and a write-up of your plans and vision how to develop the regional centre for training, education & research

Application should be sent to Mr S Sinha, Adviser, Medical Biotechnology Division-II, Department of Biotechnology, Ministry of Science & Technology, Block No 2, 8th Floor, CGO Complex, Lodhi Road, New Delhi – 110003, India or e-mail at: urc dbt@gmail.com, Telefax. 91-11-24363760; Fax: 91-11-24362884. The closing date is 18th August 2008

Note Additional information about the Centre, its structure, facilities and programmes etc is available at http://www.dbtindia.nic.in

Kuwait University

KUWAIT UNIVERSITY
FACULTY OF PHARMACY
KUWAIT

The Department of **Pharmaceutics** at the Faculty of Pharmacy in Kuwait University invites applications for appointment at the ranks of Associate and Full Professor, starting September 2008, in the following areas:

- Biopharmaceutics
- Pharmacokinetics
- Physical Pharmacy

The appointee will be expected to teach at both undergraduate and graduate levels, and to establish an active collaborative research program within the Health Sciences Faculties. Rank will be commensurate with experience and qualifications. Appointment is subject to contract.

Required Qualifications

- Ph.D. Degree in Pharmacy from a reputable University.
- The applicant's GPA in first university degree should be at least 3 out of 4 (or equivalent).
- Research experience and publications in refereed international journals.
- University teaching experience in Pharmaceutics, especially in Biopharmaceutics, Pharmacokinetics, and Physical Pharmacy.
- Full command of teaching in English.

Benefits include attractive tax-free salary according to rank and teaching experience (Professor's monthly salary varies from KD 2950 to 3192, Associate Prof.'s salary varies from KD 2265 to 2507 – KD 1 = $3.4 = £1.8), annual air tickets for the faculty member and his/her family (spouse and up to three children under the age of 20), a one time settling-in allowance, housing allowance, free national health medical care, 60 days paid summer vacation and two weeks mid-term holiday, and end-of-contract gratuity. The University also offers excellent academic environment and financial support for research projects.

To apply send by express mail/courier service or e-mail, within **two weeks** of the date of announcement, a completed application form, updated curriculum vitae (including mailing address, phone and fax numbers, e-mail address, academic qualifications, teaching and research experience, and a list of publications in professional journals), three copies of Ph.D., Master, and Bachelor certificates and transcripts, a copy of the passport, and e-mail addresses of three referees to:

Dr. Aly Nada
Chairman, Department of Pharmaceutics
Faculty of Pharmacy, Health Sciences Centre,
Kuwait University
P.O. Box 24923, Safat 13110, Kuwait
E-mail: alynada@hsc.edu.kw
Tel. (+965) 5312300 Ex. 6136
Fax. (+965) 5342807

In the pursuit of the ideals of excellence and diversity, the University of Pretoria wishes to invite applications for the following vacancies.

Application forms are available on the Internet at http://www.up.ac.za/personnel/employment/jobform.html

The University of Pretoria's commitment to quality makes us the top research university in South Africa and gives us a competitive advantage in international science and technology development.

FACULTY OF NATURAL AND AGRICULTURAL SCIENCES
DEPARTMENT OF PHYSICS

PROFESSOR/ASSOCIATE PROFESSOR/SENIOR LECTURER/LECTURER IN THEORETICAL AND IN EXPERIMENTAL PHYSICS

Several positions on different levels are available.

Minimum requirements: Lecturer: •An MSc in Physics •Sufficient experience to contribute significantly to the research outputs of the Department •Ability to teach a variety of courses in English. **Senior Lecturer:** •A PhD in Physics or allied field •Ability to teach a variety of courses in English •Proven standing as a researcher through scientific publications •Ability to supervise postgraduate students. **Associate Professor/Professor:** In addition to the requirements specified for a Senior Lecturer, the following are essential: •Proven record as an established teacher and researcher with significant scientific recognition •International scientific and scholarly recognition.

Recommended requirements: •A thorough knowledge of and experience in one of the research directions of the Department •Specialisation in theoretical physics and/or computational physics and/or nonlinear optics and/or particle-acoustic interactions and/or astrophysics and/or biophysics and/or solid state physics and/or nuclear physics and/or reactor physics and/or nanotechnology will be a strong recommendation.

Interested candidates should forward a full CV together with a list of publications, a list of postgraduate students and a brief description of current research interests as well as the names of three people who will supply, upon request, letters of recommendation, to Prof J.B. Malherbe, Department of Physics, University of Pretoria, Pretoria 0002, South Africa by **25 July 2008**.

For further information, contact Prof J.B. Malherbe, +27 (0) 12 420-2806 or e-mail: malherbe@scientia.up.ac.za

CLOSING DATE: 25 July 2008

The University of Pretoria is committed to equality, employment equity and diversity.

The University of Pretoria reserves the right not to make an appointment to the posts as advertised.

100 1908 2008

UNIVERSITEIT VAN PRETORIA
UNIVERSITY OF PRETORIA
YUNIBESITHI YA PRETORIA

http://www.up.ac.za/personnel/employment/jobform.html

CONFERENCE

2ND EUCHEMS CHEMISTRY CONGRESS

2008 SEPTEMBER 16 - 20
TORINO, ITALY

CHEMISTRY: THE GLOBAL SCIENCE

SCIENTIFIC COMMITTEE
Chair **Hartmut MICHEL** (DE)
Co-chair **Igor TKATCHENKO** (FR)

ORGANISING COMMITTEE
Chair **Giovanni NATILE** (IT)
Co-chair **Francesco DE ANGELIS** ( )

LOCAL ORGANISING COMMITTEE
Chair **Lorenza OPERTI** (IT)
Co-chair **Salvatore COLUCCIA** (IT)

PLENARY LECTURES BY
Peter AGRE (Baltimore, USA)
Avelino CORMA (Valencia, SP)
Jean M.J. FRÉCHET (Berkeley, USA)
Robert H. GRUBBS (Pasadena, USA)
Kyriacos C. NICOLAOU (La Jolla, USA)
Martyn POLIAKOFF (Nottingham, UK)
K. Barry SHARPLESS (La Jolla, USA)

KEYNOTE LECTURES BY
Varinder AGGARWAL (Bristol, UK)
Lucia BANCI (Florence, IT)
Xinhe BAO (Dalian P.R., CN)
Matthias BELLER (Rostock, DE)
Richard CATLOW (London, UK)
Ken CAULTON (Bloomington, USA)
Fritz FRIMMEL (Karlsruhe, DE)
Dante GATTESCHI (Florence, IT)
Jana HAJSLOVA (Prague, CZ)
Dino MORAS (Illkirch, FR)
Ulrich STIMMING (Munich, DE)
Philip TAYLOR (Geel, BE)
Marcel WUBBOLTS (Geleen, NL)
Jun-ichi YOSHIDA (Kyoto, JP)

www.euchems-torino2008.it

ORGANISING SECRETARIAT

Premi RAMON MARGALEF d'ecologia

The Autonomous Government of Catalonia (Spain) launches the 2008 edition of the €100,000 International Ramon Margalef Prize in Ecology

THE PRIZE

- The main objective is the recognition of a scientific career or a discovery in ecology which has significantly contributed to scientific knowledge.
- It is awarded to living individuals, to legal entities or to groups from all over the world.
- The prize is worth €100,000.

NOMINATIONS

- Nominations can be submitted by qualified representatives of universities, higher institutions of learning, research centres, winners of the Prize in previous years or former members of the Jury until June 30.
- They should be submitted through a letter or statement of well reasoned justification, accompanied by a curriculum vitae of the candidate.
- The nominations should be addressed to the Technical Secretariat of the Prize, Presidency Office of the Autonomous Government of Catalonia (Generalitat de Catalunya).

Generalitat de Catalunya

For detailed information please refer to:
www.gencat.cat/premiramonmargalef

POSITIONS OPEN

The U.S. Department of Energy, Office of Science, Office of Biological and Environmental Research (BER) is seeking a **DIRECTOR** for the Life and Medical Sciences Division. BER leads basic research supporting the energy and environmental missions of the Department of Energy. The Life and Medical Sciences Division supports research in genomics, proteomics, structural biology, plant biology, microbiology, radiation biology, radiochemistry, and development of advanced imaging instrumentation. The Division also supports the state-of-the-art Joint Genome Institute's Production Genomics Facility for high throughput DNA sequencing and genomic analysis of environmental microbes and plants. The Director leads a group of 16 program managers and support staff with a budget of over $250 million. The Director is also responsible for the Genomes to Life: Bioenergy Research Centers which are playing a leadership role in scientific innovation for sustainable bioenergy. The Director is involved in strategic planning, multiyear program planning and implementation, and budgeting. The Director is a member of the Senior Executive Service, with a salary range of $114,468 to $158,500. For further information about this position and the instructions on how to apply and submit an application, please go to website: **http://jobsearch.usajobs.gov/getjob.asp?JobID=72095978&AVSDM=2008%2D05%2D23+06%3A52%3A04&Logo=0&lid=456&FedEmp=N&sort=rv&vw=b&brd=3876&ss=0&jbf565=1&FedPub=Y&caller=/ses.asp&SUBMIT1.x=488&SUBMIT1.y=18**. It is imperative that you follow the instructions as stated on the announcement SES-SC-HQ-022 (cg). To be considered for this position, you must apply online and submit a copy of your college transcripts to meet the positive education requirement. This announcement closes on July 22, 2008.

POSTDOCTORAL FELLOWSHIP

A Postdoctoral Fellow position is immediately available in the Department of Pharmaceutical Sciences at Wayne State University to study toxicity and disposition of nanoparticles following pulmonary exposure. Strong skills in areas of cell and molecular immunology, surface chemistry, or particle engineering are desired.

Candidates are asked to submit an electronic application including curriculum vitae, letter of interest, and full contact information for three references through website: **http://jobs.wayne.edu** under this position posting at Department H1822-Pharmaceutical Sciences. Review of applications will begin on July 11, 2008, and continue until the position is filled. Direct inquiries to **Dr. Joshua Reineke at e-mail: reineke@wayne.edu.**

The Department of Pharmaceutical Sciences, website: **http://cphs.wayne.edu/psc.html,** is part of Wayne State University, a premiere institution offering 350 academic programs through 14 colleges to 34,000 students. *Wayne State is an Equal Opportunity Employer.*

POSTDOCTORAL POSITION to study molecular and cellular mechanisms of angiogenesis, with particular emphasis on neovascular eye diseases such as diabetic retinopathy. Prior background in molecular and/or cell biology would be helpful, but is not essential. Send curriculum vitae and names of three references to: **Dr. E. Duh, Johns Hopkins University School of Medicine, 1550 Orleans Street, Room 143, Baltimore, MD 21231. E-mail: eduh@jhmi.edu.** *Equal Opportunity Employer.*

POSITIONS OPEN

NAVSEA
WARFARE CENTERS
Carderock Division

SENIOR RESEARCH SCIENTIST/TECHNICAL CONSULTANT, ST-830-00
Naval Surface Warfare Center, Carderock Division
Competitive Benefits and Flexible Hours Offered

The selectee will serve as the Research Scientist/Technical Consultant who is internationally recognized as a leading expert/authority in the field of radiated flow noise signature control. This position requires extensive knowledge and experience in radiated flow noise, underwater signatures, signatures and silencing systems, ship integration and design, hull forms, structures and materials, electromagnetic signatures, propulsors, machinery systems, and associated ship and submarine susceptibility. Candidate must have achieved a nationally/internationally recognized level of excellence in the field. Scientific contributions must include solving significant Navy problems. Except under extraordinary circumstances, the selectee must have earned a Ph.D. in a directly applicable field.

Salary range: $138,380 to $158,500 per annum. Duty station: West Bethesda, Maryland.

For further job information, please review the job announcement and application procedures by accessing the information at the following link: **website: https://www.usajobs.opm.gov.** The announcement number for this position is NW8-0830-00-4G024327-FL. Applications must be received by July 22, 2008, and should be marked with the applicable announcement number. For further information, please contact **telephone: 215-897-1619.** *U.S. citizenship is required.*

The Department of the Navy is an Equal Opportunity Employer.

MARKETPLACE

RESEARCH CORPORATION

Research Corporation, a foundation for the advancement of science, is proud to announce the 2008 Cottrell Scholar Awards. The Cottrell Scholar Award, $100,000 in discretionary funds, is designed to identify early-career faculty who show promise to be future leaders in research, and who are committed to making significant contributions to teaching, especially at the undergraduate level.

For more information, see **WWW.RESCORP.ORG**

"There is no doubt in my mind that receiving the Cottrell Scholar Award as a young faculty member critically contributed to further development of my research and my group, and enabled me to pursue a novel project that led to dramatic improvements in our ability to explore the vast parameters of population synthesis models."

VASSILIKI "VICKY" KALOGERA
Associate Professor, Dept. of Physics and Astronomy, Northwestern University

RACHEL BEAN
Cornell University, Department of Astronomy
Signatures of Fundamental Physics in the Cosmos

KIRILL BELASHCHENKO
University of Nebraska, Lincoln,
Department of Physics and Astronomy
First-principles Studies of Electronic Structure and Transport in Magnetic Systems at Finite Temperatures

MATTHEW DAVID DISNEY
State University of New York at Buffalo,
Department of Chemistry
Toward the Rational Design of Small Molecules Targeting RNA

JEANNE ANN HARDY
University of Massachusetts, Amherst,
Department of Chemistry
Controlling Protein Function with Designed Allosteric Switches

NILS KROGER
Georgia Institute of Technology,
School of Chemistry and Biochemistry
Diatom Bio-Nanotechnology: A New Paradigm for the Synthesis of Functional 3D Nanomaterials

FRANKLIN WAYNE OUTTEN
University of South Carolina, Columbia,
Department of Chemistry and Biochemistry
Characterization of a Novel Fe-S Scaffold System Used by Pathogenic Bacteria Under Oxidative Stress and Iron Starvation

GIL REFAEL
California Institute of Technology, Department of Physics
Breakdown of Superfluidity in Low-dimensional Disordered Systems

CHARLES SYKES
Tufts University, Department of Chemistry
Single-Molecule Studies of Ferroelectric Self-Assembly

SERGEI URAZHDIN
West Virginia University, Department of Physics
Magnetoelectronic Phenomena in Nanostructures

TEHSHIK PETER YOON
University of Wisconsin, Madison, Department of Chemistry
Oxidative Functionalization of Hydrocarbons Using Oxaziridines

YIYING WU
Ohio State University, Columbus, Department of Chemistry
Searching for New Electrode Materials and Nanostructured Architectures for Efficient Dye-Sensitized Solar Cells

Stain DNA, not nature.

How can you protect yourself, the environment, and your DNA sample?

Answer: SYBR® Safe. Fact is, it's just as effective as ethidium bromide, yet it's not a hazardous agent. So it's not only better for the environment, but better for you. And since SYBR® Safe uses blue light for visualization, your DNA sample won't be damaged by UV, so you'll get better cloning efficiencies. Next time you're staining DNA, be sure to make the safer choice for yourself and the environment. Get SYBR® Safe. **www.invitrogen.com/sybrsafe**

invitrogen™